THESIS

Thesis title: Tissue Characterisation in Myocardial Infarction by Cardiovascular Magnetic Resonance

University: UCL

Degree: Doctor of Philosophy

Primary supervisor: Prof Derek Hausenloy

Secondary supervisor: Prof Derek Yellon

I, **Dr Heerajnarain Bulluck**, confirm that the work presented in this thesis is my own. Where information has been derived from other sources, I confirm that this has been indicated in the thesis.

Dr Heerajnarain Bulluck

Date: 26th December 2016

Abstract

Acute ST-segment elevation myocardial infarction (STEMI) and its associated co-morbidities are among the leading causes of death and disability worldwide. We used multi-parametric mapping by cardiovascular magnetic resonance (CMR) to provide insights into the pathological processes underlying the ischaemic insult and LV remodelling.

In Chapter 4 we showed that T1 mapping could quantify the AAR as well as T2 mapping. Secondly, the presence of a hypo-intense core on T1 or T2 maps performed equally well to detect intramyocardial haemorrhage (IMH). Lastly, we showed that post-contrast T1 maps could accurately delineate acute MI size.

In chapter 5, we found that 6 standard deviations (SD) was the most accurate semi-automatic method both for acute and chronic MI size quantification using paired CMR scans. However, all 4 of the promising semi-automated techniques assessed (5-SD, 6SD, full width half maximum and Otsu) were equally precise.

In chapter 6, we showed that the majority of patients with IMH had residual iron at follow-up and the latter was associated with adverse LV remodelling. Adverse LV remodelling itself was associated with delayed resolution of oedema in the MI zone. The remote extracellular volume fraction (ECV) was higher in the STEMI patients within the first week, when compared to controls, but only remained elevated in those patients who developed adverse LV remodelling.

In Chapter 7, we obtained the minimal detectable changes for percentage change in LV end-diastolic volume (%ΔLVEDV – 12%) and %Δ in LV end-systolic volume (%ΔLVESV – 13%) in paired acute and follow-up STEMI patients. Combining %ΔLVEDV and %ΔLVESV revealed 4 patterns of LV remodelling.

In conclusion, T1, T2 and T2* CMR mapping complement each other, and provide valuable insights into the pathophysiology of STEMI and adverse LV remodelling. These parameters could be used to risk-stratify, assess response to treatment and for prognostication in reperfused STEMI patients.

Acknowledgements

I would like to thank both my supervisors, Professor Derek Hausenloy and Professor Derek Yellon, for all their support, mentorship and advice during my research time.

I would also like to thank all the staff at the Heart Hospital, the nuclear medicine department at University College London Hospital NHS trust and The Hatter Cardiovascular Institute, UCL for their support.

I would also like to thank Peter Weale and Peter Kellman for supplying us with the WIPs and off-line ECV tool and the following colleagues for their support in various aspects of teaching/ training/ patient scanning etc.:

Consultants

Prof James Moon
Dr Charlotte Manisty
Dr Anna Herrey
Dr Alex Sirker
Dr Leon Menezes
Dr Ashley Grove
Dr Simon Wan

Statistical support

Dr Jennifer Nicholas
Dr Raju Maiti

Fellows

Dr Steven K White
Dr Stefania Rosmini
Dr Amna Abdel-Gadir
Dr Anish Bhuva
Dr Thomas Treibel
Dr Marianna Fontana
Dr Patricia Reant
Dr Esther Gonzalez-Lopez
Dr Manish Ramlall
Dr Ashraf Hamarneh
Dr Shane Weinmann
Dr Matthew Hammond-Haley
Dr Yun Yun Go
Dr Jennifer Bryant

Contents

1.1 Sections

1.2 Figures *(labelled as* chapter number – figure number*)*

1.3 Tables *(labelled as* chapter number – table number*)*

Abbreviations

AHA: American Heart Association

APPROACH: Alberta Provincial Project for Outcome Assessment in Coronary Heart Disease

AUC: area under the curve

BARI: Bypass Angioplasty Revascularization Investigation

CE-SSFP: contrast-enhanced steady state free precession

CI: confidence interval

CMR: cardiovascular magnetic resonance

CoV: coefficient of variability

ECM: extracellular matrix

ECV: extracellular volume fraction

EGE: early gadolinium enhancement

ESA: endocardial surface area

FB: free breathing

FFP: first pass perfusion

FWHM: full width half maximum

ICC: intra-class correlation coefficient

IMH: intramyocardial haemorrhage

IPC: ischemic preconditioning

IPost: ischemic postconditioning

IR: inversion recovery

LGE: late gadolinium enhancement

LV: left ventricle/ ventricular

LVEDV: left ventricular end-diastolic volume

LVEF: left ventricular ejection fraction

LVESV: left ventricular end-systolic volume

LVM: left ventricular mass

MACE: major adverse clinical outcome

MagIR: magnitude-reconstructed inversion recovery

MDC: minimal detectable change

MDC95: minimal detectable change with 95% confidence

MI: myocardial infarction/ infarct

MOCO: motion-corrected

MOLLI: Modified Look Locker Inversion recovery

MSI: myocardial salvage index

MVO: microvascular obstruction

PET: positron emission tomography

PPCI: primary percutaneous coronary intervention

PSIR: phase sensitive inversion recovery

RCT: randomised controlled trials

RIC: remote ischemic conditioning

ROC: receiver operator characteristic

ROI: region of interest

SD: standard deviation

SEM: standard error of the measurement

SPECT: single photon computed tomography

STEMI: ST-segment elevation myocardial infarction

STIR: short tau inversion recovery

T&P: trabeculae and papillary muscles

WIP: work in progress

%Δ: percentage change

2 Introduction

Since the introduction of thrombolysis and primary percutaneous coronary intervention (PPCI), mortality due to acute ST-elevation myocardial infarction (STEMI) has declined over the past 4 decades (1), and 1-year mortality has reached a plateau at around 11%.(2) However, despite a decline in mortality, morbidity post-myocardial infarction (MI) remains significant.(3-7) Morbidity and mortality post-STEMI is closely related to the final MI size. A recent meta-analysis of 2,632 patients showed that MI size measured by cardiovascular magnetic resonance (CMR) or Technetium-99m Sestamibi single photon computed tomography (SPECT) within 1 month post-PPCI was strongly associated with 1-year hospitalisation for heart failure and all-cause mortality.(8) For every 5% increase in MI size, there was a 20% increase in relative hazard ratio for 1-year hospitalisation for heart failure and all-cause mortality. At present, for patients presenting with an acute STEMI, the most effective therapy for limiting MI size, preserving left ventricular (LV) function, and reducing the onset of heart failure and subsequent mortality is timely reperfusion by PPCI.(9-12) Although, the process of myocardial reperfusion by PPCI has been optimised by advances in stent technology, new anti-platelet drugs (e.g. prasugrel, ticagrelor, and abciximab), and novel anti-thrombotic agents (e.g. bivalirudin therapy), the restoration of coronary blood flow comes at a price, paradoxically inducing myocardial injury and cardiomyocyte death, and has been termed myocardial reperfusion injury.

2.1 Myocardial reperfusion injury

Whether myocardial reperfusion injury exists in man has been a topic of intense debate over past decades.(13) In 1960, Jennings et al (14) first postulated the existence of myocardial reperfusion injury in a canine model of reperfused MI, characterised by cellular swelling, myofibril contracture, disruption of sarcolemma and calcium phosphate particle appearing within the mitochondria. However, the differentiation of the ischaemic component from the reperfusion component of the acute myocardial injury in the pre-clinical and clinical setting is not possible but the existence of myocardial reperfusion injury has been proven indirectly. In 2005, Staat et al. (15) first provided some evidence of the existence of myocardial reperfusion injury in the clinical setting. They showed that ischaemic postconditioning (using four 1-minute low-pressure inflations and deflations of the angioplasty balloon following direct stenting of the culprit lesion) led to a 36% reduction in MI size in PPCI-treated STEMI patients. The ability for a therapeutic intervention, applied at the onset of reperfusion, to reduce MI size has provided indirect evidence that the phenomenon of myocardial reperfusion injury exists in man. As a result, myocardial reperfusion injury has emerged as a promising target for cardioprotection.(16)

Four types of myocardial reperfusion injury have been described:

1. *Reperfusion-induced arrhythmias:* these occur on reperfusing a previously ischaemic myocardium and comprise of idioventricular rhythm and

ventricular arrhythmias. The vast majority of these arrhythmias are self-terminating or are easily treated.(17)

2. *Myocardial stunning*: this refers to the reversible contractile dysfunction that occurs on reperfusing the acutely ischaemic myocardium and is believed to be due to myocardial oxidative stress and intracellular calcium overload.(18)

3. *Coronary no-reflow and microvascular obstruction (MVO):* coronary no-reflow in the infarct-related artery following PPCI is indicative of underlying MVO – defined as the "inability to reperfuse a previously ischaemic region".(19) Some of the major contributing factors include capillary compression by swollen cardiomyocytes and endothelial cells, thrombogenic and vasomotor substance release, neutrophil plugging, capillary damage, impaired coronary vasodilatation, coronary microembolisation from the atherosclerotic plaque, and platelet micro-thrombi as illustrated in Figure 2-1.(20, 21) Intracoronary agents such as nitrates, calcium channel blockers, adenosine and nicorandil have been used to treat coronary no-reflow and improve myocardial reperfusion – although none of these have been shown to reduce MVO or improve clinical outcomes.(22)

4. *Lethal myocardial reperfusion injury:* Reperfusing a previously ischaemic cardiomyocyte induces cytosolic and mitochondrial calcium overload, oxidative stress, rapid restoration in intracellular pH, which on a background of relative adenosine triphosphate depletion, culminates in the opening of the mitochondrial permeability transition pore and irreversible cardiomyocyte hypercontracture – the hallmark of lethal myocardial reperfusion injury.(23)

Crucially, there is currently no effective therapy for reducing either MVO or lethal myocardial reperfusion injury. Therefore, novel therapeutic interventions are required to protect the heart from acute myocardial reperfusion injury in STEMI patients, in order to improve clinical outcomes.

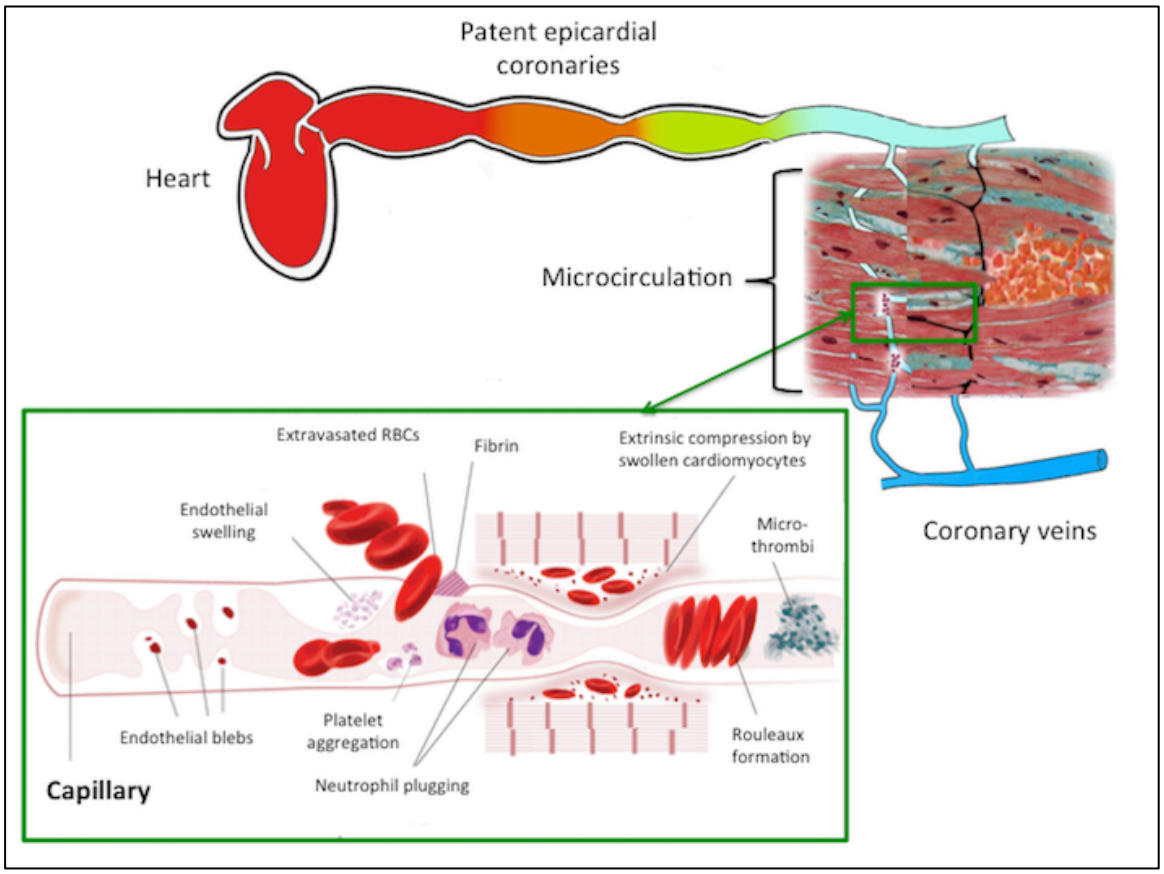

Figure 2-1: Factors contributing to the development of MVO

This figure illustrates some of the factors contributing to the development of MVO, namely external compression of capillaries by interstitial and cellular oedema, by swollen cardiomyocytes and endothelial cells, cellular plugging, capillary damage with extravasation of red blood cells, coronary microembolisation of debris and in-situ thrombosis.

2.2 The need for cardioprotection

The consequence of myocardial reperfusion injury is the death of cardiomyocytes that were still viable at the end of the index ischaemic insult, and which accounts for up to 50% of the final MI size, thereby mitigating the benefits of reperfusion, and making lethal myocardial reperfusion injury a therapeutic target for cardioprotection (Figure 2-2).

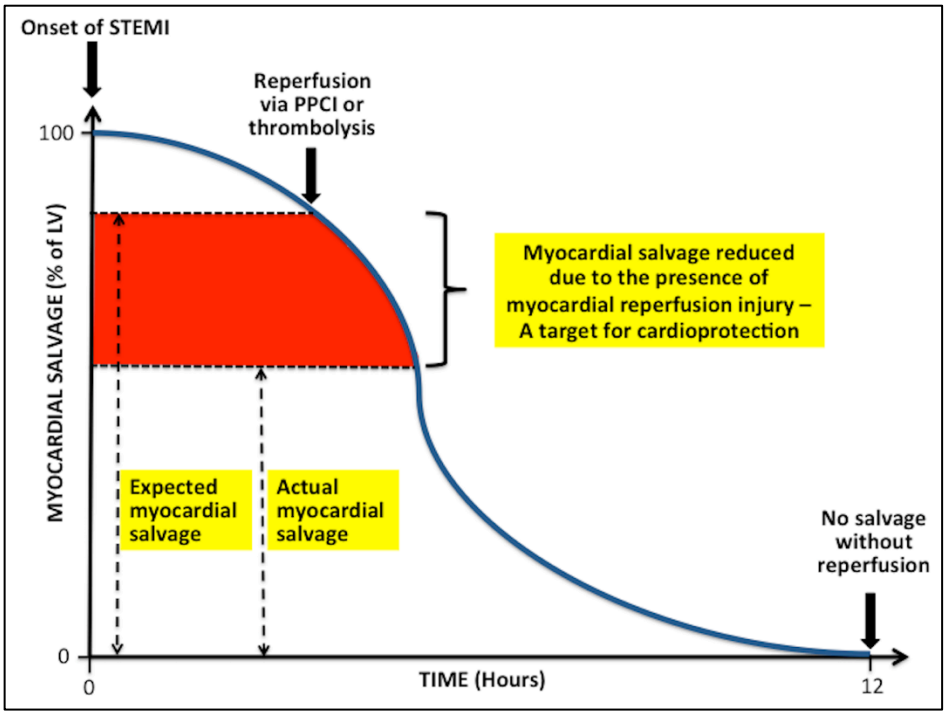

Figure 2-2: This hypothetical scheme depicts the magnitude and clinical impact of myocardial reperfusion injury in patients with ischaemic heart disease who are subjected to acute ischaemia/reperfusion injury.

The thick blue curve shows the extent of myocardial salvage (which equates to the area-at-risk subtract the myocardial infarct size and is expressed as the % of the left ventricular mass) in a theoretical patient presenting with an acute ST-segment elevation myocardial infarction (STEMI) reperfused by primary percutaneous coronary intervention (PPCI) or thrombolysis. As expected in the absence of reperfusion the extent of myocardial salvage declines with time. Although myocardial reperfusion is essential for myocardial salvage following a STEMI, the process of restoring coronary blood flow within the infarct-related artery, can paradoxically induce cardiomyocyte death – a phenomenon that has been termed 'myocardial reperfusion injury'. As a result, following reperfusion, the extent of myocardial salvage is actually smaller than expected given the duration of acute myocardial ischaemia – this attenuation in myocardial salvage is due to the presence of myocardial reperfusion injury, which can contribute up to 50% of the final myocardial infarct size.

In this regard, 'ischaemic conditioning', in which the heart is rendered tolerant to acute ischaemia/reperfusion injury (IRI) by subjecting it to cycles of brief ischaemia and reperfusion, provides an endogenous form of cardioprotection.

The therapeutic potential of ischaemic conditioning, a collective term given to the different forms of endogenous cardioprotection, include ischaemic preconditioning, ischaemic postconditioning, remote ischaemic conditioning and pharmacological conditioning.

Ischaemic preconditioning (IPC)

In 1986, Murry et al (24) made the intriguing observation that following an acute coronary artery occlusion the resultant MI size could be significantly reduced by 'preconditioning' the heart with brief episodes of ischaemia and reperfusion. As a cardioprotective strategy for protecting the heart against acute myocardial reperfusion injury, its clinical application has been limited by the need to apply the IPC stimulus directly to the heart, and prior to the index ischaemia, which is not possible in the clinical setting.

Ischaemic postconditioning

In 2003, Zhao et al (25) discovered that by interrupting myocardial reperfusion with several short-lived episodes of myocardial ischaemia, this led to a reduction in MI size to a similar extent as IPC – a phenomenon which has

been termed ‘ischaemic postconditioning’ (IPost). It has also provided confirmatory evidence for the existence of lethal myocardial reperfusion injury in man. However, IPost requires the intervention applied directly to the heart, which may not always be feasible or practical depending on the clinical situation.

Remote ischaemic conditioning

In 1993, Przyklenk et al. (26) made the interesting observation that the cardioprotective effect of IPC was not restricted to one particular coronary artery territory and it could be transferred to another coronary artery territory. This gave rise to the concept of ‘remote ischaemic conditioning’ (RIC), the term given to the cardioprotection induced by applying cycles of brief ischaemia and reperfusion to an organ or tissue away from the heart.

Pharmacological conditioning

The elucidation of the signal transduction pathways underlying ischaemic conditioning has resulted in the identification of new targets for cardioprotection, some of which can be modulated by pharmacological agents.(27, 28) However, pharmacological conditioning strategies that have shown promise in the preclinical setting or small proof-of-concept studies have failed to consistently show a benefit in the clinical setting.(29)

2.3 Challenges facing clinical cardioprotection research

There are a number of challenges facing clinical cardioprotection research. Firstly, the translation of novel cardioprotective therapies into the clinical setting for patient benefit has been extremely difficult. Over the last 30-40 years a vast number of therapies with proven efficacy for preventing myocardial reperfusion injury and reducing MI size in experimental animal studies (e.g. such as glucose-insulin-potassium (30, 31), cyclosporine (32, 33) and erythropoietin (34-36)), have produced disappointing results when investigated in the clinical setting as adjunctive therapy to reperfusion.(37) More recently, a number of promising interventions to reduce MI size in STEMI patients have also failed to meet their primary endpoint of cardioprotection - these have included studies investigating therapeutic hypothermia (38, 39), targeting mitochondrial function (40, 41), and modulation of nitric oxide signalling (42, 43) as adjuncts to myocardial reperfusion. The reasons for this failure to translate cardioprotection into the clinical setting have been attributed to a number of factors including the use of inappropriate animal MI models and poorly designed clinical studies.(44-47)

A second challenge facing clinical cardioprotection research is that clinical outcomes of STEMI patients following PPCI continue to improve, making it increasingly difficult to demonstrate an improvement in clinical outcomes with a novel cardioprotective therapy. However, although mortality following STEMI is in decline, the number of patients surviving STEMI and going on to develop heart failure remains significant. There remains, therefore, an unmet need to

discover novel therapeutic strategies capable of preventing myocardial reperfusion injury and reducing MI size, so as to preserve LV systolic function and prevent the onset of heart failure in reperfused STEMI patients.

Last but not least, it may be possible that some of the therapeutic strategies did not consistently show a cardioprotective benefit in the pre-clinical setting using different animal models and their translation to the clinical setting was premature. One such example is cyclosporin that was summarised in a meta-analysis by Lim et al.(48) They identified 20 pre-clinical studies involving 4 animal species. Cyclosporin failed to consistently reduce MI size in studies using the porcine model of MI. The porcine model is considered a closer match to human physiology (49) and therefore given the inconsistent findings of cyclosporin on MI size reduction in that model, it is likely that failure of this drug to show an improvement in outcomes in the clinical setting (32) may have been due to a lack of efficacy.

2.4 Optimising the clinical translation of cardioprotection

The failure to translate promising cardioprotective therapies from bench to bedside has been the subject of several recent review articles.(44-47) There are certain factors that need to be taken into account whilst designing clinical studies in order to improve the chances of reaping their maximum benefit in the clinical environment. In the setting of STEMI patients undergoing PPCI, these key points need to be taken into account:

- Patients that are most likely to benefit from the cardioprotective therapy should be recruited: large area-at-risk (AAR) (>30% of the LV)(50); no coronary collateralisation (Rentrop<1); occluded artery prior to PPCI (thrombolysis in myocardial infarction flow grade 0 or 1); those presenting within 2-3 hours of symptoms onset.(51, 52)
- Only therapies having shown conclusive cardioprotection in pre-clinical studies should be tested.
- The therapy should be administered prior to myocardial reperfusion via PPCI.
- Confounding factors such as age, pre-infarct angina, diabetes mellitus, hypertension, dyslipidaemia and concomitant medications (nitrates, morphine, nicorandil, sulphonamides), which can interfere with cardioprotection, should be taken into consideration when performing power calculation.(53)
- Relevant clinical endpoints for assessing cardioprotective efficacy should be selected. These include: MI size (enzymatic or CMR); myocardial salvage index; MVO; LV remodelling, LV ejection fraction (LVEF); cardiac death; and hospitalisation for heart failure.

Although the points listed above might theoretically identify a group of patients who would most likely benefit from a cardioprotective therapy, using these strict criteria in the clinical setting is not realistic. A large number of patients would need to be screened prior to recruiting only a handful of them

and this approach would make such a trial impractical and not cost-effective. Furthermore, any potentially therapy found to be effective would not be applicable to the general cohort of STEMI patients.

2.5 The role of CMR in cardioprotection studies

CMR is a well-established tool for the quantification of focal and diffuse fibrosis.(54) Late gadolinium enhancement (LGE) by CMR is considered the gold standard for MI size quantification.(55-57) CMR can also provide information on LV function, MVO and the AAR (to calculate myocardial salvage). MI size (8, 58, 59), MVO (60, 61) and myocardial salvage (62, 63) assessed by CMR performed in the first few days following PPCI in STEMI patients have all been shown to be strongly associated with prognosis. With the recent availability of T1, T2, T2* and extracellular volume fraction (ECV) mapping, more in-depth insights can be obtained into various biological processes such as oedema, intramyocardial haemorrhage (IMH), MVO, and changes in the remote myocardial interstitial space following an acute STEMI. As a result, CMR is increasingly being used as a tool, providing several surrogate endpoints, in randomised controlled trials assessing novel cardioprotective therapies for reducing MI size in reperfused STEMI patients.(64)

2.5.1 Area-at-risk (AAR)

2.5.1.1 Importance of knowing the AAR

To assess the effectiveness of a cardioprotective intervention, the actual MI size needs to be compared to the hypothetical MI size if the artery was not promptly reperfused, that is, the AAR. In the pre-clinical setting, the AAR can be obtained by measuring the regional myocardial blood flow with microspheres during coronary occlusion in vivo.(65) In the post-mortem setting, the AAR can be obtained by the injection of Evans blue dye during re-occlusion of the coronary and MI size can be obtained with triphenyl tetrazolium chloride staining.(65)

Once the AAR and MI size are known, myocardial salvage (Figure 2-5) and myocardial salvage index (MSI) can be calculated using the formula below:

$$MSI = (AAR - MI\ size)/AAR$$

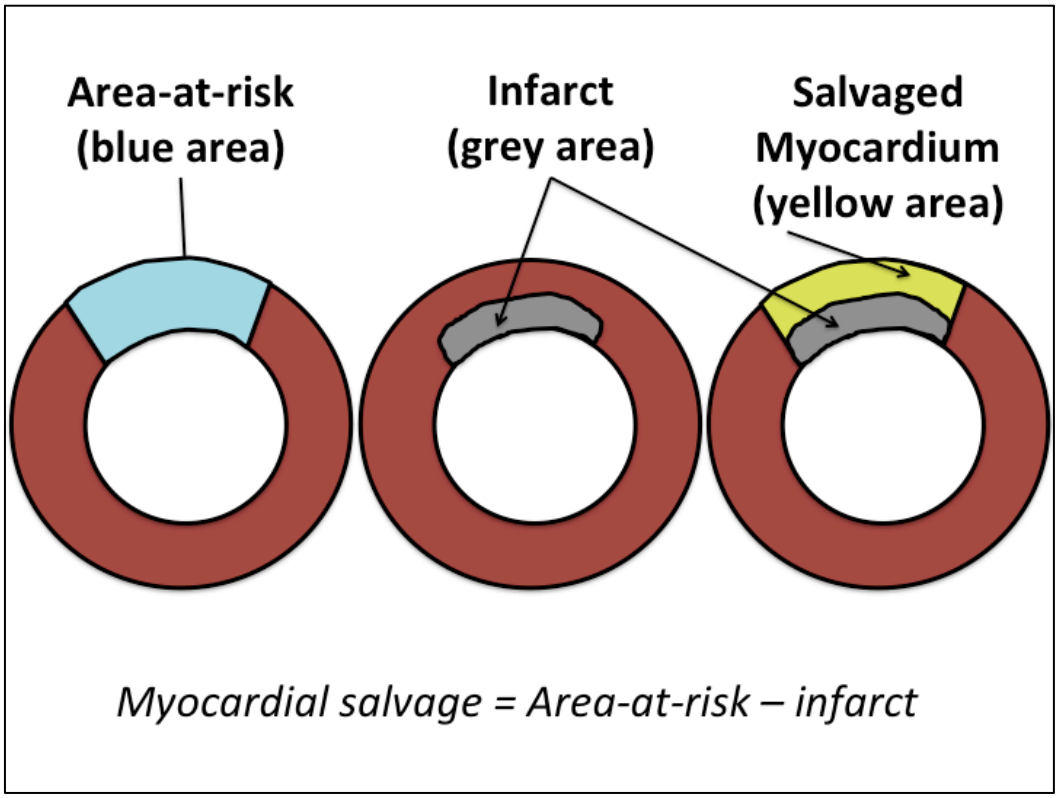

Figure 2-3: Schematic representation of the AAR (blue), infarct size (grey) and the salvaged myocardium (yellow)

MSI is considered a more sensitive measure to assess the effectiveness of a cardioprotective strategy than a reduction in absolute MI size or MI size as a percentage of the LV alone.(66, 67) Figure 2-4 below illustrates 2 patients with similar MI size in grams and as a percentage of the LV. However, Patient A has a smaller AAR but a greater transmural extent of MI than patient B. Therefore, it is clear that Patient B has a greater myocardial salvage and MSI than A. This example highlights the superiority of MSI over MI size, as a percentage of the LV or in grams; to be used as a surrogate endpoint in future studies.

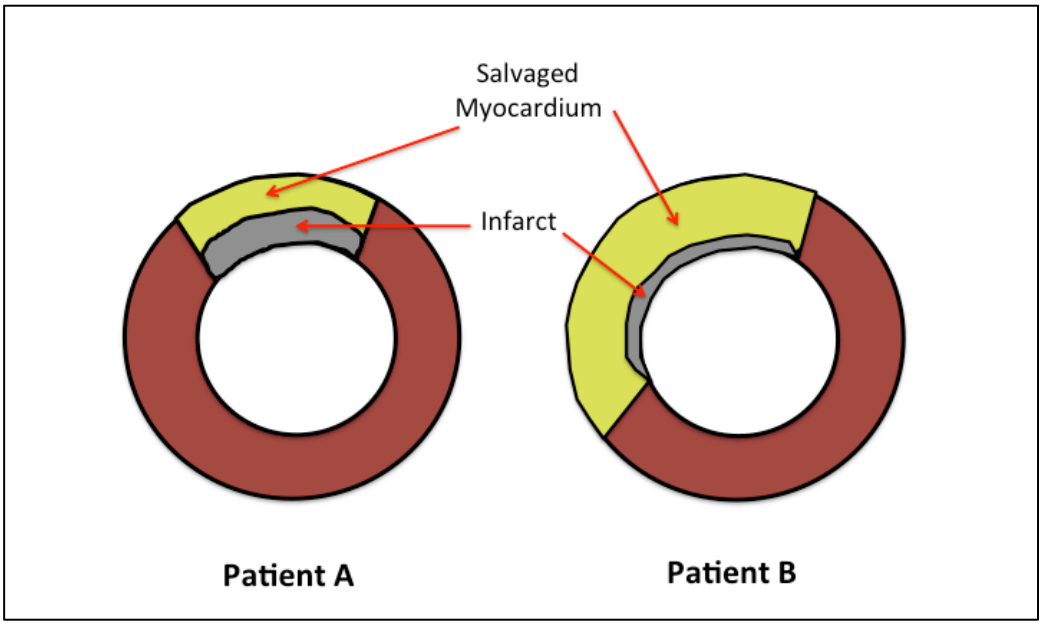

Figure 2-4: 2 patients with similar MI size as a percentage of the LV but different MSI

However, the accurate assessment of the AAR in the clinical setting using a technique that is easily accessible, reproducible, affordable and practical has been difficult and currently there is no established method.

2.5.1.2 Non-CMR based method for assessing the AAR

The well-validated method to assess the AAR in the clinical setting is by ^{99}Technetium-sestamibi SPECT.(68) However, this requires injection of ^{99}Technetium-sestamibi prior to reperfusion of the culprit artery and performing a SPECT study within 4 to 6 hours of injection. Furthermore, in order to obtain the MI size, a second scan has to be performed at a later stage, usually after 5 to 7 days (69), for an estimation of the MI size. Recently, injection of the tracer

up to 2 hours post-reperfusion has also been shown to be successful in delineating the AAR.(70) However, this is logistically difficult to perform, involves radiation exposure, is expensive, and is not widely available.(67)

The electrocardiogram has been used to estimate the AAR by using a combination of the ST-segment abnormalities and QRS complex scores but still underestimated the AAR by SPECT.(71) Furthermore, it performs less well in anterior STEMIs when compared to inferior STEMIs.(72) This technique is not robust when compared to SPECT(73) and has therefore failed to be widely adopted.

The circumferential extent of the segments with abnormal contractility by left ventriculography at the time of PPCI has also been used to assess the AAR in some cardioprotection studies (50, 74-76) but lacks prior robust validation, and can be confounded by abnormal contractility due to myocardial stunning.(77)

Three angiographic score models have been developed and can be used to assess the AAR. The Duke Jeopardy Score (78) divides the coronary tree into six segments. All segments distal to the culprit lesion are assigned 2 points and considered to be part of the AAR. The Bypass Angioplasty Revascularization Investigation (BARI) score (79) takes into account the vessels' diameter and length and grades them according to specific criteria. The scores of the vessels subtended beyond the culprit lesion are summed and divided by the total score of the whole left ventricle and expressed as a percentage of the LV. The Alberta Provincial Project for Outcome Assessment

in Coronary Heart Disease (APPROACH) score is based on previous human post-mortem studies and divides the LV according to the relative proportion of myocardium perfused by each coronary artery. This model then assigns scores to the vessels based on the location of the culprit lesion as proximal, mid, or distal and the size of the vessels.(80)

Ortiz-Perez et al (81) (83 patients) showed that the BARI and APPROACH scores matched the AAR derived by the infarct endocardial surface area (ESA) (R=0.90 and 0.87 respectively). However, Wright et al (82) (108 patients) showed that the BARI score only moderately correlated (R=0.42) with infarct-ESA but had a better correlation (R=0.77) with black blood T2-weighted short tau inversion recovery (STIR) CMR.(82) Likewise, Fuernau et al. (83) (197 patients) showed a moderate correlation between APPROACH score and infarct ESA (R=0.44) and better correlation with black blood triple inversion recovery T2-weighted imaging (R=0.87).

2.5.1.3 Assessment of the AAR by T2-weighted CMR

Due to the limitations of the above techniques for delineating the AAR, CMR has recently emerged as a promising tool for the assessment of both the MI size and the AAR in one single scan. Higgins et al (84) in the 1980s were the first investigators to study myocardial T2 in a canine model of MI. Interestingly, both T2 and T1 were shown to change similarly in the setting of an acute MI. The observed changes were theoretically consistent with myocardial oedema

and correlated with the measurements of myocardial water content estimated by wet-weight to dry-weight ratios. The changes in T2 have been described to be due to a combination of an increase in absolute tissue water, movement of water from the extracellular to the intracellular compartment, and the conversion of protein-bound water to free water.(85) In animal models of MI, Garcia-Dorado et al (86) (porcine models of MI), Boxt et al. (87) and Aletras et al. (88) (both using canine models of MI) confirmed that T2-weighted CMR images represented the AAR. Tilak et al. (89) used a canine model of permanent coronary ligation and showed that the AAR depicted by first pass perfusion on day 1 agreed well with the hyper-intense zones on T2-weighted images performed on day 2.

In the clinical setting, Friedrich et al (90) (92 patients) showed that T2-weighted images of acute MI in patients had hyper-intense regions in the distribution of the culprit coronary artery and that the hyper-intense zones were typically transmural in extent, and significantly larger than the acute MI size and could be used to assess myocardial salvage. Carlsson et al (91) (16 patients) injected sestamibi in STEMI patients prior to PPCI and imaged with SPECT to validate T2-weighted images. They found an excellent correlation between the AAR derived by SPECT and T2-weighted imaging. However, dark blood T2-weighted imaging has several limitations including the subjective interpretation of the images, variations in regional myocardial intensity due to changes in sensitivity of surface coils, blood-pooling artefacts at the subendocardial border, its relatively low contrast-to-noise ratio between normal and abnormal myocardium, and its susceptibility to breathing and motion artefacts.(66, 92)

Therefore, to overcome these limitations, bright blood T2-weighted SSFP-based sequences using a T2 preparation (93) or a turbo spin echo – SSFP hybrid approach were developed.(94) These bright blood T2-weighted sequences provide more robust image quality while preserving the contrast-to-noise ratio when compared to the dark blood T2-weighted imaging. Berry et al (95) (50 patients) used the bright-blood T2 magnetisation-preparation based sequences to delineate the AAR and compared it with angiographic measures of the AAR in patients with recent acute MI. The oedema-based AAR correlated with the APPROACH score, with a bias of about 2.5% on Bland-Altman analysis.(95) Payne et al (96) (64 patients) subsequently showed that bright blood T2-weighted imaging had higher diagnostic accuracy that dark blood T2-weighted imaging to identify and delineate the AAR.

Further progress was made in this field by Giri et al (97) developed the T2 mapping technique. They found that T2 mapping was more robust than T2-weighted imaging to detect oedema and the former did not suffer from the above limitations. Furthermore, the T2 values can be directly obtained from the pixel-wise T2 maps and does not require manual adjustment of the window settings. Verhaert et al (98) (27 patients) showed that T2 mapping performed better than T2-weighted STIR images to detect acute myocardial injury in STEMI patients, confirming the superiority of T2 mapping over T2-weighted STIR imaging. Most recently, McAlindon et al (99) (40 patients) showed that the detection of the AAR by T2 mapping was similar to T2-weighted STIR imaging, but the former was more reproducible.

2.5.1.4 Controversies surrounding the use of T2-weighted imaging for the AAR

However not all pre-clinical and clinical studies have support the notion that the areas of hyper-intensity on the T2-weighted images represent the AAR.(100) Johnston et al (101) and Miller et al (102) (both using canine models of MI) showed that T2-weighted MR images demonstrated mostly subendocardial hyper-intense regions compared to a transmural reduction in blood flow by radioactive microspheres as the reference for the AAR. Ryan et al (103) (using different occlusion times in a canine model of MI) showed that those with MI on histology had areas of hyper-intensity on T2-weighted MR images, whereas the canines without MI did not have any T2 abnormalities, despite displaying regional systolic dysfunction. In the pre-clinical setting, Kim et al (104) reported that T2-weighted imaging did not depict the AAR in anaesthetised dogs that were subjected to different durations of coronary occlusion. MI size by LGE was compared to the gold standard (triphenyl tetrazolium chloride staining) and AAR by fluorescent microspheres to T2-weighted imaging after 4±1 days reperfusion. The T2-weighted hyper-intensity correlated better and matched in shape with the MI size than with the AAR and these findings were confirmed in a small group of acute STEMI patients. Although the findings from the canine model of MI may be due to the presence of well-developed collaterals in that species, the findings in their small group of patients is in contrast with all other clinical studies published so far using T2-weighted imaging in reperfused STEMI.

In the wake of the above controversies surrounding whether T2 abnormalities depict the irreversibly injured myocardium only, or the reversibly injured (salvaged) myocardium as well, in a porcine model of MI, Ubach et al (105) showed that the AAR derived from T2-weighted imaging matched that from SPECT, both in animals with and without LGE. Recently, using hybrid positron emission tomography (PET)/MR imaging, we showed that the area of reduced 18F-fluorodeoxyglucose uptake was significantly larger than the MI size and closely matched the AAR delineated by T2, supporting the notion that T2 mapping does delineate both the reversibly and the irreversibly injury myocardium within the AAR.(106) Hammer-Hansen et al (107) provided some further insights on this topic, using a canine model of MI and T2 mapping CMR. They showed that the T2 signal was elevated in the MI zone and salvaged myocardium when compared to the remote myocardium, and the T2 values were higher in the MI zone when compared to the salvage myocardium. Furthermore, animals with CMR performed at 2 hours had higher T2 values in both the infarct and salvaged myocardium compared to those who had the scan at 48 hours, highlighting that the extent of myocardial oedema is dynamic.

The dynamic nature of oedema post-MI has been previously described in the pre-clinical setting. Johnston et al (108) showed in a serial study involving a rabbit model of non-reperfused MI that T2 relaxation times measured by nuclear magnetic resonance increased at 3 days and returned to baseline at 2 months. Using a porcine model of reperfused MI, Foltz et al (109) showed that T1 and T2 were elevated at 1 hour post reperfusion and were nearly normal at Day 2. On Day 7, T2 increased while T1 decreased. The partition coefficient was

elevated by >150% at all time points. These animals had IMH on histology and the fluctuations in T1 and T2 were explained by a combination of oedema and subsequently oxidative denaturing of haemoglobin to methaemoglobin. Recently, Fernandez-Jimenez et al (110) built on this work and looked at the interplay between myocardial water content (using desiccation) and T2 relaxation times in a similar porcine model of reperfused MI. They reported a 'bimodal' pattern of oedema, appearing at 2 hours and resolving by 24 hours and reappearing on day 4 and peaking at day 7. The first wave of oedema was attributed to reperfusion injury and the second wave of oedema was put down to inflammation during the tissue-healing phase.(111) However, they did not take the presence of MVO and IMH into account, which could have interfered with their T2 measurements, and the overall sample size for each time point was 5 pigs. Recently, Carrick et al (112) showed that although the T2 and T2* of the core of the MI followed a bimodal pattern in those with IMH assessed by T2* and in those patients without IMH, the T2 relaxation time progressively increased in the MI zone. The extent of myocardial oedema (% of the LV) in their study followed a unimodal pattern and peaked at day 3 in patients both with and without IMH. It was previously believed that oedema is stable in the first week of an MI based on the study by Carlsson et al (91) and Dall'Armellina et al (113) However both these studies only performed T2-weighted imaging on days 1 and 7 and the peak shown by Carrick et al (112) on day 3 was most probably missed.

Nordlund et al (114) recently provided some indirect evidence that there was no bimodal pattern of oedema in the clinical setting. They combined data

from 2 studies involving 215 patients and showed there was no difference in size, quality of the T2-weighted images and the ability to detect the culprit territory when patients having a CMR study on Day 1 to Day 6 onwards were compared.

The utility of T2-weighted imaging for measuring the AAR has also been put into question because certain cardioprotective therapies have been shown to reduce not only MI size but the extent of myocardial oedema as well. Ischaemic postconditioning (115) and remote ischaemic conditioning (using transient arm or leg ischaemia and reperfusion)(116, 117) has been shown to reduce MI size and the extent of oedema delineated by T2 mapping and T2-weighted imaging, leading to an underestimation of the AAR by this technique. However, these were small studies of reperfused STEMI patients and were not adequately powered to assess that endpoint. Intuitively, the fact that a cardioprotective therapy can reduce the extent of myocardial oedema, which itself is the result of myocardial reperfusion injury, should not be unexpected. However, in a recent large study of 696 STEMI patients by Eitel et al (118), ischaemic postconditioning or a combination of remote ischaemic conditioning and ischaemic postconditioning did not lead to a reduction in myocardial oedema as compared to those without any conditioning intervention. Furthermore, drugs such as metoprolol (119, 120) and exenatide (121, 122) that were effective at reducing MI size did not reduce the extent of myocardial oedema. Therefore, further studies are required to investigate the reasons for these mixed results.

2.5.1.5 Other CMR-based techniques for delineating the AAR

The infarct-ESA (81) has been proposed to assess the AAR, based on the assumption that the lateral borders of an MI are already established early after an MI, and the wave-front of ischaemic injury begins in the subendocardium and progresses in the radial direction.(123) O'Regan et al (124) (15 patients) compared the transmural and circumferential extent of T2 abnormalities and LGE. They found that the main difference between the 2 methods was in the transmural direction. Ortiz-Perez et al (81) used the infarct-ESA (Infarct-ESA = summed endocardial hyper-enhanced infarct length/total LV endocardial length x 100) in 83 patients for the AAR and showed good correlations with BARI and APPROACH angiographic scores. However, Wright et al (82) (108 patients) showed that, although black blood T2-weighted correlated well with infarct-ESA (R=0.77), the AAR by T2 was 8% larger than that derived from ESA.(82) Ubach et al (125) (37 patients) subsequently also showed that the AAR by infarct-ESA was significantly smaller than the AAR derived from T2-weighted imaging. In particular, there were a small proportion of patients with no LGE and therefore infarct-ESA could not be applied to those patients. Therefore, infarct-ESA is not considered a reliable method for the AAR, especially in those with no or very small MI.

Contrast-enhanced steady state free precession (CE-SSFP) cine imaging is another modality proposed to delineate the AAR. The SSFP-cine imaging technique is dependent on the T2/T1-weighted contrast, and in the setting of acute MI, it can sometimes display intrinsic contrast signal in the

areas of oedema due to the higher T2/T1 ratio. This ratio is further increased following gadolinium administration due to a reduction in T1 (predominantly). Therefore, this technique has shown promise to delineate the AAR but still relies on the presence of oedema in the salvaged myocardium. Sorensson et al (126) (16 STEMI patients) showed good correlation (R2=0.78) between the AAR derived from SPECT and CE-SSFP images. Ubach et al (127) (21 patients) subsequently showed good agreement between T2-weighted imaging and CE-SSFP cines. Most recently, Nordlund et al (114, 128) in a much larger cohort of patients showed good agreement between contrast-enhanced SSFP cines and T2-STIR imaging to delineate the AAR. Although there was no bias between the 2 methods, the correlation was moderate (R^2 0.71) and the limits of agreement were wide at ±12%.(114) The advantage of CE-SSFP imaging over T2-weighted imaging was that out of 200 patients with T2-STIR data, only 65% had images of diagnostic quality compared to 97% of the SSFP images being diagnostic. Furthermore, no additional breath-hold imaging, specifically for the AAR, is needed.

Early gadolinium enhancement (EGE) imaging has been proposed to assess the AAR. Matsumoto et al (129) (34 patients) showed that EGE performed 2 minutes post-contrast extended transmurally, and was consistently larger than the LGE extent. Furthermore, the AAR derived from EGE correlated well (R=0.86) with T2-weighted imaging with minimal bias (-0.8%), but the limits of agreement were quite wide at 11.8%. Hammer-Hansen et al (130) (37 patients) provided some insights into this observation using serial T1 mapping. Post contrast T1 between the salvaged and infarcted myocardium was similar at

4 minutes but different at 8 to 20 minutes post-contrast. Therefore, performing EGE before 8 minutes would also enhance the salvaged myocardium and this explains the findings from Matsumoto et al(129) However, McAlindon et al (99) (40 patients) showed that the AAR by EGE was significantly lower than that by T2 mapping and its quantification was also less reproducible.

2.5.1.6 T1 mapping for the delineation of the AAR

Native T1 mapping CMR is another modality proposed to assess the AAR. Although native T1-weighted imaging assesses the longitudinal relaxation time of the tissue compared to T2 mapping, which measures the transverse relaxation time, T1 mapping is also heavily influenced by the T2 properties of the tissue and can also detect oedema. Using a canine model of MI with microspheres as the reference standard for the AAR, Ugander et al (131) showed that native T1 mapping performed equally well along with T2 mapping to delineate the AAR. In the clinical setting, Dall'Armellina et al (132) (41 patients) confirmed that T1 mapping performed equally well to delineate the AAR when compared to T2-weighted imaging in STEMI and was superior to T2-weighted imaging to delineate the AAR in non ST-segment elevation myocardial infarction. Langhans et al (133) (n=14) found that the AAR by T1 and T2 mapping CMR at 1.5T correlated well with that obtained by SPECT but direct comparison between T1 and T2 mapping was not performed. T2 mapping is considered to be the most robust method to delineate the AAR so far. Although T1 mapping has also shown promise, the diagnostic performance of T1

mapping against T2 mapping in the clinical setting has not been performed. If T1 mapping performs equally well to detect the AAR as shown by the animal data, then this may help to keep scanning time to a minimum by not acquiring T2 mapping in cases when T1 mapping for ECV data is already being acquired.

2.5.2 Microvascular obstruction (MVO) and Intramyocardial haemorrhage (IMH)

MVO, which manifests clinically as coronary no-reflow in the infarct-related artery following PPCI, is defined as the "inability to reperfuse a previously ischaemic region".(19) IMH has been shown to be a consequence of the process of reperfusion itself (134, 135) and occurs after a period of 45 minutes of coronary occlusion in a porcine model of MI.(136) MVO is closely linked with the development of IMH (137) and clinical studies have supported the notion that MVO precedes the development of IMH in a subset of patients and is considered a more severe form of microvascular injury.(138)

2.5.2.1 Incidence and clinical significance of MVO and IMH

Despite the introduction of PPCI as the reperfusion strategy of choice in STEMI, nearly 50% of patients still develop MVO (61), and 35-40% have IMH (60, 139), as detected by CMR. The presence of MVO following PPCI, assessed by TIMI flow post-PPCI (140), a combination of ST-segment resolution and myocardial blush grade (141), myocardial contrast

echocardiography (142) and CMR (143-145), have all strongly been linked to poor outcomes.(21) In a recent meta-analysis (61) of more than 1000 STEMI patients reperfused by PPCI, there was a graded reduction in event-free survival in patients with MI size < 25% of the LV, with and without MVO, and those with MI size > 25% of the LV, with and without MVO, assessed by CMR. Both MVO and IMH are associated with larger MI size, adverse LV remodelling and poor clinical outcomes as recently summarised in 2 meta-analyses.(60, 61) Carrick et al (139) (228 patients) recently showed that both these processes are dynamic and distinct from each other, and IMH assessed by T2* mapping was more closely associated with adverse events than MVO.

2.5.2.2 Mechanisms underlying MVO and IMH

Several factors may (21) to be responsible for the development of MVO: pre-existing coronary microvascular dysfunction; individual susceptibility; the ischaemic injury; myocardial reperfusion injury; and distal embolisation of plaque and thrombus microemboli. The first 2 factors are non-modifiable. The ischaemic injury is dependent on the total ischaemic time, the AAR, TIMI flow pre-PPCI, and collateral blood flow. Tremendous efforts have already minimised the chest pain onset to balloon time. Therefore, the main focus of research to minimise the burden of MVO has been to target myocardial reperfusion injury and distal coronary embolisation. From these 2 perspectives, a number of mechanisms have been described to contribute to the occurrence of MVO as described above and illustrated in Error! Reference source not found..(20) Two

theories regarding the association of MVO with IMH have been proposed. Firstly, MVO leads to destruction of the endothelium and results in the extravasation of blood. Secondly, there is destruction of the capillaries as a direct result of myocardial reperfusion injury, which leads to IMH, the presence of which induces further external compression of the remaining microcirculation and exacerbates MVO.(60)

2.5.2.3 Detection of MVO by CMR

MVO by CMR can be divided into early MVO and late MVO. Early MVO can be assessed using first pass perfusion (FPP) or EGE performed with a fixed, high inversion time (TI) (e.g. 440 to 500ms at 1.5T), acquired at 1-4 minutes post contrast.(22, 146) Although FFP has superior temporal resolution to EGE, it suffers from relatively lower spatial resolution and full LV coverage is not currently possible.(146) On the other hand, EGE using single shot SSFP imaging, full LV short axis coverage can be achieved within one acquisition and enables more accurate quantification of early MVO.(22) Late MVO can be identified as a dark core within the areas of hyperenhancement on conventional LGE sequences acquired at 10 to 20 minutes post contrast injection.(22)

In 1995, Judd et al (147), using a canine model of MI, first reported areas of “dark zones” within areas of hyperenhancement on LGE and this correlated with areas of no-reflow by pathology. Subsequently Lima et al (148) reported similar findings by CMR in patients with large MI. Since then, several studies (149) have looked at the prognostic significance of MVO. Both early MVO and late MVO have been associated with adverse LV remodelling and MACE as

recently summarised in 2 comprehensive meta-analyses.(60, 61) Van Kranenburg et al (61) in a large meta-analysis of more than 1000 patients showed that the presence of MVO was an independent predictor of major adverse clinical outcome (MACE) at 2 years in STEMI patients, whereas MI size was not independently associated with MACE. In the meta-analysis by Hamirani et al (60), they showed that there was a weaker correlation of IMH with early MVO (R=0.30) than with late MVO (R=0.89 to 0.93). In most studies included in that review, IMH was identified only in the presence of late MVO, except in Kandler et al (150) and Husser et al (151), where some patients (5% and 9% respectively) had IMH without late MVO. However, these studies did not report whether these patients without late MVO and IMH had early MVO. Intuitively, these patients are likely to have relatively less extent of microvascular injury, and would display early MVO and with contrast eventually washing-in from the LV cavity by the time the LGE images are acquired. Interestingly, Carrick et al (139) in 286 patients did not observe any patients without MVO that had IMH. The potential explanation could be that the definition of MVO was different in these three studies. Kandler et al (150) and Husser et al (151) defined MVO on LGE images acquired at 10 to 15 minutes post contrast whereas Carrick et al (139) defined MVO on the early gadolinium enhancement images acquired at 1, 3, 5 and 7 minutes post-contrast injection. Furthermore the CMR was performed at a mean of 2.8 days in Kandler et al (150) and a median of 6 days in Husser et al (151) whereas in Carrick et al (139) the CMR scan was performed sooner at a mean of 2.1 days.

Therefore, based on both these meta-analyses (60, 61) and the recent study by Carrick et al (139) on 286 patients, our current understanding is that early MVO occurs in around 60-65%; late MVO in around 50-55%; and IMH in around 35-40% of reperfused STEMI patients. However, the detection of MVO and IMH is dependent on the CMR techniques, timing of imaging and definitions used. We believe that those with IMH but no late MVO are likely to have early MVO as illustrated in Figure 2-5 below:

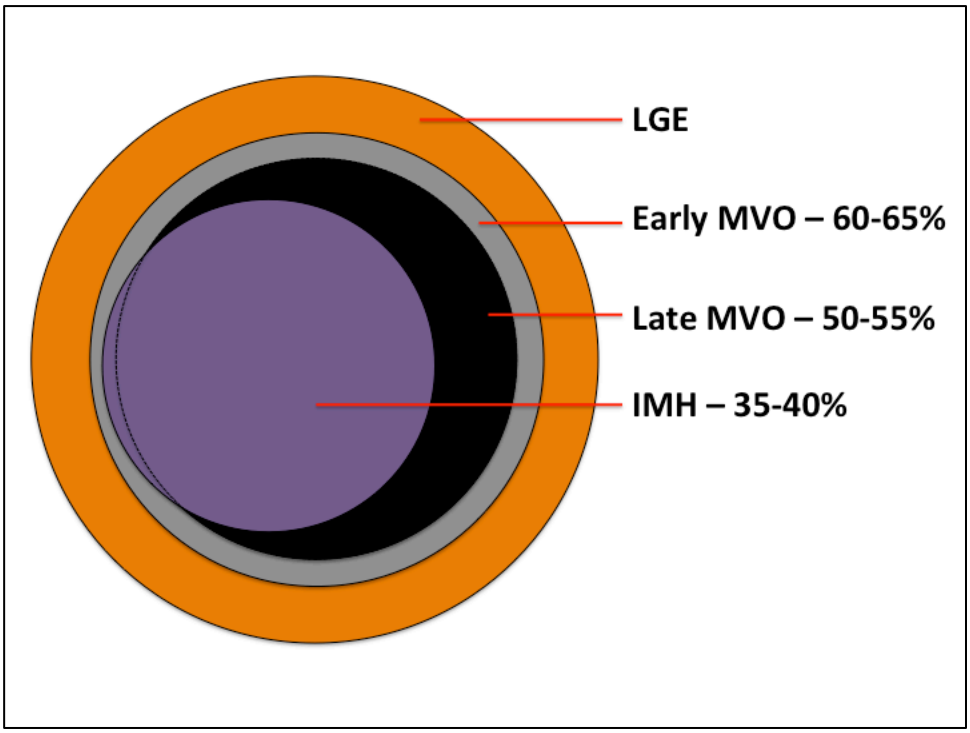

Figure 2-5: Prevalence of early MVO, late MVO and IMH

This Venn diagram depicts the prevalence of early MVO, late MVO and IMH by CMR in reperfused STEMI patients.

2.5.2.4 T2 for the detection of IMH*

T2* imaging has been shown to detect IMH in animal models of acute MI within the first week.(152, 153) Ghugre et al (152), using a porcine model of AMI, showed that T2 elevation in those pigs with IMH was blunted by the haemorrhagic by-products and manifested as a hypo-intense core on the T2* imaging. Furthermore, the reduction in T2* in the MI zone at 2 weeks was associated with IMH. Using a porcine model of AMI with IMH, Payne et al (154) showed that bright-blood T2-weighted imaging could detect IMH with high and similar diagnostic accuracy to T2* imaging when compared to histology. Using T2 mapping, dark blood T2-weight imaging and T2*-weighted imaging in a canine model of MI, Kali et al (153) showed that T2* imaging was superior than T2-weighted imaging to detect IMH due to its relative insensitivity to oedema. In the clinical setting, Kandler et al (150) (151 patients) showed that detection of IMH by T2*-weighted imaging, defined by a hypo-intense core with T* < 20ms, was superior to T2-weighted imaging.

A threshold value of T* < 20ms has subsequently been used in several clinical studies as the reference for IMH (139, 150, 155, 156) except by Zia et al (138), where they used a cut-off for T* of < 30ms. Although T2* CMR imaging is currently the reference standard for the detection of IMH, it is prone to motion, flow and off-resonance artefacts.(157) In a recent study by Carrick et al (139) involving 286 patients, only 86% of patients had analysable T2* data.

2.5.2.5 T2-weighted imaging for the detection of IMH

We know from brain imaging data that the degradation of the extravasated erythrocytes to oxyhaemoglobin, deoxyhaemoglobin, and methaemoglobin (strongly paramagnetic) is dynamic and would exhibit different T1 and T2 properties at various stages as previously described by Bradley et al(158) T2 is better at identifying deoxyhaemoglobin, whereas T1 is better at detecting methaemoglobin.(158) Breakdown of the erythrocyte membrane eventually leads to ferritin and haemosiderin deposits within macrophages.(146) Although T2-STIR imaging has been shown to have a lower diagnostic performance for detecting IMH when compared to T2* CMR imaging (150, 153), in the absence of T2* imaging or to keep scanning time to a minimum, several studies have also used T2-weighted STIR imaging rather than T2* imaging to detect IMH as the presence of a hypo-intense core within the AAR.(159-161) However, T2-weighted imaging has several limitations as already described and leads to a large number of non-diagnostic images.

2.5.2.6 Other methods to detect IMH

Susceptibility-weighted CMR imaging has been shown to improve the detection of IMH at 1.5T (162) and 3T (163), but this method still requires the acquisition of the T2*-weighted imaging. The hypo-intense core on the T1 (156, 164) and T2 maps (138, 153, 165) acquired for the detection of the oedema-based AAR has been associated with IMH and MVO. However, the diagnostic

performance of T1 and T2 maps to detect the presence of IMH and MVO following STEMI in the clinical setting has not been directly compared. If the T1 and T2 maps could identify IMH with good diagnostic accuracy, this may help to keep scanning time to a minimum in unwell STEMI patients who are not able to tolerate a comprehensive CMR scan, when T1 or T2 mapping is already being acquired as part of the study to depict the AAR. Furthermore, in cases when T2* imaging were acquired but not interpretable, the T1 or T2 maps could be used as a surrogate to detect IMH and would minimise dropout of patients from future studies.

2.5.3 MI size by CMR

CMR is considered the gold standard imaging modality for quantifying MI size (55, 56) and can detect small subendocardial MI (as little as 1 gram) with good accuracy.(55, 166, 167) Conventionally, MI can be identified by LGE with inversion recovery (IR) T1-weighted sequences and manual adjustment of the TIs to null the remote normal myocardium.(133) Gadolinium chelate is an extracellular agent and therefore it cannot cross cell membranes that are intact. In normal myocardium, the cells are densely packed. Following acute myocardial necrosis, the cell membranes are ruptured and together with interstitial oedema there is an expansion in the extracellular space. In the chronic setting, there is also expansion of the extracellular space due to the collagen deposits. Therefore, following gadolinium chelate administration, there is wash-in and wash-out of contrast and at equilibrium, a higher concentration of contrast is distributed in acute or chronic infarct tissue (leading to significant

shortening of T1) than in normal myocardium. Therefore, with appropriate nulling of the remote myocardium, the infarct territory appears bright.(64)

Both acute and chronic MI by CMR has been shown to be a stronger predictor of outcome than ejection fraction or LV volumes. (58, 168-171) Therefore, due to the robustness of CMR to assess MI size (55, 166, 167), its ability to predict outcomes (58, 168-171) and its high reproducibility (56, 172, 173) which helps to reduce sample size, both acute and chronic MI size by CMR is increasing being used as a surrogate endpoint for randomised control trials assessing the effectiveness of new cardioprotective therapies.

2.5.3.1 Optimal timing of the acute CMR post-STEMI

The optimal timing of the CMR scan following STEMI in clinical cardioprotection studies, is a topic of ongoing research. Acute MI size has been shown to be dynamic and to decrease significantly in size between Day 1 and Day 7 post-STEMI.(174, 175) In a recent study by Carrick et al (112), MI size was similar between day 1 and 3 and reduced in size by day 10. Furthermore, late MVO have also been shown to reduce in size within the first week (139, 149, 175) and those with MVO persisting at one week following STEMI was demonstrated to be more prognostic.(149) Recently, the detection of IMH has been shown to peak at day 3 and reduced in incidence by day 10 post-STEMI, and the latter was demonstrated to be more prognostic than MVO.(139)

2.5.3.2 Optimal method for MI size quantification

Several different techniques have been proposed for quantifying acute and chronic MI size including manual contouring (176) and semi-automated threshold techniques such as a signal intensity threshold of 5 standard deviations (SD)(177) or 6-SD (to identify signal intensities of 5-SD and 6-SD above the mean normal remote myocardium respectively)(178) above the normal remote myocardium, the Otsu technique (to identify the intensity threshold from the signal intensity histogram using the value with minimal intra-class variance between low and high intensities)(179, 180), and the full width half maximum (FWHM - to identify signal intensities that are above 50% of maximal signal intensity of the reference region of interest)(181-183) technique but have shown inconsistent results.

The consensus document from the Society for Cardiovascular Magnetic Resonance Board of Trustees Task Force on Standardized Post Processing recommends the semi-automated threshold technique of 5-SD for MI size quantification as it may improve reproducibility. Manual contouring is considered the gold standard (57, 176) but may be time consuming (183, 184) and subjective. FWHM has emerged as the technique having the lowest variability(182, 183), but others have shown FWHM to underestimate acute and chronic MI size.(180) (185) Recently FWHM45% and 6SD were found to perform well in paired acute and follow-up scans at 3T but they did not include Otsu in their comparison.(185) However, no studies have compared the 4

promising semi-automated techniques (5-SD, 6-SD, Otsu, FWHM) in paired acute and follow-up scans at 1.5T.

2.5.3.3 Quantification of MI size from post-contrast T1 mapping

The quantification of MI size is dependent on the accurate nulling of the remote myocardium. Using conventional magnitude reconstructed inversion recovery images, the choice of the optimal TI is done manually. Furthermore, a comprehensive CMR including information on oedema, IMH, MI size, MVO and extracellular volume fraction for research purposes in an acute STEMI patient can be challenging to perform as it may last more than an hour and requires multiple breath-holds. Therefore, keeping scanning time to a minimum with minimal user input would optimise the CMR protocol for these patients to make it more tolerable. Post-contrast T1 mapping has shown promise to detect acute MI in a small cohort of predominantly non-reperfused acute MI (186) and chronic MI patients.(186, 187) Refinements of the T1 Modified Look Locker Inversion recovery (MOLLI) prototype using inversion recovery (IR) images at different TIs initially designed to improve motion correction (188, 189), can also retrospectively create “synthetic” IR LGE images, namely magnitude-reconstructed IR (MagIR) and phase sensitive IR (PSIR) outputs. These synthetic read-outs have recently been shown to accurately detect chronic MI size in a small cohort of 17 patients.(190) To date, no studies have assessed the performance of post-contrast T1 mapping and synthetic LGE in quantifying acute MI size with full LV coverage in a cohort of reperfused STEMI patients.

2.5.4 LV remodelling post STEMI

CMR is considered the gold-standard imaging modality not only for quantifying MI size (57), but also for measuring LV volumes and LVEF (57, 191), given its high reproducibility.(57, 192) Adverse LV remodelling following STEMI has been conventionally defined as ≥ 20% increase in LV end-diastolic volume (LVEDV) from baseline. This cut-off value was determined using echocardiography, and was based on the upper limit of the 95% confidence interval of intra-observer variability for the percentage change (%Δ) in LVEDV following STEMI.(193, 194) Reverse LV remodelling has been defined as ≥10% decrease in LV end-systolic volume (LVESV) by echocardiography following cardiac resynchronization therapy, and was derived using receiver operator characteristic (ROC) curves for the optimal cut-off for the %ΔLVESV to predict mortality.(195) So far, no cut-off values for adverse and reverse LV remodelling following STEMI have been defined by CMR, and studies using CMR to assess post-STEMI LV remodelling have relied upon using these cut-off values defined by echocardiography.(196-198) Other groups have used an arbitrary cut-off of ≥15% increase in LVESV to define adverse LV remodelling by CMR.(63, 199)

Post-MI LV remodelling refers to the intricate changes occurring in both the infarcted and remote myocardium on a molecular, structural, geometric and functional level (200) and its occurrence predisposes to heart failure. The three partially overlapping phases during post-MI LV remodelling are the inflammatory phase, the proliferative phase and the maturation phase.(201)

Numerous anti-inflammatory agents such as glucocorticoids, monoclonal antibodies, C1 esterase inhibitors, metalloproteinase inhibitors, phosphoinositide-3-kinase inhibitors and immunoglobulin have had promising results in the experimental setting, but have failed to be translated into the clinical setting.(202)

2.5.4.1 Imperfect link between MI size and adverse LV remodelling

Infarct size has been linked with adverse LV remodelling.(58, 203, 204) The conventional belief has been that a larger MI leads to higher LV wall stress. The LV dilates to maintain the stroke volume as a compensatory mechanism (via the Frank-Starling principle). However, LV dilation, as described by the Laplace relationship, leads to further wall stress and begets more LV dilation. Westman et al (205) recently proposed that there was an imperfect link between MI size and adverse LV remodelling (defined as >10ml/m^2 increase in indexed LVEDV). By re-analysing previously published data (58), they showed that in 122 STEMI patients, 15% of those with MI size < 18.5% developed adverse LV remodelling and 40% of those with MI size ≥ 18.5% developed adverse LV remodelling. They postulated that an excessive inflammatory response together with MI size played an important role in the development of adverse LV remodelling.

2.5.4.2 Residual iron and inflammation

There are some emerging data that IMH leads to residual iron during the convalescent phase on an MI and may be a source of prolonged inflammation and may be pro-arrhythmic.(206) Kali et al (207) showed in a small cohort of 15 STEMI patients and in 20 canines that IMH resulted in residual myocardial iron within the MI zone, which can be a source of prolonged inflammatory burden in the chronic phase of MI. Roghi et al (208) found higher levels of non-transferrin bound iron in 7 out of 15 STEMI patients with MVO and postulated that IMH could be a source of cardiotoxicity in these patients. In a small number of STEMI patients, T2 in the infarct related territory have been shown to remain elevated on CMR performed 6 months post-PPCI.(91, 209) So far, no studies have assessed the relationship between persistently elevated T2 in some patients and residual myocardial iron and the subsequent development of adverse LV remodelling.

2.5.4.3 The role of the remote myocardium in post-MI LV remodelling

Whether changes in the extracellular matrix (ECM) in the non-infarcted remote myocardium in STEMI patients reperfused by PPCI is linked to adverse LV remodelling remains incompletely understood.(197, 210-213) It has been suggested that primary changes in the ECM that occur acutely in the non-infarct zone also contribute to LV remodelling.(214) In an experimental rat model of MI, Anversa et al (215) showed that infarcts with 50% loss of mass resulted in 83%

expansion of the spared myocardium. In a mouse model of MI, Tsuda et al (211) demonstrated that small infarcts without mechanical overload stimulated myocardial fibrosis development in the non-ischaemic myocardium distant from the infarct site as early as 72 hours. In the clinical setting, Volders et al (210) provided post-mortem histological evidence of an increase in interstitial collagen in the remote myocardium of infarcted patients when compared to control. However, the time course of acute changes and remodelling in the non-infarct zone in humans is not well understood, in part due to a prior lack of an *in vivo* imaging modality that could detect ECM expansion and quantify diffuse fibrosis. Furthermore, Marijianowski et al (212) challenged the existence of these compensatory changes in the remote myocardium. They showed that post-MI LV remodelling in patients with end-stage heart failure undergoing transplant was not associated with interstitial fibrosis in the remote myocardium.

From the tissue characterization point of view, Chan et al (213) used post-contrast T1 in 25 acute STEMI patients and found evidence of early remote expansion of the ECM, which persisted in the chronic stage. Carrick et al (197) demonstrated that native T1 of the remote myocardium of reperfused STEMI patients on the acute CMR was associated with change in LV end-diastolic volume from baseline to 6 months and was independently associated with adverse cardiac events in 267 STEMI patients after a median follow-up of 845 days. The assessment of the extracellular space in vivo by CMR can be be done by performing native and post-contrast T1 mapping and calculating ECV, after correcting for haematocrit. The availability of automated ECV map has provided a more accurate method to quantify not only focal fibrosis but also

diffuse interstitial expansion.(216, 217) The native and post-contrast T1 maps are co-registered and motion-corrected, which significantly improves the quality of the generated automated maps.(218) Whether automated ECV maps may provide valuable insights into the changes occurring in the remote myocardium during post-MI LV remodelling is not known and warrants further investigation.

2.6 T1 and T2 mapping CMR

Over the last few years, parametric mapping techniques by CMR have emerged as being superior to non-quantitative techniques to interrogate a range of pathologies as they are more objective, less prone to the sequence parameters and surface coil profiles and can detect both global and focal changes in the myocardium. These parametric maps have proven to be valuable in the field of STEMI and play a major part in this thesis. In this section, we provide a brief overview of T1 and T2 mapping techniques.

2.6.1 T1 mapping

2.6.1.1 The need for T1 Mapping

Cardiovascular magnetic resonance (CMR) is the gold standard for the non-invasive detection of focal fibrosis using gadolinium-based contrast agents.(219-222) This technique cannot be used to quantify diffuse fibrosis and endomyocardial biopsy (EMB) remains the gold standard despite being prone to

sampling error. Biopsy also carries with it inherent procedural risk and provides no information on the extent of ventricular involvement.(223, 224) With the introduction of T1 mapping, diffuse processes can now be detected and quantified – particularly for infiltrative and storage processes where the signal is high and for quantification of diffuse fibrosis which is difficult to perform, but potentially has greater impact. It offers numerous promises such as early detection of specific conditions; a surrogate marker in drug development trials; and as a prognostic marker in certain diseases. However, this is still a rapidly evolving field and numerous factors are currently precluding its standardization.(225)

2.6.1.2 T1 mapping: past and present

Late gadolinium enhancement (LGE) imaging was an advance on T1-weighted imaging in that the operator selects a tissue that was “normal” and nulls it – exaggerating the signal from any tissue with a different T1, identifying focally abnormal regions such as scar (e.g. infarction), edema or amyloid. T1 mapping requires the quantification of the exact T1 of a particular tissue and can be performed without contrast. Different tissues have specific ranges of T1 (milliseconds) at a particular magnetic field strength (226) and can be used to detect pathology.

2.6.1.3 Native T1 or non-contrast myocardial T1

The native T1 or non-contrast myocardial T1 is the longitudinal relaxation time (T1) of a given tissue without a GBCA. This provides intrinsic signal from both the myocytes and the interstitium.(227) Our current understanding is that T1 is prolonged with fibrosis (228), edema (229) and amyloid (230) and reduced in lipid accumulation (Anderson-Fabry disease) (231), cardiac siderosis (232), and hemorrhage in acute infarction.(233) However, as techniques advance, potentially other trends may be found. It does appear that pseudo-normalization of native T1 also occurs when two processes cancel out co-existing fibrosis and iron (sickle cell disease) or lipid (Anderson-Fabry disease).(234)

2.6.1.4 Post contrast T1 for extracellular volume quantification

The extracellular matrix (ECM) is a complex architectural network made up of structural and non-structural proteins contributing to strength and plasticity.(235) The matrix is hydrated with extracellular fluid – measurement of this, the extracellular volume (ECV) approximates the ECM. The ECM and ECV may expand with fibrosis, edema or amyloid.

The gadolinium contrast agent does not cross cell membranes. Post contrast T1 mapping therefore partly measures the extracellular space. However, factors such as renal excretion rate, altered wash-in and wash-out kinetics of the contrast agent in diseased myocardium(236), volume of distribution and acquisition time (237) are influencing factors. The ECV

technique intrinsically corrects for this. ECV measurement is done when the concentration of contrast is equal in the water between cells in the myocardium and in blood – a sufficient equilibrium exists, either by a primed infusion or after a bolus and sufficient time (15 minutes is adequate for all but massive interstitial expansion).(238) The ratio of a pre to post contrast signal change in myocardium and blood reflects the relative ECV of blood and myocardium – the partition coefficient. As the blood ECV is one minus the haematocrit (from a simple blood test, this can be substituted in to obtain the myocardial ECV.(238) The ECV is (1-hematocrit) x $\Delta R1_{myocardium}/\Delta R1_{blood)}$, where R1 = 1/T1.

There is no real need to use an infusion – the bolus only method(239) works for conditions with ECV < 0.4, but progressively reads a higher ECV in high interstitial expansion diseases. An alternative approach is to perform multiple T1 measurements during contrast washout rather than awaiting equilibrium.(240) The accuracy and relative precision of these approaches are not known – and currently most centers do a single pre- and post-contrast measurement. Newer approaches are to automatically register the pre- and post-contrast T1 maps to create ECV maps.(218)

2.6.1.5 Measuring the T1: techniques and sequences

2.6.1.5.1 The Look-Locker based maps

Initial methods of T1 measurement involved multiple breath-holds to obtain the recovery curve from different time points. The Look–Locker

sequence was introduced (241) to measure the T1 relaxation time at multiple time points after an initial excitation pulse and then subsequently adapted as the MOLLI (242) sequence. Colour pixel-wise “T1 maps” whereby each pixel carries the measured value of T1 can now be generated. Since this MOLLI approach, multiple incremental improvements have been made including better inversion pulses, sampling schemes, image reconstruction (236, 242), curve fitting (making shorter breath-holds) and the introduction of error maps to provide confidence in measured results.(243)

2.6.1.5.2 Non-linear curve fitting

An SSFP readout is used for the MOLLI approach. The SSFP readout allows the IR to recover quicker and reaches steady state at a lower level (the apparent T1, referred to as T1*) than the equilibrium magnetization (the actual T1). Due to the influence of the readout, the IR curve follows a 3-parameter fit exponential model, $S(t) = A - B \exp(-t/T1^*)$, where t represents the inversion time, and T1* is the apparent T1. The measured values may be fitted to this model to estimate A, B, and T1* and they can be used to approximate T1 as T1* (B/A – 1). (B/A – 1) is referred to as the “ Look- Locker” correction factor.(189)

2.6.1.5.3 Motion correction and PSIR synthetic imaging

One of the approaches to improve image reconstruction was the development of motion correction, to reduce artifacts from respiratory motion despite breath holds. A typical MOLLI sequence acquires 2 or 3 consecutive Look-Locker experiments in the same cardiac phase. Although this approach would suppress most of the influence of cardiac motion, the myocardium may not always remain still across all acquired images predominantly due to patient breathing inadvertently.(188) This would be more of a problem for subjects who are poor breath-holders. Respiratory motion due to a diaphragmatic movement, if not accounted for, could lead to errors in the pixel-wise estimation of T1 and produce poor final maps. Therefore, respiratory motion correction is necessary for accurate T1-mapping to avoid partial volume cancellation at the boundaries of tissues of different T1 resulting from the images being out of phase. Using simple pairwise image registration models is an option but can be challenging when this is applied to inversion recovery images acquired at different inversion times due to large variations in image contrast, in particular, close to the signal nulling point. A better motion-correction algorithm is now possible by firstly estimating motion-free PSIR synthetic images followed by motion correction. The PSIR synthetic images have similar contrast to original MOLLI data and are derived by using the actual polarity of the data for the initial estimate of T1 by using a partial differential equation to solve a variational energy minimisation problem (unlike magnitude reconstruction, when the negative values occurring at short TIs are reconstructed as positive to generate the single shot images).(244) The MOLLI image with the longest TI is used as a reference to

remove background phase on a pixel-by-pixel basis and the resulting images have the correct polarity of the MOLLI images. To minimise the impact of the initial misalignment on the registration process, an initial motion correction is applied to the last images of each IR experiments. A deformation field is then applied to all other images of the first IR experiment and this leads to a reduction in phase error. These images can then be registered in a frame-by-frame manner using a fast variational non-rigid image registration framework.(245) This process is now fully automated and can be done inline by the scanner to generate more accurate and robust T1 maps.(244)

2.6.1.6 Other types of T1 maps

New approaches have also been developed including saturation recovery single-shot acquisition (SASHA) sequence (246) and hybrid schemes (e.g. SAPPHIRE), which is heart rate independent and uses a combination of saturation and inversion pulses.(247, 248) Table 2-1 summarises the main differences in the T1 mapping techniques. Each technique is implemented differently by different scanner manufacturers (189, 249, 250) and there is a lack of clarity currently on which improvements are valuable or even how to measure this value. Intuitively, the best sequence would be the one that most accurately measures T1 – but even this is difficult and it is likely that precision (compared to the disease signal) and robustness across a health-care system (which is not yet done) may be more important than accuracy. Reflecting this, current advice is to have locally produced reference range from healthy

volunteers, although quality control and standardization systems are being constructed.

Table 2-1: Comparison of the various T1 mapping techniques.

Adapted from Kellman et al (189), Taylor et al (251), Roujol et al (249). ++ denotes good; + denotes fair; - denotes poor

	Multi-BH IR-FLASH	**Segmented Look-Locker**	**MOLLI**	**ShMOLLI**	**MOLLI variants**	**SASHA (3p-fit)**	**SAPPHIRE**
T1 prep type	IR	IR	IR	IR	IR	SR	SR/IR
Readout	GRE	GRE	SSFP	SSFP	SSFP	SSFP	SSFP
Influenced by T2 effects	Negligible	Negligible	Yes	Yes	Yes	No	No
Acquisition time	10 BH	≈ 20 HB	17 HB	9 HB	9-12 HB	11 HB	17 HB
HR insensitivity	-	-	-	+	+	++	++
Few image artifacts	-	-	-	++	++	-	-
Absolute accuracy	-	-	-	-	-	++	++
Precision	++	++	++	++	++	-	-
Reproducibility	-	-	-	++	++	-	-

IR: inversion recovery; SR: saturation recovery; 3p-fit: 3 parameter fit; GRE: gradient echo; BH: breath-hold; HB: heart beats; FLASH: fast low angle shot; MOLLI: modified Look-Locker sequence; SASHA: saturation recovery single shot acquisition; ShMOLLI: shortened modified Look-Locker technique; SSFP: steady-state with free precession imaging.

2.6.2 T2 mapping

The T2 or spin-spin relaxation property of a tissue refers to the exponential decay of transverse magnetisation time constant. The T2 relaxation time is dependent on the water content and can be measured by T2-weighted imaging or T2 mapping techniques. Myocardial edema can be detected in patients with acute myocardial infarction, myocarditis (98), stress cardiomyopathy (252), cardiac sarcoidosis (253), and cardiac transplant rejection.(254) T2-weighted imaging has several limitations including the subjective interpretation of the images, variations in regional myocardial intensity due to changes in sensitivity of surface coils, blood-pooling artefacts at the subendocardial border, its relatively low contrast-to-noise ratio between normal and abnormal myocardium, and its susceptibility to breathing and motion artefacts.(66, 92) T2 mapping technique can provide direct T2 relaxation times quantification and is considered more robust. Multi echo spin echo (MESE) is widely accepted as the reference technique (255), but it involves long scanning times and is prone to motion and flow artefact. An alternative method to quantify the T2 relaxation time is by using a gradient and spin echo (GRASE) sequence (256) but the as it uses an echo-planar-imaging (EPI) readout, it is susceptible to T2* weighting and can underestimate the T2 relaxation times. Furthermore, each echo is sampled at slightly different cardiac phase and could be a source of error.(257) T2 preparation technique using a balanced SSFP readout is more suitable for clinical application as it is relatively insensitive to flow and can be acquired within one breath-hold. The T2 maps are generated using a similar principle to that used for T1 maps. A T2

preparation pulse is applied to impart T2 signal contrast, and a subsequent readout is performed by using an SSFP sequence that has less sensitivity to turbo spin-echo artefacts.(258) A series of images is acquired at different T2 preparation times (typically echo times of 0, 24ms and 55ms) to calculate the T2 decay curve. A coloured T2 map consisting of pixel-wise T2 values can be generated following motion correction and fitting of the T2 decay times either in-line, by the scanner or off-line.

3 Hypotheses and Aims

3.1 T1 mapping to quantify the AAR, IMH and MI size in acute STEMI patients

Although tissue characterisation by CMR provides valuable information in acute STEMI patients, performing all the parametric maps can be time-consuming and distressing for them. Native and post-contrast T1 mapping may provide the possibility to acquire information on the AAR, IMH and MI size and will be investigated by the research questions below.

3.1.1 T1 mapping and T2 mapping CMR to quantify the AAR in reperfused STEMI patients

Ugander et al (131) showed that T1 mapping performed as well as T2 mapping to detect the AAR in a canine model of acute STEMI. Whether this is also the case in clinical patients has not yet been specifically looked at. The result from this sub-study has the potential to provide an alternative tool to measure the AAR instead of T2 mapping in acute STEMI patients.

Research question: Can T1 mapping quantify the AAR as well as T2 mapping in STEMI patients at both 1.5T and 3T?

Hypothesis: T1 mapping can quantify the AAR as well as T2 mapping in STEMI patients at both 1.5T and 3T.

3.1.2 T1 mapping versus T2 mapping for the detection of IMH

The current gold standard to detect IMH is by T2* imaging. However, T2* imaging is not routinely used in clinical studies due to its long breath hold to acquire the images, especially in patients who have recently suffered a STEMI and also due to the fact that the images are prone to breathing, motion and susceptibility artefact. In order to keep the scanning time short, IMH were being identified as a hypo-intense core on the T2-weighted images. However, T2-weighted imaging has its own inherent limitations. So far, the direct comparison of the diagnostic performance of T1 and T2 mapping to detect IMH, using T2* mapping as the reference standard, has not been performed. Therefore this study has the potential to provide an alternative modality for the detection of IMH.

Research question: Can the presence of a hypo-intense core within the area of oedema on the T1 and T2 maps be used to detect IMH in the setting of acute reperfused STEMI?

Hypothesis: In the absence of T2-weighted imaging, a hypo-intense core on the acute T1 and T2 maps can be used to detect IMH.*

3.1.3 Infarct size quantification by T1 mapping

Conventionally, MI can be identified by LGE with inversion recovery T1-weighted sequences and manual adjustment of the TIs to null the remote

normal myocardium.(133) Post-contrast T1 mapping has also shown promise to detect acute MI in a small cohort of predominantly non-reperfused acute (186) and chronic MI patients.(186, 187) The T1 MOLLI prototype (188, 189), can also retrospective create “synthetic” IR LGE images, and have recently been shown to accurately detect chronic MI size in a small cohort of 17 patients.(190) To date, no studies have assessed the performance of post-contrast T1 mapping and synthetic LGE in quantifying acute MI size with full LV coverage in a cohort of reperfused STEMI patients.

Research question: can we quantify acute MI size using post-contrast T1 maps and post-contrast T1 mapping-derived synthetic inversion recovery imaging?

Hypothesis: Acute MI size can be accurately quantified from the post-contrast T1 maps and the post-contrast T1 mapping-derived synthetic LGE images

3.2 Semi-Automated Quantification Techniques for Assessing Acute and Chronic Myocardial Infarction by CMR

Several different techniques have been proposed for quantifying acute and chronic MI size including manual contouring (176) and semi-automated threshold techniques such as a signal intensity threshold of 5 standard deviations (SD) (177) or 6-SD (178) above the normal remote myocardium, the

Otsu technique (180), and the full width half maximum (FWHM)(182, 183) technique but studies published so far have shown inconsistent results. FWHM has emerged as the technique having the lowest variability (182, 183) but others have shown FWHM to underestimate acute and chronic MI size.(180, 185) However, no studies have compared these 4 promising semi-automated techniques in paired acute and follow-up scans at 1.5T.

Research question: Which of the 4 most promising semi-automated techniques would perform best against manual MI size quantification in paired acute and follow-up scans at 1.5T?

Hypothesis: the technique that performs best against manual quantification of MI size in paired acute and follow-up CMR scans should be the method of choice when a semi-automated method is required or preferred.

3.3 Multi-parametric mapping CMR to provide insights into the pathophysiology of adverse LV remodelling post-reperfused STEMI

As discussed in the introduction, LV remodelling post-MI refers to the intricate changes occurring in both the infarcted and remote myocardium on a molecular, structural, geometric and functional level (200) and its occurrence predisposes to heart failure. IMH and its iron degradation products have been shown to result in residual myocardial iron within the MI zone and have been

proposed to have cytotoxic and pro-inflammatory effects on the myocardium.(207, 208)

Furthermore, whether expansion of the extracellular matrix (ECM) in the non-infarcted remote myocardium in STEMI patients reperfused by PPCI is linked to adverse LV remodelling remains incompletely understood.(197, 210-213)

We aimed to use multi-parametric mapping CMR to provide further insights into the pathophysiology of adverse LV remodelling post reperfused STEMI.

Research question: Do STEMI patients with post-MI LV remodelling more likely to have IMH, develop residual iron and develop remote myocardial interstitial changes as assessed by automated ECV maps?

Hypothesis: STEMI patients with IMH are more likely to have residual iron and develop subsequent adverse LV remodelling. Furthermore, those with adverse LV remodelling are also more likely to have higher ECV in the remote myocardium compared to those without.

3.4 Redefining left ventricular remodelling by CMR

Adverse LV remodelling following STEMI has been conventionally defined as ≥ 20% increase in LVEDV from baseline (193, 194) and reverse LV remodelling has been defined as ≥ 10% decrease in LVESV by echocardiography.(195) So far, no cut-off values for adverse and reverse LV remodelling following STEMI have been defined by CMR, and studies using CMR to assess post-STEMI LV remodelling have relied upon using these cut-off values defined by echocardiography for adverse (196, 197) and reverse LV remodelling.(198)

Therefore, the first aim of this chapter was to perform intra-observer and inter-observer measurements of LV parameters in paired acute and follow-up CMR scans in reperfused STEMI patients, in order to determine the minimal detectable changes (MDCs) that could be used as cut-off values for defining post-MI remodelling.

Secondly, we aimed to identify the cut-off values for clinically important %ΔLVEDV and %ΔLVESV. This would be defined as the cut-off value for %ΔLVEDV and %ΔLVESV to predict an LVEF <50% (cut-off value at follow-up by CMR previously used to define an abnormal LV function (169)).

Finally, cut-off values for %ΔLVEDV and %ΔLVESV would then be applied to a large cohort of STEMI patients with paired acute and follow-up scans to assess different patterns of post-STEMI LV remodelling.

Research question: what is the cut-off for %ΔLVEDV and %ΔLVESV by CMR to define LV remodelling post-MI, taking into account inter-observer and intra-observer measurement errors? Could the CMR definition be used to provide further insights into the different patterns of LV remodelling post STEMI?

Hypothesis: the cut-off values %ΔLVEDV and %ΔLVESV used to define adverse and reverse LV remodelling by CMR is likely to be lower that that used by echocardiography due to the superior reproducibility of the former technique.

4 General methodology

4.1 Study Population

There are 2 main cohorts of patients included in this thesis. Approval was obtained from the UK National Research Ethics Service (reference 05/Q0502/102) and all patients were prospectively recruited and provided informed written consent.

4.1.1 First cohort of patients – 1.5T cohort

50 STEMI patients reperfused by PPCI (diagnosis and treatment as per current guidelines)(259, 260) were prospectively recruited between August 2013 and July 2014 from The Heart Hospital, London.

Study exclusion criteria were previous MI and standard recognised contraindications to CMR (e.g. ferromagnetic implants, claustrophobia, estimated glomerular filtration rate <30mL/min).

All participants were scanned on a 1.5 Tesla scanner at the Heart Hospital (Magnetom Avanto, Siemens Medical Solutions) using a 32-channel phased-array cardiac coil. 48 patients completed the acute scan at 4±2 days post-PPCI and 40 of these patients had a follow-up scan at 5±2 months. 2 patients developed unexpected claustrophobia during the acute scan and were excluded. Figure 4-1 shows the screening and recruitment process.

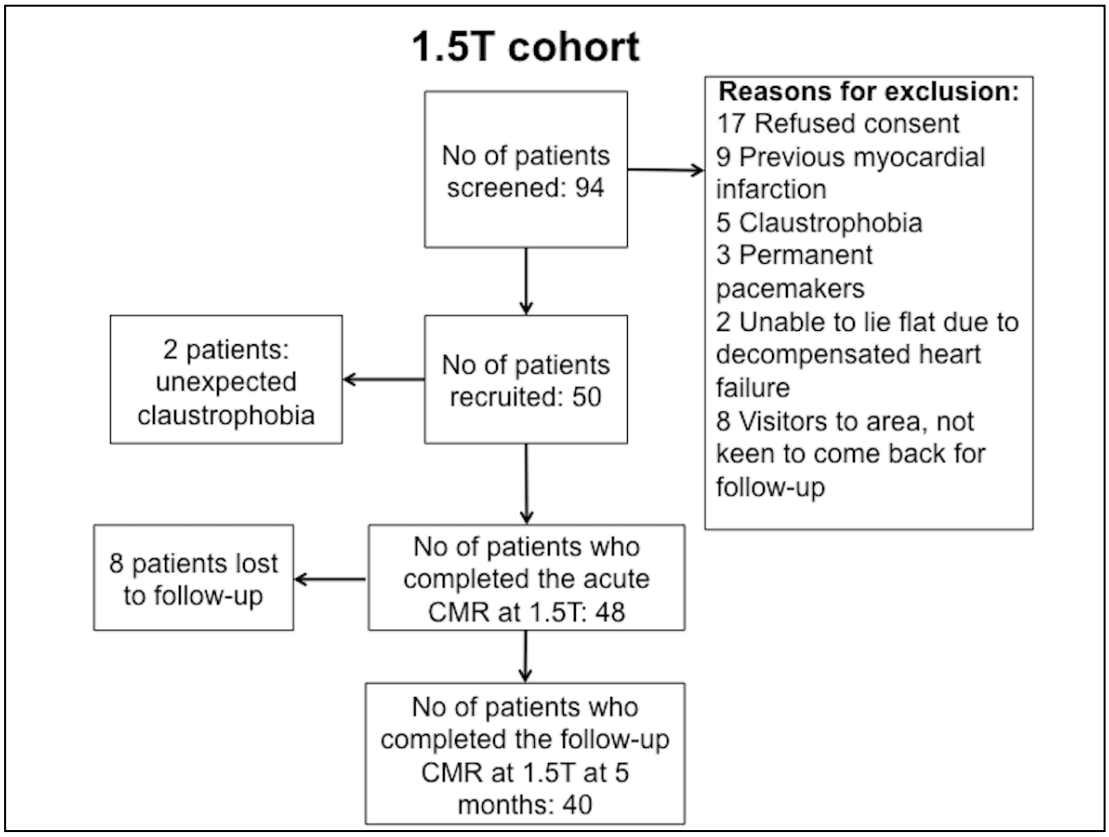

Figure 4-1: Flow diagram showing the screening and recruitment of the 1.5T cohort

4.1.2 Second cohort of patients – 3T cohort

18 STEMI patients treated by PPCI were prospectively recruited between August 2013 and March 2014 from The Heart Hospital, London and were part of a PET/MR study.(106)

As they were part of the PET/MR study, exclusion criteria were as follows: ≤45 years of age (to attenuate any theoretical higher risk from ionizing radiation in younger patients); diabetes mellitus (as pre-existing metabolic/ glycaemic derangement may affect clarity of initial results); previous MI; and standard recognised contraindications to CMR.

All patients completed the initial CMR at 5 (4– 6) days on a 3.0 Tesla scanner at the Nuclear Medicine Department, University College London Hospital (Biograph mMR; Siemens Healthcare, Erlangen, Germany). 12 patients returned for a follow-up scan at 1 year. Figure 4-2 shows the patients' screening and recruitment process.

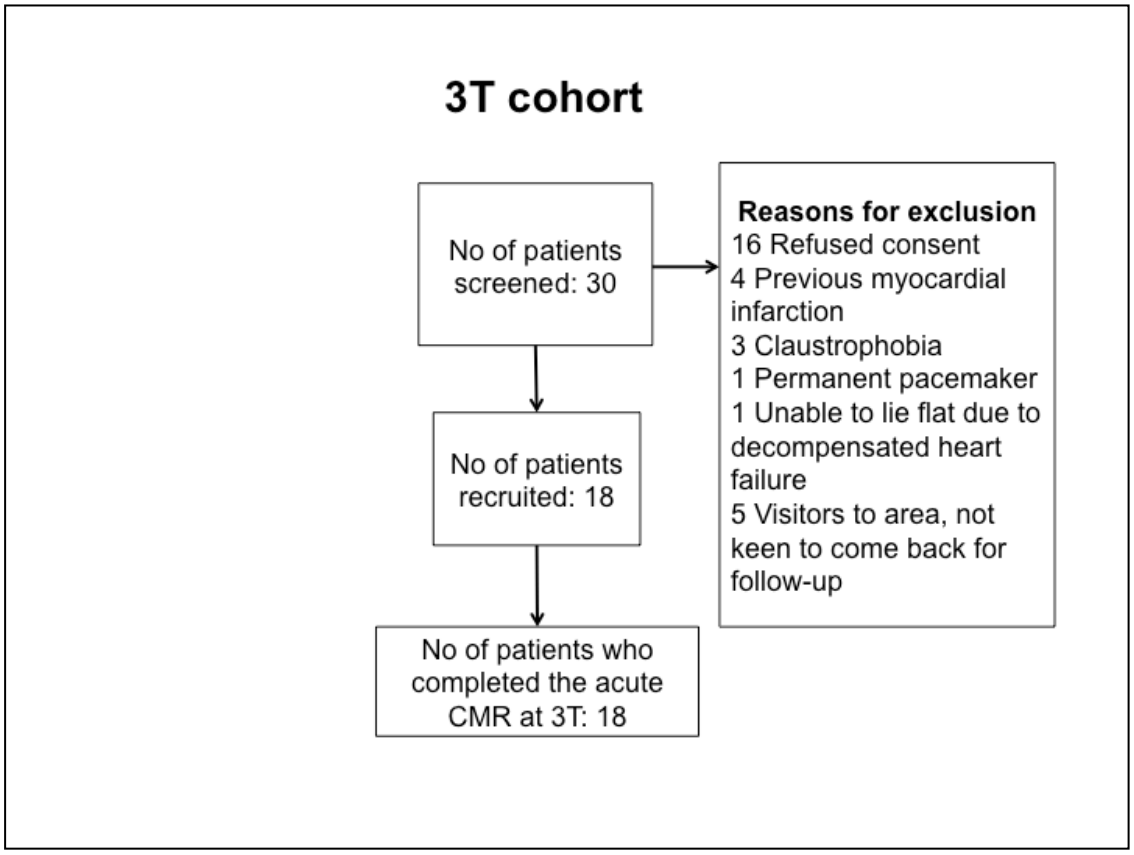

Figure 4-2: Flow diagram showing the screening and recruitment of the 3T cohort

4.2 Imaging acquisition

The CMR acquisition protocols for both cohorts are shown in Figure 4-3.

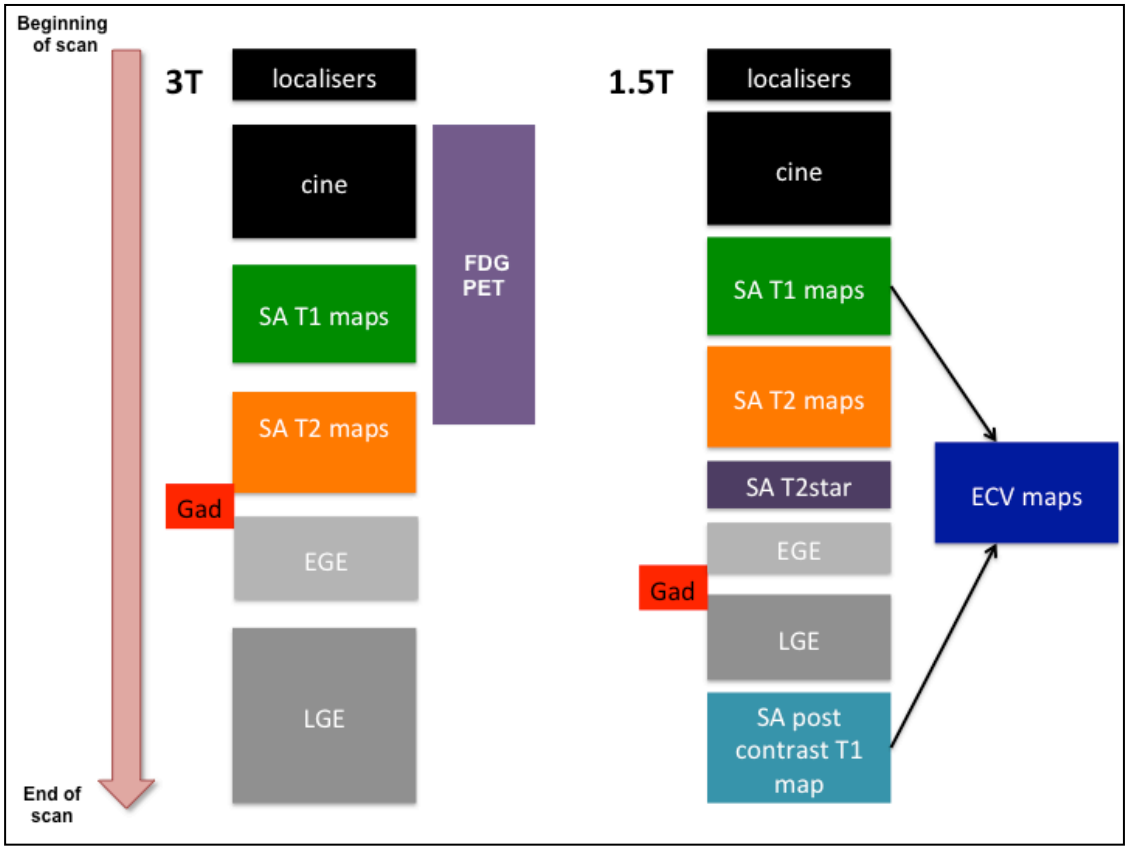

Figure 4-3: CMR protocols for the 2 cohorts

4.2.1 1.5T cohort CMR acquisition details

In the 1.5T cohort, the T1, T2 and T2* maps were part of a *Work in Progress #448B package* from Siemens via a research agreement. The CMR acquisition protocol (apart from cines, EGE and LGE) for the acute and follow-up CMR also included the following:

- All patients had full LV coverage T2 maps acquired from base to apex during the acute scan and 3 LV short-axis (base, mid and apex) T2 maps at follow-up.
- 30 patients had full LV coverage native and post-contrast MOLLI T1 maps from base to apex both during the acute scan and at follow-up. The remaining 18 patients had 3 LV short-axis (base, mid and apex) native and post-contrast T1 maps.
- All patients had 3 LV short-axis (base, mid and apex) T2* maps on both acute and follow-up scans.

Native T1 mapping

T1 maps were acquired using an SSFP-based MOLLI sequence. A 5s (3s) 3s modified MOLLI sampling protocol was used to ensure more complete recovery of the inversion pulse at higher heart rates by acquiring a set of images for at least 5 seconds after the first inversion pulse, followed by a 3-second pause and then acquiring a set of images after the second inversion pulse for at least 3 seconds(189). The acquisition parameters are provided in Table 4-1. Motion correction and a non-linear least-square curve fitting were performed with the set of images acquired at different TIs to generate a pixel-wise coloured T1 map in-line, by the scanner. Each slice was acquired during one breath hold.

T2 mapping

T2 maps were acquired as previously described.(97) In brief, 3 single-shot images at different T2 preparation times (0ms, 24ms, and 55ms, respectively) using the following parameters provided in Table 4-1. A coloured T2 map consisting of pixel-wise T2 values was generated following fitting to estimate T2 relaxation times and motion correction in-line, by the scanner. Each slice was acquired during one breath hold.

T2 mapping*

T2* maps were obtained using the parameters provided in Table 4-1. A colored pixel-wise T2* map was generated in-line, by the scanner. Each slice was acquired during one breath hold.

Early gadolinium enhancement (EGE)

EGE images were acquired 1-2 minutes after the injection of 0.1 mmol/kg of Gadoterate meglumine (Gd-DOTA marketed as Dotarem, Guerbet S.A., Paris, France) using inversion recovery single shot SSFP T1-weighted sequence at a fixed high TI of 440ms and a full LV short axis stack was acquired.(261)

Late gadolinium enhancement (LGE)

LGE imaging was acquired with a standard segmented 'fast low-angle shot' two-dimensional inversion-recovery gradient echo sequence or a respiratory motion-corrected, free-breathing single shot SSFP averaged phase sensitive inversion recovery sequence (262, 263) at 10-15 minutes after the injection of 0.1 mmol/kg of Gadoterate meglumine (Gd-DOTA marketed as Dotarem, Guerbet S.A., Paris, France).

Post-contrast T1 mapping

Post contrast T1 maps were obtained using the 4s (1s) 3s (1s) 2s sampling protocol (to improve the accuracy of T1s in the 200-600ms range as previously described)(189) 15 minutes after contrast injection (0.1 mmol/kg of Gd-DOTA) using similar acquisition parameters as for native T1 maps as provided in Table 4-1.

ECV maps

The previously described and validated automated method for producing a pixel-wise ECV map was used.(218) In brief, this method corrects for respiratory motion due to poor or inconsistent breath-holding as well as patient movement between breath-holds and relies on co-registration of the native and post-contrast T1 pixel maps. Each patient had haematocrit checked at the time of the scan and the ECV was estimated using the formula(264):

$$ECV = (1 - haematocrit) \times \frac{(1/T1_{myocardium\ post}) - (1/T1_{myocardium\ pre})}{}$$

$$(1/T1_{blood\ post}) - (1/T1_{blood\ pre})$$

An off-line software (ECV Mapping Tool Version 1.1) subsequently generated pixel-wise ECV maps using a variety of post processing steps as recently described.(218)

The coloured look up tables used for the T1, T2, T2* and ECV maps throughout this thesis are shown in Figure 4-4 below:

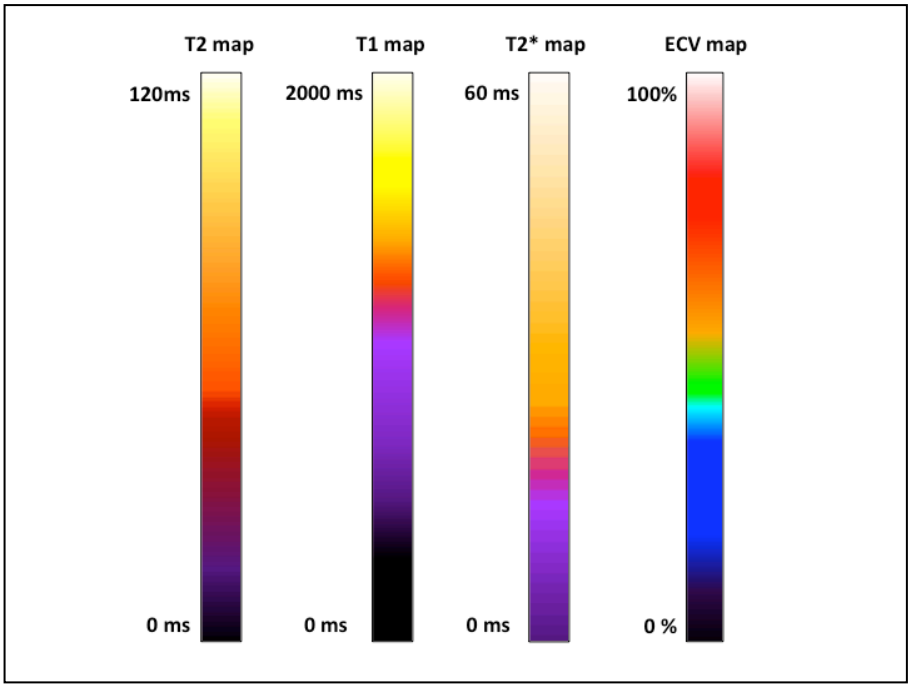

Figure 4-4: Colour scales for the various maps included in this thesis

4.2.2 3T cohort CMR acquisition details

This cohort of patients underwent a CMR protocol at 3T and was a sub-study of the PET/MR study(106) recently reported. The CMR maps were part of

a *Work in Progress #699 package* from Siemens as part of a research agreement. The acquisition protocols included cines, full LV coverage for T1 and T2 maps, EGE and LGE.

The acquisition parameters for the T1 and T2 maps are provided in Table 4-1. EGE and LGE were acquired as per the 1.5T protocol except for using a fixed TI of 500ms for the EGE images at 3T.

Table 4-1: Acquisition parameters of the T1/T2/T2* maps at 1.5T and 3T

	1.5T			**3T**	
	T1 map	**T2 map**	**T2* map**	**T1 map**	**T2 map**
WIP	*#448B*	*#448B*	*#448B*	*#699*	*#699*
Sampling protocol	5s(3s)3s for native T1 4s(1s)3s(1s)2s for post-contrast T1 maps	3 T2 preparation times: 0ms, 24ms and 55ms	8 TEs: 2.7ms, 5ms, 7.3ms, 9.6ms, 11.9ms, 14.2ms, 16.5ms and 18.8ms	5(3)3 for native T1 4(1)3(1)2 for post-contrast T1 maps	3 T2 preparation times: 0ms, 24ms and 55ms
Voxel size	1.5x1.5x6.0	2.0x2.0x6.0	1.6x1.6x8.0	1.6x1.6x6.0	2.1x2.1x6.0
TE/ ms	1.1	0, 24, 55	x8 – as above	1.1	0, 24, 55
Flip angle/ degrees	35	70	18	35	65

FoV/ mm	Variable (320-420)	Variable (320-420)	400	Variable (320-420)	Variable (320-420)
Matrix size	256x144	116x192	256x192	256x144	116x192
Bandwidth/ Hz/pixel	977	930	814	1028	930
Acceleration factor	2	2	None	2	2
Slice thickness/ mm	6	6	8	6	6
Slice gap/mm	4	4	2	4	4
Temporal Resolution/ ms	227	190	146		
Acquisition time	11 RR/ 11 seconds	7 RR	15 RR	11 RR	7 RR

4.3 Imaging analysis

Specific details pertaining to each topic are provided in their respective chapters.

Cines

All volume analysis was performed using CVI42 software (Version 5.2.2[340], Calgary, Canada). Semi-automated contours were drawn on the short-axis cine images using the threshold segmentation option for the epicardial border and the automatic detection option for the endocardial border, with minimal manual adjustment when required. The LVEDV, LVESV, LV mass (LVM) and LVEF were quantified using rounded endocardial contours and excluded the trabeculae and papillary muscles as part of the LVM and were included as part of the LV volume. The basal cine slice was included if at least 50% of the cavity circumference was surrounded by ventricular myocardium and this principle was used for both end-systole and end-diastole.

T1 and T2 maps

The T1 and T2 maps from the 3T cohort were analysed using an in-house macro written in ImageJ (Version 1.45s, National Institute of Health, USA). The in-house macro used in this study was written by Drs Steven K White, Andrew Flett and Steven G Casson. All the maps from the 1.5T cohort were analysed in CVI42 (Version 5.2.2[340], Calgary, Canada). These 2 different methods were used as at the time the 3T cohorts were analysed CVI42 was not yet available. Analysis of the maps was subsequently much easier with CVI42 and ImageJ was subsequently dropped.

For the 3T cohort, the endocardial and epicardial borders of matching LV short axis T1 maps and T2 maps were manually segmented (excluding the

papillary muscles) to obtain the myocardium volume. The basal slice with LVOT and the apical slice with no identifiable LV cavity were excluded. All subsequent quantification was performed on the pre-segmented images.

For the 1.5T cohort, the endocardial and epicardial borders were manually traced on the T2 maps and copied to the T1 maps with minimal manual adjustments using CVI42. The basal slice with LVOT present and the apical slice with no identifiable LV cavity were excluded. All subsequent quantification was performed on the pre-segmented images.

MI quantification

All LGE quantifications were performed using CVI42.

The endocardial and epicardial borders were manually drawn on all the LGE images. The basal slice with LVOT present and the apical slice with no identifiable LV cavity were excluded. MI size was quantified using Manual contouring by HB (2 and a half years experience in STEMI CMR scans analysis) and expressed as the %LV. Manual MI size quantification was performed by manually drawing a contour around the area of high signal intensities. On the acute scan, when areas of grey peri-infarct zones were present, these were excluded as part of the MI zone. Areas of hypo-intense core of MVO were included as part of the MI zone. Minimal adjustments were also performed if artefacts were present in the remote myocardium and these artefacts were manually excluded.

Thresholds of 5-SD, 6-SD, Otsu and FWHM were applied on these LGE images with pre-drawn endocardial and epicardial borders to obtain corresponding MI sizes and expressed as %LV.

For 5-SD and 6-SD (to identify signal intensities of 5-SD and 6-SD above the mean normal remote myocardium respectively), a ROI was identified in the normal remote myocardium using the automatic option from CVI42, with minimal manual adjustment when required to minimise intra-observer variability.

For the FWHM technique (to identify signal intensities that are above 50% of maximal signal intensity of the reference ROI)(181), the automatic option was also used to delineate an ROI in the area of hyper-enhancement by LGE.

The Otsu technique (to identify the intensity threshold from the signal intensity histogram using the value with minimal intra-class variance between low and high intensities)(179) did not require any additional ROIs but did require user input to identify slices with no LGE as normal.

4.4 Statistical analysis

The detailed imaging analysis descriptions will be provided in each relevant chapter. In brief, statistical analysis was performed using SPSS Version 22 (IBM Corporation, Illinois, US). Normality was assessed using Shapiro-Wilk Test. Continuous data was expressed as mean ± standard deviation (SD) or median (interquartile range) and categorical data was

reported as frequencies and percentages. Groups were compared using paired Student t-test/ Wilcoxon signed rank test or unpaired Student t-test/ Mann Whitney U test where appropriate. Correlation was assessed using either Pearson's correlation coefficient for normally distributed data or Spearman's rho for non-normally distributed data. Bland-Altman analysis was performed for inter-method measurements comparison and agreement. Inter-observer and intra-observer variability was assessed using intra-class correlation coefficient (ICC) when required. When assessment of the diagnostic performance of a parameter was required, ROC curve analyses were performed. All statistical tests were two-tailed, and $P<0.05$ was considered statistically significant.

4.5 Sample size

No formal sample size calculation was performed for the studies included in this thesis and is a limitation. I acknowledge the importance of having an appropriately powered study. Although a small sample is desirable, it would give results that are underpowered to detect a difference between two groups and the study may turn out to be falsely negative, leading to a type II error. On the other hand, a very large sample size is not recommends as it would be a waste of time and resources and not ethical for the patients.(265) 3 basic factors should be considered when performing sample size calculation; the type I or alpha error (failure to accept the null hypothesis when it is true, by convention set at 5%); the type II or beta error (failure to reject the null hypothesis when it is not true, usually set at 20%, power = 1 - type II error); and

the effect size (the larger the expected effect size, the small the sample size required).(266) A small sample size can also lead to only a small number of patients required to change their status from a non-event to an event to render a previously statistically significant result to a non-significant result. The lower this number, the more fragile the results and this is also known as the Fragility Index.(267) The sample size included in this thesis was small as recruitment was affected due to the merging of The Heart Hospital (where the initial work began) with Barts Heart Centre.

5 T1 mapping for the detection of the AAR, IMH and MI size

5.1 Background

T2-weighted STIR imaging, which has been used to delineate the AAR in reperfused STEMI patients, has also been used to detect IMH as the presence of a hypo-intense core within the AAR.(159-161) However, STIR imaging has been shown to have a lower diagnostic performance for detecting IMH when compared to T2* CMR imaging.(150, 153) Recently, *native* T1 mapping CMR (referred to as T1 mapping or T1 map throughout this chapter for simplicity) has been found to be superior to T2-weighted CMR in detecting myocardial oedema in the context of acute myocarditis (268) and acute myocardial infarction.(132) T1 mapping CMR has recently been reported to accurately quantify the AAR in the canine heart subjected to acute myocardial infarction.(131) Langhans et al (133) found that AAR by T1 and T2 mapping CMR at 1.5T correlated well with that obtained with SPECT. The direct comparison of T1 mapping against T2 mapping to quantify the AAR, to our knowledge, has not yet been performed in the clinical setting.

IMH can also manifest as a hypo-intense core on the T1 (156, 164) and T2 maps.(138, 153, 165) However, the diagnostic performance of T1 and T2 maps to detect the presence of IMH following STEMI has not been directly compared.

Conventionally, MI can be identified by LGE with inversion recovery (IR) T1-weighted sequences and manual adjustment of the inversion times (TI) to null the remote normal myocardium.(133) Post-contrast T1 mapping has also shown promise to detect acute MI in a small cohort of predominantly non-reperfused acute (186) and chronic MI patients.(186, 187) Refinements of the T1 MOLLI prototype using IR images at different TIs initially designed to improve motion correction (188, 189), can also retrospectively create “synthetic” IR LGE images, namely MagIR, PSIR outputs. These synthetic read-outs have recently been shown to accurately detect chronic MI size in a small cohort of 17 patients.(190) To date, no studies have assessed the performance of post-contrast T1 mapping and synthetic LGE in quantifying MI size with full LV coverage in a cohort of reperfused STEMI patients.

Therefore, the aim of this chapter was three-fold:

1. To assess the performance of T1 mapping to quantify the AAR as delineated by T2 mapping at 1.5T and 3T in reperfused STEMI patients.
2. To investigate the performance of T1 and T2 mapping to detect IMH and MVO within the first week in reperfused STEMI patients, using T2* mapping as the reference standard for IMH.(139, 150, 152, 153, 155, 156)
3. To investigate whether post-contrast T1 mapping and synthetic LGE images can quantify MI size (using conventional LGE as the reference).

5.2 Methods

5.2.1 Study population

5.2.1.1 T1 mapping versus T2 mapping for the AAR

This sub-study included 2 cohorts:

- 18 STEMI patients from the 3T cohort.
- 30 STEMI patients from the 1.5T cohort.

All patients had full LV coverage of T1 and T2 mapping as described in the methodology section.

The T1 and T2 maps were acquired to match the short-axis cines and LGE and to cover the entire left ventricle as shown in Figure 5-1.

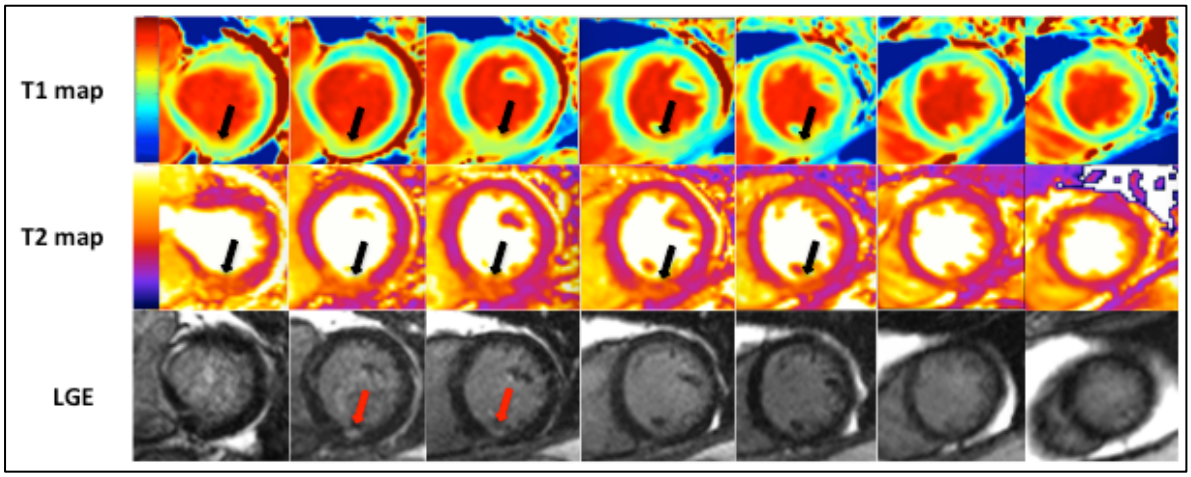

Figure 5-1: Matching T1 maps, T2 maps and LGE short axis CMR images at 3T from base to apex of a patient presenting with an acute inferior STEMI reperfused by PPCI.

Both T1 and T2 maps delineate the AAR (black arrows) and the LGE images show a small subendocardial myocardial infarct (red arrows).

5.2.1.2 T1 mapping versus T2 mapping for the detection of IMH

The 48 patients with an acute CMR study from the 1.5T cohort as described in the methodology section were included for this sub-study.

5.2.1.3 Post-contrast T1 mapping for acute MI size

28 acute STEMI patients from the 1.5T cohort described in the methodology section based on the availability of full LV coverage of post-contrast T1 mapping and the availability of the synthetic IR output dataset were included in this sub-study.

5.2.2 Imaging analysis

All LV volumes, LV mass, LV ejection fraction and MI size were analysed using CVI42 software (Version 5.2.2[340], Calgary, Canada) as described in the methodology section. MI size was quantified following manual delineation of the endocardial and epicardial borders of the short axis slices and using 5-SD threshold above the mean remote myocardium.(57)

5.2.2.1 T mapping versus T2 mapping for the AAR

For the 3T cohort, AAR by T1 mapping and T2 mapping were quantified using an in-house macro written in ImageJ (Version 1.45s, National Institute of Health, USA). The endocardial and epicardial borders of matching LV short axis T1 maps and T2 maps were manually segmented (excluding the papillary muscles) to obtain the myocardium volume. All subsequent quantification was performed on the pre-segmented images. All patients were analysed twice by HB and SKW blindly and independently, and HB performed the analysis twice, 3 months apart. The affected myocardium on the T1 maps and T2 maps were quantified using 3 analytical techniques namely manual delineation, 2SD above the mean remote normal myocardium, and the automated Otsu detection method (Otsu technique).(179) In brief, the Otsu technique uses an algorithm to automatically divide the signal intensity histogram into normal and enhanced. An exhaustive search for values that minimise the intra-class variance between two populations of signal intensities is used to establish the threshold.(269) The Otsu technique was not applied on maps that were visually normal based on the coloured look-up table and with normal wall motion on cines. Those maps

were manually marked as normal. Analysis was performed for all the slices for each patient to obtain the "enhanced" myocardium as a percentage of the whole LV (%LV). Regions of interest (ROIs) were drawn within the AAR (avoiding areas of MVO), and within the remote myocardium to obtain representative T1 and T2 values at 3T CMR. Manual correction was performed for hypo-intense areas within the MI zone (corresponding to areas of MVO) and areas of hyper-enhancement due to any obvious blood pool or pericardial partial volume effects and off-resonance artefacts in the remote myocardium. As shown in Figure 5-2, the hypo-intense area within the AAR depicted by the red arrows were manual included as part of the AAR using an option available on CVI42 for no-reflow zones. All slices were visually assessed and those with significant partial volume effects and susceptibility or motion artefacts overlapping with the affected myocardium were excluded by consensus. In cases of doubt or disagreement, the raw images were used to decide whether that slice was to be excluded or not as previously described by von Knobelsdorff-Brenkenhoff et al.(270)

For the 1.5T cohort, the endocardial and epicardial borders were manually traced on the T2 maps and copied to the T1 maps with minimal manual adjustments using CVI42 (Version 5.2.2[340], Calgary, Canada). The same 3 techniques (Manual, 2-SD and Otsu) were used to quantify the AAR. As mentioned above, the Otsu technique was not applied on maps that were visually normal based on the coloured look-up table and with normal wall motion on cines. These maps were manually selected as normal. Areas of hypo-intense core of MVO or IMH were included as part of the MI zone and

AAR. ROIs were manually drawn in MI zone and the remote myocardium to obtain representative native and post-contrast T1 and T2 values.

5.2.2.2 T1 mapping versus T2 mapping for the detection of IMH

The 2-SD threshold was also used to identify the hypo-intense core (hypo-intense area within the hyper-enhanced area) on both T1 and T2 maps to identify the hypo-intense core (Figure 5-2) in the 1.5T cohort.

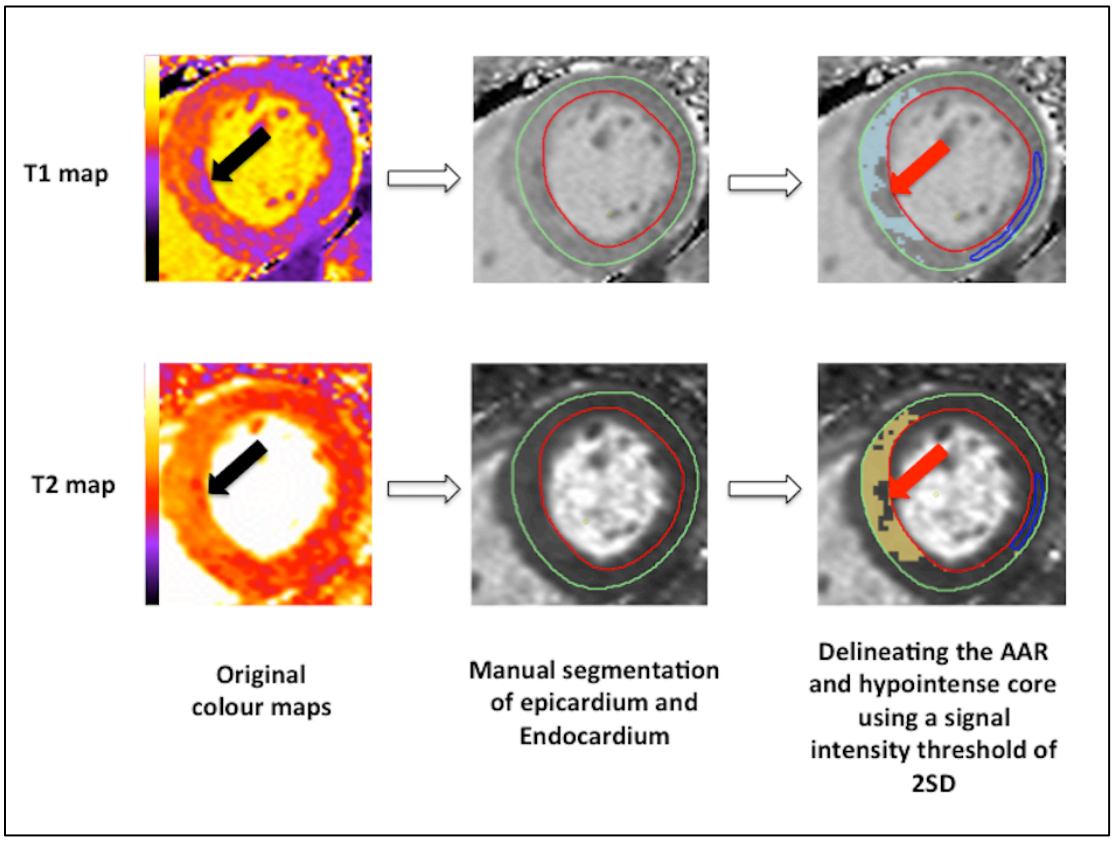

Figure 5-2: semi-automated method used to identify the hypo-intense core on the T1 and T2 maps.

So far, no studies have validated a cut-off threshold to detect IMH and MVO from these maps and we chose to use the same threshold used to

quantify the AAR to delineate the hypo-intense core as a semi-automated method to minimise bias (Figure 5-2). ROIs were manually drawn in the hypo-intense core (expressed as $T1_{Core}$ and $T2_{Core}$), the AAR (expressed as $T1_{AAR}$ and $T2_{AAR}$) and the remote myocardium (expressed as $T1_{Remote}$ and $T2_{Remote}$) on both maps. In cases when no hypo-intense core was identified, the ROI was drawn in the area of infarct. The T1 and T2 maps were also graded in a binary fashion to detect the presence or absence of a hypo-intense core (with the help of the semi-automated method as above).

10 randomly selected patients were separately analysed by 2 investigators (HB and EGL with >2½ years and 1 year experience in CMR respectively) 2 months apart for intra-observer and inter-observer variability.

Definitions

- IMH was defined as a hypo-intense core on the T2* maps with a T2* < 20ms as previously validated in pre-clinical (152) and subsequently used in several clinical STEMI studies. (139, 150, 155, 156)
- Early MVO was defined as areas of dark core within the infarcted territory visually detected (red arrow on the EGE image in Figure 5-3) on the EGE images, acquired 1-2 minutes post-contrast, as previously described.(146, 160, 261)
- Late MVO was defined as areas of dark core within the areas of LGE (red arrow on the LGE image in Figure 2) acquired 10-15 minutes post contrast on the LGE images as previously described.(149, 160, 271)

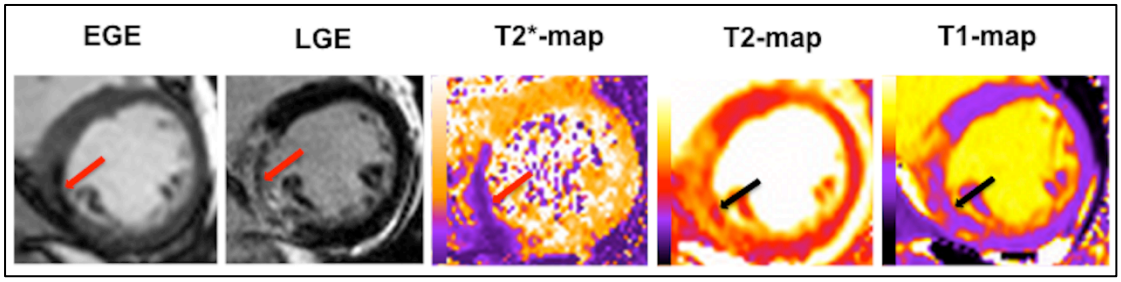

Figure 5-3: Example of a patient with an acute inferior MI depicting the evidence of MVO on EGE and LGE scans with corresponding hypo-intense cores (red and black arrows) on the basal LV short axis T2*, T1 and T2 maps.

5.2.2.3 Post-contrast mapping for acute MI size

Both the native and post-contrast MOLLI T1 mapping automatically generated 2 sets of IR images (MagIR and PSIR) in-line by the scanner for the TI range of 200 to 975ms (increments of 25ms) as illustrated in Figure 5-4.

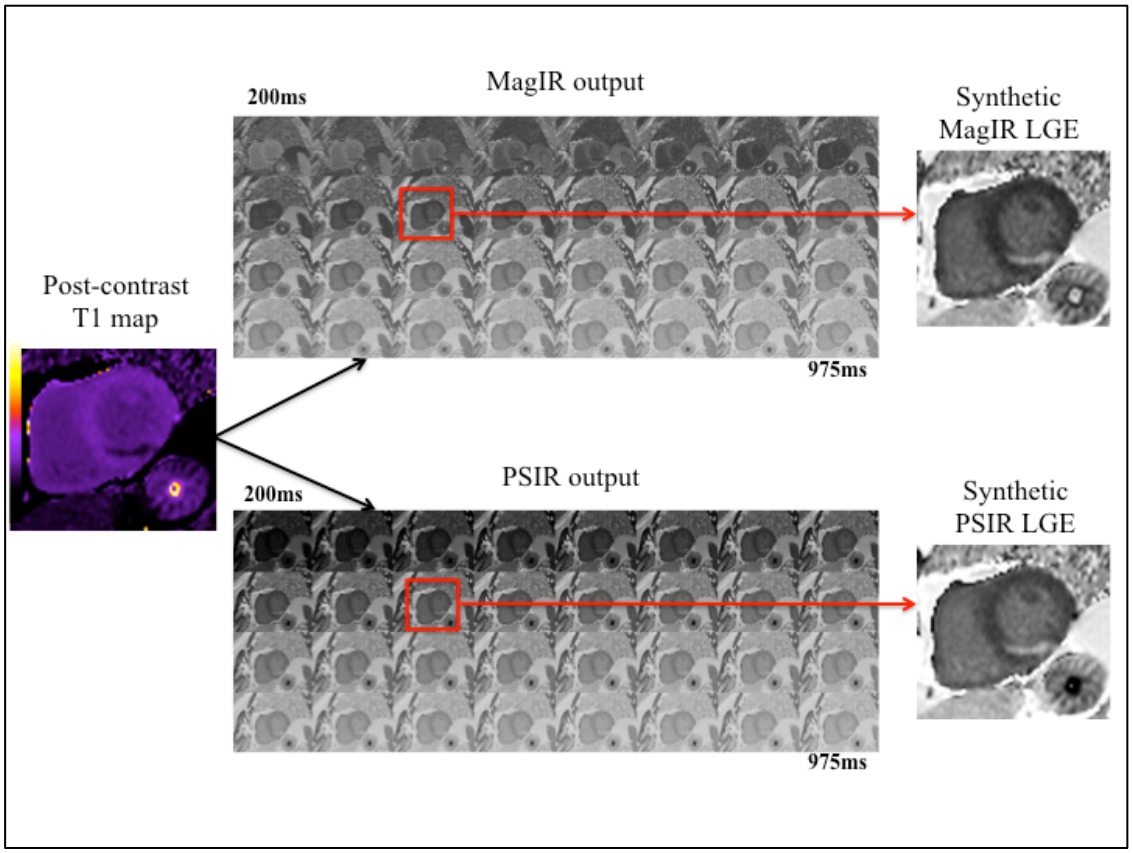

Figure 5-4: The MagIR and PSIR output from the MOLLI T1 mapping prototype

This is an illustration of the 2 additional outputs (with TI 200ms to 975ms) that were obtained from the MOLLI T1 mapping prototype for a patient with an acutely reperfused inferior STEMI. For synthetic MagIR LGE, the image with the optimal TI was manually chosen retrospectively as illustrated by the red square. For the synthetic PSIR LGE, the corresponding image from the PSIR output was chosen (red square) and was manually windowed if required.

For the synthetic MagIR LGE, the image with the optimal TI (remote normal myocardium nulled as black) was manually selected and the corresponding matching PSIR image was selected as the representative synthetic PSIR LGE image (Figure 5-4). A threshold of 5SD was also used to quantify synthetic MI size.

For the post-contrast T1 maps, we used 2 semi-automated techniques, namely a threshold of 2-SD below the mean remote myocardial post-contrast T1 and the Otsu technique (which identifies the intensity threshold from the signal intensity histogram using the value with minimal intra-class variance between low and high intensities).(179) MI size was expressed as: by conventional LGE (reference standard) as MI_{Conv}; MagIR synthetic LGE as $MI_{SynthMagIR}$; PSIR synthetic LGE as $MI_{SynthPSIR}$; post-contrast T1 MI size by 2-SD as $MI_{T1Post2SD}$; and by Otsu as $MI_{T1PostOtsu}$.

5.2.3 Statistical analysis

Pearson's correlation coefficient expressed as its square (R^2) was used to assess inter-method correlation and inter-method agreement was assessed using ICC with 95% confidence intervals (95%CI). ROC analyses were used to assess the diagnostic performance for T1 and T2 maps for detecting IMH on the acute scans and were compared using the method described by Delong et al (272) Inter-observer and intra-observer variability for T1 and T2 values of the hypo-intense core were assessed in 10 patients and expressed as ICC (95% CI). Cohen's Kappa was used to assess inter-observer and intra-observer agreement for the binary assessment of the maps. Bland-Altman analysis was performed to assess agreement and bias detection between methods and presented as average difference ± 2SD. Firstly, a per-slice and per-patient comparison was performed on the 3T cohort patients. Inter-observer and intra-observer variability was assessed for all 18 patients in the 3T cohort using ICC

and mean difference between inter-observer and intra-observer measurements of T1 and T2-derived AAR. Secondly, a per-patient comparison was performed on the 1.5T cohort. All statistical tests were two-tailed, and P-values of less than 0.05 were considered statistically significant.

5.3 Results

5.3.1 T1 mapping versus T2 mapping for the AAR

The patients' demographics and coronary angiographic and CMR characteristics are detailed in Table 5-1. The majority were male and two-thirds of the patients presented with a left anterior descending territory STEMI and one-third with a right coronary artery territory infarct. Figure 5-5 and Figure 5-6 show examples of T1 maps, T2 maps and LGE in patients from both cohorts.

Table 5-1: Patients' demographics, coronary angiographic and CMR characteristics.

Details	3T cohort	1.5T cohort
Number of patients	18	30
Male	15 (83%)	23 (77%)
Age ± SD (years)	58 ±10	55 ±12
Hypertension	5 (28%)	8 (27%)
Smoking	9 (50%)	11 (37%)
Dyslipidaemia	3 (17%)	8 (27%)
Chest pain onset to balloon time	292 (116-800)	213 (131-385)

(minutes)		
Infarct artery and location LAD Proximal/ Mid/ Distal RCA Proximal/ Mid/ Distal Cx Proximal/ Mid/ Distal	12 (67%) 5 (42%)/ 6 (50%)/ 1 (8%) 6 (33%) 3 (50%)/ 2 (33%)/ 1(17%) 0 NA	19 (63%) 13 (68%)/ 5 (26%)/ 1 (5%) 9 (30%) 8 (89%)/ 0 (0%)/ 1 (11%) 2 (7%) 2 (100%)/ 0 (0%)/ 0 (0%)
Pre-PPCI TIMI flow (%) 0/ 1/ 2/ 3	13 (72%)/ 4 (22%)/ 1 (6%)/ 0 (0%)	21 (70%)/ 1 (3%)/ 3 (10%)/ 5 (17%)
Post-PPCI TIMI flow (%) 0/ 1/ 2/ 3	1 (6%)/ 0 (0%)/ 2 (12%)/ 15 (82%)	1 (3%)/ 0(0%)/ 2 (7%)/ 27 (90%)
Days from PPCI to CMR	5 (4-6)	4±2
Left ventricular ejection fraction (%)	49±11	52±8
End diastolic volume (ml)	135±21	147±35
Left ventricular mass (g)	151±50	121±27
Presence of MVO (%)	8 (44%)	20 (67%)
Infarct size by LGE, (% LV volume)	18.8±9.4	25.6±14.1
AAR by T1 mapping, (% LV volume) Manual Otsu 2-SD	 32.0±11.5 32.3±11.5 38.4±13.6	 41.1±11.7 41.6±11.6 42.2±11.9
AAR by T2 mapping, (% LV volume) Manual Otsu 2-SD	 31.8±11.7 31.6±11.2 38.7±15.0	 41.7±11.9 41.9±11.9 42.4±11.9

SD: standard deviation; LAD: left anterior descending; RCA: right coronary artery; Cx: circumflex artery; TIMI: Thrombolysis in Myocardial Infarction; PPCI: primary percutaneous coronary intervention; CMR: cardiovascular magnetic resonance; MVO: microvascular obstruction; LGE: late gadolinium enhancement; AAR: area-at-risk; LV: left ventricle

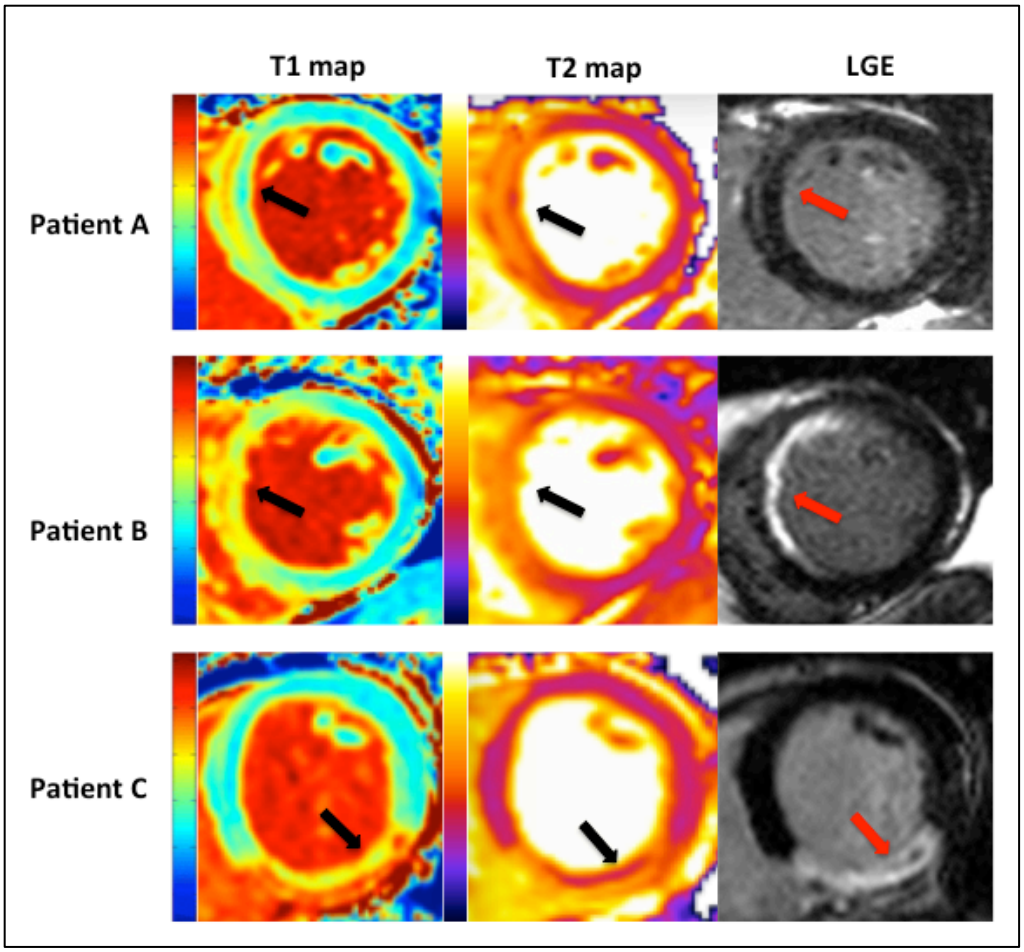

Figure 5-5: Representative mid left ventricular short axis T1 maps, T2 maps and LGE short-axis images from three patients demonstrating varying degrees of myocardial salvage at 3T

For patient A, both the T1 and T2 maps delineate a large area of myocardial oedema in the left anterior descending (LAD) territory (black arrow), corresponding to the AAR, with no significant MI on LGE image (red arrow), indicating complete myocardial salvage. For patient B, the T1 and T2 maps again delineate an area of myocardial oedema in the LAD territory (black arrow), with a subendocardial MI on the LGE image (red arrow), indicating some myocardial salvage. For patient C, the T1 and T2 maps delineate an area of myocardial oedema in the right coronary artery territory (black), with a transmural MI containing some MVO (hypo-enhancement on T2 map and LGE images) on the LGE image (red arrow), indicating minimal myocardial salvage.

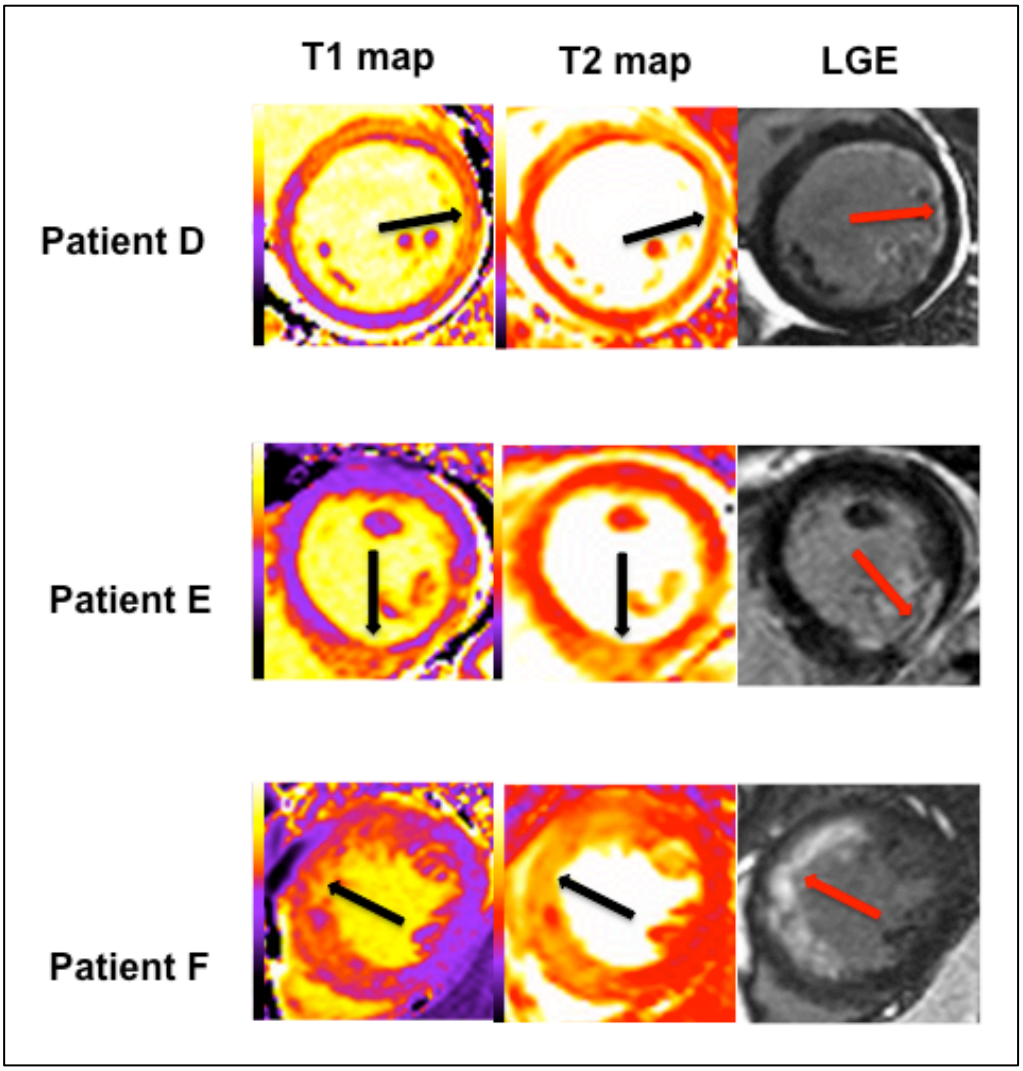

Figure 5-6: Representative examples of the native T1 and T2 maps showing the AAR and the corresponding MI extent at 1.5T

Patients D and F suffered from an acute anterior STEMI and Patient E suffered from an acute inferior STEMI – all were treated by PPCI. The black arrows indicate the territory of the AAR on the T2 and native T1 maps and the red arrows indicate the territory of the subendocardial MI (of different transmural extents) on the LGE images. All these patients had significant myocardial salvage and the areas of abnormality on the T2 and native T1 maps extended beyond the corresponding MI territory, indicating oedema in the salvaged myocardium.

5.3.1.1 Quality and acquisition times of T1 and T2 maps

The acquisition times for T1 maps and T2 maps per patient were similar both at 3T (T1 maps: 5.6 ± 1.9 minutes, T2 maps: 5.5 ± 2.0 minutes) and at 1.5T (T1 maps: 5.5 ± 1.1 minutes, T2 maps: 4.9 ± 0.7 minutes). 15% of the maps at 3T and 10% of the maps at 1.5T were excluded due to suboptimal image quality. At 3T, both T1 and T2 CMR were equally prone to susceptibility artefacts in the lateral wall. As we did not have any patients with a circumflex territory infarction, these artefacts were remote from the AAR and the slices (10/107 slices, 9%) were kept for analysis (manual correction was required). Both T1 and T2 maps were equally likely to be affected by MVO, requiring manual correction to include the core as part of the AAR at both scanner strengths. The total CMR scan time was on average 60 minutes and 90 minutes at 1.5T and 3T respectively.

5.3.1.2 Inter and intra-observer variability (3T cohort)

The AAR by the 3 techniques (manual/ Otsu/ 2-SD) were 31.8 ± 11.7%, 31.6 ± 11.2% and 38.7 ± 15.0% by T2 mapping and were 32.0 ± 11.5%, 32.3 ± 11.5% and 38.4 ± 13.6% by T1 mapping, respectively. The ICC for intra-observer and inter-observer variability of the 3 analytical techniques were excellent, both for T1 and T2 mapping and was highest for the Otsu technique. The 2-SD technique had the largest differences both for intra-observer and inter-observer measurements for both mapping techniques (

Table 5-2).

Table 5-2: Intra-observer and inter-observer variability of the AAR by T1 and T2 at 3T (n=18).

	ICC (95% CI)	Mean difference ± SD (%)	P
Intra-observer variability (n = 107)			
T1 mapping			
Manual	0.961 (0.943 – 0.973)	1.5 ± 7.1	0.04*
2-SD	0.948 (0.917 – 0.966)	2.6 ± 7.7	0.001*
Otsu	0.989 (0.984 – 0.993)	0.7 ± 3.2	0.03*
T2 mapping			
Manual	0.951 (0.928 – 0.966)	0.8 ± 6.4	0.18
2-SD	0.965 (0.942 – 0.978)	2.4 ± 6.4	0.001*
Otsu	0.996 (0.995 – 0.998)	0.2 ± 1.9	0.24
Inter-observer variability (n = 107)			
T1 mapping			
Manual	0.980 (0.972 – 0.987)	0.3 ± 4.3	0.52
2-SD	0.948 (0.925 – 0.964)	3.7 ± 7.2	0.001*
Otsu	0.993 (0.990 – 0.995)	0.2 ± 2.6	0.55
T2 mapping			
Manual	0.964 (0.947 – 0.975)	0.3 ± 6.1	0.59
2-SD	0.960 (0.914 – 0.978)	3.5 ± 6.5	0.001*
Otsu	0.993 (0.989 – 0.995)	0.7 ± 2.6	0.008*

ICC: intraclass correlation coefficient; SD: standard deviation

The 2-SD technique overestimated the AAR compared to manual delineation (as the reference standard) but there was no difference between Otsu and manual delineation for both T1 and T2 mapping (Figure 5-7). The Otsu derived T1 and T2 AAR was

herefore used for the analysis below.

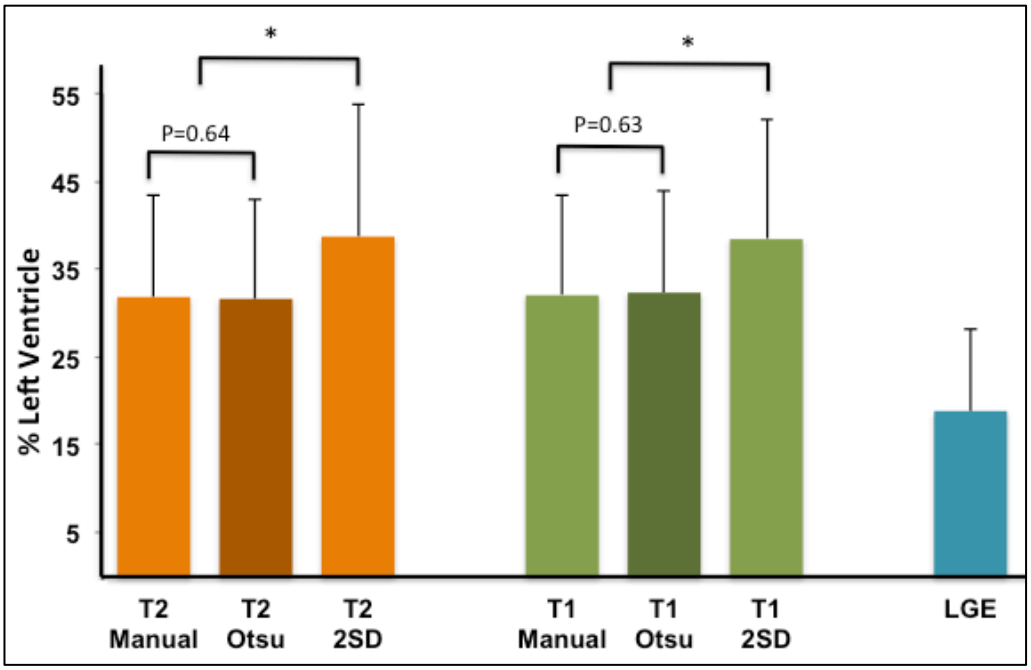

Figure 5-7: Performance of three different threshold techniques for delineating the AAR on T1 and T2 maps.

The AAR by the 2 standard deviations (2-SD) technique was significantly larger than that delineated by the manual and Otsu threshold techniques. There was no difference between the manual and Otsu techniques for both T1 and T2 mapping in delineating the AAR.

** denotes significant statistical difference with P<0.001.*

5.3.1.3 Comparison of the AAR by T1 mapping against T2 mapping at 3T

The mean MI size by LGE was 18.8 ± 9.4% of the LV, (range 2.0 - 34.0%). Myocardial salvage (AAR subtract the MI size) was 12.8 ± 10.0% of LV (range 0 – 42.0%) by T2 mapping. The MSI (myocardial salvage / AAR) was 0.40 ± 0.26 (range 0 – 0.89).

The T1 and T2 values in the AAR were significantly higher than those in the remote myocardium ($T1_{AAR}$: 1524 ± 116ms, $T1_{Remote}$: 1163 ± 78ms, P < 0.001; $T2_{AAR}$: 72 ± 7ms, $T2_{Remote}$: 46 ± 3ms, P < 0.001).

The Otsu technique failed in 4% of the maps with extensive MVO and transmural LGE and the AAR was manually delineated for these slices. On a per-slice analysis, there was an excellent correlation between the T1 mapping and T2 mapping with an R^2 of 0.95 and a regression slope 0.97 (95%CI 0.93 – 1.01). There was no bias on Bland Altman analysis (mean ± 2SD: bias 0.0 ± 9.6%) (Figure 5-8 a and b). On a per-patient analysis, the correlation and agreement remained excellent with no bias (R^2 0.95, regression slope 0.95 (95% CI 0.84 – 1.07), bias 0.7 ± 5.1%, Figure 5-8 c and d). The mean AAR (expressed as a % of the LV) quantified by T1 mapping was similar to that by T2 mapping (32.3 ± 11.5% of the LV, range 6% to 52% by T1 mapping, versus 31.6 ± 11.2% of the LV, range 5% - 48% by T2 mapping, P = 0.25).

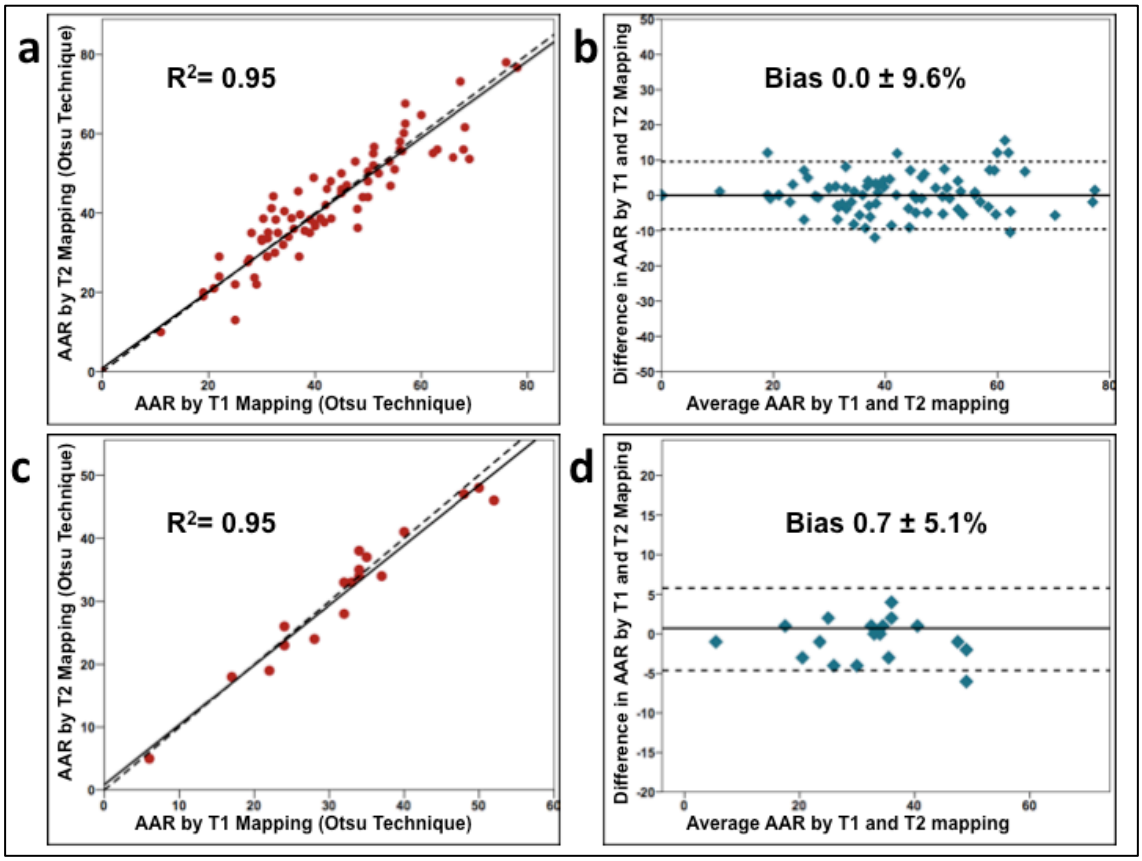

Figure 5-8: Correlation and agreement between T1 and T2 mapping to delineate the AAR.

*Both on a per-slice (a and b) and per-patient analysis (c and d), there was an excellent correlation and agreement between T1 and T2 mapping technique to delineate the AAR. The interrupted lines in **a** and **c** represent reference lines with a slope of 1.*

5.3.1.4 Comparison of the AAR by T1 mapping against T2 mapping at 1.5T

The mean MI size in this cohort of STEMI patients was 25.1±14.3%LV and the mean Manual AAR by T2 was 41.5±12.0%LV. The MSI in this cohort was 0.41±0.28.

T2 in the MI zone was significantly higher than in the remote myocardium (67±7ms versus 50±3ms, P<0.0001). Native T1 in the MI zone was also significantly higher than in the remote myocardium (1258±57ms versus 1041±57ms, P<0.001).

The Otsu technique failed in 8% of the maps with extensive MVO and transmural LGE and the AAR was manually delineated based on the transmural extension of the MI for these slices. There was an excellent correlation (R^2 0.99) and agreement (ICC 0.983 and 0.996 respectively) between the Manual T2 AAR and the 2-SD. The T2 AAR by Otsu was similar to Manual T2 AAR (41.7±12.2%LV versus 41.5±12.1%LV, P=0.38) with no bias (0.2±2.1%). However, the T2 AAR by 2-SD was significantly larger than Manual (42.2±12.1%LV versus 41.5±12.1%LV P=0.011) with a bias of 1.0±2.6%.

The same pattern was observed for T1 mapping. The T1 AAR by Otsu was similar to Manual (41.6±11.9%LV versus 41.0±12.0%LV, P=0.17) with no bias (-0.6±4.2%), and the T1 AAR by 2-SD was significantly higher than Manual (42.1±12.2%LV versus 41.0±12.0%LV, P=0.005) with a small bias of 1.0±3.9%.

T1 mapping performed as well as T2 mapping in delineating the AAR (T1 Otsu 41.6±11.9%LV versus T2 Otsu 41.7±12.2%LV, P=0.72; R^2 0.97; ICC 0.986(0.969-0.993); bias -0.1±4.2%LV). Table 5-3 and Figure 5-9 provide further details of the comparison between T2 and native T1 mapping for the quantification of the AAR using the different techniques. Figure 5-10 shows the correlation and agreement of the AAR between T1 and T2 mapping at 1.5T.

Table 5-3: Comparison of acute MI size and AAR quantification by the different techniques

Reference/ %LV	Other Techniques/ %LV	P value	R^2	ICC (95%CI)	Bias±2SD/ %LV
T2 mapping					
T2 Manual 41.5±12.1	T2 Otsu 41.7±12.2	0.38	0.99	0.983 (0.964-0.992)	0.2±2.1
	T2 2-SD 42.2±12.1	0.011*	0.99	0.993 (0.980-0.997)	1.0±2.6
T1 mapping					
T1 Manual 41.0±12.0	T1 Otsu 41.6±11.9	0.17	0.99	0.995 (0.990-0.998)	-0.6±4.2
	T1 2-SD 42.1±12.2	0.005*	0.96	0.983 (0.949-0.993)	-1.0±3.9
T2 mapping versus T1 mapping					
T2 Manual 41.5±12.1	T1 Manual 41.0±12.0	0.11	0.99	0.989 (0.977-0.995)	0.5±3.4
T2 Otsu 41.7±12.2	T1 Otsu 41.6±11.9	0.72	0.97	0.986 (0.969-0.993)	-0.1±4.2
T2 2-SD 42.2±12.1	T1 2-SD 42.1±12.2	0.86	0.97	0.985 (0.967-0.993)	0.1±4.3

LV: left ventricle; SD: standard deviation

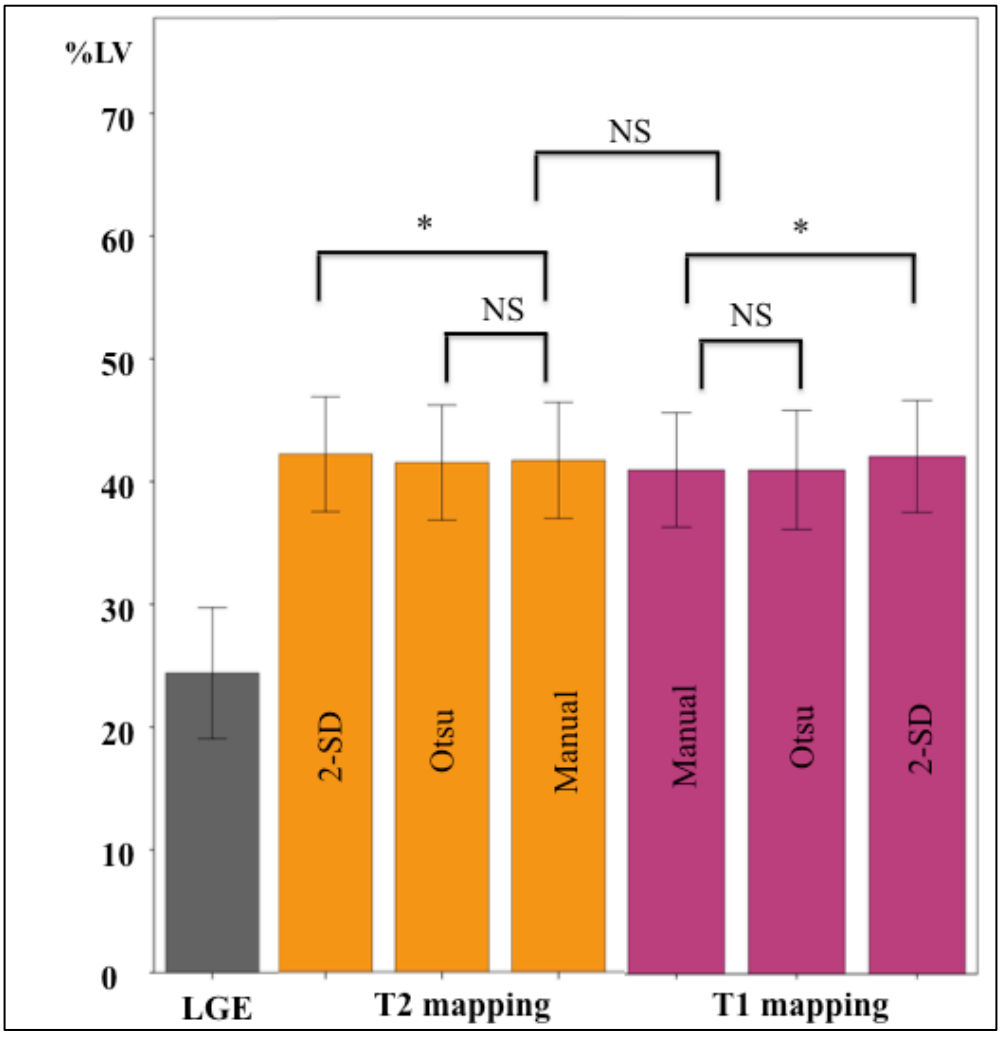

Figure 5-9: Comparison of MI size and AAR quantified by the different techniques

*This figure shows the comparison of the AAR by T2 and T1 mapping using the 3 quantification techniques. NS denotes no statistical difference and * denote P<0.05. Data presented as mean ± 95%CI.*

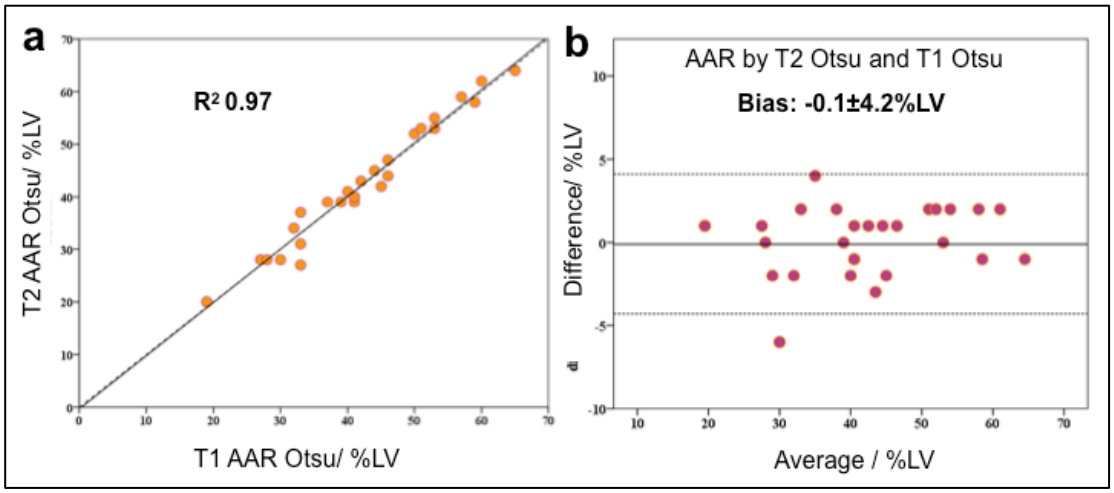

Figure 5-10: Comparison of the edema-based AAR by T2 and native T1 mapping

There was an excellent correlation and minimal bias in edema-based AAR delineated by T2 mapping versus native T1 mapping.

5.3.2 T1 mapping versus T2 mapping for the detection of IMH

Figure 5-11 provides the details of the patients' screening and recruitment into the study. 48 patients with a mean age of 59±13 years and 88% (24/48) male gender completed the CMR study at 4±2 days post-PPCI. Patients' clinical characteristics are listed in Table 5-4. The mean MI size was 27.4±14.6% of the LV and the AAR was 42.7±11.9% of the LV. Early MVO was present in 79% (38/48) of patients and late MVO in 63% (30/48) of patients. The average scanning time was 59±4 minutes, longer than a clinical CMR scan as on average an additional 15 minutes were required for T1 and T2 mapping acquisition (full LV coverage) and an additional 3 minutes for 3 short axis T2* mapping acquisition.

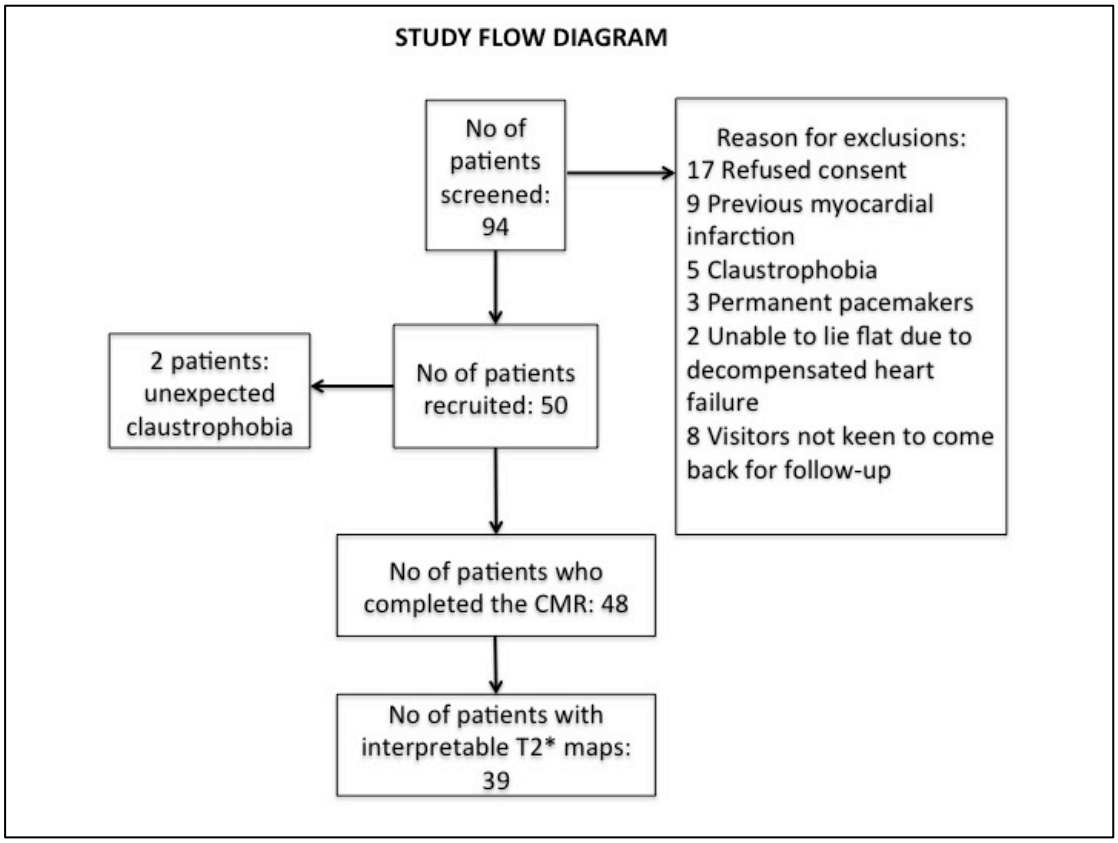

Figure 5-11: Details of the screening and recruitment of patients entering this study

Table 5-4: Clinical characteristics of STEMI patients

Details	Number
Number of patients	48
Male	40 (83%)
Age	58 ±13
Diabetes Mellitus	9 (19%)
Hypertension	15 (31%)
Smoking	15 (31%)
Dyslipidemia	15 (31%)

Chest pain onset to PPCI time (minutes)	182 [128-328]
Infarct artery (%) LAD RCA Cx	 28 (58%) 18 (38%) 2 (4%)
Pre-PPCI TIMI flow (%) 0 1 2 3	 38(80%) 1 (2%) 4 (8%) 5 (10%)
Post-PPCI TIMI flow (%) 0 1 2 3	 1 (2%) 0 (0%) 10 (21%) 37 (77%)
Treatment – during PPCI Aspirin Clopidogrel Ticagrelor Heparin Bivalirudin Glycoprotein IIbIIIa inhibitors	 100(100%) 26 (54%) 24 (50%) 40 (83%) 17 (35%) 14 (29%)
Treatment – on discharge Dual antiplatelet therapy Beta blockers ACEI/ARB Statin MRA	 48 (100%) 48 (100%) 48 (100%) 47 (98%) 11 (23%)

LAD: left anterior descending artery; RCA: right coronary artery; Cx: circumflex artery; TIMI: thrombolysis in myocardial infarction; ACEI/ARB: angiotensin converting enzyme inhibitor/ angiotensin receptor blocker; MRA: mineralocorticoid receptor antagonist.

Figure 5-3 shows an example of the different imaging modalities acquired. These are mid LV short axis images of a patient with an acute inferior STEMI with MVO and the corresponding maps showing IMH (arrows).

5.3.2.1 T2 mapping for the detection of IMH*

T2* maps were not interpretable in 19% (9/48) of the patients (due to motion, flow and off-resonance artefacts). In patients with a hypo-intense core on the T2* maps, the mean T2* value of the core was 13±3ms compared to 33±4ms in the remote myocardium, P<0.001. IMH occurred in 67% (26/39) of the patients. As expected, patients with IMH were more likely to have larger MI size (33.4±11.3% of the LV versus 17.5±9.8% of the LV, P<0.001) and worse ejection fraction (47±7% versus 53±7%, P=0.04). Further details on the CMR findings are summarised in Table 5-5.

Table 5-5 CMR characteristics of STEMI patients divided into those with and without IMH.

	With IMH (n=26)	**Without IMH (n= 13)**	**P value**
EDV/ml	172±44	152±17	0.06
ESV/ml	91±30	73±16	0.02*
EF/%	47±7	53±7	0.04*
LV Mass/g	117±44	111±23	0.66
Infarct size/ % of LV	33.4±11.3	17.5±9.8	<0.001*
Infarct size/ g	24.9±8.6	11.4±8.0	<0.001*
AAR/ %LV	46.5±10.8	37.5±13.3	0.03*
Late MVO/ % (n)	96 (25)	8 (1)	<0.001*
Early MVO/ % (n)	100 (26)	46 (6)	0.02*
$T1_{Core}$/ ms	997±79	1124±65	<0.001*
$T1_{Remote}$/ ms	1035±46	1014±55	0.03*
$T1_{AAR}$/ ms	1244±79	1267±65	0.43
$T2_{Core}$/ ms	50±4	57±4	<0.001*
$T2_{Remote}$/ ms	51±3	50±3	0.35
$T2_{AAR}$/ ms	66±6	66±7	0.85

IMH: intramyocardial haemorrhage; EDV: end diastolic volume; ESV: end systolic volume; EF: ejection fraction; LV: left ventricular mass; AAR: area-at-risk; MVO: microvascular obstruction.

**Denotes being statistically significant.*

5.3.2.2 Detection of IMH by T1 and T2 mapping

In patients with IMH, $T1_{Core}$ was lower than both $T1_{Remote}$ (997±79ms versus 1035±46ms, P=0.02) and $T1_{AAR}$ (997±79ms versus 1244±79ms, P<0.001). $T2_{Core}$ was similar to $T2_{Remote}$ (50±4ms versus 51±3ms, P=1.0) but lower than $T2_{AAR}$ (49±4ms versus 66±6ms, P<0.001). In patients without IMH, $T1_{Core}$ and $T2_{Core}$ were higher than $T1_{Remote}$ and $T2_{Remote}$ as shown in Figure 5-12 below.

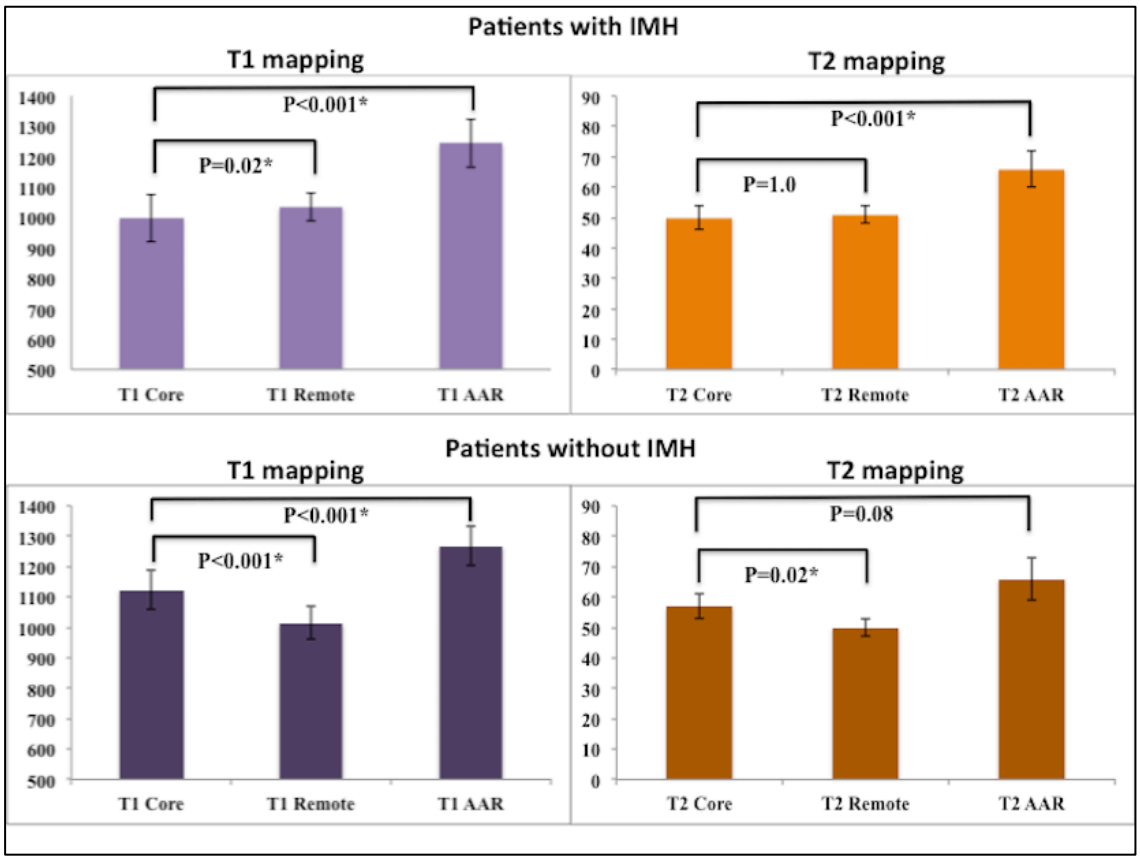

Figure 5-12: T1 and T2 values of the hypo-intense core, remote myocardium and the AAR.

** Denotes statistically significant difference.*

ROC analyses of the T1 and T2 values of the hypo-intense core showed that both mapping techniques performed equally well at detecting IMH on the acute scans (T1 maps: area under the curve (AUC) 0.86 [95%CI 0.72-0.99], cut-off value for $T1_{Core}$: <1080ms; T2 maps: AUC 0.86 [95%CI 0.74-0.99]; P=0.94, cut-off value for $T2_{Core}$: <54ms)(Figure 5-13). When using the binary assessment of either presence or absence of a hypo-intense core on the T1 and T2 maps as a measure to detect IMH, T1 and T2 performed as well the quantitative assessment of the maps (T1: AUC 0.87 [95%CI 0.73-1.00], T2: AUC 0.85 [95%CI 0.71-0.99]; P=0.90). The presence of a hypo-intense core had a sensitivity of 88% and a specificity of 85% to detect IMH on the T1 maps and a sensitivity and specificity of 85% on the T2 maps. The accuracy by T1 mapping was 87% and 85% by T2 mapping. The positive predictive value by T1 and T2 mapping were both 92%. The negative predictive values were equally high by T1 mapping and T2 mapping at 87% and 85% respectively.

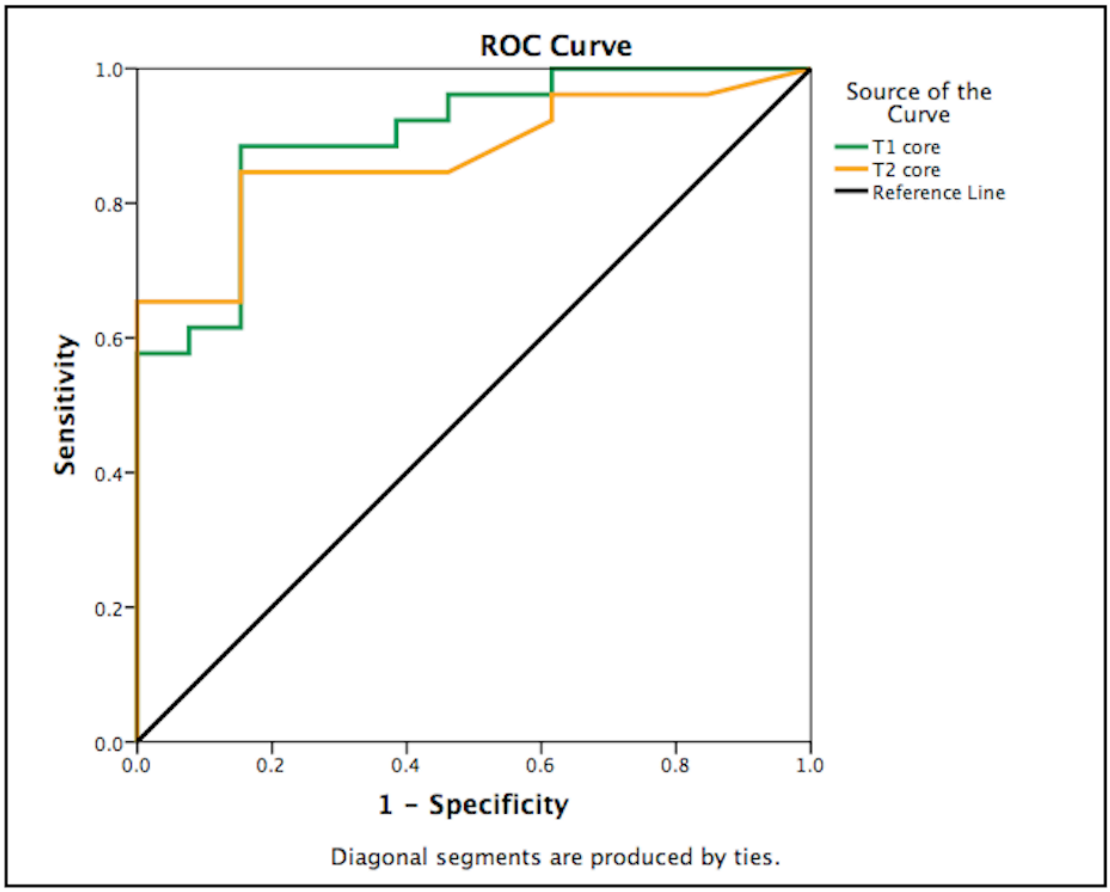

Figure 5-13: ROC curves for the diagnostic performance of T1 and T2 mapping to detect IMH on the acute scans when compared to T2* maps.

5.3.2.3 Detection of early and late MVO by T1 and T2 maps

The AUC for the presence of a hypo-intense core on the maps to detect early MVO was 0.83 (95% CI 0.70 – 0.97) for T1 (sensitivity: 76%; specificity: 90%) and 0.82 (95% CI 0.69 – 0.97) for T2 (sensitivity: 77%; specificity: 90%). For the detection of late MVO the AUC was 0.79 (95% CI 0.64 – 0.95) for T1 (sensitivity: 84%; specificity: 71%) 0.80 (95% CI 0.62 – 0.93) for T2 (sensitivity: 80%; specificity of 72%).

Table 5-6 summarises further details on the diagnostic performances of T1 and T2 maps to detect IMH, early MVO and late MVO.

Table 5-6: Summary of the diagnostic performances of T1 and T2 maps to detect IMH, early MVO and late MVO

	Sensitivity/ %	Specificity/ %	Positive predictive value/ %	Negative predictive value/ %	Accuracy/ %
IMH					
T1 map	88	85	92	79	87
T2 map	85	85	92	73	85
Early MVO					
T1 map	76	90	97	50	79
T2 map	74	90	97	47	77
Late MVO					
T1 map	84	71	87	72	81
T2 map	80	72	86	68	79

IMH: intramyocardial hemorrhage; MVO: microvascular obstruction.

5.3.2.4 ROC comparison for the detection of IMH, early MVO and late MVO

There was no significant difference in the diagnostic performance for T1 and T2 mapping to detect IMH, early MVO and late MVO (P values for ROC curves comparison for IMH versus early MVO, IMH versus late MVO, early MVO versus late MVO for T1 mapping: 0.90, 0.43, 0.37 respectively; for T2 mapping: 0.81, 0.58 and 0.42 respectively).

5.3.2.5 Early MVO with and without IMH

32 patients has analysable T2* maps and early MVO. 26/32 (81%) patients had early MVO with IMH and 6/32 (19%) patients had early MVO

without IMH. Both T1 and T2 values were significantly lower in patients with early MVO with IMH compared to those with early MVO without IMH ($T1_{Core}$: 998[954 – 1036] ms versus 1116[1085 – 1168], P<0001; $T2_{Core}$: 50[48 – 53] ms versus 55[54 – 56] ms, P=0.005). The same comparison was not performed for late MVO as only 1 patient had late MVO without IMH. All patients with early MVO and IMH developed late MVO compared to 2/6 (33%) of those with early MVO without IMH had late MVO, P<0.0001.

5.3.2.6 Inter-observer and intra-observer variability

On the quantitative mapping analysis of the hypo-intense cores, for intra-observer variability, the ICC for the quantification of the hypo-intense core for the T1 maps was 0.944 (0.792-0.986) and for T2 maps was 0.903 (0.637-0.976). For inter-observer variability, the ICC for T1 maps was 0.935 (0.746-0.984) and for T2 maps was 0.887 (0.528-0.972). On the qualitative mapping analysis for the hypo-intense core detection using the semi-automatic method, the inter-observer and intra-observer agreement was 100%, Cohen's Kappa =1.0, P<0.0001.

5.3.3 Post-contrast T1 mapping for acute MI size

Baseline characteristics of the patients included for this analysis are listed in Table 5-7. The mean age of the STEMI patients were 57±13 years old and 22/28 (79%) were male. The mean MI size (MI_{Conv}) in the STEMI patients

was 25.1±14.3%LV and the mean oedema-based AAR by T2 ($AAR_{T2Manual}$) was 41.5±12.0%LV. The myocardial salvage index in this cohort was 0.41±0.28. Post-contrast T1 was significantly lower in the MI zone compared to the remote myocardium (441±48ms versus 625±22ms, P<0.001).

Table 5-7: Patient characteristics and coronary angiographic details

Details	Number
Number of patients	28
Male	22 (79%)
Age	57 ±13
Diabetes Mellitus	8 (29%)
Hypertension	8 (29%)
Smoking	10 (36%)
Dyslipidemia	8 (29%)
Chest pain onset to PPCI time (minutes)	216 [138-422]
Infarct artery (%)	
LAD	17 (61%)
RCA	9 (33%)
Cx	2 (7%)
TIMI flow Pre/ Post PPCI (%)	
0	19 (68%)/ 1 (4%)
1	1 (4%)/ 0 (0%)
2	3 (11%)/ 1 (4%)
3	5 (17%)/ 26 (92%)

LAD: left anterior descending artery; RCA: right coronary artery; Cx: circumflex artery; TIMI: thrombolysis in myocardial infarction; PPCI: primary percutaneous coronary intervention

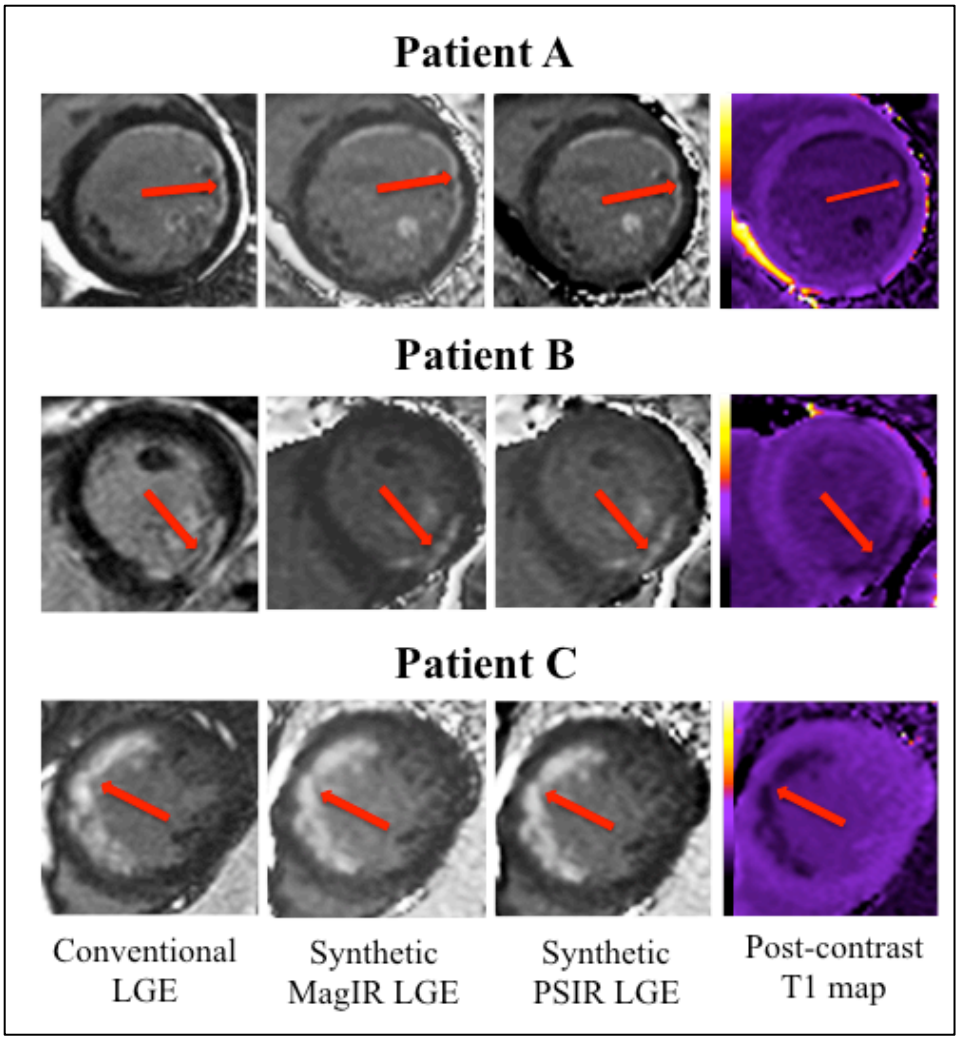

Figure 5-14: Representative examples of the T2 and native T1 maps showing the AAR and the corresponding LGE on the conventional, synthetic and post-contrast T1 maps.

Patients A and C suffered from an acute anterior STEMI and Patient B suffered from an acute inferior STEMI – all were treated by PPCI. The red arrows indicate the territory of the subendocardial MI (of different transmural extents) on the conventional and synthetic LGE images and post-contrast T1 maps. All these patients had significant myocardial salvage.

Figure 5-14 illustrates examples from 3 patients with an acute MI size by conventional LGE, synthetic MagIR LGE, synthetic PSIR LGE, and post-contrast T1 maps.

5.3.3.1 Acute MI size quantification

There was an excellent correlation (R^2 0.96 to 0.99) and inter-method agreement (ICC 0.964 to 0.996) between conventional LGE and the other techniques. There was minimal bias between MI_{Conv} and $MI_{SynthMagIR}$ (bias: 0.2±2.2%LV, P=0.35); between MI_{Conv} and $MI_{SynthPSIR}$ (bias: 0.4±2.2%LV, P=0.060); and between MI_{Conv} and $MI_{T1Post2SD}$ (bias: 0.3±1.8%LV, P=0.10), with the latter having the narrowest limits of agreement. However, $MI_{T1PostOtsu}$ underestimated MI size when compared to MI_{Conv} (bias -2.2±6.0%LV, P=0.001). Figure 5-15 shows the comparison of the various techniques used for MI size. Figure 5-16 illustrates the correlations and Bland-Altman analysis of MI_{Conv} against the 4 other techniques and further details are summarised in Table 5-8.

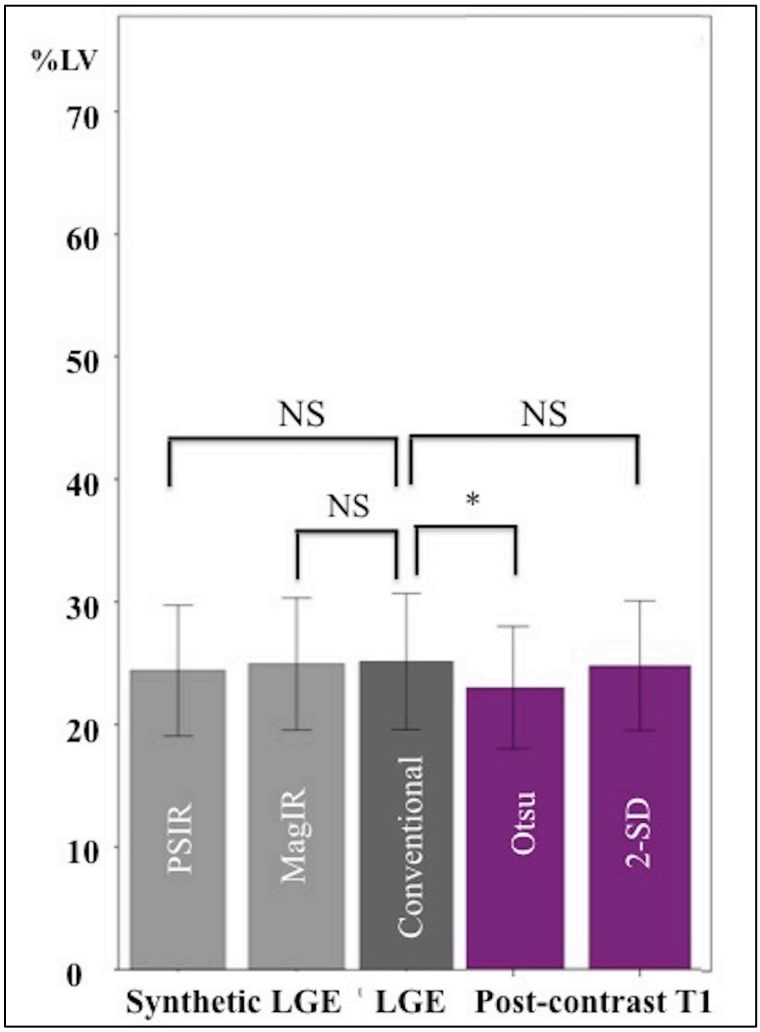

Figure 5-15: Comparison of MI size quantified by the different techniques.

This figure illustrates MI size by the conventional LGE, synthetic LGE and post-contrast T1 mapping and AAR by T2 and T1 mapping.

*NS denotes no statistical difference and * denote P<0.05. Data presented as mean ± 95%CI.*

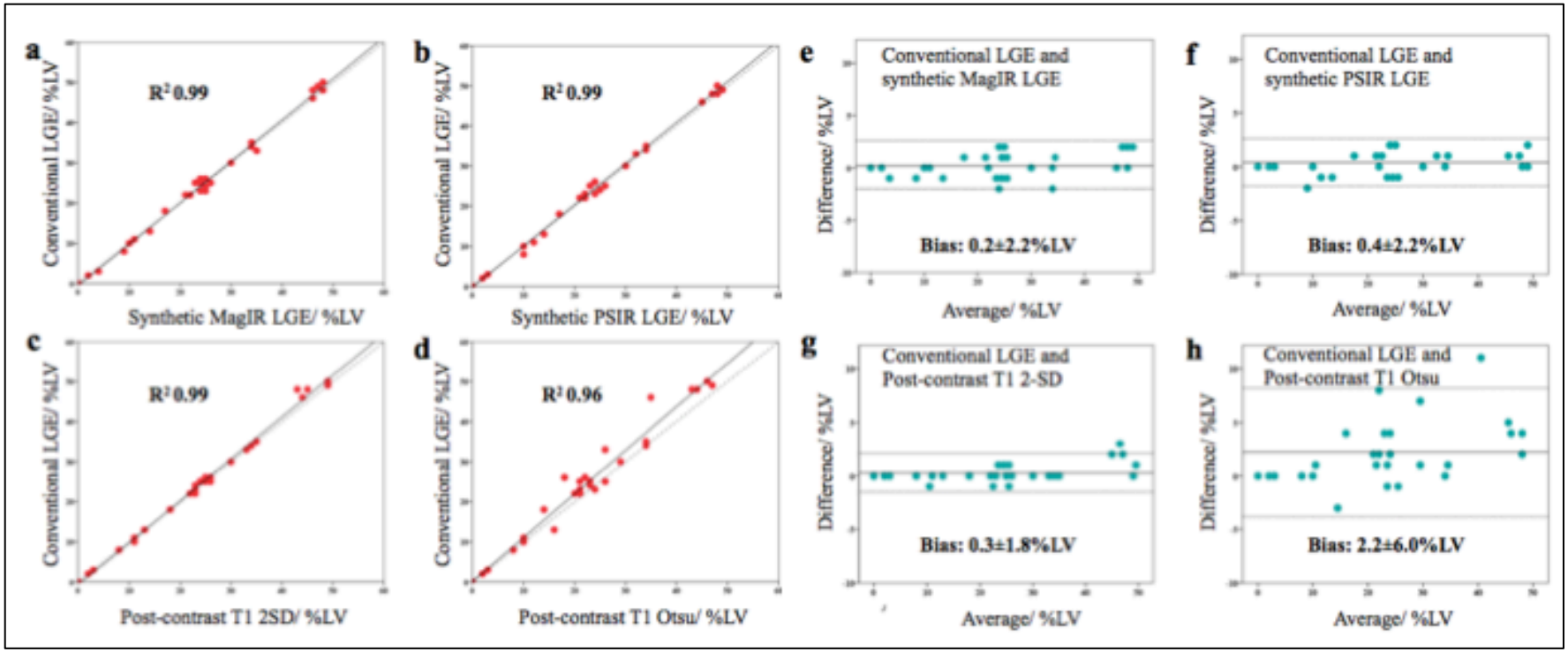

Figure 5-16: Comparison of MI size by different methods against the reference standard.

These are the correlations (a-d) and Bland-Altman analyses (e-h) of MI size by conventional LGE against each of the 4 other techniques (synthetic MagIR LGE, synthetic PSIR LGE, post-contrast T1 2-SD and post-contrast T1 Otsu).

Table 5-8: Comparison of acute MI size quantification by the different techniques.

Reference/ %LV	Other Techniques/ %LV	P value	R^2	ICC (95%CI)	Bias±2SD/ %LV
Acute MI size					
MI_{Conv} 25.1±14.3	$MI_{SynthMagIR}$ 24.9±13.8	0.35	0.99	0.996 (0.992-0.998)	0.2±2.2
	$MI_{SynthPSIR}$ 24.7±13.9	0.060	0.99	0.996 (0.992-0.998)	0.4±2.2
	$MI_{T1Post2SD}$ 24.9±13.8	0.10	0.99	0.996 (0.991-0.998)	0.3±1.8
	$MI_{T1PostOtsu}$ 23.0±12.9	0.001*	0.96	0.964 (0.859-0.987)	2.2±6.0

ICC: intraclass correlation coefficient; SD: standard deviation; MI: myocardial infarction; Conv: conventional; SynthMagIR: synthetic magnitude reconstructed inversion recovery; SynthPSIR: synthetic phase sensitive inversion recovery.

5.4 Discussion

We have demonstrated that T1 mapping CMR can perform as well as T2 mapping to delineate the AAR in reperfused STEMI patients. There was an excellent correlation and agreement between T1 and T2 mapping in delineating the AAR in both cohorts. This data confirms the findings of the pre-clinical study by Ugander et al (131) in the reperfused canine heart. Both T1 and T2 mapping CMR were equally prone to susceptibility artefacts at 3T and equally affected by MVO. The acquisition times for both mapping sequences were similar on both scanners.

We have also shown that T1 and T2 maps obtained at day 4 following a reperfused STEMI detected the presence of IMH with high specificity and sensitivity compared to the reference standard method using T2* maps. The binary assessment of presence or absence of a hypo-intense core performed as well as the quantitative assessment of the actual T1 and T2 values of the

hypo-intense core. However, T2* maps are still the modality of choice when available as the accuracy for T1 and T2 maps to detect IMH was only 87% and 85%, respectively. T1 and T2 maps provide an alternative option for the detection of IMH when T2* imaging is not available. T1 and T2 mapping performed equally well to detect early and late MVO.

Lastly, we have also showed that acute MI size can be accurately quantified from the post-contrast T1 maps (2-SD) and the synthetic LGE images when compared to conventional LGE imaging.

5.4.1 T1 mapping versus T2 mapping for the AAR

Langhans et al (133) recent looked at the reproducibility of the AAR by T1 and T2 mapping against SPECT in 14 patients with reperfused STEMI at 1.5T. Although good correlations with SPECT were reported (R=0.94 for T2 and 0.91 for T1-derived AAR), direct comparison between the two mapping techniques was not performed in terms of per slice correlation, agreement and inter and intra-observer variability.

We found that the Otsu threshold method performed best with excellent inter-observer and intra-observer variability for both mapping techniques. The algorithm automatically divides the signal intensity histogram into two classes and requires minimal user input compared to manual delineation, SD threshold and full width half maximum techniques. It automatically calculates an optimal threshold (179) and has previously been shown to be more accurate and reproducible for quantifying acute MI size by CMR.(180) However, this

technique fails in those with a higher burden of IMH (4% in our cohort) and in those situations manual input is required. Furthermore, normal slices (normal T1 and T2 values, no wall motion abnormalities on cines) need to be manually selected as normal.

Currently, it would appear that T1 and T2 mapping could be used interchangeably to assess the AAR in reperfused STEMI patients. In studies investigating post-contrast T1 and ECV in acute MI patient, there is the possibility of shortening the scanning time by omitting T2 maps as the T1 maps would be available for AAR quantification. However, T1 mapping may not be suitable in acute myocardial infarction patients who also have a chronic infarct in the remote myocardium. T1 mapping CMR has recently been shown to identify chronic infarct with high diagnostic accuracy (273) in a canine model, and using this technique in these patients would require taking into account areas of chronic infarct in the remote myocardium. Our study excluded patients with previous infarct and therefore we cannot comment on the performance of T1 mapping over T2 mapping in patients with co-existing chronic infarcts. From an MR physics point of view, these two techniques are assessing different properties of the myocardium and may explain the limits of agreement of around 10% on a per-slice comparison and of around 5% on a per-patient comparison and more work remains to be done to establish the advantage of one mapping sequence over the other.

5.4.2 T1 mapping versus T2 mapping for the detection of IMH

T1 and T2 mapping performed equally well to detect early and late MVO. This is not surprising for late MVO as most patients with late MVO also had IMH in our cohort. Although numerically the AUCs were higher for the detection of early MVO than late MVO, ROC curves comparison did not show a statistical significance. T1 and T2 mapping could differentiate between early MVO with and without IMH and predominantly those with IMH displayed late MVO. Early MVO likely represents a spectrum of aetiologies for microvascular injury and late MVO with IMH representing the most severe form. A recent study (274) using a porcine model of MI showed that T2-STIR imaging could not discriminate between IMH and MVO but imaging was performed at 8 days and no T2* data were acquired. Given the recent evidence of the dynamic nature for the detection of the paramagnetic properties of IMH (112), it is not possible to put the results of that study into context with our findings.

T1 of the infarct core was recently shown to be more prognostic than LV ejection fraction, infarct core T2 and IMH in a large cohort of STEMI patients.(156) Carrick et al (139) also showed that IMH was more closely associated with adverse LV remodelling than late MVO but their timing of CMR was a mean of 2.1 days and 87% of their patients with MVO had IMH. They also demonstrated the dynamic nature of MVO and IMH peaked at 2.9 days.(139) Whether performing CMR ≥ 3 days post PPCI (our study: mean of 4 days – 96% with MVO had IMH) may reveal more patients with MVO with IMH, which would have more prognostic significance, remains to be tested in future adequately powered studies.

The hypo-intense core on the T2 maps in reperfused STEMI patients has been thought to be due to IMH in previous studies.(98, 138) Pedersen et al (233) previously showed that T1-weighted inversion recovery images could detect IMH with high sensitivity and specificity in a porcine model of acute STEMI. However, in this work, we direct compared the diagnostic performance of T1 and T2 mapping to detect IMH against T2* mapping in the clinical setting.

The mechanism of the low signal within the areas of IMH has previously been attributed to the paramagnetic properties of haemoglobin breakdown products.(146) However, degradation of the extravasated erythrocytes to oxyhaemoglobin, deoxyhaemoglobin, and methaemoglobin (strongly paramagnetic) is dynamic and would exhibit different T1 and T2 properties at various stages as previously described by Bradley et al (158) in brain imaging. T2 is better at identifying deoxyhaemoglobin, whereas T1 is better at detecting methaemoglobin (158) and this may explain the small difference in sensitivities for T1 and T2 maps to detect IMH in our study. Breakdown of the erythrocyte membrane eventually leads to ferritin and haemosiderin deposits within macrophages.(146) Although T2* is the most sensitive to detect IMH, it is prone to motion artefacts due to relatively long breath-hold duration and this has led to the development of free-breathing T2* mapping using motion corrected averaging.(157) However this is not widely available yet and therefore T1 and T2 mapping, which is increasing becoming available in most centres performing STEMI research may be an alternative option to detect IMH and minimise patients dropping out of studies when T2* mapping was not acquired or were not interpretable.

The mechanism for a hypo-intense core on the T1 and T2 maps in patients without IMH but with MVO is not clear. It has been postulated that this may be due to a localized reduction in tissue water content due to obstruction of the capillaries by distal micro-thrombi embolisation and plaques and cellular debris and compression from extrinsic oedema.(98, 139) The alternative explanation could be that the hypo-intense core on the T1 and T2 maps may still represent IMH but the haemoglobin degradation products are not paramagnetic yet to be detected by T2* if imaged too early and more work remains to be done.

5.4.3 Post-contrast T1 mapping for acute MI size

Messroghli et al (186) has previously shown that post-contrast T1 mapping could detect both acute and chronic MI in a cohort of 24 patients but not all patients underwent coronary angiography prior to CMR and only 21% showed evidence of reperfusion. Bauner et al (187) had subsequently shown that post-contrast T1 could accurately detect chronic MI in 26 patients.

For MagIR synthetic LGE images, the negative values occurring at short TIs are reconstructed as positive and are used to reconstruct the single shot LGE images.(244) As a result, in situations when the TI is too short, the loss of polarity in the MagIR image will appear as an artifact. The PSIR technique preserves polarity and is therefore less sensitive to the TI. For PSIR synthetic LGE images, the polarity is restored and the window level can be

retrospectively leveled to display the normal myocardium as black while the MI will appear white.(263)

Synthetic LGE has also been shown to accurately quantify chronic MI size in a small cohort of patients (190), but in this study only one short-axis LV image was analysed. A previous conference abstract showed that synthetic PSIR LGE agreed well with conventional PSIR LGE in a small cohort of 17 patients with ischaemic and non-ischaemic scars.(275) In our study we performed full LV coverage and we have shown that post-contrast T1 maps can accurately quantify acute MI size (using the semi-automated 2-SD threshold) when compared to the reference standard in a cohort of reperfused STEMI patients. Using the SD technique for quantification can be variable depending on where the reference ROI is drawn. To minimise the error associated with this, we have used the automated ROI delineation option with minimal manual adjustment when required. Furthermore, we have also shown that the additional sets of IR images that can be obtained from the post-contrast MOLLI T1 maps can be used to obtain synthetic LGE images (both MagIR and PSIR) and can accurately quantify acute MI size. PSIR LGE is T1-weighted with retrospective nulling of the remote myocardium, thus being insensitive to the TI used for acquisition.(276) With the PSIR technique, the tissue with the longest TI nulls first, irrespective of the TI used (post gadolinium, the remote myocardium has the longest TI) and this sequence has previously been shown to improve MI detection more accurately by LGE compared to conventional MagIR LGE images.(277) Both synthetic LGE and post-contrast T1 map would delineate the MI zone equally well but the T1 maps would have higher spatial resolution than

the single shot SSFP synthetic images and the MI zone could be quantified on a pixel-wise basis. However, the quality of the T1 maps may be affect if there is significant motion between the single shot images that may fail to align well despite motion-correction. However, as it stands, to acquire synthetic LGE, post contrast T1 maps would also need to be acquired and therefore the synthetic PSIR output could complement post-contrast T1 maps for MI size quantification without the need for conventional LGE images.

5.4.4 Limitations

We only included a small number of patients and did not have histological validation of the AAR. We found the Otsu technique to perform best against Manual both at 1.5T and 3T but manual input was required when no oedema was present (using visual assessment of the coloured maps and cine images as reference), and when extensive MVO was present on the maps. The AAR delineated by contrast-enhanced SSFP cines in a multivendor, multi-centre setting, has been shown to perform well against T2-STIR imaging.(128) We did not acquire contrast-enhanced SSFP cines to compare against T1 and T2 mapping. The small sample size may account for the unusually high incidence of MVO (67%) when compared to the literature in the 1.5T cohort and could have been due to chance. A large number of the T2* maps were not interpretable in our study predominantly due to motion, flow and off-resonance artefacts and this highlights the challenge of performing a comprehensive CMR scan with multi-parametric mapping in acutely unwell STEMI patients (average

scanning time of 1 hour). The recent study by Carrick et al (139) also showed that 18% of T2* maps were not analysable either due to patient's intolerance of the scan or T2* maps being not evaluable. Histological validation for the low T1 and T2 of the hypo-intense core was not possible in this study and warrants further investigation. The large majority of our patients with MVO also had IMH. Therefore we could not assess whether the hypo-intense core on the T1 and T2 maps could differentiate between late MVO with IMH and late MVO without IMH. However, we did find a difference in the $T1_{Core}$ and $T2_{Core}$ between those with early MVO with IMH and early MVO without IMH and this needs to be confirmed in future studies. The conventional LGE scan (acquired 10-15 minutes post contrast) and post-contrast-T1 map (acquired 15-20 minutes post contrast) were acquired 5 minutes apart. But despite this, there was no difference in MI size. The TI range for the IR images generated in-line from the T1 maps was quite wide (200ms to 975ms and at 25ms increments). But off-line post-processing was not necessary and synthetic MagIR LGE images were interpretable and performed as well as conventional LGE for MI size quantification. Our sample size was small but still larger than previously published studies on synthetic LGE.(190) We used 2 different LGE read-outs (FLASH LGE in 22 patients and MOCO-FB LGE in 6 patients) for MI size quantification but both these sequences have been shown to perform equally well for MI size quantification.(278) Synthetic IR LGE is a single shot SSFP acquisition and therefore has lower spatial resolution than PSIR LGE. Therefore the synthetic IR LGE technique may be less useful in patients with small sub-endocardial scars and mid-wall fibrosis.

5.5 Conclusion

We have shown that T1 mapping CMR can accurately quantify the AAR delineated by T2 mapping in reperfused STEMI patients.

Furthermore, the presence of a hypo-intense core on T1 or T2 maps provides an alternative approach for the detection of IMH in situations when T2* maps are not interpretable or available. However T2* mapping currently remains the reference standard in the clinical setting and T1 and T2 mapping therefore may play a complementary role in future studies targeting IMH.

Finally, we have shown that post-contrast T1 mapping can accurately quantify acute MI size using post-contrast T1 maps or synthetic LGE outputs derived from those T1 maps. Therefore, conventional LGE imaging may be omitted in future studies when post-contrast T1 mapping is already being acquired.

6 Semi-automated quantification techniques for assessing acute and chronic myocardial infarction by CMR

6.1 Introduction

There is currently no established gold standard technique for quantifying MI size using LGE. Several different techniques have been proposed for quantifying acute and chronic MI size including manual contouring (176) and semi-automated threshold techniques such as a signal intensity threshold of 5-SD (177) or 6-SD (178) above the normal remote myocardium, the Otsu technique (180), and the FWHM (182, 183) technique. The consensus document from the Society for Cardiovascular Magnetic Resonance Board of Trustees Task Force on Standardized Post Processing recommends the semi-automated threshold technique of 5-SD for MI size quantification as it may improve reproducibility.(225) Manual contouring is considered the gold standard (57, 176) but may be time consuming (183, 184) and subjective. FWHM has emerged as the technique having the lowest variability (182, 183) but others have shown FWHM to underestimate acute and chronic MI size.(180, 185) Recently FWHM45% and 6SD were found to perform well in paired acute and follow-up scans at 3T.(185)

By convention, the FWHM technique (181) uses a threshold of above 50% of the maximal signal intensity of the ROI as the cut-off threshold and we hypothesized that areas previously occupied by MVO on the follow-up CMR are

likely to affect the highest signal intensity and impact on MI size quantification, compared to those without previous MVO. Therefore, the aim of our study was firstly to assess the impact of MVO on the performance of four most promising semi-automated techniques (5-SD, 6-SD, Otsu and FWHM) against manual contouring (referred to as Manual contouring throughout the chapter) as the reference standard (57, 176) in paired acute and follow-up CMR scans at 1.5T. Secondly, we aimed to assess the performances of acute MI size by these different techniques to predict the development of adverse LV remodelling (≥20% increase in end-diastolic volume).(197)

6.2 Methods

6.2.1 Study Population

40 STEMI patients from the 1.5T cohort with paired acute and follow-up CMR as described in the methodology section were analysed for this chapter.

6.2.2 Imaging acquisition

All CMR scans were performed on a 1.5 Tesla scanner (Magnetom Avanto, Siemens Medical Solutions) using a 32-channel phased-array cardiac coil. The imaging protocol included full LV coverage for short axis cines and LGE and automated ECV maps were available for reference (30 patients had full LV coverage and 10 patients had base, mid and apical short axis slices) as described in the methodology section.

Late gadolinium enhancement

LGE imaging was acquired using either a standard segmented 'fast low-angle shot' (FLASH) two-dimensional inversion-recovery gradient echo sequence or a free-breathing, respiratory motion-corrected (FB MOCO) single shot steady state free precession averaged inversion recovery sequence (263) between 10-15 minutes after 0.1 mmol/kg of Gd-DOTA (Dotarem).

6.2.3 Imaging analysis

All imaging analysis was performed using CVI42 software (Version 5.2.2[340], Calgary, Canada).

MI quantification

The endocardial and epicardial borders were manually drawn on all the LGE images. MI size was quantified using Manual contouring by HB (2 and a half years experience in STEMI CMR scans analysis) and expressed as the %LV. Areas of hypo-intense core of MVO were included as part of the MI zone. Minimal adjustments were also performed if artefacts were present in the remote myocardium and these artefacts were manually excluded.

Thresholds of 5-SD, 6-SD, Otsu and FWHM were applied on these LGE images with pre-drawn endocardial and epicardial borders to obtain corresponding MI sizes and expressed as %LV.

For 5-SD and 6-SD (to identify signal intensities of 5-SD and 6-SD above the mean normal remote myocardium respectively), a ROI was identified in the

normal remote myocardium using the automatic option from CVI42, with minimal manual adjustment when required to minimise intra-observer variability.

20 scans (10 acute and 10 follow-up) were randomly selected for intra-observer variability (performed by HB, 3 months apart) of MI size quantification by Manual contouring. Furthermore, the reproducibility of MI size by 5-SD and 6-SD when using manually drawn remote myocardial ROI and automatic remote myocardial ROI detection with minimal manual adjustment as illustrated in Figure 1 were compared.

For the FWHM technique (to identify signal intensities that are above 50% of maximal signal intensity of the reference ROI)(181), the automatic option was also used to delineate an ROI in the area of hyper-enhancement by LGE.

The Otsu technique (to identify the intensity threshold from the signal intensity histogram using the value with minimal intra-class variance between low and high intensities)(179) did not require any additional ROIs but did require user input to identify slices with no LGE as normal.

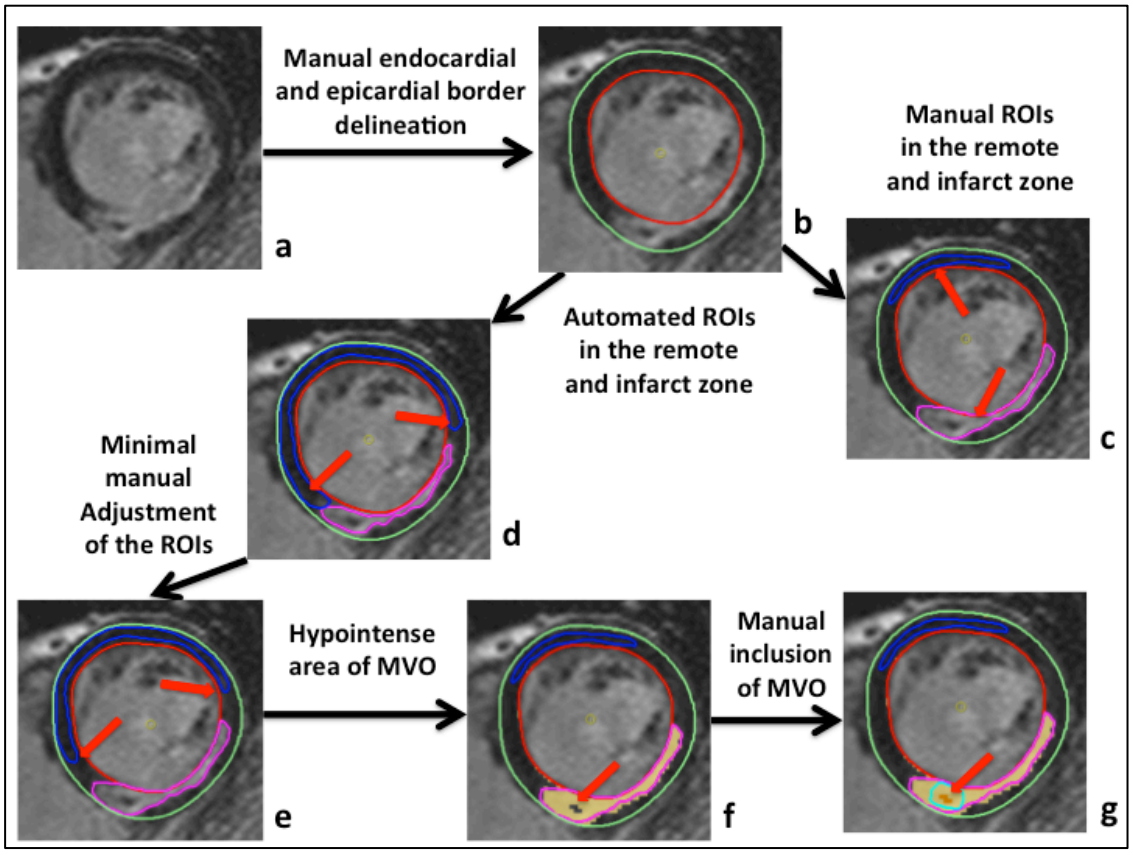

Figure 6-1: Figure 1: Illustration of the steps used in the quantification of MI size.

Endocardial and epicardial borders were first manually drawn (a to b). c illustrates the manual ROI delineation in the remote normal myocardium and Manual contouring of the MI (red arrows). d illustrates the automated ROI delineation. As shown by the red arrows in d, in this case, the ROIs need minimal manual adjustment (as shown in e by the red arrows) to make sure it was not in a segment containing LGE. Areas of MVO appears as a hypo-intense area (red arrow in f) and needed manual correction (red arrow in g) to include it as part of the MI.

Automated ECV maps

Manual ROI were drawn in the core of the MI zone (corresponding to areas of MVO in some patients with a hypo-intense core on the acute scan LGE) on the acute and matching ROIs were copied to the follow-up maps to obtained representative ECV values.

6.2.4 Statistical analysis

SPSS version 22 (IBM Corporation, Illinois, US) was used for the majority of the statistical analyses and MedCalc for Windows Version 15.6.1 (Medcalc Software, Ostend, Belgium) was used for ROC comparison using the technique described by Delong et al (272) Normality was assessed using Shapiro-Wilk test. Continuous data were expressed as mean ± SD or median (interquartile range). Groups were compared using paired Student t-test/ Wilcoxon signed rank test or unpaired Student t-test/ Mann-Whitney U test where appropriate. Categorical data were reported as frequencies and percentages.

Intra-observer reproducibility for Manual contouring and for 5-SD and 6-SD when using manual remote myocardial ROI delineation versus automatic remote myocardial ROI detection was assessed in 20 scans using ICC with 95% confidence intervals (95%CI) and Bland-Altman analysis (expressed as bias ± 2 SD for limits of agreement).

Inter-method precision and accuracy for MI size quantification was assessed as defined below:

Precision: A semi-automatic technique was considered precise when the inter-method coefficient of variability (CoV) (279) was < 10% and the ICC was > 0.900 (arbitrary cut-offs to denote good precision in the absence of a reference standard).

Accuracy: A semi-automatic technique was considered accurate when compared to Manual contouring if there was no statistically significant difference

between them on paired tests and no bias was present on Bland-Altman analysis.

ROC analyses were performed to assess the diagnostic performance for MI size by Manual contouring, 5-SD, 6-SD, Otsu and FWHM on the acute scan to predict adverse LV remodelling.

All statistical tests were two-tailed, and $P<0.05$ was considered statistically significant.

6.3 Results

The mean age of the STEMI patients was 59±13 years old and 88% were male. Further details regarding the patients' clinical, angiographic and CMR characteristics are listed in Table 6-1. The mean acute MI size was 25.0±13.7%LV (Manual contouring). The mean LVEF on the acute scan was 49±8% and at follow-up was 53±10%. As expected, there was a significant regression in MI size between the acute scan and the follow-up scan (25.0±13.7%LV versus 17.3±10.1%LV, $P<0.001$, percentage of MI regression: 32±20%). 26/40 (65%) patients had MVO on the acute scan. Figure 2 illustrates an example of MI size quantification by the 5 semi-automated techniques in a paired acute and follow-up LGE short-axis slice.

Table 6-1: Clinical, angiographic and CMR characteristics of the 40 STEMI patients.

Details	Number
Number of patients	40
Male (%)	35 (88%)
Age (age)	59 ±13
Diabetes Mellitus	8 (20%)
Hypertension	14 (35%)
Smoking	12 (30%)
Dyslipidaemia	14 (35%)
Chest pain onset to PPCI time (minutes)	267 [122-330]
Infarct artery (%) LAD RCA Cx	 24 (60%) 14 (35%) 2 (5%)
TIMI flow Pre/ Post PPCI (%) 0 1 2 3	 33 (83%)/ 1(3%) 0 (0%)/ 0 (0%) 3 (8%)/ 8 (20%) 4 (10%)/ 31 (78%)
CMR findings LV EDV/ml Acute Follow-up LV ESV/ml Acute Follow-up LV EF/% Acute Follow-up	 172±38 182±49 90±30 88±38 49±8 53±10

LV Mass/g	
Acute	112±35
Follow-up	104±26
Reference MI size/ %LV	
Acute	25.0±13.7
Follow-up	17.3±10.1
MVO/ %	26 (65%)

LAD: left anterior descending artery; RCA: right coronary artery; Cx: circumflex artery; TIMI: thrombolysis in myocardial infarction; CMR: cardiovascular magnetic resonance; LV: left ventricular; EDV: end diastolic volume; ESV: end systolic volume; EF: ejection fraction; MI: myocardial infarction; MVO: microvascular obstruction; AAR: area-at-risk.

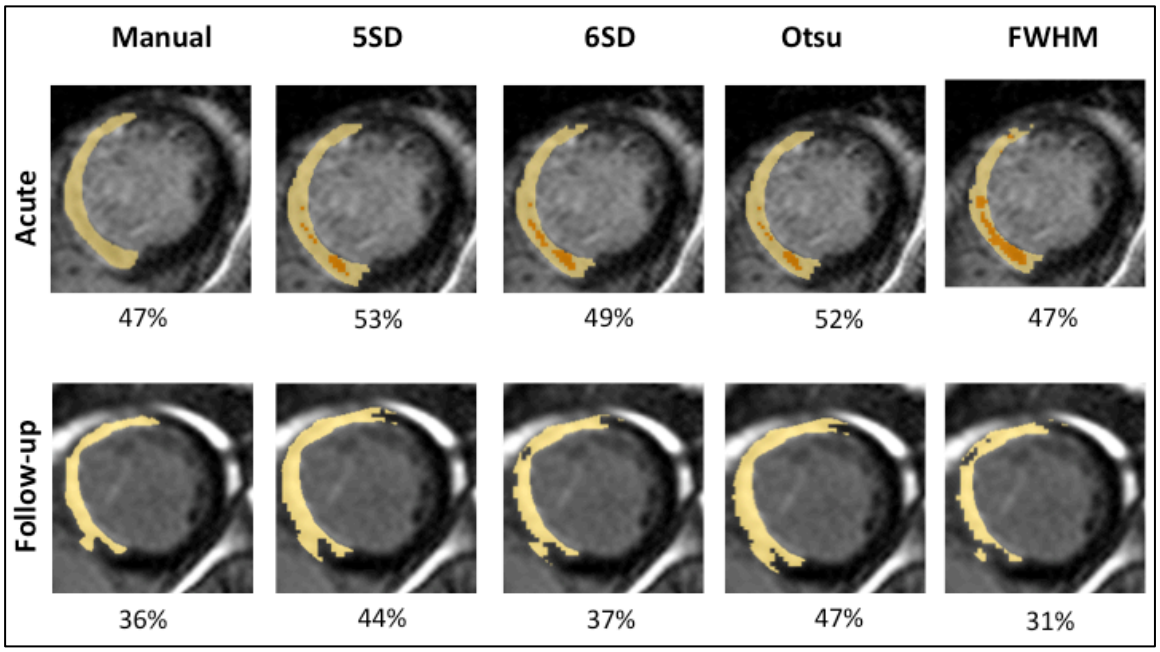

Figure 6-2: Acute and follow-up MI size quantification by different techniques.

This is an example of a paired acute (3 days) and follow-up (6 months) short axis LGE of a patient with an anterior STEMI reperfused by PPCI. This example highlights the presence of MVO on the acute scan (orange highlighted areas) and subsequent underestimation of MI size by FWHM on the follow-up scan.

6.3.1 Intra-observer variability

There was excellent intra-observer reproducibility for Manual contouring with an ICC of 0.996 (0.988-0.998) and no bias (0.5±2.2%LV, P=0.07).

There was also better intra-observer reproducibility for MI size quantification by the SD technique when automatic remote myocardial ROI delineation was used compared to manual drawing of remote myocardial ROI with a narrower 95%CI for the ICC and narrower limits of agreement on Bland-Altman analysis [manual remote ROI: ICC of 0.990 (0.981-0.995), Bias: 0.1±3.9%LV, P=0.09; automatic remote ROI: ICC of 0.999 (0.998-0.999), Bias: 0.2±1.2%LV, P=0.87].

6.3.2 Acute MI size quantification

Both 6-SD [CoV: 5.1%; ICC: 0.982 (0.966-0.991); MI size: 24.9±14.0%LV, P=0.81; bias: 0.1±5.2%LV] and FWHM [CoV: 6.4%; ICC: 0.970 (0.943-0.984); MI size: 24.1±13.1%LV, P=0.066; bias: 1.0±6.2%LV] precisely and accurately quantified acute MI size when compared to Manual contouring (25.0±13.7%LV). In contrast, both 5-SD [CoV: 6.8%; ICC: 0.971 (0.811-0.990); MI size: 27.4±14.6%LV, P<0.0001; bias: -2.4±5.0%LV] and Otsu [CoV: 8.4%; ICC: 0.953 (0.441-0.987); MI size: 28.4±13.9%LV, P<0.0001; bias: -3.4±5.2%LV] were precise but not accurate as they both overestimated acute MI size (Figure 3).

6.3.3 Chronic MI size quantification

Only 6-SD [CoV: 6.0%; ICC: 0.952 (0.911-0.974); MI size: 17.2±9.7%LV, P=0.88; bias: -0.1±6.2%LV] precisely and accurately delineated chronic MI size when compared to Manual (17.3±10.1%LV). As on the acute scan, 5-SD [CoV: 6.5%; ICC: 0.949 (0.752-0.982); MI size: 19.5±10.4%LV, P<0.0001; bias: -2.2±5.1%LV) and Otsu [CoV: 7.4%; ICC: 0.934 (0.788-0.973); MI size: 19.5±10.4%LV, P<0.001; bias -2.1±6.2%LV] were precise but not accurate as they overestimated chronic MI size. On the other hand, FWHM [CoV: 8.1%; ICC: 0.910 (0.755-0.957); MI size: 15.1±8.7%LV, P<0.001; bias: 2.2±7.1%LV) was precise but not accurate as it underestimated chronic MI size (Figure 6-3).

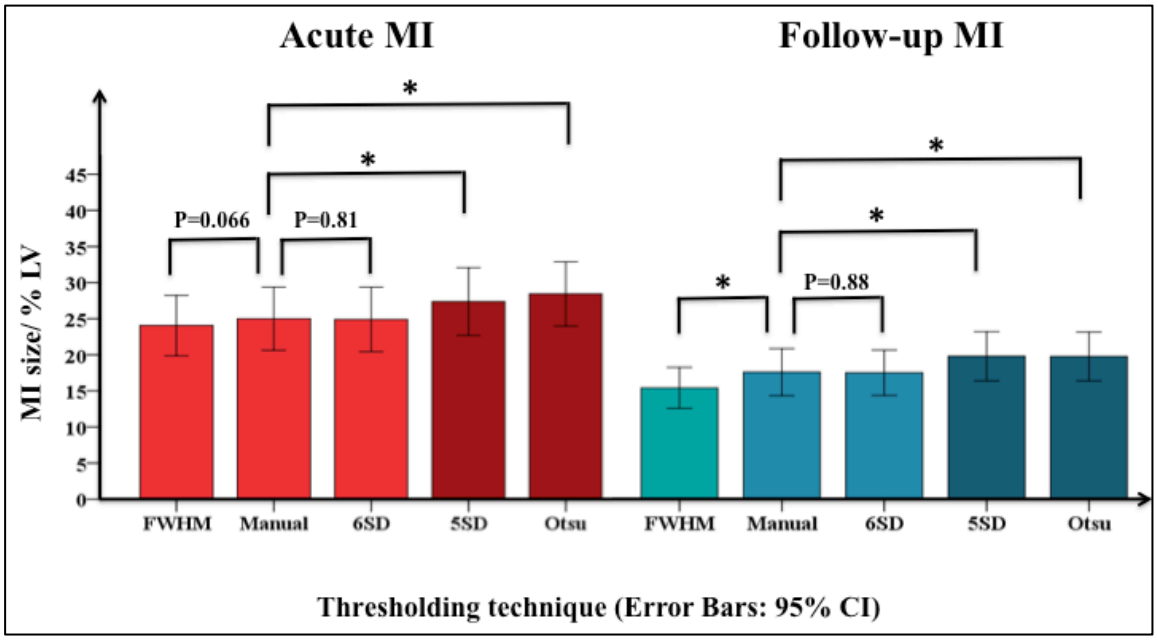

Figure 6-3: Comparison of acute and follow-up MI size quantification by different techniques

On the acute scan (red bars), MI size by FWHM and 6SD was similar to Manual whereas on the follow-up scan (blue bars), FWHM underestimated MI size and 6SD

remained similar to Manual. On the acute and follow-up scans, 5SD and Otsu overestimated MI size.

** Denotes statistically significant difference.*

6.3.4 Impact of MVO on MI size quantification

All patients with MVO (26/40) had complete resolution of the dark core on the LGE images on the follow-up scan. The percentage of MI size regression was significantly greater for those without MVO (with MVO: 27±17%, without MVO: 42±22%, P=0.028). As was the case for the whole cohort, there was no significant difference between FWHM, Manual contouring and 6-SD both for those with and without MVO, and 5-SD and Otsu overestimated acute MI size.

On the follow-up scan, FWHM remained similar to Manual contouring for those without previous MVO but underestimated chronic MI size only for those with previous MVO. The three other techniques maintained their previous relationship both for those with and without previous MVO: 6-SD was similar to Manual contouring but 5-SD and Otsu were significantly higher than Manual contouring. Further details for the comparison of MI size in those with and without MVO are available in Table 5-1 and the Bland-Altman plots in Figure 6-4.

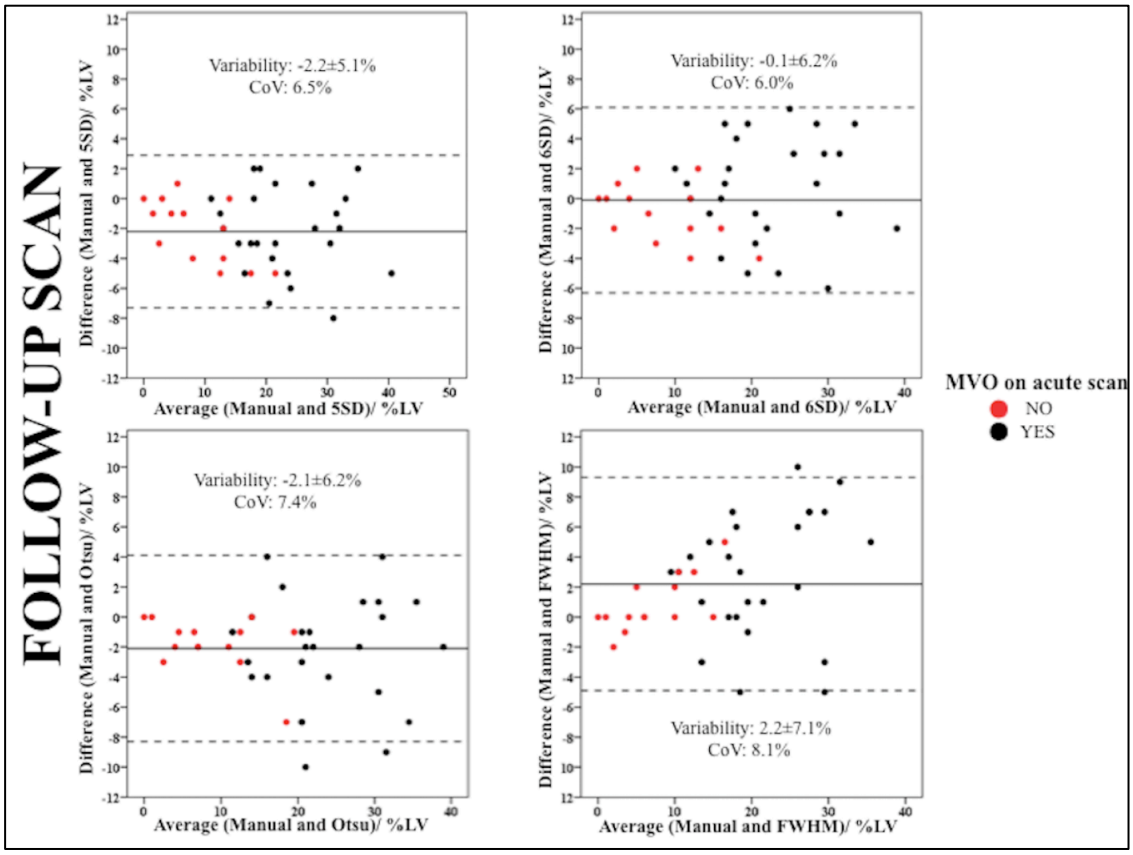

Figure 6-4: Bland-Altman plots of the chronic MI size using the 4 semi-automated methods against manual and differentiated by the previous MVO or no MVO on the acute scan.

The black dots represent patients with MVO on the acute scan and the red dots represent patients with no MVO on the acute scan. There was no bias between 6SD and Manual and all CoV were within acceptable limits. FWHM underestimated chronic MI size, especially in those with previous MVO. Both 5-SD and Otsu overestimated chronic MI size.

On the acute scan, the median ECV in the infarct core was 59 (40-72) % in those without MVO and was significantly higher than those with MVO [34 (28-40) %, P=0.02]. On the other hand, at follow-up, the median ECV in those with MVO on the acute scan was significantly higher than those without previous MVO. Figure 6-5 shows an example of 2 patients with paired acute and follow-up LGE and corresponding ECV map (Patient A had no MVO on the acute scan

and Patient B had a large area of MVO. The corresponding area of MVO on the follow-up scan had a very high ECV of 85%).

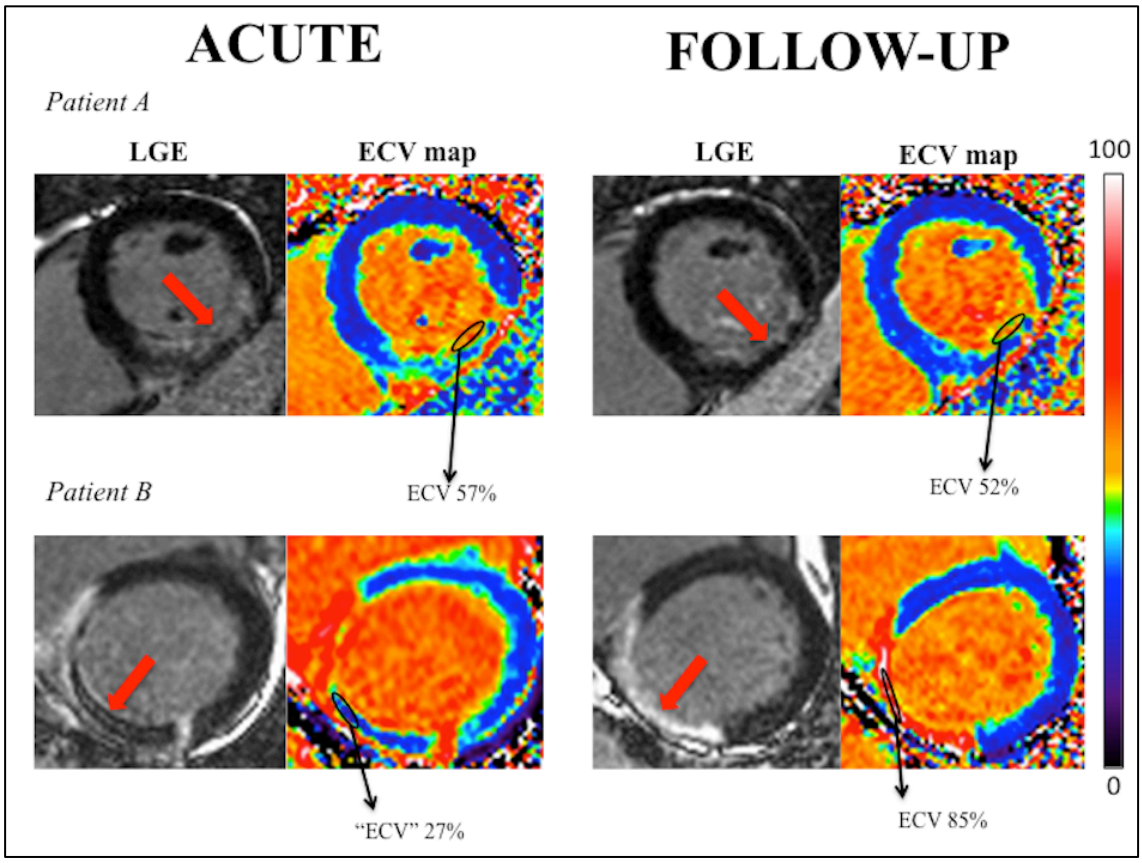

Figure 6-5: Paired LGE and automated ECV maps of 2 patients with and without MVO

Both patients presented with an inferior STEMI (red arrows). Patient A had no MVO on the acute scan and Patient B had a large area of MVO. The corresponding area of MVO on the follow-up scan had a very high ECV of 85% for Patient B compared to an ECV of 52 for Patient A.

6.3.5 Influence of LGE sequence on MI size quantification

The quantification methods were also compared for each subset of the LGE sequences (FLASH: n=16; FB MOCO: n=24). As for the whole cohort, 5SD and Otsu was significantly higher than Manual and 6SD was similar to Manual contouring for both LGE sequences on the acute and follow-up scans. FWHM was significantly lower than Manual contouring for both LGE sequences on the follow-up scans. However, on the acute scans, FWHM was similar to Manual for FLASH but significantly lower for the FB MOCO sequence (FB MOCO: Manual: 23.4±15.9%LV versus FWHM: 22.6±15.5%LV, P=0.001). Further details are shown in Table 6-2 and the Bland-Altman plots in Figure 6-6 below.

Table 6-2: MI size quantification using different LGE sequences

Manual	Other thresholds	P value	Manual	Other thresholds	P value
FB MOCO LGE sequence (n=16)					
Acute MI size/ %LV			**Chronic MI size/ %LV**		
23.4±15.9	5SD 26.3±17.4	0.02*	17.1±12.3	5SD 19.7±13.1	0.001*
	6SD 24.3±15.9	0.13		6SD 18.0±12.2	0.21
	Otsu 25.9±16.8	0.003*		Otsu 18.1±11.7	0.03*
	FWHM 22.6±15.5	0.001*		FWHM 14.3±9.7	0.005*
FLASH LGE sequence (n=24)					
Acute MI size/ %LV			**Chronic MI size/ %LV**		
26.0±12.2	5SD 28.1±12.8	<0.0001*	17.5±8.5	5SD 19.3±8.7	0.001*
	6SD 25.3±12.1	0.15		6SD 16.7±7.8	0.25
	Otsu 30.1±12.1	<0.0001*		Otsu 20.3±9.7	0.001*
	FWHM 25.0±11.5	0.24		FWHM 15.7±8.2	0.033*

FB MOCO LGE: free breathing and motion corrected late gadolinium enhancement; MVO: microvascular obstruction; MI: myocardial infarction; LV: left ventricle; SD: standard deviation; FWHM: full width half maximum; FLASH LGE: fast low angle shot late gadolinium enhancement.

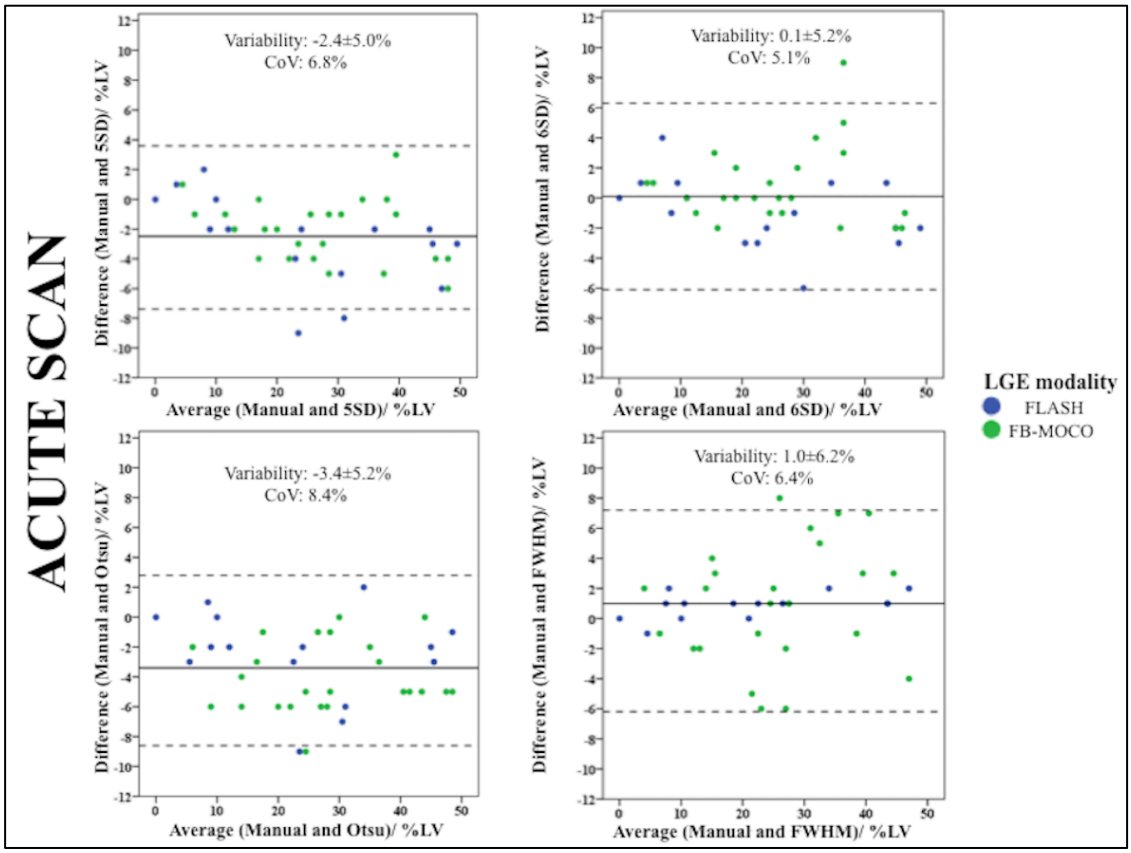

Figure 6-6: Bland-Altman plots of the acute MI size using the 4 semi-automated methods against Manual and differentiated by the LGE sequence used.

The blue dots represent patients with FLASH LGE sequence and the green dots represent patients with FB MOCO LGE sequence. There was no bias between 6SD and Manual and FWHM and Manual and all CoV were within acceptable limits. However, compared to Manual, FWHM was dependent of the LGE sequence used. Both 5-SD and Otsu overestimated acute MI size.

6.3.6 Acute MI size quantification and adverse LV remodelling

8/40 (20%) patients developed adverse LV remodelling. The diagnostic performances of Manual contouring, 5-SD, 6-SD, Otsu and FWHM were all very high with all 5 AUC of ≥ 0.90 as shown in Table 6-3 and Figure 6-7. ROC comparisons showed no significant differences between them (Manual

contouring versus: 5-SD, P=0.14; 6-SD, P=1.0; Otsu, P=0.14; FWHM, P=0.56). The sensitivities and specificities and cut-off values for acute MI size to predict adverse LV remodelling by the different techniques are listed in Table 6-3 below.

Table 6-3: Performance of the 5 techniques for quantifying acute MI size on predicting adverse LV remodelling at follow-up.

Acute MI quantification	AUC (95%CI)	Sensitivity/ %	Specificity/ %	Acute MI cut-off value/ %LV
Manual contouring	0.93 (0.82-1.00)	88	91	37
5-SD	0.91 (0.79-1.00)	88	87	38
6-SD	0.90 (0.83-1.00)	88	95	35
Otsu	0.90 (0.77-1.00)	88	91	41
FWHM	0.92 (0.80-1.00)	88	95	35

MI: myocardial infarction; AUC: area under the curve; CI: confidence interval; LV: left ventricle; SD: standard deviation; FWHM: full width half maximum.

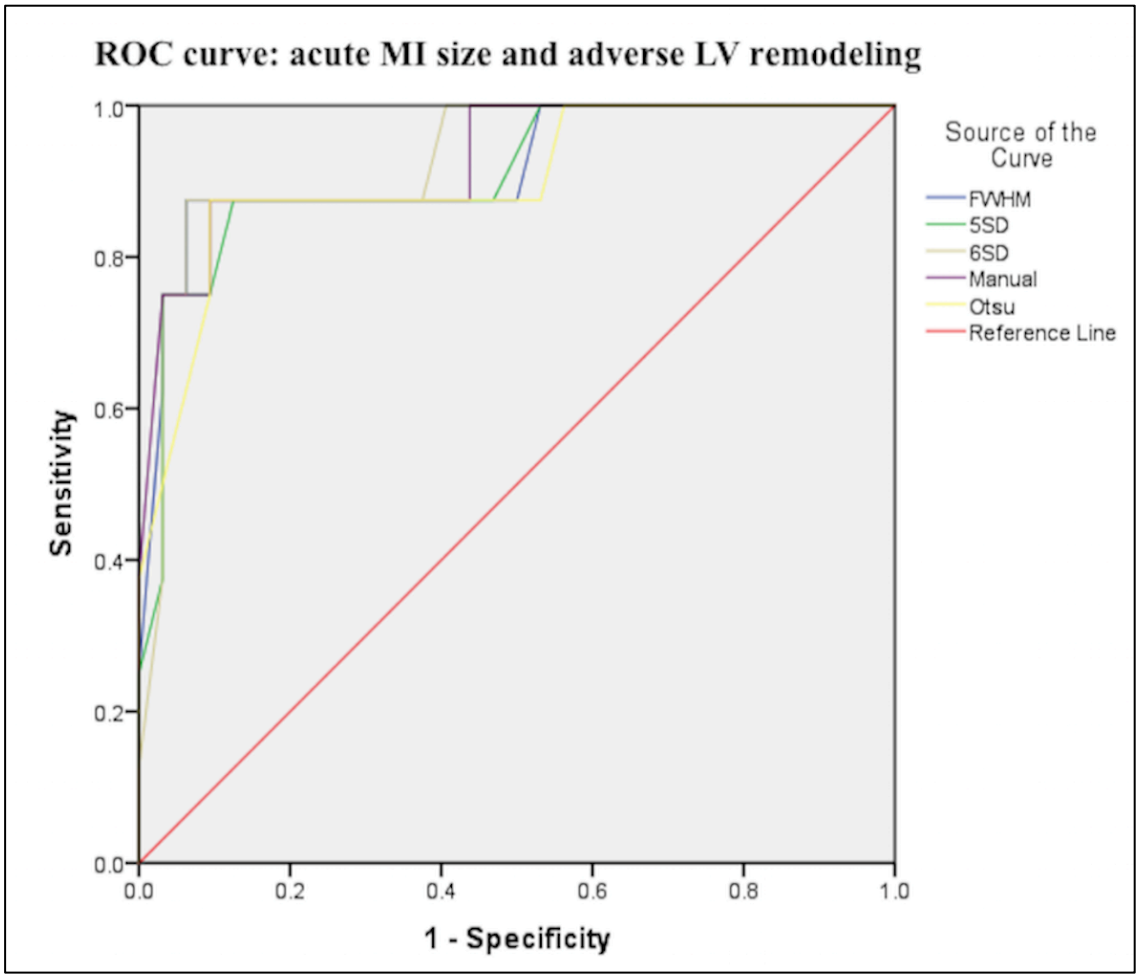

Figure 6-7: ROC curves for acute MI size by 5 techniques to predict adverse LV remodelling.

This is the ROC curves comparison to assess the diagnostic performance of the 5 quantification techniques to predict adverse LV remodelling.

6.4 Discussion

The main findings from this study are: (a) the 6-SD technique was as accurate as Manual contouring in quantifying acute and chronic MI size, irrespective of the LGE acquisition sequence used, whereas the FWHM only performed as well as Manual for FLASH and underestimated acute MI size by

FB MOCO LGE sequence. (b) FWHM underestimated chronic MI size and this predominantly occurred in patients with MVO on the acute scan. These patients had very high ECV of the MI core that was previously occupied by MVO compared to those without previous MVO. (c) 5-SD and Otsu consistently overestimated both acute and chronic MI size when compared to Manual contouring; (d) All 4 semi-automated techniques were precise (all with acceptable CoV and excellent inter-method agreement), and on the acute scan, they all performed equally well to predict the development of adverse LV remodelling.

There are several implications from our study. Firstly, 6-SD is the most suitable semi-automated technique in studies where accurate quantification of acute MI size is important (e.g. randomised controlled trials assessing the effectiveness of cardioprotective therapies on reducing acute and chronic MI size), as it performed as well as Manual contouring. Secondly, the performance of FWHM against Manual is influenced by the LGE sequence used and in studies requiring an accurate quantification of chronic MI size as an endpoint, 6-SD would be preferred to FWHM given that the latter appeared to underestimate chronic MI size especially in patients who had MVO on the acute scan. Thirdly, for those clinical studies only requiring precise (good agreement but with some residual bias) MI size quantification, such as registries or prospective observational studies, and for those aiming to assess other surrogate markers such as LVEF or adverse LV remodelling, any of these 4 semi-automatic techniques may be acceptable for quantifying MI size.

The reason for FWHM underestimating chronic MI size was due to the very high signal intensities on the follow-up scans in the location previously occupied by MVO on the acute scan. The likely explanation is that resorption of the MVO results in a relatively large interstitial space. These spaces are filled with contrast at a higher concentration than the surrounding scar tissues and displayed higher signal intensity than those without previous MVO as shown by the ECV maps. The “ECV” of the MVO on the acute scan was low but this was a reflection of the inability of LGE to penetrate areas of MVO and failure to achieve pseudo-equilibrium rather than a true MVO ECV value. As the FWHM uses the signal intensities that are above 50% of the maximal signal intensity within the scar, some of the scar tissue with “intermediate” signal intensities may have been classified as having signal intensities within “normal” range in these patients, resulting in an underestimation of chronic MI size.

Several studies have investigated the optimal technique for MI size quantification and these are summarised in Table 9-1. Manual contouring is considered the reference standard (57, 176) and in experienced hands, has been shown to have the lowest variability.(176) However, the manual delineation of MI size can be time consuming.(183, 184) A semi-automated technique is highly desirable as this would improve workflow considerably and would be more objective. Although FWHM has consistently been shown to be more reproducible (176, 180, 182, 183), other studies have shown FWHM to underestimate acute and chronic MI size.(180) (185) Recently FWHM45% (185) instead was found to be similar to Manual in chronic MI. However, not all

specialist software for MI size quantification allows the adjustment of the signal intensity threshold for the FWHM technique.

We showed that in patients with MVO on the acute scan, FWHM underestimates chronic MI size on the follow-up scan at 5 months and provided some mechanistic insights using automated ECV maps. Beek et al (178) previously showed that 6-SD had the highest accuracy to predict segment wall recovery in a cohort of chronic MI patients with hibernating myocardium. Flett et al (182) showed no difference between Manual contouring and 6-SD in both their acute and chronic MI cohorts and Dash et al (280) in a conference abstract showed that 6-SD was the most accurate to quantify MI size in a porcine model when compared to histology. Most recently, Zhang et al (185) have also shown that 6SD was similar to Manual contouring for both acute and follow-up MI size at 3T. However they did not compare Otsu in their study and they did not investigate the impact of MVO. We assessed the performance of the 4 most promising semi-automated techniques against Manual in paired acute and follow-up scans and our findings of the 6-SD technique being the most robust is consistent with some of the previous studies.(178, 182, 185, 280) McAlindon et al (176) recently showed that Manual contouring provided the lowest inter-observer, intra-observer and inter-scan variability, but they did not assess 6-SD in their study. Of note, our intra-observer reproducibility for Manual contouring was similar to their study. However, Khan et al (183) recently showed 6-SD to be higher than Manual contouring in acute MI size quantification, but they only included 10 patients and the remote myocardial ROI was manually drawn. We

used the automatic option for ROI delineation with minimal user input when required and we showed that the reproducibility of the n-SD technique is improved when using this approach.

6.4.1 Limitations

We only compared 4 semi-automated techniques against Manual contouring but we specifically chose those techniques with the most promising results so far and that are widely available in most commercial software for MI size quantification. The automated method previously shown to be very promising and accounts for partial volume effect by Heiberg et al (281) is only available from one CMR analysis software and we were not able to include it in this study using CVI42. We did not perform intra-observer and inter-observer variability for all techniques as this has already been performed in several previous studies (176, 180, 182, 183, 185) and was not the main focus of our study. We used Manual contouring as the reference standard (176) given that histological validation was not possible in this study. We were underpowered to assess the performance of these different semi-automated techniques on clinical outcomes and this warrants further evaluation in larger studies. Despite using automated threshold techniques, user input was required if the automated reference ROIs in the remote myocardium were extending to the salvaged myocardium; when pixels with high signal intensity in the remote myocardium were enhanced due to artefact; or when the Otsu method were picking abnormalities in slices with no LGE. These user inputs would likely introduce

some intra-observer and inter-observer variability but would not affect the overall results in experienced hands.

6.5 Conclusions

The optimal semi-automated technique for the quantification of MI size depends on the research question. For randomised controlled trials requiring the accurate assessment of MI size, 6-SD would be preferred. However, for registries or observational studies where precise MI size quantification may be adequate, any one of the four techniques may be an acceptable semi-automated option.

7 Multi-parametric mapping CMR to provide insights into the pathophysiology of adverse LV remodelling post-reperfused STEMI

7.1 Introduction

Although improvements in evidence-based therapies during PPCI have substantially reduced mortality following an acute STEMI, the onset of heart failure is on the rise.(3, 4, 282) MVO occurs in up to 50% of reperfused STEMI patients (61), and approximately 40% of STEMI patients develop IMH (139) detected by CMR. Both MVO and IMH are associated with larger MI size, adverse LV remodelling and worse clinical outcomes.(60, 61, 149, 159, 161, 283, 284)

IMH and its iron degradation products have been shown to result in residual myocardial iron within the MI zone and have been proposed to have cytotoxic and pro-inflammatory effects on the myocardium(207) (208). In some STEMI patients, T2 values in the surrounding myocardium have been shown to be elevated on CMR performed 6 months post-PPCI.(91, 209) The aetiology of the persistently elevated T2 signal and its relationship to adverse LV remodelling remains to be determined.

Whether changes in the ECM in the non-infarcted remote myocardium in STEMI patients reperfused by primary PPCI is linked to adverse LV remodelling remains incompletely understood.(197, 210-213) Although native T1 mapping (197) and post-contrast T1 mapping (213) CMR have been used to interrogate

the remote myocardial ECM, the availability of automated ECV mapping CMR provides a more robust method for quantifying not only focal fibrosis but also diffuse interstitial expansion in the myocardium (216, 217) as the native and post-contrast T1 maps are co-registered and motion-corrected, thereby improving the quality of the generated automated maps.(218)

We aimed to use multi-parametric mapping CMR to provide further insights into the pathophysiology of adverse LV remodelling in reperfused STEMI patients in order to identify potential future therapeutic targets. We hypothesized that patients with adverse LV remodelling were more likely (a) to have MVO/IMH on the acute scan; (b) to have residual iron at follow-up; (c) to have persistently high T2 around areas of residual iron that may suggest delayed infarct healing due to ongoing inflammation; (d) and have higher ECV in the remote myocardium due to remote compensatory changes.

7.2 Methods

7.2.1 Study Population

40 STEMI patients reperfused by PPCI from the 1.5T cohort with paired acute and follow-up CMR scans described in the methodology section were included in the analysis for this chapter.

20 age and sex-matched healthy volunteers served as control (all free of cardiovascular disease). All participants were scanned at the same centre and on the same scanner.

7.2.2 CMR acquisition

CMR was performed on a 1.5 Tesla scanner (Magnetom Avanto, Siemens Medical Solutions) using a 32-channel phased-array cardiac coil as described in the methodology section.

In the 1.5T STEMI cohort all patients had T2 maps acquired from base to apex during the acute scan. As for native T1 and post-contrast T1 maps, 30 patients had full LV short axis coverage and the remaining 10 patients had three (basal, mid and apical) left ventricular short axis T1 maps acquired during both scans.

The 20 healthy volunteers had one mid ventricular short axis native T1, T2 and post-contrast T1 maps acquired. All participants had full LV coverage for LV short axis cines and LGE acquired.

Figure 7-1 shows an example of the basal short axis images acquire during the acute scan and at follow-up in a patient with an inferior STEMI.

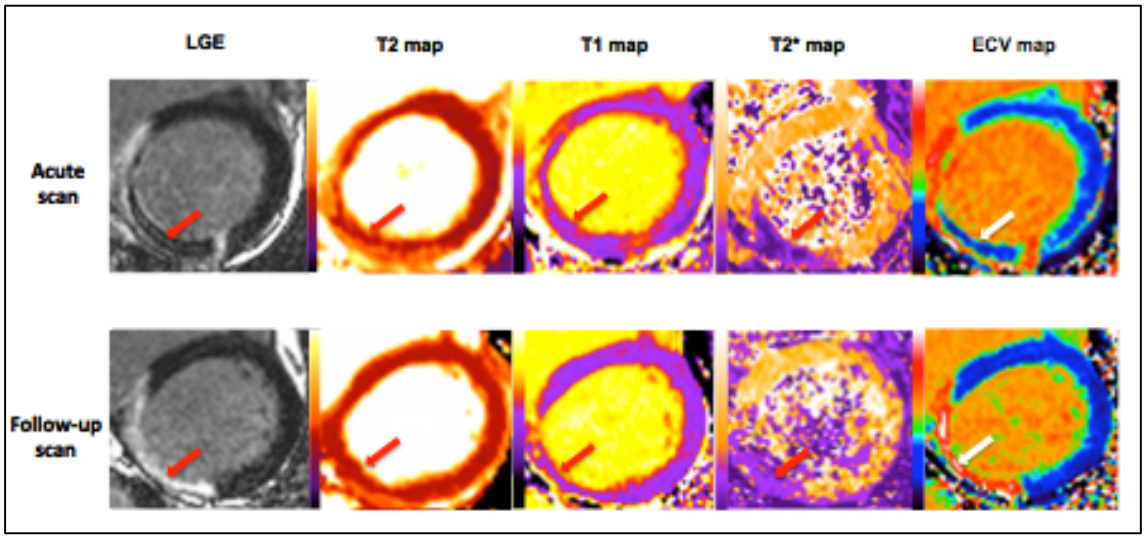

Figure 7-1: Multiparametric map acquisition.

Basal left ventricular short axis of a patient with an acute inferior MI depicting MVO on LGE scans with corresponding hypo-intense cores (red and white arrows) on the basal LV short axis T1, T2, T2 and ECV maps and the follow-up scan with corresponding maps and areas of residual myocardial iron on the T2* map.*

7.2.3 CMR analysis

Imaging analysis was performed using CVI42 software (Version 5.2.2[340], Calgary, Canada) as described in the methods section.

7.2.3.1 LGE and AAR quantification

MI size was quantified as a percentage of the LV (%LV) using signal intensity threshold of 5-SD (57) above the mean remote myocardium. The presence of MVO (late MVO) was defined as areas of hypo-enhancement on the LGE images, and was quantified and expressed as %LV. Areas of MVO were included as part of the MI zone and AAR.

Once the above method was used to highlight the LGE area, the anterior and inferior RV insertion points were identified and using a dedicated tool on CVI42, the transmural extent of LGE was obtained quantitatively (by averaging the values from 100 chords from each slice, which was done automatically) to obtain the mean transmural extent of LGE for each of the 16 AHA segments (Figure 7-2).

Adverse LV remodelling was defined as a ≥20% increase in LV end-diastolic volume (LVEDV) between the acute and follow-up scans.(193, 194, 197)

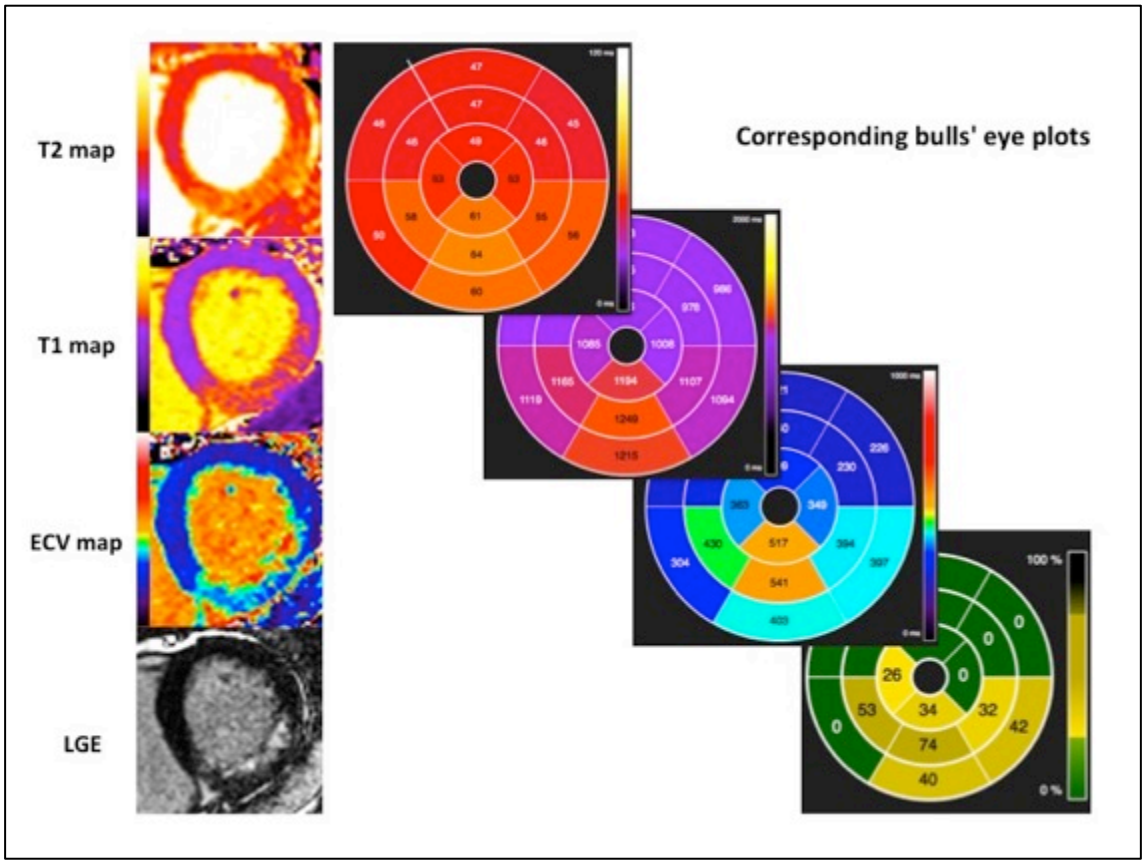

Figure 7-2: Example of generated bull's eye plots with AHA segments from the maps and LGE images.

7.2.3.2 Analysis of IMH and residual iron

A hypo-intense core on the T2* maps with a T2* value of <20ms was used to identify the presence of IMH on the acute scans and "residual myocardial iron" on the follow-up scans.(150, 153, 156, 285, 286) The extent of IMH and residual iron was quantified using manual ROI delineation around the hypo-intense core on the basal, mid and apical slices and expressed as %LV.

For the follow-up T1 and T2 maps, a ROI was manual drawn in hyper-enhanced areas using a signal intensity threshold of 2SD from the remote

myocardium (using the LGE images as reference) and was denoted as $T1_{Infarct}$ and $T2_{Infarct}$ respectively.

A second ROI was copied from the hypo-intense core of the T2* map on to the T1 and T2 maps and denoted as $T1_{Core}$ and $T2_{Core}$ as illustrated in Figure 7-3.

In cases when there were no areas of hyper-enhancement on the follow-up maps using a 2SD threshold, a ROI from the areas of LGE was copied on to the maps for representative values. An ROI was also drawn in the remote myocardium and expressed as $T1_{Remote}$ and $T2_{Remote}$.

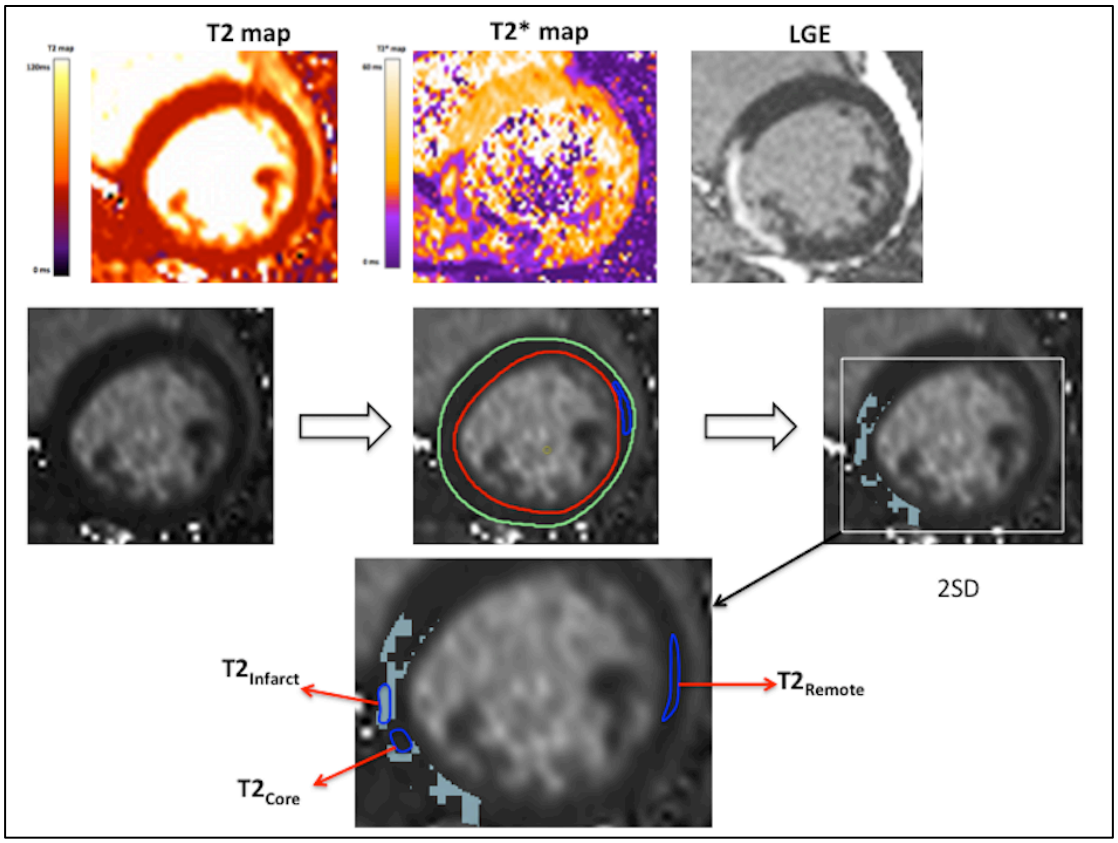

Figure 7-3: Quantification of follow-up T2 maps.

Method used to detect the area of high T2 ($T2_{Infarct}$) around the area of residual myocardial iron ($T2_{Core}$) and the remote myocardium ($T2_{Remote}$) using a threshold of 2SD from the remote myocardium.

7.2.3.3 Analysis of the T1, T2 and ECV maps

The endocardial and epicardial borders were manually delineated on the native T1 maps and T2 maps and copied on the ECV maps. The left ventricular outflow track and apical LV short axis slices were excluded and a 10% erosion of the wall thickness was applied to the endocardial and epicardial borders to minimise partial volume effects. Mean segmental T1, T2 and ECV values were then generated and displayed as a Bull's eye plots using the 16 AHA segments (Figure 7-2). For assessing inter-method agreement, in 10 patients, manual ROI were also drawn with care to avoid partial volume effects in the remote myocardium and the infarcted segments for comparison with mean segmental values for ECV. The remote myocardium was defined as the AHA segment 180^{o} from the infarct territory with normal wall motion and no LGE. T1, T2 and ECV values in the remote myocardium were represented by $T1_{Remote}$, $T2_{Remote}$ and ECV_{Remote}. T1 values of the core ($T1_{Core}$) of the infarct were obtained by manually drawing the ROI within the hypo-enhanced regions inside areas of hyper-enhancement within 2SD of the remote myocardium on the T1 maps and were represented as $T1_{Core}$. Mean segmental ECV of the infarcted segments was represented as $ECV_{Infarct}$.

7.2.4 Statistical analysis

Statistical analysis was performed using SPSS Version 22 (IBM Corporation, Illinois, US). Continuous data was expressed as mean ± SD or median [interquartile range] and categorical data was reported as frequencies and percentages. Normality was assessed using Shapiro-Wilk test. Independent groups (those with and without IMH; with and without paired CMR scan; with and without residual iron at follow-up; with and without adverse LV remodelling; without adverse LV remodelling but with and without residual iron) were compared with unpaired Student t-test for normally distributed parameters and with Mann Whitney U test for non-normally distributed parameters. Comparison between paired acute and follow-up scans were performed using paired Student t-test for normally distributed parameters and Wilcoxon signed rank test for non-normally distributed parameters. To compare T1 and T2 values in the remote, core and infarct territories between patients and divided between those with and without residual iron, a linear mixed model was used with the patients as a random factor and the territory within patients (remote, core, infarct) being a fixed factor. Comparison of 3 independent groups (no residual iron, residual iron only, residual iron and adverse LV remodelling) was performed using Kruskal-Wallis test and post hoc pairwise comparisons. Categorically variables such as incidence of MVO or IMH were compared using Chi square test or Fisher's exact test. Pearson rho correlation coefficient was assessed between MVO, acute MI size, IMH and adverse LV remodelling as a continuous variable respectively and their correlations were compared. ROC curve was also used to compare the diagnostic performance of MVO, acute MI

size and IMH to predict adverse LV remodelling. All statistical tests were two-tailed, and P <0.05 was considered statistically significant.

7.3 Results

The 40 patients with paired acute and follow-up CMR from the 1.5T cohort were used for this chapter and their characteristics are listed in Table 7-1. CMR details of these 40 patients are shown in Table 7-2. The median chest pain onset to PPCI time was 267 (122-330) minutes. The MI size was 27.4±14.6%LV. MVO was present in 65% (26/40) of patients (mean MVO size among those with MVO was 13.6±7.2%LV). In 24% of the patients, the paired T2* maps (acute and follow-up) had to be excluded as they were not interpretable due to motion and off-resonance artefacts.

Table 7-1: Clinical characteristics of STEMI patients.

Details	Number
Number of patients	40
Male (%)	35 (88%)
Age (age)	59 ±13
Diabetes Mellitus	8 (20%)
Hypertension	14 (35%)
Smoking	12 (30%)
Dyslipidaemia	14 (35%)
Chest pain onset to PPCI time	267 (122-330)

(minutes)	
Infarct artery (%) LAD RCA Cx	 24 (60%) 14 (35%) 2 (5%)
Treatment – on discharge Dual antiplatelet therapy Beta blockers ACEI/ARB Statin MRA	 40 (100%) 40 (100%) 40 (100%) 39 (98%) 10 (25%)

LAD: left anterior descending artery; RCA: right coronary artery; Cx: circumflex artery; TIMI: thrombolysis in myocardial infarction; ACEI/ARB: angiotensin converting enzyme inhibitor/ angiotensin receptor blocker; MRA: mineralocorticoid receptor antagonist.

Table 7-2: CMR characteristics of STEMI patients

	Controls (n=20)	**Acute Scan (n=40)**	**Follow-up Scan (n=40)**	**P value**
EDV/ml	148±34	172±38	182±49	0.027
ESV/ml	55±16	90±30	88±38	0.60
EF/%	63±5	49±8	53±10	0.001
LV Mass/g	108±21	112±35	104±26	0.051
LV wall thickness in remote myocardium – diastole/mm	7.2±0.7	7.1±1.3	6.7±1.3	NS
LV wall thickness in remote myocardium – systole/mm	12.0±1.3	12.0±1.8	11.2±1.8	NS
LV wall thickening in remote myocardium / %	66±14	77±40	75±26	NS
LV wall motion in remote myocardium/mm	7.7±2.5	9.2±2.6	8.9±2.6	0.04† 0.10*

Infarct size/ % of LV	NA	27.4±14.6	19.5±10.5	0.0001
Infarct size/ g	NA	20.2±13.6	14.4±9.4	0.0001
AAR/ % of LV	NA	42.0±12%	-	NA
MVO/ n (%)	NA	26 (65)	-	NA
MVO (n=26)/ %LV	NA	5.1±3.5		NA
IMH (n=15)/%LV	NA	14.0 (6.0-21.2)	-	NA
Residual iron (n=13)/ %LV	NA	-	9.0 (4.0-10.3)	NA
$T2_{Remote}$/ ms T2*<20ms (n=15) T2*≥20ms (n=13)	50±4	 51 (48-53) 49 (48-51)	 49 (46-51) 47 (45-48)	 0.056 0.060
$T2_{Infarct}$/ ms T2*<20ms (n=15) T2*≥20ms (n=13)	NA	 64 (62-68) 64 (62-69)	 60 (58-64) 53 (51-55)	 0.017 0.001
$T2_{Core}$/ ms T2*<20ms (n=15) T2*≥20ms (n=13)	NA	 50 (46-53) 55 (52-59)	 47 (45-50) 47 (45-49)	 0.111 0.001
$T1_{Remote}$/ ms T2*<20ms (n=15) T2*≥20ms (n=13)	1000±25	 1051 (1023-1094) 990 (968-1018)	 1015 (989-1020) 1007 (966-1039)	 0.002 0.74
$T1_{Infarct}$/ ms T2*<20ms (n=15) T2*≥20ms (n=13)	NA	 1232 (1163-1338) 1262 (1198-1286)	 1162 (1132-1216) 1113 (1092-1140)	 0.014 0.001
$T1_{Core}$/ ms T2*<20ms (n=15) T2*≥20ms (n=13)	NA	 1016 (949-1061) 1140 (1086-1160)	 1004 (990-1028) 1042 (1015-1140)	 0.78 0.11
$T2^*_{Remote}$ (n=28)	NA	32 (30-35)	34 (31-35)	0.52
$T2^*_{Infarct}$ (n=13)	NA	29 (24-36)	33 (28-35)	0.80
$T2^*_{Core}$ (n=15)	NA	10 (11-13)	15 (13-17)	0.013
ECV_{Remote}/ % Whole cohort (n=40)	26.4±2.1	27.9±2.1	27.0±2.1	0.01† 0.30*

With adverse LV remodelling (n=8)	NA	29.5±1.4	28.6±1.5	0.27
Without adverse LV remodelling (n=32)	NA	27.4±2.0	26.6±2.1	0.02
$ECV_{Infarct}$/ %	NA	69.2±9.6	70.4±19.9	0.71

EDV: end diastolic volume; ESV: end systolic volume; EF: ejection fraction; LV: left ventricle; AAR: area-at-risk; MVO: microvascular obstruction; IMH: intramyocardial haemorrhage; NA: not applicable.

† control versus acute scan; * control versus follow-up scan; NS: not statistically significant.

7.3.1 IMH and oedema-based AAR

Patients with IMH had lower $T2_{Core}$ (50[46-53] ms versus 55[52-49] ms, P=0.001) but similar $T2_{Infarct}$ (64[62-64] ms versus 64[62-69] ms, P=0.29) and T2 in the salvaged myocardium (65[61-68] ms versus 63[62-67] ms, P=0.43). However, in patients with IMH, oedema-based AAR was larger (46[40-55] %LV versus 31[24-43] %LV, P=0.009) and myocardial salvage index was smaller (0.24[0.16-0.43] versus 0.61[0.36-0.88], P=0.009), when compared to those without IMH.

7.3.2 Residual myocardial iron on the follow-up scan in a subset of patients

A subset of 28 patients who completed the follow-up scans had matching and interpretable T2* maps. There was no difference in the CMR parameters between those with paired T2* maps (n=28) and those without (n=12) (see Table 7-3). On the acute scan, 15/28 (54%) patients had IMH and 18/28 (64%)

had MVO. 15/18 (83%) patients had MVO with IMH. On the follow-up scan, 13/15 (87%) patients had evidence of residual myocardial iron.

Table 7-3: CMR characteristics patients with and without paired T2* maps.

	Patients with paired T2* maps (n=28)	Patients without paired T2* maps (n=12)	P value
EDV/ml	173±40	170±31	0.79
ESV/ml	91±32	87±24	0.71
EF/%	48±9	50±7	0.58
Mass/ g	119±33	104±24	0.15
Change in EDV/ ml	7±16	3±13	0.44
Acute infarct size/ %LV	26.7±15.2	28.8±13.6	0.69
Chronic Infarct size/ %LV	18.5±11.1	22.0±9.8	0.36
AAR/ % of LV	42.7±12.3	40.3±11.8	0.56
MVO/ n (%)	18 (64)	8 (67%)	0.59
Adverse LV remodelling/ n (%)	6 (21%)	2 (17%)	0.55
Acute scan			
T2 remote	50 (48-52)	50 (48-52)	0.85
T2 core	52 (48-55)	51 (48-54)	0.96
T2 infarct	64 (62-68)	65 (64-66)	0.80
Follow-up scan			
T2 remote	48 (46-50)	47 (45-49)	0.63
T2 core	47 (45-49)	47 (46-48)	0.90
T2 infarct	57 (53-61)	54 (52-57)	0.25

EDV: end diastolic volume; ESV: end systolic volume; EF: ejection fraction; LV: left ventricle; AAR: area-at-risk; MVO: microvascular obstruction.

7.3.3 T1 and T2 of the core, infarct zone and remote myocardium at follow-up

Using a linear mixed model to adjust for within patient interaction, in patients without residual myocardial iron, there was no difference between $T1_{Core}$ and $T1_{Infarct}$ (1042 [1015 – 1140] ms versus 1113 [1092 – 1140] ms, P=0.20) and $T1_{Infarct}$ was significantly higher than $T1_{Remote}$ (1113 [1092 – 1140] ms versus 1007 [966 – 1039] ms, P<0.001). However, $T2_{Core}$ was lower than $T2_{Infarct}$ (47 [45 – 49] ms versus 53 [51 – 55] ms, P=0.001) and similar to $T2_{Remote}$ (47 [45 – 49] ms versus 47 [45 – 48] ms, P=1.0) and $T2_{Infarct}$ was significantly higher than $T2_{Remote}$ (53 [51 – 55] ms versus 47 [45 – 48] ms, P<0.001) (Figure 7-4).

In patients with residual myocardial iron, both $T1_{Core}$ and $T2_{Core}$ were similar to $T1_{Remote}$ and $T2_{Remote}$ (T1: 1004 [90 – 1028] ms versus 1015 [989 – 1020] ms, P=1.0; T2: 47 [45 – 50] ms versus 49 [46 – 51] ms, P=1.0) but significantly lower than $T1_{Infarct}$ and $T2_{Infarct}$ (T1: 1004 [90 – 1028] ms versus 1162 [1132 – 1216] ms, P<0.001; T2: 47 [45 – 50] ms versus 60 [58 – 64] ms, P<0.001) respectively (Figure 7-4).

Patients with residual myocardial iron had lower $T1_{Core}$, similar $T2_{Core}$ and higher $T1_{Infarct}$ and $T2_{Infarct}$ when compared to patients without. There was no difference in the $T1_{Remote}$ and $T2_{Remote}$ between these two groups as illustrated in Figure 7-4.

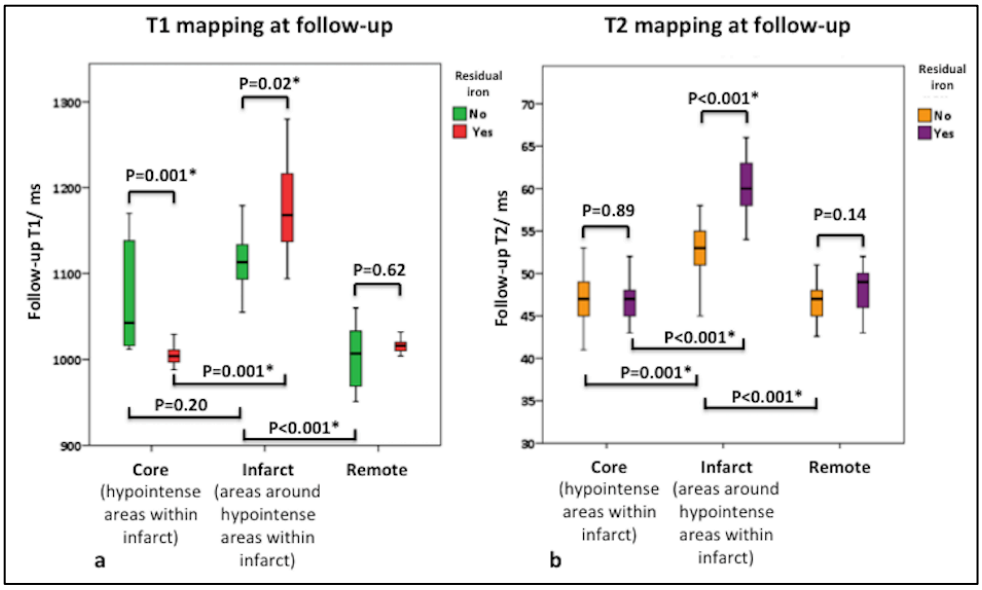

Figure 7-4: Box-plots of T1 and T2 values of the core, infarct and remote myocardium in patients with and without residual myocardial iron.

Figure 7-5 shows an example of 3 patients with acute and follow-up CMR images showing MVO, IMH, residual myocardial iron and persistently elevated T2 in the surrounding myocardium within the infarct zone at follow-up.

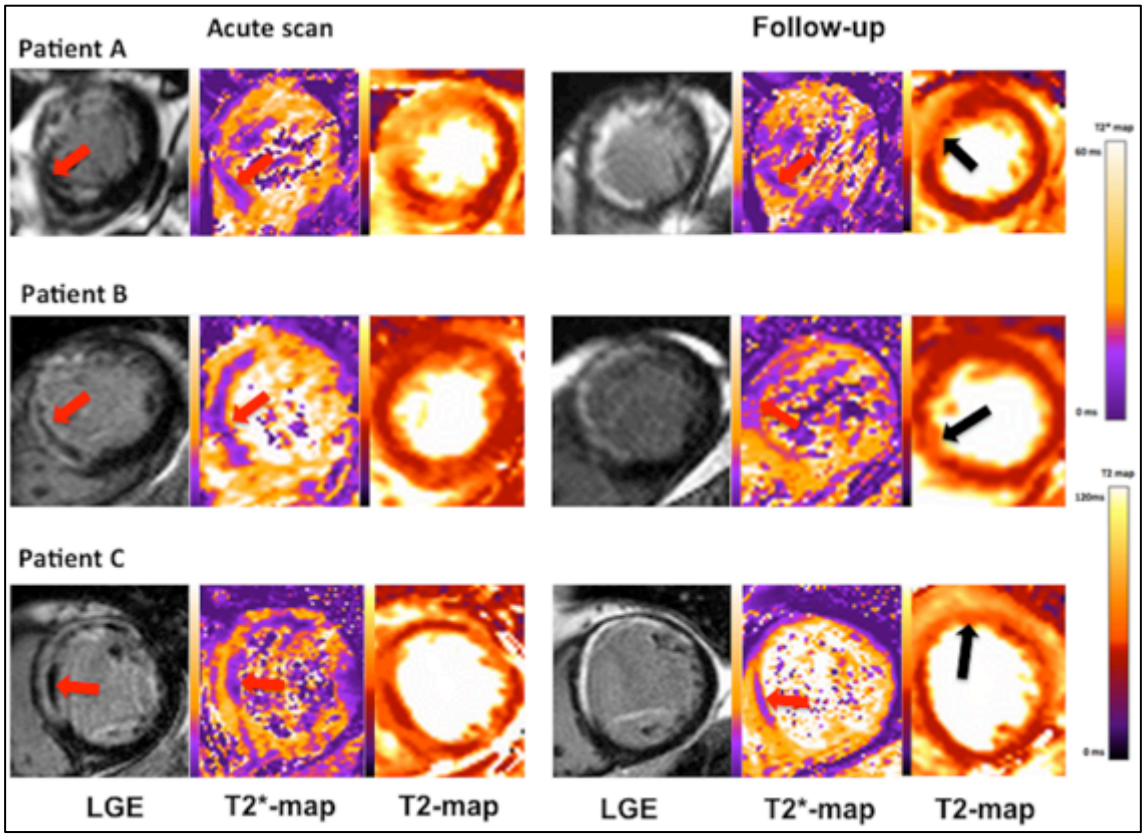

Figure 7-5: Acute and follow-up T2* maps.

Examples of 3 patients (A, B and C) with acute and follow-up scans and the red arrows showing areas of MVO, IMH and residual myocardial iron and the black arrows showing areas of hyper-enhancement on the T2 maps.

7.3.4 IMH and adverse LV remodelling

Eight out of forty (20%) patients developed adverse LV remodelling. Patients with adverse LV remodelling had larger MI size (30.1±7.3%LV versus 16.9±9.8%LV, P=0.01), had an increased incidence (100% versus 50% P=0.10) and extent of MVO (8.0±3.2%LV versus 3.6±2.6%LV; P=0.001), and were more likely to have IMH (100% versus 60%, P=0.04) on the acute scans when compared to those without adverse LV remodelling.

7.3.5 Residual myocardial iron and adverse LV remodelling

In patients with adverse LV remodelling, $T2_{Infarct}$ was significant higher than those without adverse LV remodelling and without residual myocardial iron (60 [54 – 64] ms versus 53 [51 – 56] ms, P=0.025), but similar to those with residual myocardial iron but no adverse LV remodelling (60 [54 – 64] ms versus 60 [58 – 63] ms, P=1.0) as shown in Figure 7-6a.

However, when looking at those patients that did not develop adverse LV remodelling, those with residual iron had a significantly higher change in EDV (8 [-2 – 14] % versus -4 [-7 – 5] %, P=0.043), when compared to those patients without residual myocardial iron (Figure 7-6b).

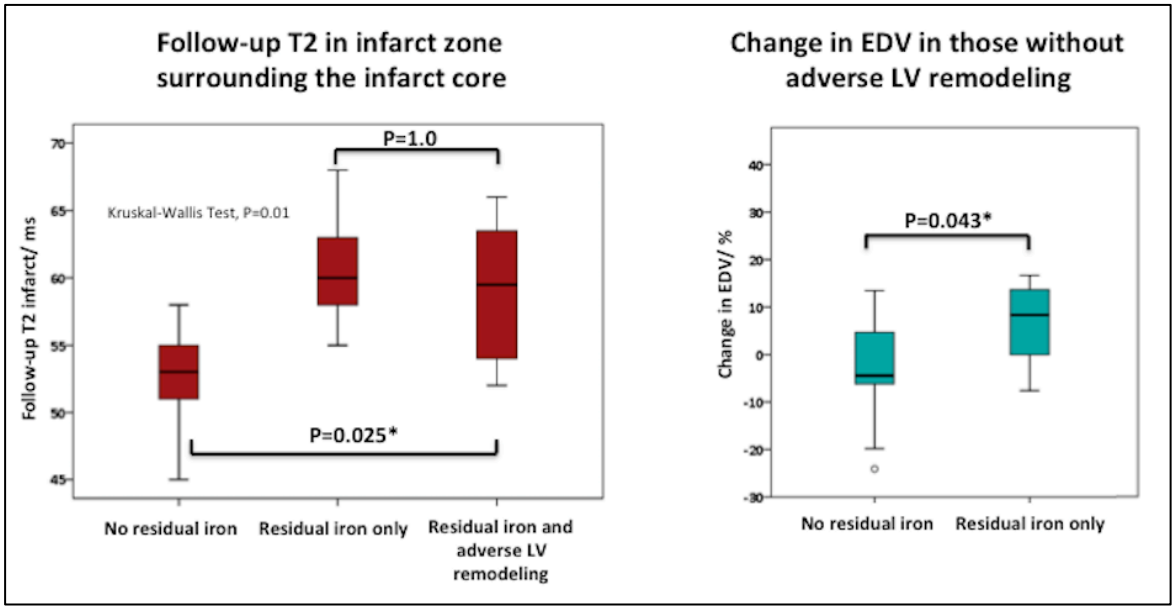

Figure 7-6: (a) T2 values in the infarct zone in patients with and without residual myocardial iron; (b) Change in EDV in patients with and without residual myocardial iron.

7.3.6 Relationship between acute MI size, MVO and IMH and adverse LV remodelling

Acute MI size, extent of MVO and IMH correlated with the change in LV end diastolic volume (Pearson's rho of 0.64, 0.59, and 0.66 respectively, P values of 0.18 and 0.62 respectively for correlation coefficient comparison), and performed equally well on ROC curve for predicting adverse LV remodelling (area under the curve: 0.99, 0.94, and 0.95 respectively, P=0.19 for ROC curve comparison).

7.3.7 Intra-observer and inter-observer variability for ECV measurements

There was less intra-observer and inter-observer variability when ECV_{Remote} and $ECV_{Infarct}$ were assessed by mean segmental analysis when compared to manual ROI (Table 7-4). For intra-observer measurements, the limits of agreement for ECV_{Remote} were ±1.22% when using mean segmental values compared to ±1.59% when using manual ROI. For inter-observer measurements, the limits of agreement for ECV_{Remote} were ±0.99% when using mean segmental values compared to ±1.40% when using manual ROI. The limits of agreement for the two techniques were even wider for $ECV_{Infarct}$ (Table 7-4).

Table 7-4: Intra-observer and inter-observer variability for ECV using 2 different techniques (mean segmental values and manual ROI, n=10).

	Intra-class correlation coefficient (95% CI)	Bias ± limits of agreement (%)
Intra-observer variability (n = 10)		
ECV_{Remote}		
Mean segmental values	0.994 (0.976-0.998)	0.11 ± 1.22
Manual ROI	0.981 (0.922-0.995)	0.42 ± 1.59
$ECV_{Infarct}$		
Mean segmental values	0.992 (0.967-0.998)	0.53 ± 2.44
Manual ROI	0.972 (0.886-0.993)	0.13 ± 5.02
Inter-observer variability (n = 10)		
ECV_{Remote}		
Mean segmental values	0.996 (0.984-0.999)	0.10 ± 0.99
Manual ROI	0.989 (0.958-0.997)	0.18 ± 1.40
$ECV_{Infarct}$		
Mean segmental values	0.991 (0.949-0.998)	0.81 ± 2.21
Manual ROI	0.963 (0.850-0.991)	0.10 ± 5.96

ECV: extracellular volume fraction; ROI: region of interest.

Changes in the remote myocardial ECV

For both the acute and follow-up scans, there were no differences in LV diastolic and systolic wall thickness and LV wall thickening in the remote myocardium between the STEMI patients and controls (Table 7-2). However, on the acute scan, LV wall motion in the remote myocardium was higher in the STEMI patients when compared to controls (9.2±2.6mm versus 7.7±2.5mm,

P=0.04) but there was no statistically significant difference between them on the follow-up scan (8.9±2.6 mm versus 7.7±2.5mm, P=0.10).

There were no significant differences in the $T2_{Remote}$ values between the STEMI patients and controls on either the acute scan or the follow-up scans. Native $T1_{Remote}$ and ECV_{Remote} were both significantly higher in the STEMI patients when compared to controls on the acute scan (T1: 1032±51ms versus 1000±25ms, P=0.001; ECV: 27.9±2.1% versus 26.4±2.1%, P=0.01), but this difference was not present on the follow-up scan (T1: 1004±39ms versus 1000±25ms, P=0.66; ECV: 27.0±2.1% versus 26.4±2.1%, P=0.30) (Table 7-2).

7.3.8 LV remodelling and remote myocardial ECV

Out of 40 STEMI patients who had a follow-up scan, 8 (20%) patients had adverse LV remodelling. In these 8 patients, the ECV_{Remote} was higher acutely when compared to those 32 patients without adverse LV remodelling (29.5±1.4% vs. 27.4±2.0%; P=0.01) and this difference in ECV_{remote} persisted on the follow-up scan (28.6±1.5% vs. 26.6±2.1%; P=0.02). There were no significant differences in $T2_{Remote}$ between those with and without adverse LV remodelling both on the acute and follow-up scans (Figure 7-7).

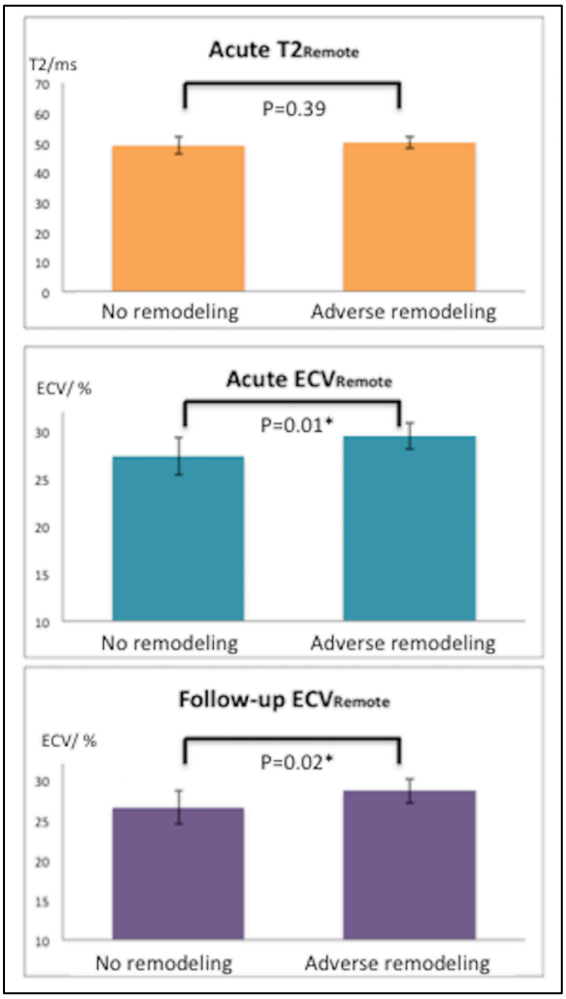

Figure 7-7: T2 and ECV of the remote myocardium in STEMI patients with (n=8) and without LV remodelling (n=32).

7.3.9 Multi-parametric CMR prediction of remodelling

Percentage increase in LVEDV as a continuous variable was used as a surrogate for adverse LV remodelling for univariable and multivariable linear regression analysis. MI size quantified by LGE (R^2 0.36, coefficient 0.64, 95% CI 0.37-0.9, P=0.0001) was the single most significant predictor of adverse LV remodelling after adjusting for $T1_{Remote}$, MVO and LVEDV on the acute scan in a multivariable analysis. In order to account for both MI size and AAR, MSI was used in the regression model instead of MI size. $T1_{Remote}$ and ECV_{Remote}, $T1_{Core}$,

MSI and MVO on the acute scan were significantly associated with adverse LV remodelling on univariable analysis and these were then included in a multivariable analysis. MSI and then ECV_{Remote} were most associated with adverse LV remodelling after adjusting for $T1_{Remote}$, $T1_{Core}$ and MVO on the acute scan (Table 7-5 below).

Table 7-5: Univariable and multivariable associates of LV remodelling (n=40).

	Univariable analysis			**Multivariable analysis**	
	Regression slope	R^2	P	Regression slope	P
MSI	-29	0.25	0.001	-25	0.008
ECV_{Remote}	3.5	0.24	0.001	2.6	0.03
MVO/g	2.7	0.26	0.001		NS
T1 remote	0.13	0.20	0.03		NS
$T1_{Core}$	-0.06	0.14	0.001		NS

NS: not statistically significant.

7.4 Discussion

Our study confirms that MVO is a strong precursor for the development of adverse LV remodelling. The majority of patients with MVO also had IMH

(83%). A large proportion of those with IMH had residual iron at follow-up (87%). Those with residual iron had higher T2 in the surrounding infarct areas suggestive of delayed resolution of oedema in these patients. All patients with adverse LV remodelling had residual iron and higher T2 in the surrounding infarct areas. Furthermore, those with residual iron but not meeting the definition for adverse LV remodelling had larger percentage increase in LVEDV than those without residual iron. Although T1 values were also higher in the MI zone surrounding areas of residual iron compared to those without, this difference in T1 may have been due to the complex interplay between fibrosis, oedema and the development of early fatty metaplasia (287) in the convalescent phase of a STEMI. We also showed that ECV_{Remote} in STEMI patients was acutely elevated and this elevation persisted in those who developed adverse remodelling at 5 months, suggesting that remote compensatory changes in the ECM occurred in this subset of patients. There was no difference in T2 values observed in the remote myocardium of the STEMI patients when compared to the controls suggesting that the increased ECV_{Remote} on the acute scan was unlikely due to oedema in the remote myocardium. As expected, those with adverse LV remodelling had significantly more infarct regression predominantly due to MVO resorption as demonstrated by the very high ECV of 82±8% at follow-up in regions previously occupied by MVO.

7.4.1 IMH, residual iron and adverse LV remodelling

It is recognised that IMH is associated with larger MI size, adverse LV remodelling and poor clinical outcomes (160, 161, 261) and residual iron may be a source of prolonged inflammation (207) and may be pro-arrhythmic.(206) Although our study was purely based on tissue characterisation, these findings add to the current literature that residual iron may play a role in the inflammatory phase of adverse LV remodelling. Using T2* imaging, Kali et al (207) have recently shown in a small cohort of 15 STEMI patients that the presence of IMH on the acute scans was associated with residual iron at 6 months. They also used immuno-histochemical analysis of canine heart models of acute MI to show evidence of localized accumulation of macrophages at the sites of residual iron at follow-up suggesting a prolonged inflammatory response due to the residual iron.(207) Roghi et al (208) showed in a small cohort of 15 STEMI patients that those with MVO and IMH had higher levels of non-transferrin bound iron, which have previously been linked with cardiotoxicity in thalassemia major patients with iron overload. Although oedema has been shown to be present in some patients up to 6 months post reperfused STEMI, we have showed that the delayed resolution of oedema by T2 mapping was associated with residual iron due to IMH.

7.4.2 Remote myocardial ECV and adverse LV remodelling

In a murine model of acute MI, Tsuda et al (211) found molecular and immuno-histochemical evidence of interstitial fibrosis in the remote myocardium

as early as 72 hours post MI. Volders et al (210) provided post-mortem histological evidence of an increase in interstitial collagen in the remote myocardium of infarcted patients when compared to control. However, Marijianowski et al (212) showed that post-MI LV remodelling in patients with end-stage heart failure undergoing transplant was not associated with interstitial fibrosis in the remote myocardium. From the tissue characterization point of view, Chan et al (213) used post-contrast T1 in 25 acute STEMI patients and found evidence of early remote expansion of the ECM, which persisted in the chronic stage. Carrick et al (197) demonstrated that increased native T1 values in remote myocardium of reperfused STEMI patients were independently associated with adverse LV remodelling. We interrogated the remote myocardium using automated ECV maps and we have demonstrated that only in a subset of patients who developed adverse LV remodelling had increased ECV_{Remote} as early as 4 days and persisted at 5 months. The cause of this expansion in ECV_{Remote} acutely could due to increase in the intravascular compartment due to compensatory hyperaemia in the remote myocardium and at follow-up, there is compensation in the remote myocardium to maintain cardiac output and a subset of patients develop remote myocardial LV remodelling with left ventricular hypertrophy and increased interstitial fibrosis. Interestingly, Carberry et al (288) recently showed that change in ECV in remote myocardium, calculated from native and post contrast MOLLI T1 maps in 140 patients, was a multivariate associate of LV remodelling. However, due to lack of power, ECV_{Remote} was not associated with all-cause death and heart failure.

7.4.3 Limitations

A significant proportion of the T2* maps were not interpretable in our study and this partly highlights the challenge of performing a comprehensive CMR scan with multi-parametric mapping in patients with an acute STEMI. Of note, 18% of T2* data were not available in the large study by Carrick et al (139) either due to patient's intolerance of the scan or T2* maps being not evaluable. We did not measure blood inflammation markers to support the notion of persistent inflammation due to residual iron in these patients. Histological validation to elucidate whether persistently elevated T2 may be due to inflammation around the areas of residual iron was beyond the scope of this work and needs to be confirmed in future animal studies of IMH and MVO. We only included a relatively small number of patients and therefore we were underpowered to determine the interplay between $T1_{Remote}$ (197), $T1_{Core}$ (156), IMH (139) and ECV_{Remote} on major adverse cardiovascular events. Furthermore, the Fragility Index (described in section 3.5 on Sample size) of this analysis was low due to the small number of patients and we only showed an association rather than causality. These findings need to be confirmed in future adequately powered studies.

7.5 Conclusion

The majority of patients with IMH had residual iron at follow-up, which was associated with adverse LV remodelling. Adverse LV remodelling itself was associated with delayed resolution of oedema in the MI zone that may be

suggestive of ongoing inflammation. These patients also displayed expansion of the remote myocardial ECV as early as 4 days and persisted at 5 months. Therefore, patients with IMH or residual iron could be future potential targets for therapeutic interventions with anti-inflammatory agents or chelation therapy aiming to prevent adverse LV remodelling and improve clinical outcome in these patients (except in those with established heart failure where iron supplementation can improve outcomes (289)).

8 Redefining post-MI left ventricular remodelling by CMR

8.1 Introduction

Adverse LV remodelling following STEMI has been conventionally defined as ≥20% increase in LVEDV from baseline. This cut-off value was determined using echocardiography, and was based on the upper limit of the 95% confidence interval of intra-observer variability for the %Δ in LVEDV following STEMI.(193, 194) Reverse LV remodelling has been defined as ≥10% decrease in LVESV by echocardiography following cardiac resynchronization therapy, and was derived using ROC curves for the optimal cut-off for the %ΔLVESV to predict mortality.(195) So far, no cut-off values for adverse and reverse LV remodelling following STEMI have been defined by CMR, and studies using CMR to assess post-STEMI LV remodelling have relied upon using these cut-off values defined by echocardiography for adverse (196, 197) and reverse LV remodelling.(198)

Therefore, the first aim of this study was to perform intra-observer and inter-observer measurements of LV parameters in paired acute and follow-up CMR scans in reperfused STEMI patients, in order to determine the minimal detectable changes (MDCs) that could be used as cut-off values for defining post-STEMI remodelling.

Secondly, we aimed to identify the cut-off values for clinically important %ΔLVEDV and %ΔLVESV to predict LVEF <50% at follow-up.(169)

Finally, cut-off values for %ΔLVEDV and %ΔLVESV would then be applied to a cohort of 146 STEMI patients with paired acute and follow-up scans to assess different patterns of post-STEMI LV remodelling.

8.2 Methods

Patients included in this study are those from cohorts 1 and 2 with paired acute and follow-up scans and from 2 published studies (117, 290) as summarised in Table 8-1. All patients provided informed consent at the time of recruitment and the studies were conducted according to the Declaration of Helsinki. Only patients with a paired acute CMR within the first week post PPCI and a follow-up CMR were included in this study.

8.2.1 Cohort for inter-observer and intra-observer analysis

Analysis was performed using CVI42 software (Version 5.2.2[340], Calgary, Canada). 15 STEMI patients reperfused by PPCI, with a minimum of 6 months between the acute and follow-up scan were randomly chosen from cohort 1 and were used for inter and intra-observer variability. Semi-automated contours were drawn on the short-axis cine images using the threshold segmentation option for the epicardial border and the automatic detection option for the endocardial border, with minimal manual adjustment when required. The LVEDV, LVESV, LV mass (LVM) and LVEF were quantified using 2 methods as shown in Figure 8-1. In method 1, we used rounded endocardial contours and excluded the trabeculae and papillary muscles (T&P) as part of the LVM and they were included as part of the LV volume.

Table 8-1: CMR acquisition details of the 2 additional studies included together with Cohort 1 and 2.

	Number of patients with paired CMR	Aim	Scanner and contrast	MVO and MI size	Outcome
Ludman 2011 (290)	29 patients, 4 months apart (RCT)	To assess benefit of erythropoiet in during PPCI	1.5T Siemens Dotarem 0.2mmol/kg at 10 minutes	MVO: Hypo-intense core on LGE images at 10 minutes MI size: manual	High dose of erythropoietin as an adjunct to PPCI failed to reduce MI size
Crimi 2013 (117)	65 patients, 4 months apart (RCT) LAD only included	To assess benefit of remote ischaemic post conditioning during PPCI	1.5T Siemens Magnevist 0.2mmol/kg at 15 minutes	Hypo-intense core on LGE images at 5 minutes MI size: manual	Remote ischaemic conditioning at the time of PPCI was associated with a reduction in enzymatic MI size but this study was underpowered for MI size by CMR
3T cohort	12 patients, 1 year apart (cohort study)		3T Siemens Dotarem 0.1mmol/kg at 10-15 minutes	Hypo-intense core on LGE images at 10-15 minutes MI size: Otsu	
1.5T cohort	40 patients, 5 months apart (cohort study)		1.5T Siemens Dotarem 0.1mmol/kg at 10-15 minutes	Hypo-intense core on LGE images at 10-15 minutes MI size: 5-SD	

RCT: randomised controlled trial; LGE: late gadolinium enhancement; MVO: microvascular obstruction; MI: myocardial infarction; PPCI: primary percutaneous coronary intervention; PET/MR: positron emission tomography/ magnetic resonance; SD: standard deviation.

In method 2, the T&P were included as part of the LVM and were excluded from the LV volume. The basal cine slice was included if at least 50% of the cavity circumference was surrounded by ventricular myocardium and this principle was used for both end-systole and end-diastole. %ΔLVEDV, %ΔLVESV, %ΔLVM and %ΔLVEF were calculated as the difference between the follow-up parameters and the corresponding baseline parameters and expressed as a percentage of the baseline parameters. All 15 acute and matching follow-up scans were analysed by 2 experienced CMR operators (twice by HB, 3 years' experience in CMR, 2 months apart and blinded to previous results, and once by YYG, 1 and a half years' experience in CMR).

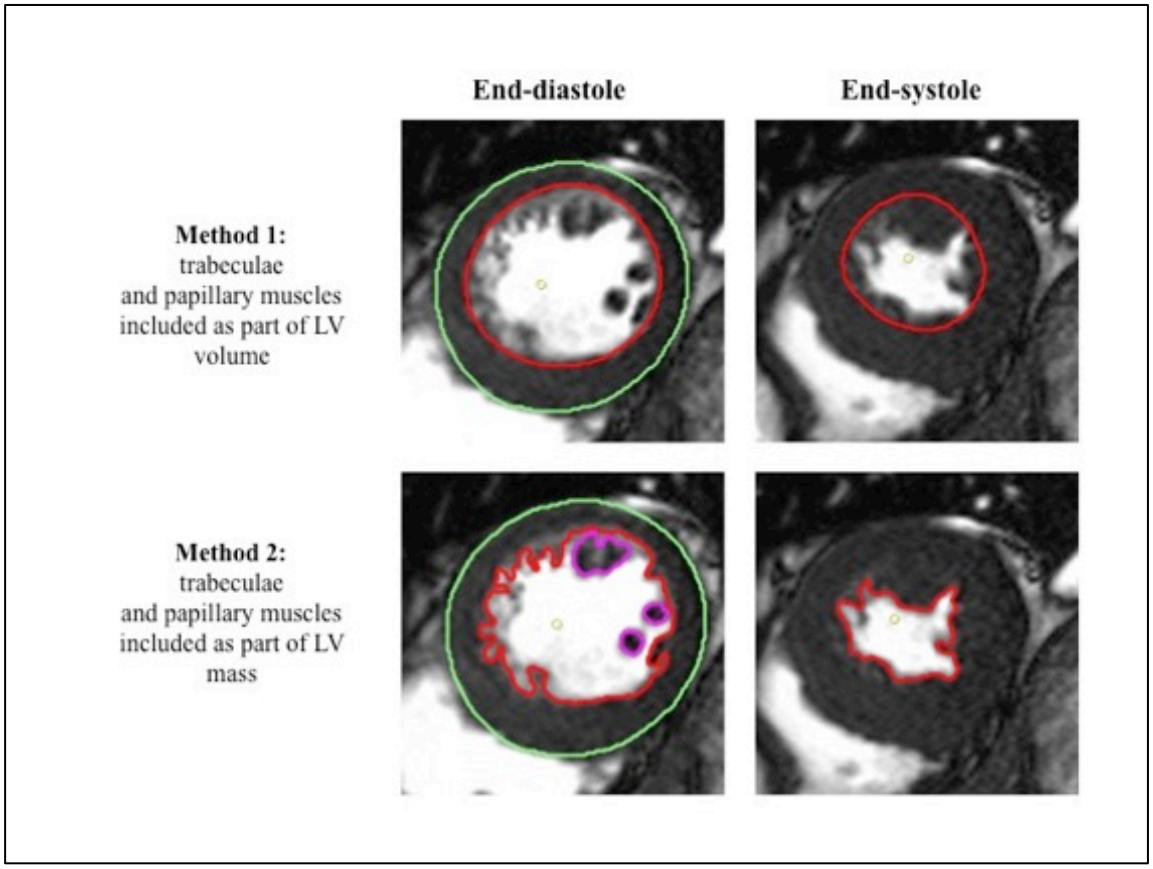

Figure 8-1: Quantification of LV parameters with T&P part of LV volume (method 1) and part of LV mass (method 2).

8.2.2 Cohort for LV remodelling

Patient level data were obtained from the 2 previous randomised controlled trials (117, 290) and from the 3T and 1.5T cohorts described in the methodology section as listed in Table 8-1. Only patients with paired acute and follow-up CMR scans were included. The LV parameters reported by the original studies were used for analysis. All cines were acquired using steady-state free precession based cines as previously described in their respective publications.(117, 290) The CMR details for the acute MI size and MVO detection by the 4 different cohorts of patients included are summarised in Table 8-1.

8.2.3 Statistical analysis

Statistical analysis was performed using SPSS Version 22 (IBM Corporation, Illinois, US). Normality was assessed using Shapiro-Wilk Test. Continuous data was expressed as mean ± standard deviation (SD) or median (interquartile range) and categorical data was reported as frequencies and percentages. Groups were compared using paired Student t test/ Wilcoxon signed rank test or unpaired Student t test/ Mann Whitney U test where appropriate. One-way analysis of variance was used to obtain the mean squared error for each LV parameter for inter and intra-observer measurements and their corresponding square root provided their standard error of the measurement (SEM). The 95% confidence interval (CI) for each SEM was calculated as previously described.(291) Coefficient of variation (CoV) was

expressed as the standard deviation of the difference divided by the mean and expressed as a percentage and Levene's test for homogeneity of variance was used to compare CoV between the 2 methods used for LV parameters quantification (T&P being part of the LV mass or LV volume). Bland-Altman analysis was performed for inter and intra-observer measurements of the LV parameters for comparison. The MDCs with 95% confidence (MDC95) for intra and inter-observer measurements for %ΔLVEDV, %ΔLVESV, % LVM and %ΔLVEF was calculated as 1.96 x SEM x square root of 2. ROC curve analysis was performed to predict an LVEF of <50% at follow-up to identify clinically significant cut-off values for %ΔLVEDV and %ΔLVESV. All statistical tests were two-tailed, and $P<0.05$ was considered statistically significant.

8.3 Results

The median age of the 15 STEMI patients used for intra-observer and inter-observer measurements were 57 (44-62) years old and 12 (80%) were male. Details of the paired acute and follow-up CMR scans are shown in Table 8-2. The acute CMR scan was performed at 2±1 days post-PPCI and the follow-up CMR scan was performed at 7±1 months.

Table 8-2: CMR characteristics of STEMI patients for intra-observer and inter-observer study.

	Acute Scan (n=15)	Follow-up Scan (n=15)	P value
T&P part of the LV volume			

LVEDV/ml	156±38	171±51	0.05
LVESV/ml	78±24	82±34	0.48
LVM/g	107 (81-121)	87 (82-106)	0.07
LVEF/%	50±7	53±9	0.15
T&P part of the LV mass			
LVEDV/ ml	141±39	156±49	0.09
LVESV/ ml	64±20	68±31	0.44
LVM/g	118 (98-135)	99 (94-128)	0.25
LVEF/%	54±7	58±10	0.07

LVEDV: left ventricular end-diastolic volume; LVESV: left ventricular end-systole volume; LVM: left ventricular mass; LVEF: left ventricular ejection fraction.

8.3.1 Variability of LV parameters between the acute and follow-up CMR scans

Table 8-3 summarises the SEM (95%CI), CoV and Bland-Altman analysis of the LV parameters divided into acute and follow-up scans and quantification method. Comparison of CoV did not show any statistical difference for inter-observer or intra-observer measurements (LVEDV, LVESV, LVM, LVEF) on both the acute or follow-up scans between both LV quantification methods (T&P included as part of the LV volume or LV mass) (P values between 0.26 to 0.93).

The LVEDV and LVESV were significantly higher and the LVM and LVEF were significantly lower both on the acute and follow-up scans when the T&P were included as part of the LV volume as shown in Figure 8-2. When they were included as part of the LVM, they contributed the same extent to the LV

mass on the acute and the follow-up scans (13.5±5.0% and 14.5±5.7% respectively, P=0.53).

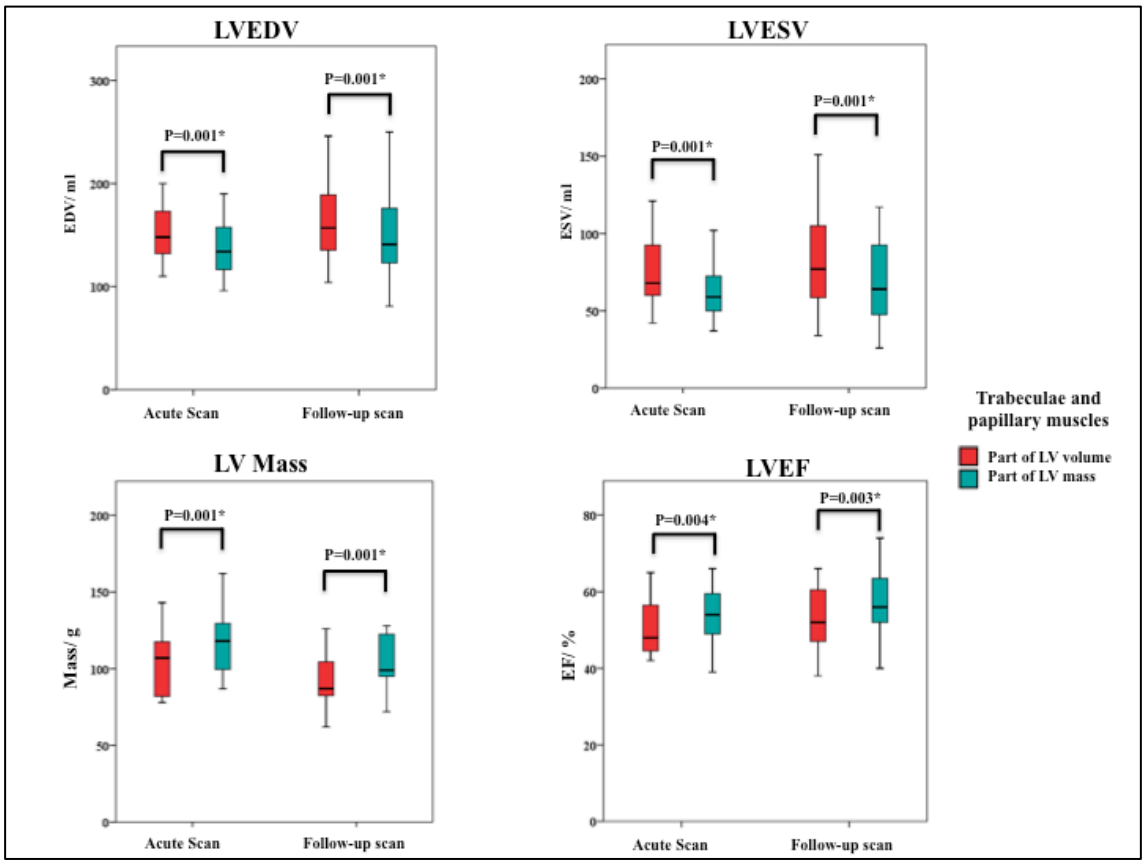

Figure 8-2: Comparison of LV parameters on the acute and follow-up scans with T&P as part of LV volume or as part of LV mass

8.3.2 Variability of %Δ in LV parameters

Details on the intra-observer and inter-observer measurements for %ΔLVEDV, %ΔLVESV, %ΔLVM and %ΔLVEF, both for when T&P was included as part of either LV volume or LV mass, are provided in

Table 8-4. The MDC95 values for these LV parameters were different for inter-observer and intra-observer measurements, and whether the T&P were included as part of the LV volume or mass.

Table 8-3: Intra-observer and inter-observer variability for LV parameters.

	Intra- observer			Inter-observer		
	SEM (95% CI)	**CoV**	**Bias ± limits of agreement**	**SEM (95% CI)**	**CoV**	**Bias ± limits of agreement**
T&P included as part of the LV volume						
LVEDV						
Acute (n=15)	2.0 (1.5 to 3.2) ml	1.3 %	-0.5±5.8 ml	4.6 (3.4 to 7.3) ml	2.9 %	-2.9±13.0 ml
Chronic (n=15)	3.4 (2.5 to 5.3) ml	2.0 %	0±9.6 ml	6.5 (4.7 to 10.2) ml	3.8%	0.7±18.2 ml
LVESV						
Acute (n=15)	1.8 (1.3 to 2.9) ml	2.3 %	-0.3±5.2 ml	3.6 (2.6 to 5.7) ml	4.7 %	1.7±10.2 ml
Chronic (n=15)	1.4 (1.1 to 2.3) ml	1.8 %	-0.5±4.2 ml	2.7 (2.0 to 4.3) ml	3.3 %	1.0±8.0 ml
LVM						
Acute (n=15)	2.2 (1.6 to 3.5) g	2.2 %	0.5±6.2 g	4.2 (3.1 to 6.6) g	4.1 %	-2.7±11.8 g
Chronic (n=15)	2.7 (1.9 to 4.2) g	2.8 %	0.5±9.2 g	3.3 (2.4 to 5.1) g	3.3 %	-1.5±9.8 g
LVEF						
Acute (n=15)	1.3 (1.0 to 2.1) %	2.6 %	0.1±3.8 %	1.9 (1.4 to 3.0) %	3.8 %	-1.4±5.4 %
Chronic (n=15)	1.2 (0.9 to 1.9) %	2.3 %	0.1±4.8 %	1.7 (1.2 to 2.6) %	3.2 %	0.1±8.4 %

Table 8-3 continued: Intra-observer and inter-observer variability for LV parameters.

	Intra- observer			Inter-observer		
	SEM (95% CI)	**CoV**	**Bias ± limits of agreement**	**SEM (95% CI)**	**CoV**	**Bias ± limits of agreement**
T&P included as part of the LV mass						
LVEDV						
Acute (n=15)	3.0 (2.2 to 4.8) ml	2.1 %	0.1±8.6 ml	4.2 (3.1 to 6.7) ml	2.9 %	-2.7±12.0 ml
Chronic (n=15)	3.3 (2.4 to 5.2) ml	2.1 %	0.7±9.4 ml	4.1 (3.0 to 6.5) ml	2.7 %	1.6±11.6 ml
LVESV						
Acute (n=15)	1.4 (1.0 to 2.1) ml	2.1 %	0.5±3.8 ml	3.1 (2.2 to 4.8) ml	4.7 %	-1.2±8.6 ml
Chronic (n=15)	1.5 (1.1 to 2.4) ml	2.3 %	0.7±4.4 ml	3.2 (2.3 to 5.0) ml	4.6 %	-0.5±9.0 ml
LVM						
Acute (n=15)	3.0 (2.2 to 4.8) g	2.6 %	0±8.6 g	3.6 (2.6 to 5.6) g	3.0 %	-2.3±12.4 g
Chronic (n=15)	3.3 (2.4 to 5.2) g	2.9 %	-0.7±9.4 g	4.4 (3.2 to 7.0) g	3.9 %	-0.5±12.4 g
LVEF						
Acute (n=15)	1.5 (1.1 to 2.4) %	2.8 %	-0.7±4.4 %	2.2 (1.6 to 3.5) %	4.1 %	-0.4±6.4 %
Chronic (n=15)	1.3 (1.0 to 2.1)%	2.3 %	0.3±4.2 %	2.1 (1.5 to 3.3) %	3.6 %	1.1±6.4 %

SEM: standard error of the measurement; CoV: coefficient of variation; LVEDV: left ventricular end-diastolic volume; LVESV: left ventricular end-systole volume; LVM: left ventricular mass; LVEF: left ventricular ejection fraction.

Table 8-4: Intra-observer and inter-observer variability for %Δ in LVEDV, LVESV, LVM and LVEF.

	Intra- observer			Inter-observer		
	SEM (95%CI)	**Bias ± limits of agreement**	**MDC95**	**SEM (95%CI)**	**Bias ± limits of agreement**	**MDC95**
T&P included as part of the LV volume						
%ΔLVEDV (n=15)	2.4 (1.8 to 3.8) %	0.2±6.8 %	**7%**	3.5 (2.6 to 5.6) %	1.7±8.2 %	**10%**
%ΔLVESV (n=15)	3.5 (2.6 to 5.6) %	0.5±10.0 %	**10%**	4.8 (3.3 to 7.1) %	-0.5±12.0%	**13%**
%ΔLVM (n=15)	3.4 (2.5 to 5.3) %	0.2±9.6 %	**9%**	4.1 (3.0 to 6.5) %	0.4±11.6 %	**11%**
%ΔLVEF (n=15)	4.0 (2.9 to 6.3) % [Absolute change 2.3(1.7 to 3.6)%]	0.8±11.4 %	**11% (5.5% absolute change from an acute LVEF 50%)**	4.8 (3.6 to 7.7) % [Absolute change 2.7(2.0 to 4.3)%]	2.2±12.8 %	**13% (6.5% absolute change from an acute LVEF 50%)**

Table 8-4 continued: Intra-observer and inter-observer variability for %Δ in LVEDV, LVESV, LVM and LVEF.

	Intra- observer			Inter-observer		
	SEM (95%CI)	**Bias ± limits of agreement**	**MDC95**	**SEM (95%CI)**	**Bias ± limits of agreement**	**MDC95**
T&P included as part of the LV mass						
%ΔLVEDV (n=15)	2.8 (2.0 to 4.4) %	0.8±7.8 %	**8%**	4.3 (3.2 to 6.9) %	4.2±12.2 %	**12%**
%ΔLVM (n=15)	3.1 (2.3 to 4.9) %	-0.5±8.8 %	**9%**	4.4 (3.2 to 7.0) %	1.8±12.6 %	**12%**
%ΔLVEF (n=15)	3.7 (2.7 to 5.9) % [Absolute change 2.0 (1.4 to 3.1) %]	1.4±10.6%	**10% (5% absolute change from an acute LVEF 50%)**	4.3 (3.1 to 6.7) % [Absolute change 2.1 (1.5 to 3.3) %]	2.2±12.0 %	**12% (6.0% absolute change from an acute LVEF 50%)**

SEM: standard error of the measurement; MDC95: minimal detectable change in 95% confidence; LVEDV: left ventricular end-diastolic volume; LVESV: left ventricular end-systole volume; LVM: left ventricular mass; LVEF: left ventricular ejection fraction.

Irrespective of how the T&P were dealt with, the highest MDC95 was 8% for %ΔLVEDV and 10% for %ΔLVESV for intra-observer measurements. The corresponding values for inter-observer measurements were 12% and 13%, respectively. Further details for %ΔLVM and %ΔLVEF are provided in Table 8-5.

Table 8-5: Cut-off values for LVEDV and LVESV in STEMI patients in our cohort (irrespective of whether T&P considered as part of LV volume or LV mass).

	MDC95	
	Intra-observer	**Inter-observer**
%ΔLVEDV	8%	12%
%ΔLVESV	10%	13%
%ΔLVM	9%	12%
%ΔLVEF	11% (5.5% absolute change)	13% (6.5% absolute change)

MDC95: minimal detectable change in 95% confidence; %Δ: percentage change; LVEDV: left ventricular end-diastolic volume; LVESV: left ventricular end-systole volume; LVM: left ventricular mass; LVEF: left ventricular ejection fraction.

8.3.3 Clinically significant %Δ in LVEDV and LVESV

A total of 146 STEMI patients had matching acute (mean of 4±2 days) and follow-up CMR scans (median of 4 months). 12/146 (8%) patients had their scans on a 3T scanner and the rest were acquired on 1.5T scanners. Table 8-6 summarises the clinical and CMR details of these 146 patients.

Table 8-6: Total number of patients with paired acute and follow-up scan from 4 studies.

Details	Number
Number of patients	146
Ludman 2011 Crimi 2013 Cohort 2 Cohort 1	29 (20%) 65 (45%) 12 (8%) 40 (27%)
Male	129 (88%)
Age (years)	59±12
Diabetes Mellitus	15 (10%)
Hypertension	67 (46%)
Smoking	64 (44%)
Dyslipidaemia	47 (32%)
Chest pain onset to PPCI time (minutes)	184 [135-282]
Infarct artery (%) LAD RCA Cx	 109 (75%) 29 (20%) 8 (6%)
TIMI flow pre-PPCI 0 1 2 3	 129 (89%) 7 (5%) 4 (3%) 4 (3%)
TIMI flow post-PPCI 0 1 2 3	 2 (1%) 2 (1%) 23 (16%) 117 (82%)

Timing of acute CMR	4±2 days
Timing of follow-up CMR	4 (4-5) months
CMR findings- acute	
LVEDV	156 (132-183) ml
LVESV	80 (64-103) ml
LVM	121 (104-145) g
LVEF	47±9 %
MI size	24.6±12.1 %LV
MVO	96 (66%)
CMR findings- follow-up	
LVEDV	165 (141-201) ml
LVESV	82 (60-109) ml
LVM	106 (90-132) g
LVEF	50±11 %
MI size	17.8±10.1 %LV

LAD: left anterior descending artery; RCA: right coronary artery; Cx: circumflex artery; TIMI: thrombolysis in myocardial infarction; LVEDV: left ventricular end-diastolic volume; LVESV: left ventricular end-systole volume; LVM: left ventricular mass; LVEF: left ventricular ejection fraction.

As expected, ROC curve analysis showed that %ΔLVESV was a better predictor of LVEF of <50% at follow-up, with an AUC of 0.83 (95% CI 0.77 to 0.90), when compared to an AUC of 0.75 (95% CI 0.67 to 0.83) for %ΔLVEDV, P=0.03 for ROC curves comparison (Figure 8-3). A %ΔLVEDV of 11% had a sensitivity of 72% and a specificity of 70%, and a %ΔLVESV of 5% had a sensitivity and specificity of 78%.

These cut-off values were lower than the MDC95 for inter-observer measurements. Therefore, using the cut-off values for MDC95 for inter-observer measurements (given that the scans from different studies were by different

observers), an increase in LVEDV of 12% had a sensitivity of 73% and a specificity of 69% and an increase in LVESV of 13% had a sensitivity of 90% and a specificity of 60% to detect an LVEF of <50%.

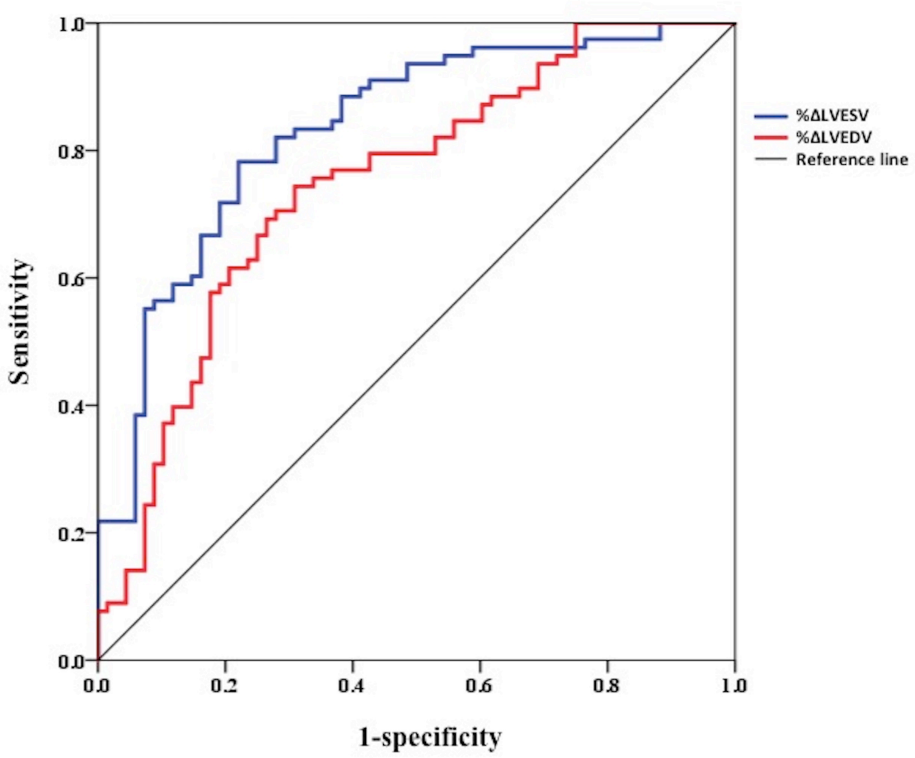

Figure 8-3: ROC curve comparison for %ΔLVEDV and %ΔLVESV to detect LVEF<50% at follow-up.

8.3.4 Relationship between %ΔLVESV, %ΔLVEDV, %ΔLVEF on post-STEMI LV remodelling

Figure 8-4 shows the relationship between %ΔLVESV and %ΔLVEDV. The dashed lines represent the cut-off values of +12 and -12% for %ΔLVEDV (vertical dashed lines) and of +13 and -13% for %ΔLVESV (horizontal dashed lines). Patients were divided into 3 groups for %ΔLVEF based on the MDC95 cut-off of 13% for inter-observer measurements, namely: blue circles - no change in LVEF at follow-up; green circles - increase in LVEF at follow-up compared to acute scan; red circles - decrease in LVEF at follow-up compared to acute scan. Those with a reduction in LVEF at follow-up were more likely to have an increase in both LVEDV and LVESV, and tended to be in the right upper quadrant (RUQ) of the graph (adverse LV remodelling group). Those with an improvement in LVEF were more likely to have in improvement in LVESV and LVEDV and tended to be in the middle lower quadrant (MLQ) and left lower quadrant (LLQ) of the graph (reverse LV remodelling group). Some patients had an increase in LVEDV only with or without an improvement in LVEF, and tended to lie in the right middle quadrant (RMQ) of the graph (adverse LV remodelling with compensation). Those in the middle quadrant (MQ) of the graph had no change in LVEDV or LVESV and predominantly no change in LVEF (no remodelling group).

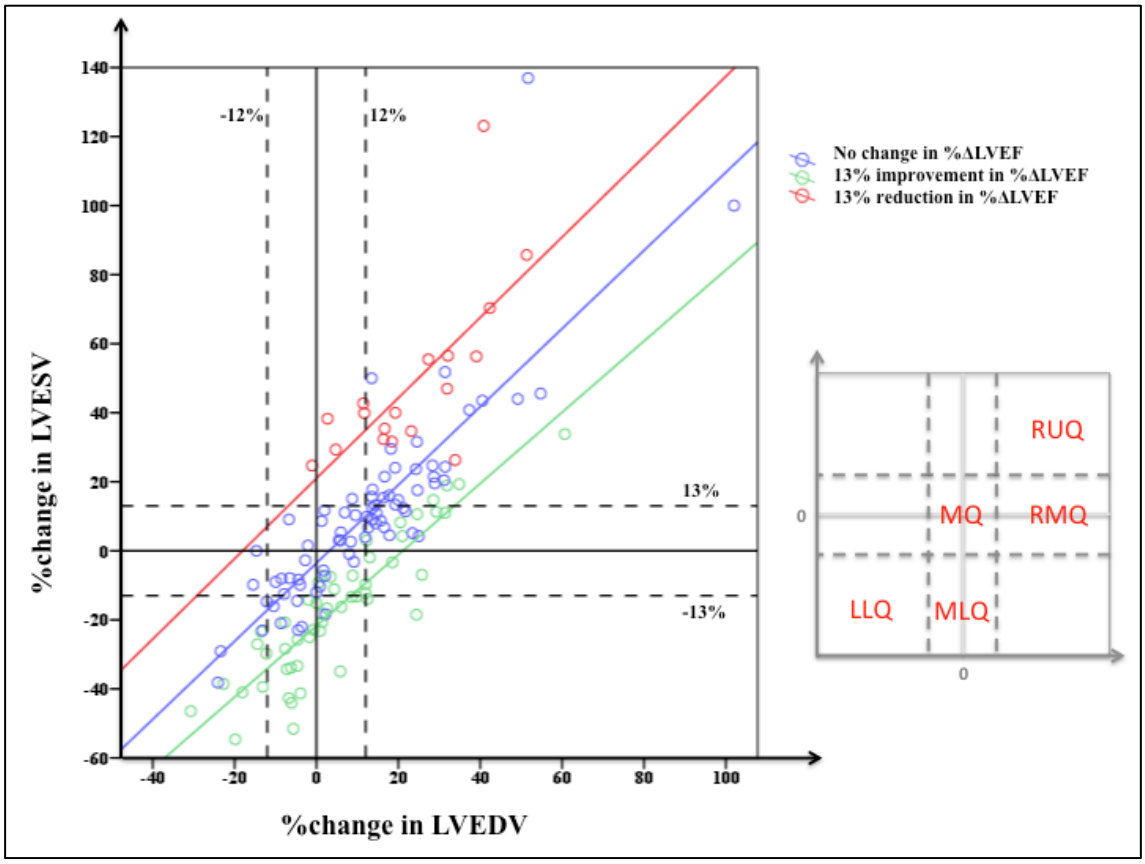

Figure 8-4: Relationship between %ΔLVEDV, %ΔLVESV and %ΔLVEF.

The vertical dashed lines represent the cut-off values of +12 and -12% change in LVEDV and the horizontal dashed lines represent +13 and -13% %ΔLVESV. Patients were divided into 3 groups for %ΔLVEF based on the MDC95 cut-off of 13%, namely: blue circles - no change in LVEF at follow-up; green circles - increase in LVEF at follow-up compared to acute scan; red circles - decrease in LVEF at follow-up compared to follow-up. Those with a reduction in LVEF at follow-up were more likely to have an increase in both LVEDV and LVESV, and tended to be in the right upper quadrant (RUQ) of the graph (adverse LV remodelling group). Those with an improvement in LVEF were more likely to have in improvement in LVESV and LVEDV and tended to be in the middle lower quadrant (MLQ) and left lower quadrant (LLQ) of the graph (reverse LV remodelling group). Some patients had an increase in LVEDV only with or without an improvement in LVEF, and tended to lie in the right middle quadrant (RMQ) of the graph (adverse LV remodelling with compensation). Those in the middle quadrant (MQ) of the graph had no change in LVEDV or LVESV and predominantly no change in LVEF (no remodelling group).

Figure 8-5a provides a schematic representation for evaluating LV remodelling post-STEMI from %ΔLVEDV and %ΔLVESV, using a 2-step approach: firstly the %ΔLVEDV is evaluated (in this case a cut-off value of 12% was used) and secondly, the %ΔLVESV is assessed as shown in Figure 8-5b (in this case a cut-off value of 13% was used). Using this approach, 4 main patterns of post-STEMI LV remodelling were observed: Group 1: adverse LV remodelling (with LVEF unchanged or worsened, 30%); Group 2: adverse LV remodelling with compensation (with LVEF predominantly improved, 16%); Group 3: no LV remodelling (with LVEF predominantly unchanged, 20%); and Group 4: reverse LV remodelling (with LVEF predominantly improved, 27%).

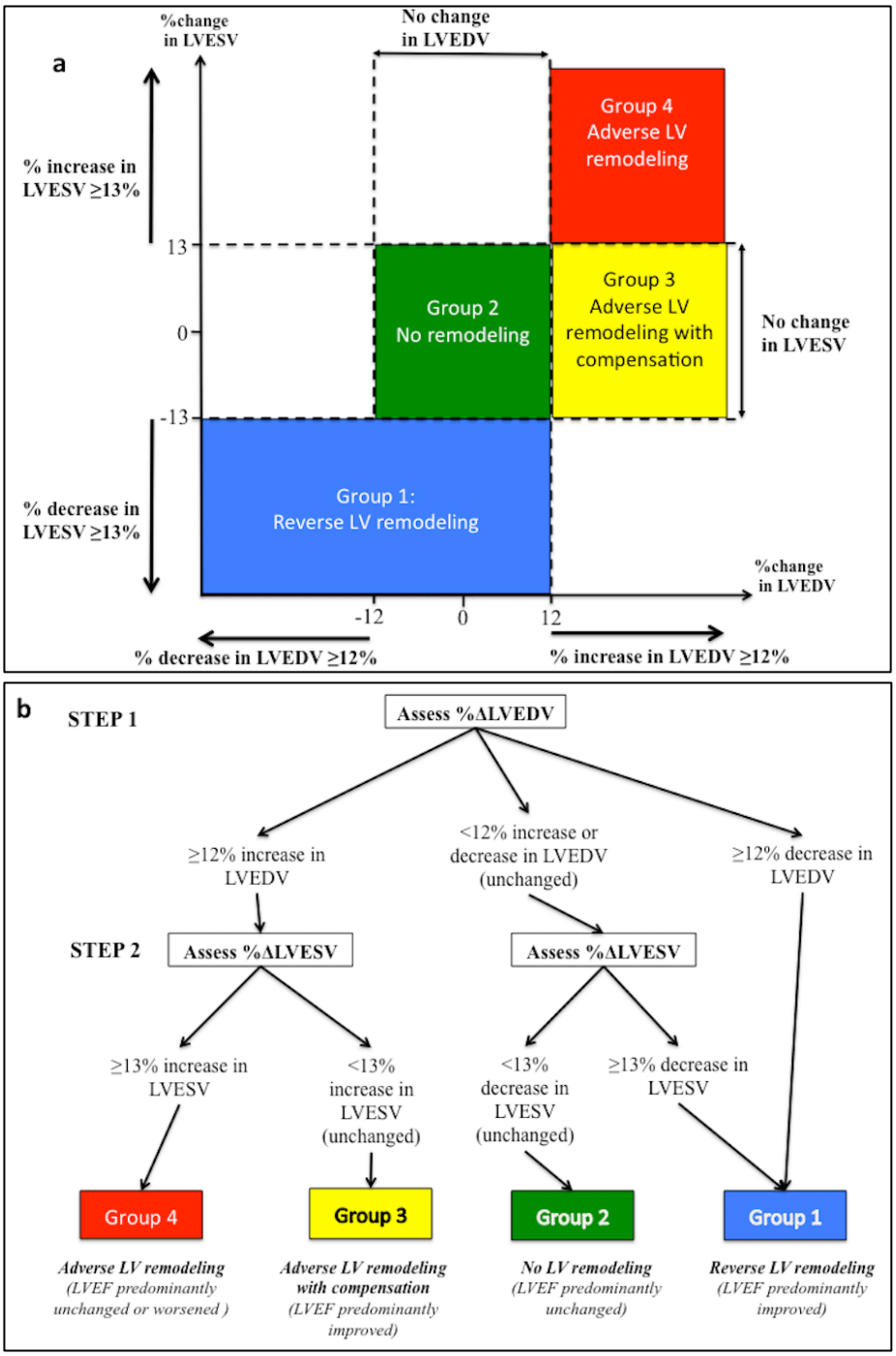

Figure 8-5: (a) Schematic representation of the different groups of remodelling; (b) The evaluation of LV remodelling using a 2-step approach.

Based on the %ΔLVEDV and %ΔLVESV between the follow-up and acute CMR, patients would predominantly fall into these 4 main patterns of LV remodelling groups. Using a 2-step approach and a combination of %ΔLVEDV and %ΔLVESV, patients can be easily classified into these 4 groups.

8.3.5 Relationship between %ΔLVESV/ %ΔLVEDV, MI size and MVO

The acute MI size was divided into quartiles as follows: <15%, 15 to <24%, 24 to <33% and ≥33%. Figure 6 shows the distribution of acute MI size divided by quartiles and between those without MVO (Figure 8-6a) and those with MVO (Figure 6b). Although those with larger MI size and MVO were more likely to have adverse LV remodelling (red box), there were also patients with small MI sizes and no MVO who went on to develop adverse LV remodelling (green dots within the red margins in Figure 6a) and adverse LV remodelling with compensation (green dots within the yellow margins). Likewise, there were also a notable number of patients with large MI size and MVO who developed reverse LV remodelling (black dots within the blue margins in Figure 8-6b).

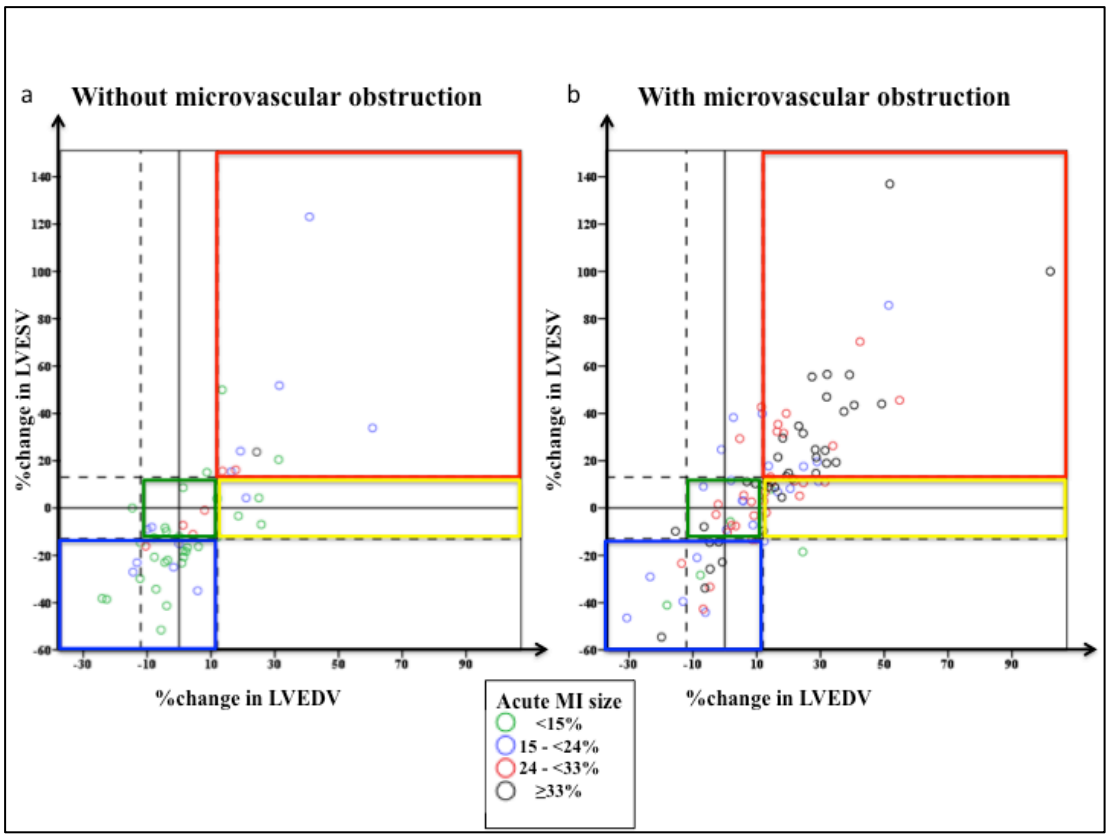

Figure 8-6: Relation between %ΔLVEDV/ %ΔLVEV and different quartiles of acute MI size in (a) patients without MVO and (b) patients with MVO.

Some patients with small MI and no MVO (green dots in 6a) developed adverse LV remodelling (falling within the red margin or yellow margin in 6a) with others with large MI and MVO (black dots in 6b) developed reverse LV remodelling or no remodelling (falling within the green or blue box in 6b).

8.4 Discussion

The main findings of this study are as follows: (a) The MDC95 in %ΔLVEDV and %ΔLVESV of 12% and 13% respectively, and was higher than the corresponding cut-off values for predicting LVEF<50% at follow-up (11% for %ΔLVEDV, and 5% for %ΔLVESV), providing cut-off values for assessing adverse and reverse LV remodelling following STEMI by CMR; (b) The minimal

detectable changes in %ΔLVM and %ΔLVEF from the acute to follow-up CMR scan were 12% and 13%, respectively, providing cut-off values for assessing changes in these LV parameters following STEMI by CMR; (c) By assessing the combined %ΔLVEDV and %ΔLVESV between the acute and follow-up CMR, we observed 4 different patterns of LV remodelling following STEMI.

In this study, we measured both intra-observer and inter-observer variability, and as expected the MDC95s for all these LV parameters were greater for inter-observer than intra-observer measurements. Our analyses on the whole cohort mainly focused on the inter-observer rather than the intra-observer measurements because different operators analysed the scans from each study. We found that the inter-observer MDC95s for %ΔLVEDV and %ΔLVESV between the acute and the follow-up CMR were 12% and 13%, respectively. These provide cut-off values for defining LV remodelling following STEMI, and suggest that a combination an increase in LVEDV (≥12%) and in LVESV (≥13%) could be used to identify adverse LV remodelling, whereas a decrease in LVESV (≥13%) with or without a decrease in LVEDV (≥12%) could be used to identify reverse LV remodelling. However, further studies are required to investigate the prognostic implications of these proposed cut-off values for defining adverse and reverse LV remodelling following STEMI.

Currently there is no consensus on whether T&P should be included as part of the LV volume or as part of LV mass during LVEF and LVM assessment by CMR. (57) We therefore provided MDC95 for %ΔLVEDV, %ΔLVESV, %ΔLVM, and %ΔLVEF using both approaches. It is already known that the T&P can significantly affect LV volumes, LV mass, and LVEF.(292, 293) We found

that LVEDV and LVESV were higher, and LVM and LVEF were lower when T&P were included as part of the LV volume and this is consistent with previous reports.(292-294) As their inclusion as part of the LV mass is not always practical depending on the software, both methods are currently considered acceptable.(57) Although the LV parameters differed depending on how the T&P were dealt with, there was no difference in the CoV both for inter or intra-observer measurements for LVEDV, LVESV, LVM and LVEF when T&P were included as part of the LV volume or LV mass. However, the MDC95 for intra-observer and inter-observer measurements for %Δ in LV parameters varied by 1-2% depending on whether the T&P were included as part of the LV volume or LV mass. We therefore provided the highest MDC95 for each LV parameter in Table 5, irrespective of how the T&P were dealt with.

Using LVEF <50% at follow-up as a clinically important surrogate marker for assessing adverse LV remodelling following STEMI, we obtained cut-off values for %ΔLVEDV and %ΔLVESV of 10% and 5%, respectively. The diagnostic performance of %ΔLVEDV and %ΔLVESV was not as high as expected and could be related to the fact that some patients have LV remodelling with compensation (group 3) and therefore would maintain LVEF above 50% despite an increase in %ΔLVEDV. On the other hand, %ΔLVESV performed slightly better, which is not surprising as LVEF is calculated from the formula (LVEDV-LVESV)/LVEDV, and there was an element of mathematical coupling.(295) But the diagnostic performance for %ΔLVESV was not as high as expected as it is dependent on a change in %ΔLVEDV to lead to a reduction in LVEF. These cut-off values obtained were lower than that defined by our

MDC95 cut-off values for %ΔLVEDV of 12%, and for %ΔLVESV of 13%. The minimal detectable change and the clinically significant change are independent of each other as they are derived in different ways and in our case, the former turned out to be larger than the later. Therefore we chose the cut-off values of MDC95 to define LV remodelling in the whole cohort.

Westman et al (205) recently showed that there was an imperfect link between MI size and adverse LV remodelling (defined as >10ml/m^2 increase in indexed LVEDV). Several studies have also shown that MVO was a strong predictor of adverse LV remodelling.(60) Using the definition in our study for adverse LV remodelling, we also showed that there was an imperfect link between acute MI size and adverse LV remodelling as well between MVO and adverse LV remodelling. Some patients with large MI size and MVO developed reverse LV remodelling and some patients with small MI size and no MVO developed adverse LV remodelling. As eluded by Westman et al(205), the development of adverse LV remodelling is complex and multi-factorial, and more work is warranted in this field.

We found the MDC95 in %ΔLVM between acute and follow-up scans to be ≥12%, suggesting that this would be the minimal change in LVM that is unlikely due to inter-observer measurement errors. However, the interpretation of changes in LVM following STEMI is complicated by the fact that on the acute scan, the presence of myocardial oedema also contributes to the changes in LVM acutely and therefore we did not investigate %ΔLVM in post-STEMI LV remodelling. However, it would be interesting to determine the MDC for assessing %ΔLVM in patients with LV hypertrophy (LVH) related to

hypertension or aortic valve disease, in order to provide cut-off values which can be used in studies assessing the regression of LVH.

Finally, we found the MDC95 for %ΔLVEF to be ≥13% in STEMI patients when using CMR. This finding suggests that only a relative change in LVEF of 13% or more can be reliably detected by CMR as being beyond inter-observer measurement errors. This is equivalent to an absolute change of 6.5% in a patient with an acute LVEF of 50%. This needs to be taken into consideration when planning future studies designed to investigate new treatments for improving LVEF following STEMI.

8.4.1 Limitations

Inter-observer and intra-observer measurements were performed in 15 patients only (30 scans) but this is similar in numbers to the previous study providing the minimal detectable change in LVEF by echocardiography in patients undergoing chemotherapy (10 patients with echocardiography at 2 time-points).(291) We only used one analysis tool and LV parameters were quantified using the semi-automated method. We did not have matching echocardiography data for comparison. Crimi et al (117) included LAD STEMIs only and there was an element of selection bias. However LAD STEMIs are associated with larger MIs and with poor prognosis (296) and therefore despite having only 146 patients with paired CMR scans, they represented a higher risk cohort with 75% presenting with LAD STEMI. We did not have a large enough cohort to provide information on clinical outcomes and therefore used an LVEF

at follow-up of <50% to be clinically important. There was heterogeneity in the performance of CMR for acute MI size and MVO (scanner strength, dosage and type of contrast, timing of LGE for MVO and MI, quantification technique used – Table 1) and our findings need to be confirmed by other studies.

8.5 Conclusions

The MDCs for %ΔLVEDV and %ΔLVESV of 12% and 13% respectively, between acute and follow-up CMR scans, may be used to help define adverse and reverse LV remodelling post-STEMI. Combining %ΔLVEDV and %ΔLVESV following STEMI may provide additional insights into the different patterns of LV remodelling, but their prognostic impact needs to be assessed in future studies. Finally, the MDC for %ΔLVEF of 13% relative to baseline provides the minimal effect size that needs to be taken into consideration when investigating treatments aimed at improving LVEF following acute STEMI.

9 General discussion

In this thesis, we have shown that multi-parametric mapping CMR provides in-depth insight into the various components of an acute STEMI, namely the MI zone, the MI core, the AAR and remote myocardium. However, performing all these parameters can be time-consuming, especially in acutely unwell STEMI patients. Therefore, these multi-parametric mapping techniques should be used judiciously in order to obtain the maximum information with the least number of CMR sequences.

9.1 T1 mapping for the delineation of the AAR, IMH and MI size

A comprehensive CMR study in a reperfused acute STEMI patient requiring data on the AAR, IMH, MVO, MI size and ECV, would take on average, an hour to perform. Based on the results from Chapter 5, either native T1 mapping or T2 mapping and conventional LGE could be omitted. This approach would substantially shorten the scanning time by 15-20 minutes (see Figure 9-1 *a and b*) in centres performing comprehensive CMR studies, without compromising data acquisition. Furthermore, this would improve patient workflow, make the CMR scan more tolerable to acute STEMI patients, and may help minimise patient dropout in future clinical studies. If data on ECV were required, then native T1 mapping would be preferred over T2 mapping. By acquiring native (for AAR) and post contrast T1 mapping (for LGE), ECV maps can be derived (Figure 9-1*d*), and this process may also be accelerated if the synthetic or in-line ECV tool available on the Siemens platform is used.(297)

Alternatively, If only data on AAR and MI are required, then T2 mapping could be replaced by T1 mapping (Figure 9-1*c*).

We would still recommend performing T2* weighted imaging or T2* mapping when available as the accuracy of T1 mapping and T2 mapping to detect IMH was only 85% and 87% respectively. However, in situations when T2* imaging is not interpretable or not available, T1 or T2 mapping could then be used as surrogates to identify IMH and this approach would minimise patients' dropping out from future studies. The wider availability of free breathing and motion corrected T2* mapping (157) would make this modality more bearable for STEMI patients and full LV coverage (for accurate IMH quantification) would be possible with minimal discomfort to the patients.

Last but not least, performing post-contrast cine as shown in Figure 9-1 would provide an alternative modality for assessing the AAR. AAR from contrast-enhanced SSFP (CE-SSFP) cine has been shown to provide similar estimates of the AAR when compared to T2-STIR and CE-SSFP had significantly more images of diagnostic quality (97% versus 65%) in a large study of 215 STEMI patients.(114)

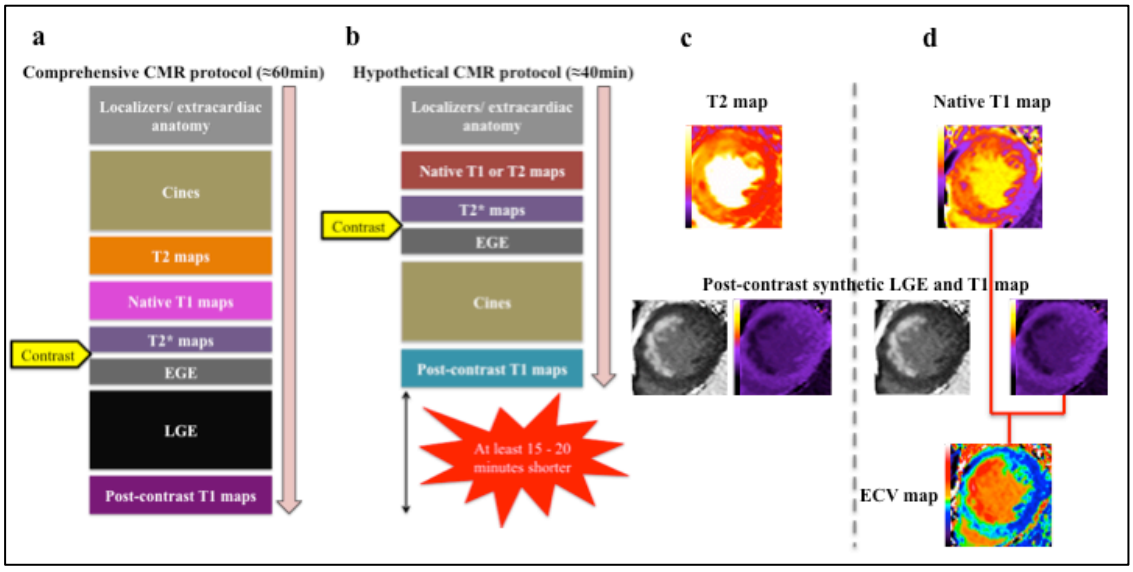

Figure 9-1: Duration of the CMR scan.

Figure 6a and b illustrate the duration for a comprehensive STEMI CMR acquisition protocol providing data on AAR, IMH, MVO, MI size and ECV and on average takes around one hour to acquire. Based on the results from this study, T1 mapping may allow T2 mapping and LGE to be omitted thereby shortening the scanning time by 15-20 minutes. Figure 6c and d illustrates the options of either doing T2 mapping and post-contrast T1 mapping or native T1 mapping and post-contrast T1 mapping depending on the research question.

Certain cardioprotective therapies such as ischaemic postconditioning (115) and remote ischaemic conditioning (using transient arm or leg ischaemia and reperfusion) (116, 117) have been shown not only to reduce MI size, but also reduced the extent of oedema delineated by T2 mapping and T2-weighted imaging, leading to an underestimate of the AAR in reperfused STEMI patients. Whether these therapeutic interventions also affect the AAR delineated by T1 mapping needs to be investigated in future studies.

It was previously believed that the AAR delineated by T2-weighted imaging is maximum and constant within the first week following an acute

myocardial infarction.(91, 164) A recent pre-clinical study using a porcine model of acute MI has suggested that myocardial oedema delineated by T2-weighted imaging vary over the first week and displays a bimodal phase of oedema.(110) However, recently Carrick et al (112) showed that although the T2 and T2* of the core of the MI followed a bimodal pattern and was more pronounced in those with IMH, the extent of myocardial oedema in the clinical setting followed a unimodal pattern and peaked at day 3. Nordlund et al (114) also recently provided some indirect evidence and no change in size or quality of the AAR over the first week in 215 STEMI patients. More work is warranted in this field to compare the performance and stability of CE-SSFP cines, T1 mapping and T2 mapping to delineate the AAR within the first week of an MI and when is the optimal timing for CMR imaging.

Although free breathing and motion corrected T2* mapping (157) sounds very appealing and promising for use in the setting of STEMI research, its performance against the conventional T2* mapping to detect and quantify different extents of IMH, remains to be tested. Furthermore, although IMH has been showed to peak on day 3 (112), whether those with IMH at a later stage (day 5 to 7) may be more prognostic remains to be tested in future studies.

Advances in real-time cines for LVEF (298) and future refinements in MR fingerprinting techniques (299) (for robust and fast acquisition of simultaneous T1 and T2 mapping data per slice within one breath-hold) would further reduce scan time and would be highly desirable in the STEMI setting.

9.2 The optimal method for MI size quantification

Several studies (177, 178) have investigated the optimal semi-automated method for quantifying MI size, but there is currently no established gold standard recommendation. Manual contouring is considered the reference standard (57, 176) but it can be time consuming (183) and may be subjective. Several semi-automated techniques have been proposed for quantifying acute and chronic MI size such as a signal intensity threshold of 5-SD (177) or 6-SD (178) above the normal remote myocardium, the Otsu technique (180), and the FWHM (182, 183) and the automated quantification accounting for partial volume effects (281) as summarised in Table 9-1. The consensus document from the Society for Cardiovascular Magnetic Resonance (SCMR) Board of Trustees Task Force on Standardized Post Processing (57) currently recommends the semi-automated threshold technique of 5-SD for MI size quantification, in the absence of clear gold standard semi-automated technique, as it may improve reproducibility. However, some studies have shown that 5-SD overestimates acute MI size (180, 280) and we showed a similar finding, as described in chapter 6. 6-SD was better that 5-SD, FWHM and Otsu to quantify both acute and follow-up MI size and this was most recently confirmed by Zhang et al at 3T.(185) Although FWHM has been shown to have the lowest variability (182, 183) and performed well for acute MI size in our cohort, it was dependent on the imaging sequence we used for LGE. Furthermore, we showed that in patients with MVO on the acute scan, FWHM underestimated the chronic MI size. However, we have also shown that acute MI size by all 4 of

these promising techniques performed equally well to predict adverse LV remodelling.

Whether MI size quantified by the 4 different semi-automated techniques would perform equally well to predict clinical outcomes, needs to be tested in future studies.

Table 9-1: Main studies comparing difference techniques for IS and AAR quantification.

Study	No of patients	Techniques compared	Software	Result
Zhang 2016 (185)	114 AMI patients with matching follow-up scan at 6 months at 3T	Manual, FWHM (20 to 50%), 1 to 9-SDs	Mass	FWHM30% and 3-SD was closest to manual for total infarct size and FWHM45% and 6-SD was closest to manual for core MI size
Dash 2015 (280) (conference abstract)	19 AMI porcine models	FWHM 5-SD 6-SD	CVI42	6-SD was more accurate to quantify MI size. FWHM and 5-SD overestimated MI size when compared to histology
McAlindon 2015 (176)	40 AMI	Manual 2,3,5 SDs Otsu FWHM	CVI42	Manual and FWHM provided the lowest inter, intra-observer variability for infarct size
Khan 2015 (183)	10 AMI 1.5T and 10AMI 3T	5-8 SDs FWHM Otsu	CVI42	FWHM is accurate and reproducible. 5-SD and OAT overestimates infarct size at both fields. FWHM correlated strongest with LV EF
Vermes 2013 (180)	28 AMI 30 myocarditis	Visual 2,3,5 SDs Otsu FWHM	CVI42	Otsu and 5-SD did not differ. Otsu similar to visual 5-SD and FWHM overestimated LGE compared to visual
Varga-	AMI in 6	2-6 SD,	ImageJ	6-SD provided the most

Szemes 2012 (300)	swines	FWHM, TTC		accurate measure of MI size
Flett 2011 (182)	20 AMI 20 CMI 20 HCM	Manual 2 - 6 SDs FWHM	ImageJ (purpose-written macro)	No difference between FWHM, manual, 6-SD and 5-SD. FWHM similar to manual and more reproducible (reducing required sample size by one-half)
Beek 2009 (178)	38 CMI	2-8 SDs FWHM	Mass	6-SD showed the highest accuracy to predict segmental functional recovery
Bondarenko 2005 (177)	15 CMI	2-6 SDs		No difference between visual analysis and 5-SD.
Hsu 2006/ Hsu 2006 (301, 302)	11 canine - AMI 11 AMI and 9 CMI	Manual 2SD FWHM FACT	Interactive Display Language/ Microsoft Visual C++	FACT accurately measured MI size in vivo and ex-vivo – more accurate than manual and SD. Manual and 2-SD overestimated infarct size compared to FACT
Amado 2004 (181)	13 canine – AMI	Manual 1-6 SDs FWHM	Cine tool, GE	FWHM correlated best with post-mortem data. No difference in MI between 6 and 30 minutes after contrast

AMI: acute myocardial infarction; SD: standard deviation; MI: myocardial infarction; FWHM: full width half maximum; FACT: feature analysis and combined thresholding; LGE: late gadolinium enhancement; CMI: chronic myocardial infarction; HCM: hypertrophic cardiomyopathy.

9.3 IMH as a future therapeutic target to prevent adverse LV remodelling

It is well recognised that IMH is associated with larger MI size, adverse LV remodelling and poor clinical outcomes (160, 161, 261, 283) and may be pro-arrhythmic. (206, 303) Although our study was purely based on tissue characterisation, these findings support the current literature (207, 208) that residual myocardial iron may play a role in the inflammatory phase of adverse

LV remodelling. We used T2 mapping for the detection of delayed resolution of oedema associated with residual myocardial iron in patients with IMH.

Recently Carrick et al (139) performed serial scanning in 30 patients and elegantly described the time course of MVO and IMH. MVO was already present at 4 to 12 hours and remained stable up to a mean of 2.9 days and then reduced by day 10. IMH, on the other hand, peaked at a mean of 2.9 days and decreased by day 10. 13 patients had IMH on day 2.9 and only 4 patients displayed residual myocardial iron by 6 months. Based on brain imaging data (158), degradation of haemoglobin eventually leads to ferritin and hemosiderin deposits and the fact that the majority of their patients had no residual myocardial iron in their study may suggest that those patients had small areas of IMH that were rapidly cleared by the macrophages. They reported the presence of IMH in 41% of their total cohort of 245 patients with analysable T2* data and it is likely that this may be an underestimation of the true prevalence of IMH, as the CMR was performed at a mean of 2.1 days, which is earlier than the timing for peak IMH (2.9 days). Pooling the results of these 3 studies demonstrating residual myocardial iron following STEMI, Kali et al (207) (acute scan: 11 out of 15 patients with IMH; follow-up scan: 11 with residual myocardial iron), Carrick et al (139) (acute scan: 13 out of 30 patients with IMH; follow-up scan: 4 with residual myocardial iron) and our study (acute scan: 15 out of 28 patients with IMH; follow-up scan: 13 with residual myocardial iron), the incidence of IMH by T2* mapping was 53% (39/73) and 72% (28/39) had residual myocardial iron at follow-up. Although IMH is likely to be confounded by larger infarct size, whether specifically targeting these patients with anti-

inflammatory agents or chelation therapy needs to be investigated in future studies aiming to prevent adverse LV remodelling.

9.4 Prognostic significance of the remote myocardial ECV

Chan et al (213) used post-contrast T1 in 25 acute STEMI patients and found evidence of early remote systolic dysfunction and expansion of the ECM, which persisted in the chronic stage and their findings partly differs from ours. We did not find evidence of systolic dysfunction in the remote myocardium but paradoxically found an increase in wall motion in the remote myocardium on the acute scan only. These differences may partly be due to the smaller number of patients, and methodology used in their study (definition of a remote sector: any segment without LGE as defined in their study may potentially have included adjacent segments with oedema and stunning; they only analysed base, mid and an apical cine compared to full LV short axis analysis and we used averaged values of the mid ventricular segments in our study). Furthermore, not all STEMI patients showed persistence of ECV_{Remote} expansion at follow-up when using automated ECV maps and this may be due to the fact that we included more patients with a wider range of MI size (acute MI size in our study 27.4±14.6% versus 19.2±10.5% in their study) and the higher use of angiotensin converting enzyme inhibitors/ angiotensin receptor blockers (ACEI/ARB) and mineralocorticoid receptor antagonist (MRA) in our study (ACEI/ARB 92% versus 100%: MRA 16% versus 25%).

Carrick et al (197) demonstrated that increased native T1 values in remote myocardium of reperfused STEMI patients were independently

associated with adverse LV remodelling after adjusting for LVEDV, MI size and MVO on the acute scan. In a separate publication, Carrick et al (156) also showed that native T1 of the hypo-intense infarct core was inversely associated with the risk of all-cause mortality or hospitalization for heart failure in the same cohort of patients although they did not adjust for native T1 of the remote myocardium.

In our cohort, although the number of patients were significantly less, we showed that MI size was the single most significant predictor of adverse LV remodelling after adjusting for similar parameters including native T1 of the remote myocardium. Although MI size is known to be a strong predictor of outcome (58, 59), MSI is a more sensitive marker to assess the effectiveness of a reperfusion strategy (66, 67) in randomised controlled trials and it was recently shown that MSI significantly reduced sample size.(304) Therefore, we opted to use MSI instead of MI size expressed as a percentage of the LV. We found that acute ECV_{Remote} together with MSI were also strongly associated with LV remodelling after adjusting for $T1_{Remote}$, $T1_{Core}$ and MVO.

Although the sample size was significantly smaller in our study, our findings may also differ from the studies by Carrick et al (156, 197) as we used mean segmental values for T1, T2 and ECV rather than manual ROI (The ICC for reliability of remote T1 in Carrick et al (197) was 0.92 and had quite a wide 95% CI (0.80, 0.97)). Furthermore, the majority of our patients (>70%) had full LV coverage for the T1 maps and ECV maps. These maps were averaged to derive the mean segmental values as per the AHA classification and therefore

were more likely to be a better representation of the changes in the remote myocardium.

Carberry et al (288) most recently showed in 131 STEMI patients that the change in remote zone ECV was a multivariable associate of the change in left ventricular end-diastolic volume at 6 months, but they were underpowered to show an association with clinical outcomes. Whether change in ECV in the remote myocardium can be used as a surrogate to predict those at high risk of adverse LV remodelling and poor clinical outcomes needs to be assessed in future adequately powered studies.

9.5 Redefining LV remodelling by CMR

Conventionally, adverse LV remodelling post-STEMI has been defined by %ΔLVEDV and CMR studies have used the echocardiography derived cut-off value of 20%.(196, 197) Other groups have used an arbitrary cut-off of ≥15% increase in LVESV to define adverse LV remodelling by CMR.(63, 199) We found that the cut-off values for %ΔLVEDV and %ΔLVESV between the acute and the follow-up CMR were 12% and 13%, respectively.

As expected, the cut-off value of 12% or more for %ΔLVEDV to define adverse LV remodelling obtained in our cohort is significantly lower than that defined by echocardiography. This is due to the better spatial resolution of CMR, with results in lower intra-observer and inter-observer variability.(191) On the other hand, the cut-off value for defining reverse LV remodelling as ≥13% ΔLVESV from our study is higher than the 10% cut-off value currently proposed by echocardiography (195), although the MDC95 for intra-observer

measurements by CMR was identical at 10%. The echocardiography-based method was derived using ROC curve for the optimal cut-off for decrease in ESV to predict mortality in patients undergoing cardiac resynchronization therapy and they did not perform inter-observer and intra-observer variability for %ΔLVESV. It is highly likely that the inter-observer and intra-observer for %ΔLVESV by echocardiography in STEMI patients would be higher than the CMR cut-off value we obtained.

Our data, suggests that assessing both %ΔLVEDV and %ΔLVESV provides further insights into different patterns of LV remodelling following STEMI, and this approach may allow one to customise heart failure therapy to prevent adverse LV remodelling or promote reverse LV remodelling. Orn et al (149) described 3 patterns of LV remodelling based on the presence and persistence of MVO by CMR within the first week of an acute STEMI in a serial CMR study of 42 patients. Most LV remodelling occurred by 2 months and continued to at least 1 year. Those with no MVO had a normal pattern of wound healing; those with MVO on day 2 only dilated their ventricle but adapted functionally; and the last group were those with persistent MVO at 1 week and they dilated their ventricle without the ability to adapt functionally. These 3 groups bear some resemblance to the groups of LV remodelling we identified but we did not have serial CMR data on MVO for comparison. Other factors that determine the pattern of LV remodelling post-STEMI also require further study.

We also found that in STEMI patients, only a relative change in LVEF of 13% or more can be reliably detected by CMR as being beyond inter-observer measurement errors. This is equivalent to an absolute change of 6.5% in a

patient with an acute LVEF of 50%. This needs to be taken into consideration when planning future studies designed to investigate new treatments for improving LVEF following STEMI.

We have provided new definitions to define LV remodelling post-STEMI by CMR. Combining %ΔLVEDV and %ΔLVESV following STEMI may provide additional insights into the different patterns of LV remodelling, but their prognostic impact needs to be assessed in future studies.

9.6 Summary of major findings

1. T1 mapping can quantify the AAR as well as T2 mapping in STEMI patients both at 1.5T and 3T. T1 mapping provides a reliable alternative method to quantify the AAR.
2. A hypo-intense core within the AAR on a T1 or T2 map can be used to detect IMH in cases when T2* mapping is not available or is not interpretable.
3. Post-contrast T1 maps and the post-contrast T1 mapping derived synthetic LGE can be used to accurately delineate the acute MI size and by acquiring post-contrast T1 maps may obviate the need for conventional LGE imaging.
4. When accurate MI size quantification is required (e.g. randomised controlled trials), 6-SD is the optimal semi-automatic threshold method both in the acute and follow-up setting. However, when precise MI size quantification is required (e.g. registries or observational studies), any

one of these 4 semi-automated techniques (5-SD, 6-SD, FWHM or Otsu) may be suitable.

5. A proportion of reperfused STEMI patients with IMH go on to have residual myocardial iron at 5 months and is associated with persistently elevated T2 in the areas of the chronic MI surrounding the residual iron. IMH and residual myocardial iron are potential future therapeutic targets to prevent adverse LV remodelling.
6. The remote ECV is increased within the first few days of a reperfused STEMI but only remains persistently elevated in a subset of patients who develop adverse LV remodelling.
7. The cut-off values to define %ΔLVEDV and %ΔLVESV in paired acute and follow-up STEMI patients are 12% and 13% respectively. These cut-off values could be used to define LV remodelling post STEMI by CMR. Combining %ΔLVEDV and %ΔLVESV would provide additional insights into the different patterns of LV remodelling.

Bibliography

1. Nabel EG, Braunwald E. A tale of coronary artery disease and myocardial infarction. The New England journal of medicine. 2012;366(1):54-63.

2. Pedersen F, Butrymovich V, Kelbaek H, Wachtell K, Helqvist S, Kastrup J, et al. Short- and long-term cause of death in patients treated with primary PCI for STEMI. Journal of the American College of Cardiology. 2014;64(20):2101-8.

3. Torabi A, Cleland JG, Khan NK, Loh PH, Clark AL, Alamgir F, et al. The timing of development and subsequent clinical course of heart failure after a myocardial infarction. European heart journal. 2008;29(7):859-70.

4. Ezekowitz JA, Kaul P, Bakal JA, Armstrong PW, Welsh RC, McAlister FA. Declining in-hospital mortality and increasing heart failure incidence in elderly patients with first myocardial infarction. Journal of the American College of Cardiology. 2009;53(1):13-20.

5. Spencer FA, Meyer TE, Gore JM, Goldberg RJ. Heterogeneity in the management and outcomes of patients with acute myocardial infarction complicated by heart failure: the National Registry of Myocardial Infarction. Circulation. 2002;105(22):2605-10.

6. Fokkema ML, James SK, Albertsson P, Akerblom A, Calais F, Eriksson P, et al. Population trends in percutaneous coronary intervention: 20-year results from the SCAAR (Swedish Coronary Angiography and Angioplasty Registry). Journal of the American College of Cardiology. 2013;61(12):1222-30.

7. Terkelsen CJ, Jensen LO, Tilsted HH, Trautner S, Johnsen SP, Vach W, et al. Health care system delay and heart failure in patients with ST-segment elevation myocardial infarction treated with primary percutaneous coronary intervention: follow-up of population-based medical registry data. Annals of internal medicine. 2011;155(6):361-7.

8. Stone GW, Selker HP, Thiele H, Patel MR, Udelson JE, Ohman EM, et al. Relationship Between Infarct Size and Outcomes Following Primary PCI: Patient-Level Analysis From 10 Randomized Trials. 2016(1558-3597 (Electronic)).

9. Dobrzycki S, Kralisz P, Nowak K, Prokopczuk P, Kochman W, Korecki J, et al. Transfer with GP IIb/IIIa inhibitor tirofiban for primary percutaneous coronary intervention vs. on-site thrombolysis in patients with ST-elevation myocardial infarction (STEMI): a randomized open-label study for patients admitted to community hospitals. European heart journal. 2007;28(20):2438-48.

10. Dieker HJ, van Horssen EV, Hersbach FM, Brouwer MA, van Boven AJ, van 't Hof AW, et al. Transport for abciximab facilitated primary angioplasty versus on-site thrombolysis with a liberal rescue policy: the randomised Holland Infarction Study (HIS). Journal of thrombosis and thrombolysis. 2006;22(1):39-45.

11. Svensson L, Aasa M, Dellborg M, Gibson CM, Kirtane A, Herlitz J, et al. Comparison of very early treatment with either fibrinolysis or percutaneous coronary intervention facilitated with abciximab with respect to ST recovery and infarct-related artery epicardial flow in patients with acute ST-segment elevation

myocardial infarction: the Swedish Early Decision (SWEDES) reperfusion trial. Am Heart J. 2006;151(4):798 e1-7.

12. Armstrong PW, Committee WS. A comparison of pharmacologic therapy with/without timely coronary intervention vs. primary percutaneous intervention early after ST-elevation myocardial infarction: the WEST (Which Early ST-elevation myocardial infarction Therapy) study. European heart journal. 2006;27(13):1530-8.

13. Kloner RA. Does reperfusion injury exist in humans? Journal of the American College of Cardiology. 1993;21(2):537-45.

14. Jennings RB, Sommers HM, Smyth GA, Flack HA, Linn H. Myocardial necrosis induced by temporary occlusion of a coronary artery in the dog. Archives of pathology. 1960;70:68-78.

15. Staat P, Rioufol G, Piot C, Cottin Y, Cung TT, L'Huillier I, et al. Postconditioning the human heart. Circulation. 2005;112(14):2143-8.

16. Yellon DM, Hausenloy DJ. Mechanisms of disease: Myocardial reperfusion injury. New England Journal of Medicine. 2007;357(11):1121-35.

17. Manning AS, Hearse DJ. Reperfusion-induced arrhythmias - mechanisms and prevention. Journal of molecular and cellular cardiology. 1984;16(6):497-518.

18. Bolli R, Marban E. Molecular and cellular mechanisms of myocardial stunning. Physiological reviews. 1999;79(2):609-34.

19. Krug A, Du Mesnil de R, Korb G. Blood supply of the myocardium after temporary coronary occlusion. Circulation research. 1966;19(1):57-62.

20. Niccoli G, Burzotta F, Galiuto L, Crea F. Myocardial no-reflow in humans. Journal of the American College of Cardiology. 2009;54(4):281-92.

21. Niccoli G, Scalone G, Lerman A, Crea F. Coronary microvascular obstruction in acute myocardial infarction. European heart journal. 2016;37(13):1024-33.

22. White SK, Hausenloy DJ, Moon JC. Imaging the myocardial microcirculation post-myocardial infarction. Current heart failure reports. 2012;9(4):282-92.

23. Frohlich GM, Meier P, White SK, Yellon DM, Hausenloy DJ. Myocardial reperfusion injury: looking beyond primary PCI. European heart journal. 2013;34(23):1714-22.

24. Murry CE, Jennings RB, Reimer KA. Preconditioning with ischemia: a delay of lethal cell injury in ischemic myocardium. Circulation. 1986;74(5):1124-36.

25. Zhao ZQ, Corvera JS, Halkos ME, Kerendi F, Wang NP, Guyton RA, et al. Inhibition of myocardial injury by ischemic postconditioning during reperfusion: comparison with ischemic preconditioning. American Journal of Physiology-Heart and Circulatory Physiology. 2003;285(2):H579-H88.

26. Przyklenk K, Bauer B, Ovize M, Kloner RA, Whittaker P. Regional ischemic 'preconditioning' protects remote virgin myocardium from subsequent sustained coronary occlusion. Circulation. 1993;87(3):893-9.

27. Yellon DM, Hausenloy DJ. Myocardial reperfusion injury. The New England journal of medicine. 2007;357(11):1121-35.

28. Sharma V, Bell RM, Yellon DM. Targeting reperfusion injury in acute myocardial infarction: a review of reperfusion injury pharmacotherapy. Expert opinion on pharmacotherapy. 2012;13(8):1153-75.

29. Bulluck H, Yellon DM, Hausenloy DJ. Reducing myocardial infarct size: challenges and future opportunities. Heart. 2016;102(5):341-8.

30. Mehta SR, Yusuf S, Diaz R, Zhu J, Pais P, Xavier D, et al. Effect of glucose-insulin-potassium infusion on mortality in patients with acute ST-segment elevation myocardial infarction: the CREATE-ECLA randomized controlled trial. JAMA : the journal of the American Medical Association. 2005;293(4):437-46.

31. Selker HP, Beshansky JR, Sheehan PR, Massaro JM, Griffith JL, D'Agostino RB, et al. Out-of-hospital administration of intravenous glucose-insulin-potassium in patients with suspected acute coronary syndromes: the IMMEDIATE randomized controlled trial. JAMA : the journal of the American Medical Association. 2012;307(18):1925-33.

32. Cung TT, Morel O, Cayla G, Rioufol G, Garcia-Dorado D, Angoulvant D, et al. Cyclosporine before PCI in Patients with Acute Myocardial Infarction. The New England journal of medicine. 2015;373(11):1021-31.

33. Latini R, Limbruno U, La Vecchia L, Locuratolo N, Costalunga A, Sicuro M, et al. Abstract 15211: Effect of Cyclosporine a on Infarct Size Reduction in Reperfused Acute Myocardial Infarction Treated with Primary Angioplasty. Circulation. 2014;130(Suppl 2):A15211-A.

34. Najjar SS, Rao SV, Melloni C, Raman SV, Povsic TJ, Melton L, et al. Intravenous erythropoietin in patients with ST-segment elevation myocardial infarction: REVEAL: a randomized controlled trial. JAMA : the journal of the American Medical Association. 2011;305(18):1863-72.

35. Prunier F, Biere L, Gilard M, Boschat J, Mouquet F, Bauchart JJ, et al. Single high-dose erythropoietin administration immediately after reperfusion in patients with ST-segment elevation myocardial infarction: results of the erythropoietin in myocardial infarction trial. Am Heart J. 2012;163(2):200-7 e1.

36. Ott I, Schulz S, Mehilli J, Fichtner S, Hadamitzky M, Hoppe K, et al. Erythropoietin in patients with acute ST-segment elevation myocardial infarction undergoing primary percutaneous coronary intervention: a randomized, double-blind trial. Circulation Cardiovascular interventions. 2010;3(5):408-13.

37. Kloner RA. Current state of clinical translation of cardioprotective agents for acute myocardial infarction. Circulation research. 2013;113(4):451-63.

38. Erlinge D, Gotberg M, Lang I, Holzer M, Noc M, Clemmensen P, et al. Rapid endovascular catheter core cooling combined with cold saline as an

adjunct to percutaneous coronary intervention for the treatment of acute myocardial infarction. The CHILL-MI trial: a randomized controlled study of the use of central venous catheter core cooling combined with cold saline as an adjunct to percutaneous coronary intervention for the treatment of acute myocardial infarction. Journal of the American College of Cardiology. 2014;63(18):1857-65.

39. Nichol G, Strickland W, Shavelle D, Maehara A, Ben-Yehuda O, Genereux P, et al. Prospective, multicenter, randomized, controlled pilot trial of peritoneal hypothermia in patients with ST-segment- elevation myocardial infarction. Circulation Cardiovascular interventions. 2015;8(3):e001965.

40. Atar D, Arheden H, Berdeaux A, Bonnet JL, Carlsson M, Clemmensen P, et al. Effect of intravenous TRO40303 as an adjunct to primary percutaneous coronary intervention for acute ST-elevation myocardial infarction: MITOCARE study results. European heart journal. 2015;36(2):112-9.

41. Lincoff AM, Roe M, Aylward P, Galla J, Rynkiewicz A, Guetta V, et al. Inhibition of delta-protein kinase C by delcasertib as an adjunct to primary percutaneous coronary intervention for acute anterior ST-segment elevation myocardial infarction: results of the PROTECTION AMI Randomized Controlled Trial. European heart journal. 2014;35(37):2516-23.

42. Siddiqi N, Neil C, Bruce M, MacLennan G, Cotton S, Papadopoulou S, et al. Intravenous sodium nitrite in acute ST-elevation myocardial infarction: a randomized controlled trial (NIAMI). European heart journal. 2014;35(19):1255-62.

43. Jones DA, Pellaton C, Velmurugan S, Rathod KS, Andiapen M, Antoniou S, et al. Randomized phase 2 trial of intracoronary nitrite during acute myocardial infarction. Circulation research. 2015;116(3):437-47.

44. Hausenloy DJ, Baxter G, Bell R, Botker HE, Davidson SM, Downey J, et al. Translating novel strategies for cardioprotection: the Hatter Workshop Recommendations. Basic research in cardiology. 2010;105(6):677-86.

45. Schwartz Longacre L, Kloner RA, Arai AE, Baines CP, Bolli R, Braunwald E, et al. New horizons in cardioprotection: recommendations from the 2010 National Heart, Lung, and Blood Institute Workshop. Circulation. 2011;124(10):1172-9.

46. Hausenloy DJ, Erik Botker H, Condorelli G, Ferdinandy P, Garcia-Dorado D, Heusch G, et al. Translating cardioprotection for patient benefit: position paper from the Working Group of Cellular Biology of the Heart of the European Society of Cardiology. Cardiovascular research. 2013;98(1):7-27.

47. Heusch G. Cardioprotection: chances and challenges of its translation to the clinic. Lancet. 2013;381(9861):166-75.

48. Lim WY, Messow CM, Berry C. Cyclosporin variably and inconsistently reduces infarct size in experimental models of reperfused myocardial infarction: a systematic review and meta-analysis. British journal of pharmacology. 2012;165(7):2034-43.

49. Rossello X, Yellon DM. A critical review on the translational journey of cardioprotective therapies! International journal of cardiology. 2016;220:176-84.

50. Sorensson P, Saleh N, Bouvier F, Bohm F, Settergren M, Caidahl K, et al. Effect of postconditioning on infarct size in patients with ST elevation myocardial infarction. Heart. 2010;96(21):1710-5.

51. Garcia-Dorado D, Garcia-Del-Blanco B, Otaegui I, Rodriguez-Palomares J, Pineda V, Gimeno F, et al. Intracoronary injection of adenosine before reperfusion in patients with ST-segment elevation myocardial infarction: A randomized controlled clinical trial. International journal of cardiology. 2014;177(3):935-41.

52. Lonborg J, Kelbaek H, Vejlstrup N, Botker HE, Kim WY, Holmvang L, et al. Exenatide reduces final infarct size in patients with ST-segment-elevation myocardial infarction and short-duration of ischemia. Circulation Cardiovascular interventions. 2012;5(2):288-95.

53. Ferdinandy P, Hausenloy DJ, Heusch G, Baxter GF, Schulz R. Interaction of risk factors, comorbidities, and comedications with ischemia/reperfusion injury and cardioprotection by preconditioning, postconditioning, and remote conditioning. Pharmacological reviews. 2014;66(4):1142-74.

54. Bulluck H, Maestrini V, Rosmini S, Abdel-Gadir A, Treibel TA, Castelletti S, et al. Myocardial T1 mapping. Circulation journal : official journal of the Japanese Circulation Society. 2015;79(3):487-94.

55. Wagner A, Mahrholdt H, Holly TA, Elliott MD, Regenfus M, Parker M, et al. Contrast-enhanced MRI and routine single photon emission computed tomography (SPECT) perfusion imaging for detection of subendocardial myocardial infarcts: an imaging study. Lancet. 2003;361(9355):374-9.

56. Thiele H, Kappl MJ, Conradi S, Niebauer J, Hambrecht R, Schuler G. Reproducibility of chronic and acute infarct size measurement by delayed enhancement-magnetic resonance imaging. Journal of the American College of Cardiology. 2006;47(8):1641-5.

57. Schulz-Menger J, Bluemke DA, Bremerich J, Flamm SD, Fogel MA, Friedrich MG, et al. Standardized image interpretation and post processing in cardiovascular magnetic resonance: Society for Cardiovascular Magnetic Resonance (SCMR) board of trustees task force on standardized post processing. Journal of cardiovascular magnetic resonance : official journal of the Society for Cardiovascular Magnetic Resonance. 2013;15:35.

58. Wu E, Ortiz JT, Tejedor P, Lee DC, Bucciarelli-Ducci C, Kansal P, et al. Infarct size by contrast enhanced cardiac magnetic resonance is a stronger predictor of outcomes than left ventricular ejection fraction or end-systolic volume index: prospective cohort study. Heart. 2008;94(6):730-6.

59. Roes SD, Kelle S, Kaandorp TA, Kokocinski T, Poldermans D, Lamb HJ, et al. Comparison of myocardial infarct size assessed with contrast-enhanced magnetic resonance imaging and left ventricular function and volumes to predict

mortality in patients with healed myocardial infarction. The American journal of cardiology. 2007;100(6):930-6.

60. Hamirani YS, Wong A, Kramer CM, Salerno M. Effect of microvascular obstruction and intramyocardial hemorrhage by CMR on LV remodeling and outcomes after myocardial infarction: a systematic review and meta-analysis. JACC Cardiovascular imaging. 2014;7(9):940-52.

61. van Kranenburg M, Magro M, Thiele H, de Waha S, Eitel I, Cochet A, et al. Prognostic value of microvascular obstruction and infarct size, as measured by CMR in STEMI patients. JACC Cardiovascular imaging. 2014;7(9):930-9.

62. Eitel I, Desch S, Fuernau G, Hildebrand L, Gutberlet M, Schuler G, et al. Prognostic significance and determinants of myocardial salvage assessed by cardiovascular magnetic resonance in acute reperfused myocardial infarction. Journal of the American College of Cardiology. 2010;55(22):2470-9.

63. Masci PG, Ganame J, Strata E, Desmet W, Aquaro GD, Dymarkowski S, et al. Myocardial salvage by CMR correlates with LV remodeling and early ST-segment resolution in acute myocardial infarction. JACC Cardiovascular imaging. 2010;3(1):45-51.

64. Kim HW, Farzaneh-Far A, Kim RJ. Cardiovascular Magnetic Resonance in Patients With Myocardial Infarction. Journal of the American College of Cardiology. 2009;55(1):1-16.

65. Ibanez B, Heusch G, Ovize M, Van de Werf F. Evolving therapies for myocardial ischemia/reperfusion injury. Journal of the American College of Cardiology. 2015;65(14):1454-71.

66. Pennell D. Myocardial salvage: retrospection, resolution, and radio waves. Circulation. 2006;113(15):1821-3.

67. Botker HE, Kaltoft AK, Pedersen SF, Kim WY. Measuring myocardial salvage. Cardiovascular research. 2012;94(2):266-75.

68. Verani MS, Jeroudi MO, Mahmarian JJ, Boyce TM, Borges-Neto S, Patel B, et al. Quantification of myocardial infarction during coronary occlusion and myocardial salvage after reperfusion using cardiac imaging with technetium-99m hexakis 2-methoxyisobutyl isonitrile. Journal of the American College of Cardiology. 1988;12(6):1573-81.

69. Gibbons RJ. Tc-99m SPECT sestamibi for the measurement of infarct size. Journal of cardiovascular pharmacology and therapeutics. 2011;16(3-4):321-31.

70. Kaltoft A, Bottcher M, Sand NP, Rehling M, Andersen NT, Zijlstra F, et al. Sestamibi single photon emission computed tomography immediately after primary percutaneous coronary intervention identifies patients at risk for large infarcts. Am Heart J. 2006;151(5):1108-14.

71. van Hellemond IE, Bouwmeester S, Olson CW, Botker HE, Kaltoft AK, Nielsen SS, et al. Consideration of QRS complex in addition to ST-segment abnormalities in the estimated "risk region" during acute anterior myocardial infarction. Journal of electrocardiology. 2011;44(3):370-6.

72. van Hellemond IE, Bouwmeester S, Olson CW, Hassell M, Botker HE, Kaltoft AK, et al. Consideration of QRS complex in addition to ST segment abnormalities in the estimation of the 'risk region' during acute inferior myocardial infarction. Journal of electrocardiology. 2013;46(3):215-20.

73. Christian TF, Gibbons RJ, Clements IP, Berger PB, Selvester RH, Wagner GS. Estimates of myocardium at risk and collateral flow in acute myocardial infarction using electrocardiographic indexes with comparison to radionuclide and angiographic measures. Journal of the American College of Cardiology. 1995;26(2):388-93.

74. Piot C, Croisille P, Staat P, Thibault H, Rioufol G, Mewton N, et al. Effect of cyclosporine on reperfusion injury in acute myocardial infarction. The New England journal of medicine. 2008;359(5):473-81.

75. Roubille F, Mewton N, Elbaz M, Roth O, Prunier F, Cung TT, et al. No post-conditioning in the human heart with thrombolysis in myocardial infarction flow 2-3 on admission. European heart journal. 2014;35(25):1675-82.

76. Mewton N, Thibault H, Roubille F, Lairez O, Rioufol G, Sportouch C, et al. Postconditioning attenuates no-reflow in STEMI patients. Basic research in cardiology. 2013;108(6):383.

77. Feild BJ, Russell RO, Dowling JT, Rackley CE. Regional left ventricular performance in the year following myocardial infarction. . Circulation 1972;46:679-89.

78. Dash H, Johnson RA, Dinsmore RE, Harthorne JW. Cardiomyopathic syndrome due to coronary-artery disease .1. relation to angiographic extent of coronary-disease and to remote myocardial-infarction. British heart journal. 1977;39(7):733-9.

79. Alderman EL, Stadius M. The angiographic definitions of the Bypass Angioplasty Revascularization Investigation. Coronary artery disease. 1992;3(12):1189-207.

80. Graham MM, Faris PD, Ghali WA, Galbraith PD, Norris CM, Badry JT, et al. Validation of three myocardial jeopardy scores in a population-based cardiac catheterization cohort. American Heart Journal. 2001;142(2):254-61.

81. Ortiz-Perez JT, Meyers SN, Lee DC, Kansal P, Klocke FJ, Holly TA, et al. Angiographic estimates of myocardium at risk during acute myocardial infarction: validation study using cardiac magnetic resonance imaging. European heart journal. 2007;28(14):1750-8.

82. Wright J, Adriaenssens T, Dymarkowski S, Desmet W, Bogaert J. Quantification of myocardial area at risk with T2-weighted CMR: comparison with contrast-enhanced CMR and coronary angiography. JACC Cardiovascular imaging. 2009;2(7):825-31.

83. Fuernau G, Eitel I, Franke V, Hildebrandt L, Meissner J, de Waha S, et al. Myocardium at risk in ST-segment elevation myocardial infarction comparison of T2-weighted edema imaging with the MR-assessed endocardial surface area and validation against angiographic scoring. JACC Cardiovascular imaging. 2011;4(9):967-76.

84. Higgins CB, Herfkens R, Lipton MJ, Sievers R, Sheldon P, Kaufman L, et al. Nuclear magnetic resonance imaging of acute myocardial infarction in dogs: alterations in magnetic relaxation times. The American journal of cardiology. 1983;52(1):184-8.

85. Friedrich MG. Myocardial edema--a new clinical entity? Nature reviews Cardiology. 2010;7(5):292-6.

86. Garcia-Dorado D, Oliveras J, Gili J, Sanz E, Perez-Villa F, Barrabes J, et al. Analysis of myocardial oedema by magnetic resonance imaging early after coronary artery occlusion with or without reperfusion. Cardiovascular research. 1993;27(8):1462-9.

87. Boxt LM, Hsu D, Katz J, Detweiler P, McLaughlin S, Kolb TJ, et al. Estimation of myocardial water content using transverse relaxation time from dual spin-echo magnetic resonance imaging. (0730-725X (Print)).

88. Aletras AH, Tilak GS, Natanzon A, Hsu LY, Gonzalez FM, Hoyt RF, Jr., et al. Retrospective determination of the area at risk for reperfused acute myocardial infarction with T2-weighted cardiac magnetic resonance imaging: histopathological and displacement encoding with stimulated echoes (DENSE) functional validations. Circulation. 2006;113(15):1865-70.

89. Tilak GS, Hsu LY, Hoyt RF, Arai AE, Aletras AH. In vivo T2-weighted magnetic resonance imaging can accurately determine the ischemic area at risk for 2-day-old nonreperfused myocardial infarction. (0020-9996 (Print)).

90. Friedrich MG, Abdel-Aty H, Taylor A, Schulz-Menger J, Messroghli D, Dietz R. The salvaged area at risk in reperfused acute myocardial infarction as visualized by cardiovascular magnetic resonance. J Am Coll Cardiol. 2008;51(16):1581-7.

91. Carlsson M, Ubachs JF, Hedstrom E, Heiberg E, Jovinge S, Arheden H. Myocardium at risk after acute infarction in humans on cardiac magnetic resonance: quantitative assessment during follow-up and validation with single-photon emission computed tomography. JACC Cardiovascular imaging. 2009;2(5):569-76.

92. Arai AE. Using magnetic resonance imaging to characterize recent myocardial injury: utility in acute coronary syndrome and other clinical scenarios. Circulation. 2008;118(8):795-6.

93. Kellman P, Aletras AH, Mancini C, McVeigh ER, Arai AE. T2-prepared SSFP improves diagnostic confidence in edema imaging in acute myocardial infarction compared to turbo spin echo. Magnetic resonance in medicine : official journal of the Society of Magnetic Resonance in Medicine / Society of Magnetic Resonance in Medicine. 2007;57(5):891-7.

94. Aletras AH, Kellman P, Derbyshire JA, Arai AE. ACUT2E TSE-SSFP: a hybrid method for T2-weighted imaging of edema in the heart. Magnetic resonance in medicine : official journal of the Society of Magnetic Resonance in Medicine / Society of Magnetic Resonance in Medicine. 2008;59(2):229-35.

95. Berry C, Kellman P, Mancini C, Chen MY, Bandettini WP, Lowrey T, et al. Magnetic resonance imaging delineates the ischemic area at risk and

myocardial salvage in patients with acute myocardial infarction. Circ Cardiovasc Imaging. 2010;3(5):527-35.

96. Payne AR, Casey M, McClure J, McGeoch R, Murphy A, Woodward R, et al. Bright-blood T2-weighted MRI has higher diagnostic accuracy than dark-blood short tau inversion recovery MRI for detection of acute myocardial infarction and for assessment of the ischemic area at risk and myocardial salvage. Circulation Cardiovascular imaging. 2011;4(3):210-9.

97. Giri S, Chung YC, Merchant A, Mihai G, Rajagopalan S, Raman SV, et al. T2 quantification for improved detection of myocardial edema. Journal of cardiovascular magnetic resonance : official journal of the Society for Cardiovascular Magnetic Resonance. 2009;11:56.

98. Verhaert D, Thavendiranathan P, Giri S, Mihai G, Rajagopalan S, Simonetti OP, et al. Direct T2 quantification of myocardial edema in acute ischemic injury. JACC Cardiovascular imaging. 2011;4(3):269-78.

99. McAlindon EJ, Pufulete M, Harris JM, Lawton CB, Moon JC, Manghat N, et al. Measurement of myocardium at risk with cardiovascular MR: comparison of techniques for edema imaging. Radiology. 2015;275(1):61-70.

100. Croisille P, Kim HW, Kim RJ. Controversies in cardiovascular MR imaging: T2-weighted imaging should not be used to delineate the area at risk in ischemic myocardial injury. Radiology. 2012;265(1):12-22.

101. Johnston DL, Brady TJ, Ratner AV, Rosen BR, Newell JB, Pohost GM, et al. Assessment of myocardial ischemia with proton magnetic-resonance - effects of a 3 hour coronary-occlusion with and without reperfusion. Circulation. 1985;71(3):595-601.

102. Miller DD, Johnston DL, Dragotakes D, Newell JB, Aretz T, Kantor HL, et al. Effect of hyperosmotic mannitol on magnetic-resonance relaxation parameters in reperfused canine myocardial-infarction. Magnetic Resonance Imaging. 1989;7(1):79-88.

103. Ryan T, Tarver RD, Duerk JL, Sawada SG, Hollenkamp NC. Distinguishing viable from infarcted myocardium after experimental-ischemia and reperfusion by using nuclear-magnetic-resonance imaging. Journal of the American College of Cardiology. 1990;15(6):1355-64.

104. Kim HW, Van Assche L, Jennings RB, Wince WB, Jensen CJ, Rehwald WG, et al. Relationship of T2-Weighted MRI Myocardial Hyperintensity and the Ischemic Area-At-Risk. Circulation research. 2015;117(3):254-65.

105. Ubachs JF, Engblom H, Koul S, Kanski M, Andersson P, van der Pals J, et al. Myocardium at risk can be determined by ex vivo T2-weighted magnetic resonance imaging even in the presence of gadolinium: comparison to myocardial perfusion single photon emission computed tomography. European heart journal cardiovascular Imaging. 2013;14(3):261-8.

106. Bulluck H, White SK, Frohlich GM, Casson SG, O'Meara C, Newton A, et al. Quantifying the Area at Risk in Reperfused ST-Segment-Elevation Myocardial Infarction Patients Using Hybrid Cardiac Positron Emission

Tomography-Magnetic Resonance Imaging. Circulation Cardiovascular imaging. 2016;9(3):e003900.

107. Hammer-Hansen S, Ugander M, Hsu LY, Taylor J, Thune JJ, Kober L, et al. Distinction of salvaged and infarcted myocardium within the ischaemic area-at-risk with T2 mapping. European heart journal cardiovascular Imaging. 2014;15(9):1048-53.

108. Johnston DL, Homma S, Liu P, Weilbaecher DG, Rokey R, Brady TJ, et al. Serial changes in nuclear magnetic resonance relaxation times after myocardial infarction in the rabbit: relationship to water content, severity of ischemia, and histopathology over a six-month period. Magnetic resonance in medicine : official journal of the Society of Magnetic Resonance in Medicine / Society of Magnetic Resonance in Medicine. 1988;8(4):363-79.

109. Foltz WD, Yang Y, Graham JJ, Detsky JS, Wright GA, Dick AJ. MRI relaxation fluctuations in acute reperfused hemorrhagic infarction. Magnetic Resonance in Medicine. 2006;56(6):1311-9.

110. Fernandez-Jimenez R, Sanchez-Gonzalez J, Aguero J, Garcia-Prieto J, Lopez-Martin GJ, Garcia-Ruiz JM, et al. Myocardial Edema After Ischemia/Reperfusion Is Not Stable and Follows a Bimodal Pattern: Advanced Imaging and Histological Tissue Characterization. Journal of the American College of Cardiology. 2014.

111. Fernandez-Jimenez R, Garcia-Prieto J, Sanchez-Gonzalez J, Aguero J, Lopez-Martin GJ, Galan-Arriola C, et al. Pathophysiology Underlying the Bimodal Edema Phenomenon After Myocardial Ischemia/Reperfusion. Journal of the American College of Cardiology. 2015;66(7):816-28.

112. Carrick D, Haig C, Ahmed N, Rauhalammi S, Clerfond G, Carberry J, et al. Temporal Evolution of Myocardial Hemorrhage and Edema in Patients After Acute ST-Segment Elevation Myocardial Infarction: Pathophysiological Insights and Clinical Implications. Journal of the American Heart Association. 2016;5(2):Advance online publication.

113. Dall'Armellina E, Karia N, Lindsay AC, Karamitsos TD, Ferreira V, Robson MD, et al. Dynamic changes of edema and late gadolinium enhancement after acute myocardial infarction and their relationship to functional recovery and salvage index. Circ Cardiovasc Imaging. 2011;4(3):228-36.

114. Nordlund D, Klug G, Heiberg E, Koul S, Larsen TH, Hoffmann P, et al. Multi-vendor, multicentre comparison of contrast-enhanced SSFP and T2-STIR CMR for determining myocardium at risk in ST-elevation myocardial infarction. European heart journal cardiovascular Imaging. 2016.

115. Thuny F, Lairez O, Roubille F, Mewton N, Rioufol G, Sportouch C, et al. Post-conditioning reduces infarct size and edema in patients with ST-segment elevation myocardial infarction. Journal of the American College of Cardiology. 2012;59(24):2175-81.

116. White SK, Frohlich GM, Sado DM, Maestrini V, Fontana M, Treibel TA, et al. Remote Ischemic Conditioning Reduces Myocardial Infarct Size and Edema

in Patients With ST-Segment Elevation Myocardial Infarction. JACC Cardiovascular interventions. 2014.

117. Crimi G, Pica S, Raineri C, Bramucci E, De Ferrari GM, Klersy C, et al. Remote ischemic post-conditioning of the lower limb during primary percutaneous coronary intervention safely reduces enzymatic infarct size in anterior myocardial infarction: a randomized controlled trial. JACC Cardiovascular interventions. 2013;6(10):1055-63.

118. Eitel I, Stiermaier T, Rommel KP, Fuernau G, Sandri M, Mangner N, et al. Cardioprotection by combined intrahospital remote ischaemic perconditioning and postconditioning in ST-elevation myocardial infarction: the randomized LIPSIA CONDITIONING trial. European heart journal. 2015.

119. Ibanez B, Macaya C, Sanchez-Brunete V, Pizarro G, Fernandez-Friera L, Mateos A, et al. Effect of early metoprolol on infarct size in ST-segment-elevation myocardial infarction patients undergoing primary percutaneous coronary intervention: the Effect of Metoprolol in Cardioprotection During an Acute Myocardial Infarction (METOCARD-CNIC) trial. Circulation. 2013;128(14):1495-503.

120. Pizarro G, Fernandez-Friera L, Fuster V, Fernandez-Jimenez R, Garcia-Ruiz JM, Garcia-Alvarez A, et al. Long-term benefit of early pre-reperfusion metoprolol administration in patients with acute myocardial infarction: results from the METOCARD-CNIC trial (Effect of Metoprolol in Cardioprotection During an Acute Myocardial Infarction). Journal of the American College of Cardiology. 2014;63(22):2356-62.

121. Woo JS, Kim W, Ha SJ, Kim JB, Kim SJ, Kim WS, et al. Cardioprotective effects of exenatide in patients with ST-segment-elevation myocardial infarction undergoing primary percutaneous coronary intervention: results of exenatide myocardial protection in revascularization study. Arteriosclerosis, thrombosis, and vascular biology. 2013;33(9):2252-60.

122. Lonborg J, Vejlstrup N, Kelbaek H, Botker HE, Kim WY, Mathiasen AB, et al. Exenatide reduces reperfusion injury in patients with ST-segment elevation myocardial infarction. European heart journal. 2012;33(12):1491-9.

123. Reimer KA, Jennings RB. Wavefront phenomenon of myocardial ischemic cell-death .2. transmural progression of necrosis within the framework of ischemic bed size (myocardium at risk) and collateral flow. Laboratory Investigation. 1979;40(6):633-44.

124. O'Regan DP, Ahmed R, Neuwirth C, Tan Y, Durighel G, Hajnal JV, et al. Cardiac MRI of myocardial salvage at the peri-infarct border zones after primary coronary intervention. American journal of physiology Heart and circulatory physiology. 2009;297(1):H340-6.

125. Ubachs JF, Engblom H, Erlinge D, Jovinge S, Hedstrom E, Carlsson M, et al. Cardiovascular magnetic resonance of the myocardium at risk in acute reperfused myocardial infarction: comparison of T2-weighted imaging versus the circumferential endocardial extent of late gadolinium enhancement with transmural projection. Journal of cardiovascular magnetic resonance : official journal of the Society for Cardiovascular Magnetic Resonance. 2010;12:18.

126. Sorensson P, Heiberg E, Saleh N, Bouvier F, Caidahl K, Tornvall P, et al. Assessment of myocardium at risk with contrast enhanced steady-state free precession cine cardiovascular magnetic resonance compared to single-photon emission computed tomography. Journal of cardiovascular magnetic resonance : official journal of the Society for Cardiovascular Magnetic Resonance. 2010;12:25.

127. Ubachs JF, Sorensson P, Engblom H, Carlsson M, Jovinge S, Pernow J, et al. Myocardium at risk by magnetic resonance imaging: head-to-head comparison of T2-weighted imaging and contrast-enhanced steady-state free precession. European heart journal cardiovascular Imaging. 2012;13(12):1008-15.

128. Nordlund D, Heiberg E, Carlsson M, Frund ET, Hoffmann P, Koul S, et al. Extent of Myocardium at Risk for Left Anterior Descending Artery, Right Coronary Artery, and Left Circumflex Artery Occlusion Depicted by Contrast-Enhanced Steady State Free Precession and T2-Weighted Short Tau Inversion Recovery Magnetic Resonance Imaging. Circulation Cardiovascular imaging. 2016;9(7).

129. Matsumoto H, Matsuda T, Miyamoto K, Shimada T, Mikuri M, Hiraoka Y. Peri-infarct zone on early contrast-enhanced CMR imaging in patients with acute myocardial infarction. JACC Cardiovascular imaging. 2011;4(6):610-8.

130. Hammer-Hansen S, Bandettini WP, Hsu LY, Leung SW, Shanbhag S, Mancini C, et al. Mechanisms for overestimating acute myocardial infarct size with gadolinium-enhanced cardiovascular magnetic resonance imaging in humans: a quantitative and kinetic study. European heart journal cardiovascular Imaging. 2016;17(1):76-84.

131. Ugander M, Bagi PS, Oki AJ, Chen B, Hsu LY, Aletras AH, et al. Myocardial edema as detected by pre-contrast T1 and T2 CMR delineates area at risk associated with acute myocardial infarction. JACC Cardiovascular imaging. 2012;5(6):596-603.

132. Dall'Armellina E, Piechnik SK, Ferreira VM, Si QL, Robson MD, Francis JM, et al. Cardiovascular magnetic resonance by non contrast T1-mapping allows assessment of severity of injury in acute myocardial infarction. Journal of cardiovascular magnetic resonance : official journal of the Society for Cardiovascular Magnetic Resonance. 2012;14:15.

133. Langhans B, Nadjiri J, Jahnichen C, Kastrati A, Martinoff S, Hadamitzky M. Reproducibility of area at risk assessment in acute myocardial infarction by T1- and T2-mapping sequences in cardiac magnetic resonance imaging in comparison to Tc99m-sestamibi SPECT. The international journal of cardiovascular imaging. 2014;30(7):1357-63.

134. Bresnahan GF, Roberts R, Shell WE, Ross J, Sobel BE. DELETERIOUS EFFECTS DUE TO HEMORRHAGE AFTER MYOCARDIAL REPERFUSION. American Journal of Cardiology. 1974;33(1):82-6.

135. Reffelmann T, Kloner RA. Microvascular reperfusion injury: rapid expansion of anatomic no reflow during reperfusion in the rabbit. American

Journal of Physiology-Heart and Circulatory Physiology. 2002;283(3):H1099-H107.

136. Garcia-Dorado D, Theroux P, Solares J, Alonso J, Fernandez-Aviles F, Elizaga J, et al. Determinants of hemorrhagic infarcts. Histologic observations from experiments involving coronary occlusion, coronary reperfusion, and reocclusion. Am J Pathol. 1990;137(2):301-11.

137. Driesen RB, Zalewski J, Vanden Driessche N, Vermeulen K, Bogaert J, Sipido KR, et al. Histological correlate of a cardiac magnetic resonance imaged microvascular obstruction in a porcine model of ischemia-reperfusion. Cardiovasc Pathol. 2012;21(3):129-31.

138. Zia MI, Ghugre NR, Connelly KA, Strauss BH, Sparkes JD, Dick AJ, et al. Characterizing myocardial edema and hemorrhage using quantitative T2 and T2* mapping at multiple time intervals post ST-segment elevation myocardial infarction. Circulation Cardiovascular imaging. 2012;5(5):566-72.

139. Carrick D, Haig C, Ahmed N, McEntegart M, Petrie MC, Eteiba H, et al. Myocardial Hemorrhage After Acute Reperfused ST-Segment-Elevation Myocardial Infarction: Relation to Microvascular Obstruction and Prognostic Significance. Circulation Cardiovascular imaging. 2016;9(1):e004148.

140. Morishima I, Sone T, Okumura K, Tsuboi H, Kondo J, Mukawa H, et al. Angiographic no-reflow phenomenon as a predictor of adverse long-term outcome in patients treated with percutaneous transluminal coronary angioplasty for first acute myocardial infarction. Journal of the American College of Cardiology. 2000;36(4):1202-9.

141. Sorajja P, Gersh BJ, Costantini C, McLaughlin MG, Zimetbaum P, Cox DA, et al. Combined prognostic utility of ST-segment recovery and myocardial blush after primary percutaneous coronary intervention in acute myocardial infarction. European heart journal. 2005;26(7):667-74.

142. Bolognese L, Carrabba N, Parodi G, Santoro GM, Buonamici P, Cerisano G, et al. Impact of microvascular dysfunction on left ventricular remodeling and long-term clinical outcome after primary coronary angioplasty for acute myocardial infarction. Circulation. 2004;109(9):1121-6.

143. Wu KC, Zerhouni EA, Judd RM, Lugo-Olivieri CH, Barouch LA, Schulman SP, et al. Prognostic significance of microvascular obstruction by magnetic resonance imaging in patients with acute myocardial infarction. Circulation. 1998;97(8):765-72.

144. Hombach V, Grebe O, Merkle N, Waldenmaier S, Hoher M, Kochs M, et al. Sequelae of acute myocardial infarction regarding cardiac structure and function and their prognostic significance as assessed by magnetic resonance imaging. European heart journal. 2005;26(6):549-57.

145. Weir RA, Murphy CA, Petrie CJ, Martin TN, Balmain S, Clements S, et al. Microvascular obstruction remains a portent of adverse remodeling in optimally treated patients with left ventricular systolic dysfunction after acute myocardial infarction. Circulation Cardiovascular imaging. 2010;3(4):360-7.

146. Wu KC. CMR of microvascular obstruction and hemorrhage in myocardial infarction. Journal of cardiovascular magnetic resonance : official journal of the Society for Cardiovascular Magnetic Resonance. 2012;14:68.

147. Judd RM, Lugo-Olivieri CH, Arai M, Kondo T, Croisille P, Lima JA, et al. Physiological basis of myocardial contrast enhancement in fast magnetic resonance images of 2-day-old reperfused canine infarcts. Circulation. 1995;92(7):1902-10.

148. Lima JA, Judd RM, Bazille A, Schulman SP, Atalar E, Zerhouni EA. Regional heterogeneity of human myocardial infarcts demonstrated by contrast-enhanced MRI. Potential mechanisms. Circulation. 1995;92(5):1117-25.

149. Orn S, Manhenke C, Greve OJ, Larsen AI, Bonarjee VV, Edvardsen T, et al. Microvascular obstruction is a major determinant of infarct healing and subsequent left ventricular remodelling following primary percutaneous coronary intervention. European heart journal. 2009;30(16):1978-85.

150. Kandler D, Lucke C, Grothoff M, Andres C, Lehmkuhl L, Nitzsche S, et al. The relation between hypointense core, microvascular obstruction and intramyocardial haemorrhage in acute reperfused myocardial infarction assessed by cardiac magnetic resonance imaging. European radiology. 2014;24(12):3277-88.

151. Husser O, Monmeneu JV, Sanchis J, Nunez J, Lopez-Lereu MP, Bonanad C, et al. Cardiovascular magnetic resonance-derived intramyocardial hemorrhage after STEMI: Influence on long-term prognosis, adverse left ventricular remodeling and relationship with microvascular obstruction. International journal of cardiology. 2013;167(5):2047-54.

152. Ghugre NR, Ramanan V, Pop M, Yang Y, Barry J, Qiang B, et al. Quantitative tracking of edema, hemorrhage, and microvascular obstruction in subacute myocardial infarction in a porcine model by MRI. Magnetic resonance in medicine : official journal of the Society of Magnetic Resonance in Medicine / Society of Magnetic Resonance in Medicine. 2011;66(4):1129-41.

153. Kali A, Tang RL, Kumar A, Min JK, Dharmakumar R. Detection of acute reperfusion myocardial hemorrhage with cardiac MR imaging: T2 versus T2. Radiology. 2013;269(2):387-95.

154. Payne AR, Berry C, Kellman P, Anderson R, Hsu LY, Chen MY, et al. Bright-blood T(2)-weighted MRI has high diagnostic accuracy for myocardial hemorrhage in myocardial infarction: a preclinical validation study in swine. Circulation Cardiovascular imaging. 2011;4(6):738-45.

155. O'Regan DP, Ahmed R, Karunanithy N, Neuwirth C, Tan Y, Durighel G, et al. Reperfusion hemorrhage following acute myocardial infarction: assessment with T2* mapping and effect on measuring the area at risk. Radiology. 2009;250(3):916-22.

156. Carrick D, Haig C, Rauhalammi S, Ahmed N, Mordi I, McEntegart M, et al. Prognostic significance of infarct core pathology revealed by quantitative non-contrast in comparison with contrast cardiac magnetic resonance imaging

in reperfused ST-elevation myocardial infarction survivors. European heart journal. 2015;10.1093/eurheartj/ehv372.

157. Kellman P, Xue H, Spottiswoode BS, Sandino CM, Hansen MS, Abdel-Gadir A, et al. Free-breathing T2* mapping using respiratory motion corrected averaging. Journal of cardiovascular magnetic resonance : official journal of the Society for Cardiovascular Magnetic Resonance. 2015;17(1):3.

158. Bradley WG, Jr. MR appearance of hemorrhage in the brain. Radiology. 1993;189(1):15-26.

159. Beek AM, Nijveldt R, van Rossum AC. Intramyocardial hemorrhage and microvascular obstruction after primary percutaneous coronary intervention. The international journal of cardiovascular imaging. 2010;26(1):49-55.

160. Bekkers SC, Smulders MW, Passos VL, Leiner T, Waltenberger J, Gorgels AP, et al. Clinical implications of microvascular obstruction and intramyocardial haemorrhage in acute myocardial infarction using cardiovascular magnetic resonance imaging. European radiology. 2010;20(11):2572-8.

161. Eitel I, Kubusch K, Strohm O, Desch S, Mikami Y, de Waha S, et al. Prognostic value and determinants of a hypointense infarct core in T2-weighted cardiac magnetic resonance in acute reperfused ST-elevation-myocardial infarction. Circulation Cardiovascular imaging. 2011;4(4):354-62.

162. Durighel G, Tokarczuk PF, Karsa A, Gordon F, Cook SA, O'Regan DP. Acute myocardial infarction: susceptibility-weighted cardiac MRI for the detection of reperfusion haemorrhage at 1.5 T. (1365-229X (Electronic)).

163. Kidambi A, Biglands JD, Higgins DM, Ripley DP, Zaman A, Broadbent DA, et al. Susceptibility-weighted cardiovascular magnetic resonance in comparison to T2 and T2 star imaging for detection of intramyocardial hemorrhage following acute myocardial infarction at 3 Tesla. Journal of cardiovascular magnetic resonance : official journal of the Society for Cardiovascular Magnetic Resonance. 2014;16:86.

164. Dall'Armellina E, Ferreira VM, Kharbanda RK, Prendergast B, Piechnik SK, Robson MD, et al. Diagnostic value of pre-contrast T1 mapping in acute and chronic myocardial infarction. JACC Cardiovascular imaging. 2013;6(6):739-42.

165. Zaman A, Higgins DM, Motwani M, Kidambi A, Kouwenhoven M, Kozerke S, et al. Robust myocardial T and T * mapping at 3T using image-based shimming. Journal of magnetic resonance imaging : JMRI. 2014.

166. Kim RJ, Fieno DS, Parrish TB, Harris K, Chen EL, Simonetti O, et al. Relationship of MRI delayed contrast enhancement to irreversible injury, infarct age, and contractile function. Circulation. 1999;100(19):1992-2002.

167. Ibrahim T, Nekolla SG, Hornke M, Bulow HP, Dirschinger J, Schomig A, et al. Quantitative measurement of infarct size by contrast-enhanced magnetic resonance imaging early after acute myocardial infarction: comparison with single-photon emission tomography using Tc99m-sestamibi. Journal of the American College of Cardiology. 2005;45(4):544-52.

168. Lonborg J, Vejlstrup N, Kelbaek H, Holmvang L, Jorgensen E, Helqvist S, et al. Final infarct size measured by cardiovascular magnetic resonance in patients with ST elevation myocardial infarction predicts long-term clinical outcome: an observational study. European heart journal cardiovascular Imaging. 2013;14(4):387-95.

169. Larose E, Rodes-Cabau J, Pibarot P, Rinfret S, Proulx G, Nguyen CM, et al. Predicting late myocardial recovery and outcomes in the early hours of ST-segment elevation myocardial infarction traditional measures compared with microvascular obstruction, salvaged myocardium, and necrosis characteristics by cardiovascular magnetic resonance. Journal of the American College of Cardiology. 2010;55(22):2459-69.

170. Roes SD, Kelle S, Kaandorp TAM, Kokocinski T, Poldermans D, Lamb HJ, et al. Comparison of myocardial infarct size assessed with contrast-enhanced magnetic resonance imaging and left ventricular function and volumes to predict mortality in patients with healed myocardial infarction. American Journal of Cardiology. 2007;100(6):930-6.

171. Kwon DH, Halley CM, Carrigan TP, Zysek V, Popovic ZB, Setser R, et al. Extent of left ventricular scar predicts outcomes in ischemic cardiomyopathy patients with significantly reduced systolic function: a delayed hyperenhancement cardiac magnetic resonance study. JACC Cardiovascular imaging. 2009;2(1):34-44.

172. Mahrholdt H, Wagner A, Holly TA, Elliott MD, Bonow RO, Kim RJ, et al. Reproducibility of chronic infarct size measurement by contrast-enhanced magnetic resonance imaging. Circulation. 2002;106(18):2322-7.

173. Wagner A, Mahrholdt H, Thomson L, Hager S, Meinhardt G, Rehwald W, et al. Effects of time, dose, and inversion time for acute myocardial infarct size measurements based on magnetic resonance imaging-delayed contrast enhancement. Journal of the American College of Cardiology. 2006;47(10):2027-33.

174. Ibrahim T, Hackl T, Nekolla SG, Breuer M, Feldmair M, Schomig A, et al. Acute myocardial infarction: serial cardiac MR imaging shows a decrease in delayed enhancement of the myocardium during the 1st week after reperfusion. Radiology. 2010;254(1):88-97.

175. Mather AN, Fairbairn TA, Artis NJ, Greenwood JP, Plein S. Timing of cardiovascular MR imaging after acute myocardial infarction: effect on estimates of infarct characteristics and prediction of late ventricular remodeling. Radiology. 2011;261(1):116-26.

176. McAlindon E, Pufulete M, Lawton C, Angelini GD, Bucciarelli-Ducci C. Quantification of infarct size and myocardium at risk: evaluation of different techniques and its implications. European heart journal cardiovascular Imaging. 2015;16(7):738-46.

177. Bondarenko O, Beek AM, Hofman MB, Kuhl HP, Twisk JW, van Dockum WG, et al. Standardizing the definition of hyperenhancement in the quantitative assessment of infarct size and myocardial viability using delayed contrast-

enhanced CMR. Journal of cardiovascular magnetic resonance : official journal of the Society for Cardiovascular Magnetic Resonance. 2005;7(2):481-5.

178. Beek AM, Bondarenko O, Afsharzada F, van Rossum AC. Quantification of late gadolinium enhanced CMR in viability assessment in chronic ischemic heart disease: a comparison to functional outcome. Journal of cardiovascular magnetic resonance : official journal of the Society for Cardiovascular Magnetic Resonance. 2009;11:6.

179. Otsu N. A threshold selection method from gray-level histograms. IEEE Trans Syst Man Cyberb 1979(9):62–6.

180. Vermes E, Childs H, Carbone I, Barckow P, Friedrich MG. Auto-threshold quantification of late gadolinium enhancement in patients with acute heart disease. Journal of magnetic resonance imaging : JMRI. 2013;37(2):382-90.

181. Amado LC, Gerber BL, Gupta SN, Rettmann DW, Szarf G, Schock R, et al. Accurate and objective infarct sizing by contrast-enhanced magnetic resonance imaging in a canine myocardial infarction model. Journal of the American College of Cardiology. 2004;44(12):2383-9.

182. Flett AS, Hasleton J, Cook C, Hausenloy D, Quarta G, Ariti C, et al. Evaluation of techniques for the quantification of myocardial scar of differing etiology using cardiac magnetic resonance. JACC Cardiovascular imaging. 2011;4(2):150-6.

183. Khan JN, Nazir SA, Horsfield MA, Singh A, Kanagala P, Greenwood JP, et al. Comparison of semi-automated methods to quantify infarct size and area at risk by cardiovascular magnetic resonance imaging at 1.5T and 3.0T field strengths. BMC research notes. 2015;8:52.

184. Mewton N, Revel D, Bonnefoy E, Ovize M, Croisille P. Comparison of visual scoring and quantitative planimetry methods for estimation of global infarct size on delayed enhanced cardiac MRI and validation with myocardial enzymes. European journal of radiology. 2011;78(1):87-92.

185. Zhang L, Huttin O, Marie PY, Felblinger J, Beaumont M, Chillou C, et al. Myocardial infarct sizing by late gadolinium-enhanced MRI: Comparison of manual, full-width at half-maximum, and n-standard deviation methods. Journal of magnetic resonance imaging : JMRI. 2016.

186. Messroghli DR, Walters K, Plein S, Sparrow P, Friedrich MG, Ridgway JP, et al. Myocardial T1 mapping: application to patients with acute and chronic myocardial infarction. Magnetic resonance in medicine : official journal of the Society of Magnetic Resonance in Medicine / Society of Magnetic Resonance in Medicine. 2007;58(1):34-40.

187. Bauner KU, Biffar A, Theisen D, Greiser A, Zech CJ, Nguyen ET, et al. Extracellular volume fractions in chronic myocardial infarction. Investigative radiology. 2012;47(9):538-45.

188. Xue H, Shah S, Greiser A, Guetter C, Littmann A, Jolly MP, et al. Motion correction for myocardial T1 mapping using image registration with synthetic image estimation. Magnetic resonance in medicine : official journal of the

Society of Magnetic Resonance in Medicine / Society of Magnetic Resonance in Medicine. 2012;67(6):1644-55.

189. Kellman P, Hansen MS. T1-mapping in the heart: accuracy and precision. Journal of cardiovascular magnetic resonance : official journal of the Society for Cardiovascular Magnetic Resonance. 2014;16:2.

190. Varga-Szemes A, van der Geest RJ, Spottiswoode BS, Suranyi P, Ruzsics B, De Cecco CN, et al. Myocardial Late Gadolinium Enhancement: Accuracy of T1 Mapping-based Synthetic Inversion-Recovery Imaging. Radiology. 2016;278(2):374-82.

191. Grothues F, Smith GC, Moon JC, Bellenger NG, Collins P, Klein HU, et al. Comparison of interstudy reproducibility of cardiovascular magnetic resonance with two-dimensional echocardiography in normal subjects and in patients with heart failure or left ventricular hypertrophy. The American journal of cardiology. 2002;90(1):29-34.

192. American College of Cardiology Foundation Task Force on Expert Consensus D, Hundley WG, Bluemke DA, Finn JP, Flamm SD, Fogel MA, et al. ACCF/ACR/AHA/NASCI/SCMR 2010 expert consensus document on cardiovascular magnetic resonance: a report of the American College of Cardiology Foundation Task Force on Expert Consensus Documents. Circulation. 2010;121(22):2462-508.

193. Bolognese L, Cerisano G, Buonamici P, Santini A, Santoro GM, Antoniucci D, et al. Influence of infarct-zone viability on left ventricular remodeling after acute myocardial infarction. Circulation. 1997;96(10):3353-9.

194. Cerisano G, Bolognese L, Carrabba N, Buonamici P, Santoro GM, Antoniucci D, et al. Doppler-derived mitral deceleration time: an early strong predictor of left ventricular remodeling after reperfused anterior acute myocardial infarction. Circulation. 1999;99(2):230-6.

195. Yu CM, Bleeker GB, Fung JW, Schalij MJ, Zhang Q, van der Wall EE, et al. Left ventricular reverse remodeling but not clinical improvement predicts long-term survival after cardiac resynchronization therapy. Circulation. 2005;112(11):1580-6.

196. Symons R, Masci PG, Francone M, Claus P, Barison A, Carbone I, et al. Impact of active smoking on myocardial infarction severity in reperfused ST-segment elevation myocardial infarction patients: the smoker's paradox revisited. European heart journal. 2016.

197. Carrick D, Haig C, Rauhalammi S, Ahmed N, Mordi I, McEntegart M, et al. Pathophysiology of LV Remodeling in Survivors of STEMI: Inflammation, Remote Myocardium, and Prognosis. JACC Cardiovascular imaging. 2015;8(7):779-89.

198. Bodi V, Monmeneu JV, Ortiz-Perez JT, Lopez-Lereu MP, Bonanad C, Husser O, et al. Prediction of Reverse Remodeling at Cardiac MR Imaging Soon after First ST-Segment-Elevation Myocardial Infarction: Results of a Large Prospective Registry. Radiology. 2016;278(1):54-63.

199. Symons R, Masci PG, Goetschalckx K, Doulaptsis K, Janssens S, Bogaert J. Effect of infarct severity on regional and global left ventricular remodeling in patients with successfully reperfused ST segment elevation myocardial infarction. Radiology. 2015;274(1):93-102.

200. Pfeffer JM, Pfeffer MA, Braunwald E. Influence of chronic captopril therapy on the infarcted left ventricle of the rat. Circulation research. 1985;57(1):84-95.

201. Frangogiannis NG. The immune system and the remodeling infarcted heart: cell biological insights and therapeutic opportunities. Journal of cardiovascular pharmacology. 2014;63(3):185-95.

202. Seropian IM, Toldo S, Van Tassell BW, Abbate A. Anti-inflammatory strategies for ventricular remodeling following ST-segment elevation acute myocardial infarction. Journal of the American College of Cardiology. 2014;63(16):1593-603.

203. O'Regan DP, Shi W, Ariff B, Baksi AJ, Durighel G, Rueckert D, et al. Remodeling after acute myocardial infarction: mapping ventricular dilatation using three dimensional CMR image registration. Journal of cardiovascular magnetic resonance : official journal of the Society for Cardiovascular Magnetic Resonance. 2012;14:41.

204. Masci PG, Ganame J, Francone M, Desmet W, Lorenzoni V, Iacucci I, et al. Relationship between location and size of myocardial infarction and their reciprocal influences on post-infarction left ventricular remodelling. European heart journal. 2011;32(13):1640-8.

205. Westman PC, Lipinski MJ, Luger D, Waksman R, Bonow RO, Wu E, et al. Inflammation as a Driver of Adverse Left Ventricular Remodeling After Acute Myocardial Infarction. Journal of the American College of Cardiology. 2016;67(17):2050-60.

206. Cokic I, Kali A, Wang X, Yang HJ, Tang RL, Thajudeen A, et al. Iron deposition following chronic myocardial infarction as a substrate for cardiac electrical anomalies: initial findings in a canine model. PloS one. 2013;8(9):e73193.

207. Kali A, Kumar A, Cokic I, Tang RL, Tsaftaris SA, Friedrich MG, et al. Chronic manifestation of postreperfusion intramyocardial hemorrhage as regional iron deposition: a cardiovascular magnetic resonance study with ex vivo validation. Circulation Cardiovascular imaging. 2013;6(2):218-28.

208. Roghi A, Poggiali E, Duca L, Mafrici A, Pedrotti P, Paccagnini S, et al. Role of Non-Transferrin-Bound Iron in the pathogenesis of cardiotoxicity in patients with ST-elevation myocardial infarction assessed by Cardiac Magnetic Resonance Imaging. International journal of cardiology. 2015;199:326-32.

209. Dall'Armellina E, Karia N, Lindsay AC, Karamitsos TD, Ferreira V, Robson MD, et al. Dynamic changes of edema and late gadolinium enhancement after acute myocardial infarction and their relationship to functional recovery and salvage index. Circulation Cardiovascular imaging. 2011;4(3):228-36.

210. Volders PG, Willems IE, Cleutjens JP, Arends JW, Havenith MG, Daemen MJ. Interstitial collagen is increased in the non-infarcted human myocardium after myocardial infarction. Journal of molecular and cellular cardiology. 1993;25(11):1317-23.

211. Tsuda T, Gao E, Evangelisti L, Markova D, Ma X, Chu ML. Post-ischemic myocardial fibrosis occurs independent of hemodynamic changes. Cardiovascular research. 2003;59(4):926-33.

212. Marijianowski MM, Teeling P, Becker AE. Remodeling after myocardial infarction in humans is not associated with interstitial fibrosis of noninfarcted myocardium. Journal of the American College of Cardiology. 1997;30(1):76-82.

213. Chan W, Duffy SJ, White DA, Gao XM, Du XJ, Ellims AH, et al. Acute left ventricular remodeling following myocardial infarction: coupling of regional healing with remote extracellular matrix expansion. JACC Cardiovascular imaging. 2012;5(9):884-93.

214. Jugdutt BI. Ventricular remodeling after infarction and the extracellular collagen matrix: when is enough enough? Circulation. 2003;108(11):1395-403.

215. Anversa P, Beghi C, Kikkawa Y, Olivetti G. Myocardial infarction in rats. Infarct size, myocyte hypertrophy, and capillary growth. Circulation research. 1986;58(1):26-37.

216. Ugander M, Oki AJ, Hsu LY, Kellman P, Greiser A, Aletras AH, et al. Extracellular volume imaging by magnetic resonance imaging provides insights into overt and sub-clinical myocardial pathology. European heart journal. 2012;33(10):1268-78.

217. Kellman P, Wilson JR, Xue H, Bandettini WP, Shanbhag SM, Druey KM, et al. Extracellular volume fraction mapping in the myocardium, part 2: initial clinical experience. Journal of cardiovascular magnetic resonance : official journal of the Society for Cardiovascular Magnetic Resonance. 2012;14:64.

218. Kellman P, Wilson JR, Xue H, Ugander M, Arai AE. Extracellular volume fraction mapping in the myocardium, part 1: evaluation of an automated method. Journal of cardiovascular magnetic resonance : official journal of the Society for Cardiovascular Magnetic Resonance. 2012;14:63.

219. Assomull RG, Prasad SK, Lyne J, Smith G, Burman ED, Khan M, et al. Cardiovascular magnetic resonance, fibrosis, and prognosis in dilated cardiomyopathy. Journal of the American College of Cardiology. 2006;48(10):1977-85.

220. Jiji RS, Kramer CM. Cardiovascular magnetic resonance: applications in daily practice. Cardiology in review. 2011;19(5):246-54.

221. Karamitsos TD, Neubauer S. The prognostic value of late gadolinium enhancement CMR in nonischemic cardiomyopathies. Current cardiology reports. 2013;15(1):326.

222. Kramer CM, Barkhausen J, Flamm SD, Kim RJ, Nagel E, Society for Cardiovascular Magnetic Resonance Board of Trustees Task Force on Standardized P. Standardized cardiovascular magnetic resonance imaging

(CMR) protocols, society for cardiovascular magnetic resonance: board of trustees task force on standardized protocols. Journal of cardiovascular magnetic resonance : official journal of the Society for Cardiovascular Magnetic Resonance. 2008;10:35.

223. Schalla S, Bekkers SC, Dennert R, van Suylen RJ, Waltenberger J, Leiner T, et al. Replacement and reactive myocardial fibrosis in idiopathic dilated cardiomyopathy: comparison of magnetic resonance imaging with right ventricular biopsy. European journal of heart failure. 2010;12(3):227-31.

224. Mewton N, Liu CY, Croisille P, Bluemke D, Lima JA. Assessment of myocardial fibrosis with cardiovascular magnetic resonance. Journal of the American College of Cardiology. 2011;57(8):891-903.

225. Moon JC, Messroghli DR, Kellman P, Piechnik SK, Robson MD, Ugander M, et al. Myocardial T1 mapping and extracellular volume quantification: a Society for Cardiovascular Magnetic Resonance (SCMR) and CMR Working Group of the European Society of Cardiology consensus statement. Journal of cardiovascular magnetic resonance : official journal of the Society for Cardiovascular Magnetic Resonance. 2013;15:92.

226. Piechnik SK, Ferreira VM, Lewandowski AJ, Ntusi NA, Banerjee R, Holloway C, et al. Normal variation of magnetic resonance T1 relaxation times in the human population at 1.5 T using ShMOLLI. Journal of cardiovascular magnetic resonance : official journal of the Society for Cardiovascular Magnetic Resonance. 2013;15:13.

227. Coelho-Filho OR, Shah RV, Mitchell R, Neilan TG, Moreno H, Jr., Simonson B, et al. Quantification of cardiomyocyte hypertrophy by cardiac magnetic resonance: implications for early cardiac remodeling. Circulation. 2013;128(11):1225-33.

228. Bull S, White SK, Piechnik SK, Flett AS, Ferreira VM, Loudon M, et al. Human non-contrast T1 values and correlation with histology in diffuse fibrosis. Heart. 2013;99(13):932-7.

229. Ferreira VM, Piechnik SK, Dall'Armellina E, Karamitsos TD, Francis JM, Choudhury RP, et al. Non-contrast T1-mapping detects acute myocardial edema with high diagnostic accuracy: a comparison to T2-weighted cardiovascular magnetic resonance. Journal of cardiovascular magnetic resonance : official journal of the Society for Cardiovascular Magnetic Resonance. 2012;14:42.

230. Karamitsos TD, Piechnik SK, Banypersad SM, Fontana M, Ntusi NB, Ferreira VM, et al. Noncontrast T1 mapping for the diagnosis of cardiac amyloidosis. JACC Cardiovascular imaging. 2013;6(4):488-97.

231. Sado DM, White SK, Piechnik SK, Banypersad SM, Treibel T, Captur G, et al. Identification and assessment of Anderson-Fabry disease by cardiovascular magnetic resonance noncontrast myocardial T1 mapping. Circulation Cardiovascular imaging. 2013;6(3):392-8.

232. Sado DM, Maestrini V, Piechnik SK, Banypersad SM, White SK, Flett AS, et al. Noncontrast myocardial T mapping using cardiovascular magnetic

resonance for iron overload. Journal of magnetic resonance imaging : JMRI. 2014.

233. Pedersen SF, Thrysoe SA, Robich MP, Paaske WP, Ringgaard S, Botker HE, et al. Assessment of intramyocardial hemorrhage by T1-weighted cardiovascular magnetic resonance in reperfused acute myocardial infarction. Journal of cardiovascular magnetic resonance : official journal of the Society for Cardiovascular Magnetic Resonance. 2012;14:59.

234. Jellis CL, Kwon DH. Myocardial T1 mapping: modalities and clinical applications. Cardiovascular diagnosis and therapy. 2014;4(2):126-37.

235. Rienks M, Papageorgiou AP, Frangogiannis NG, Heymans S. Myocardial extracellular matrix: an ever-changing and diverse entity. Circulation research. 2014;114(5):872-88.

236. Messroghli DR, Greiser A, Frohlich M, Dietz R, Schulz-Menger J. Optimization and validation of a fully-integrated pulse sequence for modified look-locker inversion-recovery (MOLLI) T1 mapping of the heart. Journal of magnetic resonance imaging : JMRI. 2007;26(4):1081-6.

237. Chin CW, Semple S, Malley T, White AC, Mirsadraee S, Weale PJ, et al. Optimization and comparison of myocardial T1 techniques at 3T in patients with aortic stenosis. European heart journal cardiovascular Imaging. 2014;15(5):556-65.

238. Flett AS, Sado DM, Quarta G, Mirabel M, Pellerin D, Herrey AS, et al. Diffuse myocardial fibrosis in severe aortic stenosis: an equilibrium contrast cardiovascular magnetic resonance study. European heart journal cardiovascular Imaging. 2012;13(10):819-26.

239. White SK, Sado DM, Fontana M, Banypersad SM, Maestrini V, Flett AS, et al. T1 Mapping for Myocardial Extracellular Volume Measurement by CMR: Bolus Only Versus Primed Infusion Technique. JACC Cardiovascular imaging. 2013.

240. Jerosch-Herold M, Sheridan DC, Kushner JD, Nauman D, Burgess D, Dutton D, et al. Cardiac magnetic resonance imaging of myocardial contrast uptake and blood flow in patients affected with idiopathic or familial dilated cardiomyopathy. American journal of physiology Heart and circulatory physiology. 2008;295(3):H1234-H42.

241. Look DC, Locker DR. Time saving in measurement of NMR and EPR relaxation times. . Rev Sci Instrum. 1970(41):250–1

242. Messroghli DR, Radjenovic A, Kozerke S, Higgins DM, Sivananthan MU, Ridgway JP. Modified Look-Locker inversion recovery (MOLLI) for high-resolution T1 mapping of the heart. Magnetic resonance in medicine : official journal of the Society of Magnetic Resonance in Medicine / Society of Magnetic Resonance in Medicine. 2004;52(1):141-6.

243. Piechnik SK, Ferreira VM, Dall'Armellina E, Cochlin LE, Greiser A, Neubauer S, et al. Shortened Modified Look-Locker Inversion recovery (ShMOLLI) for clinical myocardial T1-mapping at 1.5 and 3 T within a 9

heartbeat breathhold. Journal of cardiovascular magnetic resonance : official journal of the Society for Cardiovascular Magnetic Resonance. 2010;12:69.

244. Xue H, Greiser A, Zuehlsdorff S, Jolly MP, Guehring J, Arai AE, et al. Phase-sensitive inversion recovery for myocardial T1 mapping with motion correction and parametric fitting. Magnetic resonance in medicine : official journal of the Society of Magnetic Resonance in Medicine / Society of Magnetic Resonance in Medicine. 2013;69(5):1408-20.

245. Xue H, Ding Y, Guetter C, Jolly MP, Guehring J, Zuehlsdorff S, et al. Motion compensated magnetic resonance reconstruction using inverse-consistent deformable registration: application to real-time cine imaging. Med Image Comput Comput Assist Interv. 2011;14(Pt 1):564-72.

246. Chow K, Flewitt JA, Green JD, Pagano JJ, Friedrich MG, Thompson RB. Saturation recovery single-shot acquisition (SASHA) for myocardial T(1) mapping. Magnetic resonance in medicine : official journal of the Society of Magnetic Resonance in Medicine / Society of Magnetic Resonance in Medicine. 2014;71(6):2082-95.

247. Weingartner S, Akcakaya M, Basha T, Kissinger KV, Goddu B, Berg S, et al. Combined saturation/inversion recovery sequences for improved evaluation of scar and diffuse fibrosis in patients with arrhythmia or heart rate variability. Magnetic resonance in medicine : official journal of the Society of Magnetic Resonance in Medicine / Society of Magnetic Resonance in Medicine. 2013.

248. Higgins DM, Moon JC. Review of T1 Mapping Methods: Comparative Effectiveness Including Reproducibility Issues. Current Cardiovascular Imaging Reports. 2014;7(3).

249. Roujol S, Weingartner S, Foppa M, Chow K, Kawaji K, Ngo LH, et al. Accuracy, precision, and reproducibility of four T1 mapping sequences: a head-to-head comparison of MOLLI, ShMOLLI, SASHA, and SAPPHIRE. Radiology. 2014;272(3):683-9.

250. Fontana M, White SK, Banypersad SM, Sado DM, Maestrini V, Flett AS, et al. Comparison of T1 mapping techniques for ECV quantification. Histological validation and reproducibility of ShMOLLI versus multibreath-hold T1 quantification equilibrium contrast CMR. Journal of cardiovascular magnetic resonance : official journal of the Society for Cardiovascular Magnetic Resonance. 2012;14:88.

251. Taylor AJ, Salerno M, Dharmakumar R, Jerosch-Herold M. T1 Mapping: Basic Techniques and Clinical Applications. JACC Cardiovascular imaging. 2016;9(1):67-81.

252. Thavendiranathan P, Walls M, Giri S, Verhaert D, Rajagopalan S, Moore S, et al. Improved detection of myocardial involvement in acute inflammatory cardiomyopathies using T2 mapping. Circulation Cardiovascular imaging. 2012;5(1):102-10.

253. Crouser ED, Ono C, Tran T, He X, Raman SV. Improved detection of cardiac sarcoidosis using magnetic resonance with myocardial T2 mapping. Am J Respir Crit Care Med. 2014;189(1):109-12.

254. Usman AA, Taimen K, Wasielewski M, McDonald J, Shah S, Giri S, et al. Cardiac magnetic resonance T2 mapping in the monitoring and follow-up of acute cardiac transplant rejection: a pilot study. Circulation Cardiovascular imaging. 2012;5(6):782-90.

255. Baessler B, Schaarschmidt F, Stehning C, Schnackenburg B, Maintz D, Bunck AC. Cardiac T2-mapping using a fast gradient echo spin echo sequence - first in vitro and in vivo experience. (1532-429X (Electronic)).

256. Bonner F, Janzarik N, Jacoby C, Spieker M, Schnackenburg B, Range F, et al. Myocardial T2 mapping reveals age- and sex-related differences in volunteers. Journal of cardiovascular magnetic resonance : official journal of the Society for Cardiovascular Magnetic Resonance. 2015;17(1):9.

257. Sprinkart AM, Luetkens JA, Traber F, Doerner J, Gieseke J, Schnackenburg B, et al. Gradient Spin Echo (GraSE) imaging for fast myocardial T2 mapping. Journal of cardiovascular magnetic resonance : official journal of the Society for Cardiovascular Magnetic Resonance. 2015;17:12.

258. Giri S, Chung Y-C, Merchant A, Mihai G, Rajagopalan S, Raman SV, et al. T2 quantification for improved detection of myocardial edema. Journal of Cardiovascular Magnetic Resonance. 2009;11.

259. O'Gara PT, Kushner FG, Ascheim DD, Casey DE, Jr., Chung MK, de Lemos JA, et al. 2013 ACCF/AHA guideline for the management of ST-elevation myocardial infarction: executive summary: a report of the American College of Cardiology Foundation/American Heart Association Task Force on Practice Guidelines: developed in collaboration with the American College of Emergency Physicians and Society for Cardiovascular Angiography and Interventions. Catheterization and cardiovascular interventions : official journal of the Society for Cardiac Angiography & Interventions. 2013;82(1):E1-27.

260. Steg PG, James SK, Atar D, Badano LP, Blomstrom-Lundqvist C, Borger MA, et al. ESC Guidelines for the management of acute myocardial infarction in patients presenting with ST-segment elevation. European heart journal. 2012;33(20):2569-619.

261. Mather AN, Fairbairn TA, Ball SG, Greenwood JP, Plein S. Reperfusion haemorrhage as determined by cardiovascular MRI is a predictor of adverse left ventricular remodelling and markers of late arrhythmic risk. Heart. 2011;97(6):453-9.

262. Ledesma-Carbayo MJ, Kellman P, Hsu LY, Arai AE, McVeigh ER. Motion corrected free-breathing delayed-enhancement imaging of myocardial infarction using nonrigid registration. Journal of magnetic resonance imaging : JMRI. 2007;26(1):184-90.

263. Kellman P, Arai AE. Cardiac imaging techniques for physicians: late enhancement. Journal of magnetic resonance imaging : JMRI. 2012;36(3):529-42.

264. Arheden H, Saeed M, Higgins CB, Gao DW, Bremerich J, Wyttenbach R, et al. Measurement of the distribution volume of gadopentetate dimeglumine at echo-planar MR imaging to quantify myocardial infarction: comparison with 99mTc-DTPA autoradiography in rats. Radiology. 1999;211(3):698-708.

265. Nayak BK. Understanding the relevance of sample size calculation. Indian Journal of Ophthalmology. 2010;58(6):469-70.

266. Biau DJ, Kernéis S, Porcher R. Statistics in Brief: The Importance of Sample Size in the Planning and Interpretation of Medical Research. Clinical Orthopaedics and Related Research. 2008;466(9):2282-8.

267. Walsh M, Srinathan SK, McAuley DF, Mrkobrada M, Levine O, Ribic C, et al. The statistical significance of randomized controlled trial results is frequently fragile: a case for a Fragility Index. Journal of clinical epidemiology. 2014;67(6):622-8.

268. Ferreira VM, Piechnik SK, Dall'Armellina E, Karamitsos TD, Francis JM, Ntusi N, et al. T(1) mapping for the diagnosis of acute myocarditis using CMR: comparison to T2-weighted and late gadolinium enhanced imaging. JACC Cardiovascular imaging. 2013;6(10):1048-58.

269. Abdel-Aty H, Cocker M, Friedrich MG. Myocardial edema is a feature of Tako-Tsubo cardiomyopathy and is related to the severity of systolic dysfunction: insights from T2-weighted cardiovascular magnetic resonance. International journal of cardiology. 2009;132(2):291-3.

270. von Knobelsdorff-Brenkenhoff F, Prothmann M, Dieringer MA, Wassmuth R, Greiser A, Schwenke C, et al. Myocardial T1 and T2 mapping at 3 T: reference values, influencing factors and implications. Journal of cardiovascular magnetic resonance : official journal of the Society for Cardiovascular Magnetic Resonance. 2013;15:53.

271. de Waha S, Desch S, Eitel I, Fuernau G, Zachrau J, Leuschner A, et al. Impact of early vs. late microvascular obstruction assessed by magnetic resonance imaging on long-term outcome after ST-elevation myocardial infarction: a comparison with traditional prognostic markers. European heart journal. 2010;31(21):2660-8.

272. DeLong ER, DeLong DM, Clarke-Pearson DL. Comparing the areas under two or more correlated receiver operating characteristic curves: a nonparametric approach. Biometrics. 1988;44(3):837-45.

273. Kali A, Cokic I, Tang RL, Yang HJ, Sharif B, Marban E, et al. Determination of location, size, and transmurality of chronic myocardial infarction without exogenous contrast media by using cardiac magnetic resonance imaging at 3 T. Circulation Cardiovascular imaging. 2014;7(3):471-81.

274. Hansen ES, Pedersen SF, Pedersen SB, Kjaergaard U, Schmidt NH, Botker HE, et al. Cardiovascular MR T2-STIR imaging does not discriminate between intramyocardial haemorrhage and microvascular obstruction during the subacute phase of a reperfused myocardial infarction. Open Heart. 2016;3(1):e000346.

275. Abdula G, Sörensson P, Lundin M, Svedin J, Klein M, Kellman P, et al. Synthetic phase sensitive inversion recovery late gadolinium enhancement from post-contrast T1-mapping shows excellent agreement with conventional PSIR-LGE for diagnosing myocardial scar. Journal of Cardiovascular Magnetic Resonance. 2014;16(Suppl 1):P213-P.

276. Kellman P, Arai AE, McVeigh ER, Aletras AH. Phase-sensitive inversion recovery for detecting myocardial infarction using gadolinium-delayed hyperenhancement. Magnetic resonance in medicine : official journal of the Society of Magnetic Resonance in Medicine / Society of Magnetic Resonance in Medicine. 2002;47(2):372-83.

277. Huber AM, Schoenberg SO, Hayes C, Spannagl B, Engelmann MG, Franz WM, et al. Phase-sensitive inversion-recovery MR imaging in the detection of myocardial infarction. Radiology. 2005;237(3):854-60.

278. Piehler KM, Wong TC, Puntil KS, Zareba KM, Lin K, Harris DM, et al. Free-breathing, motion-corrected late gadolinium enhancement is robust and extends risk stratification to vulnerable patients. Circulation Cardiovascular imaging. 2013;6(3):423-32.

279. Bland JM, Altman DG. Statistical Methods for Assessing Agreement between Two Methods of Clinical Measurement. Lancet. 1986;1(8476):307-10.

280. Dash R, Tachibana A, Mitsutake Y, Dawoud F, Ikeno F, Lyons JK, et al. Cardiac MRI detection of infarct size reduction with hypothermia in porcine ischemia reperfusion injury model. Journal of Cardiovascular Magnetic Resonance. 2015;17(1):1-2.

281. Heiberg E, Ugander M, Engblom H, Gotberg M, Olivecrona GK, Erlinge D, et al. Automated quantification of myocardial infarction from MR images by accounting for partial volume effects: animal, phantom, and human study. Radiology. 2008;246(2):581-8.

282. Levi F, Lucchini F, Negri E, La Vecchia C. Trends in mortality from cardiovascular and cerebrovascular diseases in Europe and other areas of the world. Heart. 2002;88(2):119-24.

283. Ganame J, Messalli G, Dymarkowski S, Rademakers FE, Desmet W, Van de Werf F, et al. Impact of myocardial haemorrhage on left ventricular function and remodelling in patients with reperfused acute myocardial infarction. European heart journal. 2009;30(12):1440-9.

284. de Waha S, Desch S, Eitel I, Fuernau G, Lurz P, Leuschner A, et al. Relationship and prognostic value of microvascular obstruction and infarct size in ST-elevation myocardial infarction as visualized by magnetic resonance imaging. Clinical research in cardiology : official journal of the German Cardiac Society. 2012;101(6):487-95.

285. O'Regan DP, Ariff B, Neuwirth C, Tan Y, Durighel G, Cook SA. Assessment of severe reperfusion injury with T2* cardiac MRI in patients with acute myocardial infarction. Heart. 2010;96(23):1885-91.

286. Kidambi A, Mather AN, Motwani M, Swoboda P, Uddin A, Greenwood JP, et al. The effect of microvascular obstruction and intramyocardial

hemorrhage on contractile recovery in reperfused myocardial infarction: insights from cardiovascular magnetic resonance. Journal of cardiovascular magnetic resonance : official journal of the Society for Cardiovascular Magnetic Resonance. 2013;15:58.

287. Kellman P, Bandettini WP, Mancini C, Hammer-Hansen S, Hansen MS, Arai AE. Characterization of myocardial T1-mapping bias caused by intramyocardial fat in inversion recovery and saturation recovery techniques. Journal of cardiovascular magnetic resonance : official journal of the Society for Cardiovascular Magnetic Resonance. 2015;17:33.

288. Carberry J, Carrick D, Haig C, Rauhalammi SM, Ahmed N, Mordi I, et al. Remote Zone Extracellular Volume and Left Ventricular Remodeling in Survivors of ST-Elevation Myocardial Infarction. Hypertension. 2016.

289. Jankowska EA, von Haehling S, Anker SD, Macdougall IC, Ponikowski P. Iron deficiency and heart failure: diagnostic dilemmas and therapeutic perspectives. European heart journal. 2013;34(11):816-29.

290. Ludman AJ, Yellon DM, Hasleton J, Ariti C, Babu GG, Boston-Griffiths E, et al. Effect of erythropoietin as an adjunct to primary percutaneous coronary intervention: a randomised controlled clinical trial. Heart. 2011;97(19):1560-5.

291. Thavendiranathan P, Grant AD, Negishi T, Plana JC, Popovic ZB, Marwick TH. Reproducibility of echocardiographic techniques for sequential assessment of left ventricular ejection fraction and volumes: application to patients undergoing cancer chemotherapy. Journal of the American College of Cardiology. 2013;61(1):77-84.

292. Chuang ML, Gona P, Hautvast GL, Salton CJ, Blease SJ, Yeon SB, et al. Correlation of trabeculae and papillary muscles with clinical and cardiac characteristics and impact on CMR measures of LV anatomy and function. JACC Cardiovascular imaging. 2012;5(11):1115-23.

293. Weinsaft JW, Cham MD, Janik M, Min JK, Henschke CI, Yankelevitz DF, et al. Left ventricular papillary muscles and trabeculae are significant determinants of cardiac MRI volumetric measurements: effects on clinical standards in patients with advanced systolic dysfunction. International journal of cardiology. 2008;126(3):359-65.

294. Kozor R, Callaghan F, Tchan M, Hamilton-Craig C, Figtree GA, Grieve SM. A disproportionate contribution of papillary muscles and trabeculations to total left ventricular mass makes choice of cardiovascular magnetic resonance analysis technique critical in Fabry disease. Journal of cardiovascular magnetic resonance : official journal of the Society for Cardiovascular Magnetic Resonance. 2015;17:22.

295. Walsh TS, Lee A. Mathematical coupling in medical research: lessons from studies of oxygen kinetics. British journal of anaesthesia. 1998;81(2):118-20.

296. Morrow DA, Antman EM, Charlesworth A, Cairns R, Murphy SA, de Lemos JA, et al. TIMI risk score for ST-elevation myocardial infarction: A convenient, bedside, clinical score for risk assessment at presentation: An

intravenous nPA for treatment of infarcting myocardium early II trial substudy. Circulation. 2000;102(17):2031-7.

297. Treibel TA, Fontana M, Maestrini V, Castelletti S, Rosmini S, Simpson J, et al. Automatic Measurement of the Myocardial Interstitium: Synthetic Extracellular Volume Quantification Without Hematocrit Sampling. JACC Cardiovascular imaging. 2016;9(1):54-63.

298. Kido T, Kido T, Nakamura M, Watanabe K, Schmidt M, Forman C, et al. Compressed sensing real-time cine cardiovascular magnetic resonance: accurate assessment of left ventricular function in a single-breath-hold. Journal of Cardiovascular Magnetic Resonance. 2016;18(1):50.

299. Hamilton JI, Jiang Y, Chen Y, Ma D, Lo WC, Griswold M, et al. MR fingerprinting for rapid quantification of myocardial T1 , T2 , and proton spin density. Magnetic resonance in medicine : official journal of the Society of Magnetic Resonance in Medicine / Society of Magnetic Resonance in Medicine. 2016.

300. Varga-Szemes A, Ruzsics B, Kirschner R, Singh SP, Kiss P, Brott BC, et al. Determination of infarct size in ex vivo swine hearts by multidetector computed tomography using gadolinium as contrast medium. Investigative radiology. 2012;47(5):277-83.

301. Hsu LY, Ingkanisorn WP, Kellman P, Aletras AH, Arai AE. Quantitative myocardial infarction on delayed enhancement MRI. Part II: Clinical application of an automated feature analysis and combined thresholding infarct sizing algorithm. Journal of magnetic resonance imaging : JMRI. 2006;23(3):309-14.

302. Hsu LY, Natanzon A, Kellman P, Hirsch GA, Aletras AH, Arai AE. Quantitative myocardial infarction on delayed enhancement MRI. Part I: Animal validation of an automated feature analysis and combined thresholding infarct sizing algorithm. Journal of magnetic resonance imaging : JMRI. 2006;23(3):298-308.

303. Cokic I, Kali A, Yang HJ, Yee R, Tang R, Tighiouart M, et al. Iron-Sensitive Cardiac Magnetic Resonance Imaging for Prediction of Ventricular Arrhythmia Risk in Patients With Chronic Myocardial Infarction: Early Evidence. Circulation Cardiovascular imaging. 2015;8(8).

304. Engblom H, Heiberg E, Erlinge D, Jensen SE, Nordrehaug JE, Dubois-Rande JL, et al. Sample Size in Clinical Cardioprotection Trials Using Myocardial Salvage Index, Infarct Size, or Biochemical Markers as Endpoint. Journal of the American Heart Association. 2016;5(3):Advance online publication.

Publications related to this thesis

1. **Bulluck H**, Rosmini S, Abdel-Gadir A, Bhuva AN, Treibel TA, Fontana M, Weinmann S, Sirker A, Herrey AS, Manisty C, Moon JC, Hausenloy DJ (2016) Impact of microvascular obstruction on semi-automated techniques for quantifying acute and chronic myocardial infarction by cardiovascular magnetic resonance. **Open Heart** 3:e000535

2. **Bulluck H**, Rosmini S, Abdel-Gadir A, White SK, Bhuva AN, Treibel TA, Fontana M, Ramlall M, Hamarneh A, Sirker A, Herrey AS, Manisty C, Yellon DM, Kellman P, Moon JC, Hausenloy DJ (2016) Residual Myocardial Iron Following Intramyocardial Hemorrhage During the Convalescent Phase of Reperfused ST-Segment–Elevation Myocardial Infarction and Adverse Left Ventricular Remodeling. **Circulation: Cardiovascular Imaging** 9:e004940

3. **Bulluck H**, Rosmini S, Abdel-Gadir, A, White, S. K, Bhuva, A. N, Treibel, T.A, Fontana, M, Gonzalez-Lopez, E, Reant, P, Ramlall, M, Hamarneh, A, Sirker, A, Herrey, A.S, Manisty, C, Yellon, D, Kellman, P, Moon, J. C, Hausenloy, D.J. Automated ECV mapping provides insights into the pathophysiology of LV remodeling post reperfused STEMI. **J Am Heart Assoc.** 2016 Jul 11;5(7). pii: e003555. doi: 10.1161/JAHA.116.003555.

4. **Bulluck H**, White SK, Fröhlich GM, Casson SG, O'Meara C, Newton A, Nicholas J, Weale P, Wan SM, Sirker A, Moon JC, Yellon DM, Groves A, Menezes L, Hausenloy DJ. Quantifying the Area-at-risk in Reperfused ST-Segment-Elevation Myocardial Infarction Patients Using Hybrid Cardiac Positron Emission Tomography-Magnetic Resonance Imaging. **Circ Cardiovasc Imaging.** 2016 Mar;9(3):e003900. doi: 10.1161/CIRCIMAGING.115.003900.

5. **Bulluck H**, Yellon RL, Yellon DM. Promising strategies to minimize reperfusion injury in STEMI. **Minerva Cardioangiol.** 2016 Feb 9. [Epub ahead of print]

6. **Bulluck H**, Yellon DM, Hausenloy DJ. Reducing myocardial infarct size: challenges and future opportunities. **Heart.** 2016 Mar 1;102(5):341-8. doi: 10.1136/heartjnl-2015-307855. Epub 2015 Dec 16.

7. **Bulluck H**, Hausenloy DJ. Microvascular Obstruction: The Bane of Myocardial Reperfusion. **Rev Esp Cardiol** (Engl Ed). 2015 Nov;68(11):919-20. doi: 10.1016/j.rec.2015.06.022.

8. **Bulluck H**, White SK, Rosmini S, Bhuva A, Treibel TA, Fontana M, Abdel-Gadir A, Herrey A, Manisty C, Wan SM, Groves A, Menezes L, Moon JC, Hausenloy DJ. T1 mapping and T2 mapping at 3T for

quantifying the area-at-risk in reperfused STEMI patients. **J Cardiovasc Magn Reson.** 2015 Aug 12;17(1):73. doi: 10.1186/s12968-015-0173-6.

9. **Bulluck H**, Hausenloy DJ. Ischaemic conditioning: are we there yet? **Heart.** 2015 Jul;101(13):1067-77. doi: 10.1136/heartjnl-2014-306531. Epub 2015 Apr 17.

10. **Bulluck H**, Maestrini V, Rosmini S, Abdel-Gadir A, Treibel TA, Castelletti S, Bucciarelli-Ducci C, Manisty C, Moon JC (2015) Myocardial T1 mapping. **Circ J** 79:487-494

Under review/ accepted

1. Diagnostic performance of T1 and T2 mapping to detect intramyocardial hemorrhage in reperfused STEMI patients – **JMRI – accepted**

2. Quantification of both the Area-At-Risk and Acute Myocardial Infarct Size in ST-segment Elevation Myocardial Infarction using T1-mapping – **EHJCI – de-novo submission after revision**

3. Defining left ventricular remodeling following acute ST-segment elevation myocardial infarction using cardiovascular magnetic resonance – **JCMR - revision**